

DESIGN AND EVALUATION  
OF ANTI-STEAP2 ANTIBODIES TO  
TREAT AGGRESSIVE PROSTATE CANCER

presented by  
Aimy Nguyen Chi

DISSERTATION

Submitted to  
Swansea University in  
fulfilment of the requirements for the Degree of

DOCTOR OF PHILOSOPHY

Swansea University  
May 2020



# SUMMARY

**Introduction:** Prostate cancer is the second most frequent male cancer worldwide. Although prostate cancer is not always life-threatening when confined to the gland, the 5-year survival rate remains poor for men with advanced disease at approximately 30%. For such patients, there is an unmet need for patient-tailored drugs to improve their clinical management and quality of life, since current therapy options are accompanied with severe side-effects. The Six-Transmembrane Epithelial Antigen of the Prostate2 (STEAP2) is a cell surface protein highly expressed in advanced prostate cancer but not in the normal prostate. STEAP2 drives cancer invasive traits associated with prostate cancer progression *in vitro* and represents a promising drug target. The aim of this thesis was therefore to evaluate, whether STEAP2 is a viable drug target *in vitro*, with a focus on the application of antibodies (Abs) and Ab-Drug-Conjugates (ADCs), to treat advanced prostate cancer.

**Methods:** Immunohistochemistry (IHC) analysis of tissue-microarrays (TMAs) containing 33 tissues across the human body was conducted to assess the normal tissue profile of STEAP2. Structural analysis of STEAP2 was performed to identify targetable regions for the use of Ab therapeutics. One commercial polyclonal anti-STEAP2 Ab (anti-STEAP2 pAb) was selected for proof-of-concept studies based on the ability to detect both linear and native STEAP2 by confocal microscopy and protein analysis in prostate cancer cells (PC3) and normal prostate epithelial cells (PNT2). The effect of the anti-STEAP2 pAb on cancer invasive traits was studied in PC3 and PNT2 cells. Receptor internalisation of STEAP2 was evaluated upon anti-STEAP2 pAb binding to confirm the suitability of the ADC technology by confocal microscopy. A polyclonal anti-STEAP2-monomethylauristatin-E (MMAE) ADC (anti-STEAP2 pADC) was produced to compare its effect on reducing the cell viability of PC3 cells versus the unconjugated anti-STEAP2 pAb alone. Monoclonal anti-STEAP2 Ab (anti-STEAP2 mAb) was generated by the hybridoma technology using Balb/C mice. The specificity of the mAbs to STEAP2 was analysed by ELISA, Western blot and confocal microscopy.

**Results:** IHC/TMA analysis showed low STEAP2 protein levels in 33 different organs across the human body. Structural analysis of STEAP2 identified five targetable domains (Peptides1 - 5) specific to the extracellular loops1 - 3 (ECL1 - 3) of STEAP2. Peptide5/ECL3, „GWKRAFEEEEYYRFY“, appeared as the most promising immunogen region and was used as the antigen for mAb development. Anti-pAb treatment reduced cancer cell migration, invasion and viability of PC3 cells and triggered receptor internalisation of STEAP2. The anti-STEAP2- pADC was 3-fold more efficient than the unconjugated anti-STEAP2 pAb in decreasing the cell viability at a dose of 100 µg/ml. Peptide5/ECL3 elicited a moderate immune response in Balb/C mice. Four anti-STEAP2 mAbs were developed and their specificity to STEAP2 was confirmed by ELISA.

**Conclusion:** The low tissue expression profile of STEAP2 implies few off-target side-effects are likely to occur if STEAP2 is to be utilised as a future drug target. Peptide1 - 5 specific to the ECL1 - 3 of STEAP2 are potential antigen regions for future mAb development. When ECL3 was evaluated, the anti-STEAP2 pAb targeting this region was indeed capable of significantly reducing cancer invasive traits and triggered receptor internalisation in PC3 cells. Assessment of the anti-STEAP2 pADC demonstrated the potential utility of the ADC technology in the future. These promising findings highlight the therapeutic value of Ab-based strategies against STEAP2 to block cancer invasive traits. Evaluation of the four generated anti-STEAP2 mAbs indicated their specificity to STEAP2, albeit future validation is required. The *in-vitro* findings presented herein provide proof-of-concept, that supports STEAP2 as a viable drug target, with a focus on Abs and ADCs, prior to preclinical *in-vivo* studies for the treatment of patients with advanced prostate cancer.



# DECLARATION

- This work has not previously been accepted in substance for any degree and is not being concurrently submitted in candidature for any degree.
- This thesis is the result of my own investigations, except where otherwise stated. Where correction services have been used, the extent and nature of the correction is clearly marked in a footnote(s). Other sources are acknowledged by footnotes giving explicit references. A bibliography is appended.
- I hereby give consent for my thesis, if accepted, to be available for photocopying and for inter-library loan, and for the title and summary to be made available to outside organisations.

Munich, Germany, 30<sup>th</sup> of May, 2020



Aimy Nguyen Chi



# TABLE OF CONTENTS

<b>1</b>	<b>General Introduction.....</b>	<b>1</b>
1.1	The prostate.....	1
1.2	Prostate cancer .....	2
1.2.1	Prevalence .....	2
1.2.2	Prostate cancer types .....	3
1.2.3	Diagnosis .....	4
1.2.4	Treatments.....	9
1.3	Current challenges .....	15
1.4	The STEAP family .....	16
1.4.1	STEAP1 .....	19
1.4.2	STEAP2.....	20
1.4.3	STEAP3.....	23
1.4.4	STEAP4.....	24
1.4.5	The STEAP family as therapeutic targets .....	25
1.5	Antibodies and their use as therapeutics .....	27
1.5.1	Antibody structure.....	27
1.5.2	Therapeutic antibodies.....	28
1.5.3	Monoclonal antibody production (hybridoma technology).....	29
1.6	Antibody-Drug Conjugates .....	33
1.6.1	ADC structure .....	33
1.6.2	ADC receptor internalisation .....	34
1.7	Thesis aims .....	40
<b>2</b>	<b>Material and Methods.....</b>	<b>41</b>
2.1	Material .....	41
2.1.1	Reagents.....	41
2.1.2	Material.....	42
2.1.3	Equipment.....	42
2.1.4	Buffers and solutions.....	42
2.1.5	Cell lines.....	43
2.1.6	Cell culture and subculture .....	45
2.2	Methods .....	47
2.2.1	Immunohistochemistry .....	47
2.2.2	Structural analysis of the human STEAP2 protein.....	48
2.2.3	Western blotting .....	49

2.2.4	Fluorescence microscopy .....	56
2.2.5	Anti-STEAP2 Ab effects <i>in-vitro</i> .....	57
2.2.6	Anti-STEAP2 ADC development (CellMosaic) .....	59
2.2.7	Monoclonal anti-STEAP2 development (APS).....	60
2.2.8	Programs.....	62
2.2.9	Statistical analysis.....	62
<b>3</b>	<b>“Evaluation of STEAP2 as a drug target.”.....</b>	<b>64</b>
3.1	Introduction .....	64
3.2	Material and methods .....	68
3.2.1	Tissue micro-array (TMA) description .....	68
3.2.2	Immunohistochemistry of the tissue-microarray .....	70
3.2.3	TMA semi-quantitative scoring system and statistical analysis....	70
3.2.4	Structural analysis of the human STEAP2 protein.....	72
3.2.5	Polyclonal, commercial lead anti-STEAP2 pAb candidates.....	74
3.2.6	Protein extraction .....	74
3.2.7	Western blotting .....	74
3.2.8	Fluorescence Microscopy .....	76
3.3	Results .....	78
3.3.1	STEAP2 is expressed at minimal levels in over 33 normal tissues across the human body .....	78
3.3.2	Structural analysis of the human STEAP2 protein revealed three Ab-accessible extracellular loops (ECLS).....	82
3.3.3	Ab mapping to STEAP2’s ECLs suggested three targetable immunogens leading to selection of four commercial Abs.....	87
3.3.4	Peptide5 is the most suitable peptide sequence for immunogen design for hybridoma Ab development .....	90
3.3.5	Ab panel detected overexpressed STEAP2 in PC3 cells and low expression levels in PNT2 cells .....	95
3.3.6	Ab panel detected intracellular STEAP2, whilst Ab4 demonstrated exclusive cell surface location.....	96
3.4	Discussion .....	100
3.4.1	Normal tissue distribution of STEAP2 .....	100
3.4.2	Structural modelling of STEAP2 to identify targetable peptide sequences for immunogen design to generate mAbs.....	104
3.4.3	Ab panel evaluation and candidate selection .....	109
3.5	Conclusion.....	112
<b>4</b>	<b>“Impact of an anti-STEAP2 Ab on invasive properties of prostate cancer cells <i>in-vitro</i>.” .....</b>	<b>113</b>

4.1	Introduction .....	113
4.2	Methods .....	116
4.2.1	Cell culture.....	116
4.2.2	Assays to study the Ab's effect on cancer invasive traits .....	116
4.2.3	Fluorescence microscopy .....	118
4.2.4	Cell surface STEAP2 staining of 3D PC3 spheroid cells.....	121
4.2.5	Cell viability (3D PC3 spheroid cells).....	122
4.2.6	Statistical analysis.....	122
4.3	Results .....	123
4.3.1	Anti-STEAP2 pAbs exposure substantially inhibit cancer cell migration in PC3 cells .....	123
4.3.2	Anti-STEAP2 pAb (ECL3) reduced cell invasion in PC3 cells...	127
4.3.3	Receptor internalisation was triggered by anti-STEAP2 pAb (AB4/ECL3) and indicates acidic organelle localisation.....	130
4.3.4	Anti-STEAP2 pAb (AB4/ECL3) exposure reduces cell viability	136
4.3.5	STEAP2 is overexpressed in 3D PC3 cells.....	138
4.3.6	The anti-STEAP2 pAb (AB4/ECL3) has no significant effect on reducing the cell viability in 3D PC3 spheroid cells .....	141
4.4	Discussion .....	143
4.4.1	Cell migration .....	143
4.4.2	Cell invasion.....	146
4.4.3	Receptor internalisation .....	148
4.4.4	Cell viability.....	150
4.4.5	STEAP2 cell-surface expression and cell viability assessment after anti-STEAP2 pAb (AB4/ECL3) treatment in 3D PC3 spheroid cells .....	155
4.5	Conclusion.....	157
<b>5</b>	<b>“Generation and <i>in-vitro</i> assessment of anti-STEAP2 antibodies.”</b>	<b>158</b>
5.1	Introduction .....	158
5.2	Material and methods .....	160
5.2.1	Cell lines.....	160
5.2.2	Cell culture.....	160
5.2.3	Polyclonal anti-STEAP2-MMAE ADC generation .....	160
5.2.4	Polyclonal anti-STEAP2 ADC quality control .....	160
5.2.5	Cell viability assay .....	161
5.2.6	Monoclonal anti-STEAP2 Ab development at APS.....	163
5.2.7	Ab screening methods .....	164
5.2.8	Statistical analysis.....	166
5.3	Results .....	167

5.3.1	SEC to determine the DAR of the anti-STEAP2 pADC .....	167
5.3.2	Poor anti-STEAP2 pADC cell killing efficiency in PC3 cells.....	170
5.3.3	IC <sub>50</sub> of anti-STEAP2 pADC indicates poor quality.....	174
5.3.4	Test sera1 (linear) contain Abs specific to linear STEAP2 antigen . .....	175
5.3.5	Test sera1 (cyclic) contain Abs specific to cyclic STEAP2 antigen . .....	177
5.3.6	Test sera2 (linear) contain Abs specific to linear STEAP2 antigen . .....	178
5.3.7	Test sera2 (linear) do not recognise cyclic STEAP2 antigen .....	179
5.3.8	Test sera2 (cyclic) contain Abs specific to cyclic STEAP2.....	180
5.3.9	Test sera2 (cyclic) do not recognise linear STEAP2 antigen .....	181
5.3.10	Test sera2 (linear/cyclic) detect native STEAP2 in PC3 cells....	182
5.3.11	Test sera2 (linear and cyclic) contain a heterogenous pool of anti- STEAP2 pAbs by western blotting .....	189
5.3.12	Anti-STEAP2 mAbs recognise linear STEAP2 antigen by ELISA .. .....	189
5.3.13	Anti-STEAP2 mAbs show distinct IgG heavy and light chains by Nu-PAGE analysis.....	191
5.3.14	Anti-STEAP2 mAbs do not detect native STEAP2.....	193
5.3.15	Anti-STEAP2 mAbs poorly detect linear STEAP2 .....	195
5.4	Discussion .....	198
5.4.1	PC3 cell viability following anti-STEAP2 pADC and anti-STEAP2 pAb drug exposure.....	198
5.4.2	Anti-STEAP2 mAb development (Phase I) .....	204
5.4.3	Anti-STEAP2 mAb development (Phase II).....	209
5.4.4	Anti-STEAP2 mAb development (Phase IV) .....	212
5.5	Conclusion.....	214
<b>6</b>	<b>General Discussion .....</b>	<b>215</b>
6.1	Future Outlook .....	227
6.2	Conclusion.....	228
<b>7</b>	<b>Bibliography.....</b>	<b>229</b>
<b>8</b>	<b>Appendices.....</b>	<b>255</b>



# ACKNOWLEDGEMENTS

First and foremost, I would like to express my sincerest gratitude to my first supervisor, Professor Shareen Doak, for the opportunity to pursue this PhD in her lab. Your guidance has incredibly supported me throughout this thesis. Many thanks to my second advisor, Professor Steve Conlan, for your antibody expertise and the initiation of the mAb development with Shareen. Thank you both for your time to thoroughly review this thesis, your suggestions and effort. Also, thank you so much to Steve's group members Jezabel Garcia-Parra, Belen Pan-Castillo, and Gareth Healey who provided invaluable guidance for this project.

My sister Vivan, Mom (Mẹ) and Sven, have tremendously supported me to conquer this PhD. Vivan - your ongoing mental support has helped me to weather this process. I am so fortunate to have had you as my „third“ mentor. Thanks for your advice on the „art of becoming a PhD“, including the “figure formatting sessions” you gave, despite the 9 h time shift between our homes. Mẹ - thank you for your permanent support in every possible way. The past three years have glued us together and I am extremely glad to be able to see you more often in the future. Con cảm ơn Mẹ bạn vì tất cả mọi thứ và yêu Mẹ rất nhiều. Sven - your tireless motivation and moral support have been by far my biggest cheerleaders. Your effort to travel all the way to Wales and the adventures we went on to take some time out to recharge were exceptional.

Lastly, thanks to my dearest and best friends, Ena, Isabel and Heike, for your open ear and your energy to constantly push me, despite the long distance. I am glad to have you in my life. Also, this PhD would have been much less joy without my fellow lab mates Kulsoom, Irene, Mike, Jeff, Rifaik, Joana and Rui. Thank you all for creating a more pleasant working atmosphere, for sharing your expertise and the fruitful discussions.



# LIST OF FIGURES

Figure 1.1 Anatomy of the prostate .....	2
Figure 1.2 The Gleason pattern grading.....	7
Figure 1.3 Structural overview of the STEAP family of proteins.....	16
Figure 1.4 BLAST protein sequence alignment of the members of STEAP family ..	18
Figure 1.5 Cellular localisation and function of the STEAP2 protein .....	21
Figure 1.6 Immunoglobulin G (IgG) Ab structure .....	27
Figure 1.7 mAb development (hybridoma technology) .....	31
Figure 1.8 Antibody-Drug Conjugate structure.....	34
Figure 1.9 ADC receptor internalisation .....	35
Figure 1.10 Linkers used in commercial ADCs.....	37
Figure 1.11 Payloads used in commercial ADCs .....	39
Figure 2.1 Representatives images of the cell lines used in this thesis .....	44
Figure 2.2 Hemocytometer chamber used for cell counting.....	47
Figure 2.3 The BCA assay for protein quantification.....	50
Figure 2.4 Protein standard curve against the absorbance (nm).....	51
Figure 2.5 Material assembly prior to electro blotting .....	54
Figure 2.6 PVDF membrane cut .....	54
Figure 3.1 Drug target properties to consider for Ab drug development.....	65
Figure 3.2 Example TMA layout with IHC staining .....	68
Figure 3.3 PVDF membrane cut after electro-blotting.....	75
Figure 3.4 STEAP2 expression in high grade prostate cancer tissues .....	78
Figure 3.5 Tissue profile of STEAP2 in 33 human tissues by IHC/TMA .....	80
Figure 3.6 Tissue expression of STEAP2 in 33 human tissues by IHC/TMA .....	81
Figure 3.7 2D and 3D structures of STEAP2.....	82
Figure 3.8 AbDesigner output for STEAP2 protein .....	86
Figure 3.9 Identified immunogen regions on the ECLs of STEAP2 .....	89
Figure 3.10 AbDesigner output for Peptide1 and 2 (STEAP2/ECL1) .....	92
Figure 3.11 AbDesigner output for Peptide3 and4 (STEAP2/ECL2) .....	93
Figure 3.12 AbDesigner output for Peptide5 (STEAP2/ECL3) .....	94
Figure 3.13 STEAP2 protein analysis using the anti-STEAP2 pAb panel.....	95
Figure 3.14 Higher STEAP2 expression in PC3 cells by confocal microscopy.....	98
Figure 3.15 Lower STEAP2 expression in PNT2 cells by confocal microscopy .....	99
Figure 3.16 Differences in the tissue profile of STEAP2 by the HPA/ Chapter3... 102	
Figure 4.1 Anti-STEAP2 pAb (AB4/ECL3) inhibits cell migration of PC3 cells in a dose-dependent manner .....	124
Figure 4.2 Single and dual anti-STEAP2 pAb exposure block cell migration in PC3 cells.....	125
Figure 4.3 Anti-STEAP2 pAb (AB4/ECL3) does not affect the cell migration in PNT2 cells.....	127
Figure 4.4 Anti-STEAP2 pAb (AB4/ECL3) reduces cancer cell invasion of PC3 cells .....	129

Figure 4.5 STEAP2 is located to the cell membrane prior to receptor internalisation in cancerous PC3 cells but not in HFF cells.....	131
Figure 4.6 STEAP2 receptor internalisation was triggered after anti-STEAP2 pAb pHAb Amine Reactive Dye Conjugate (ECL3) binding .....	133
Figure 4.7 STEAP2's is localised in the endosomal/lysosomal organelles after 240 min of receptor internalisation in PC3 cells but is absent in HFF1 cells.....	134
Figure 4.8 Internalised STEAP2 does not co-localise with the Golgi apparatus indicating endosomal/ lysosomal accumulation after 240 min time point in PC3 cells .....	135
Figure 4.9 Anti-STEAP2 pAb (AB4/ECL3) reduces cell viability after 24 h exposure in PC3 and PNT2 cells.....	137
Figure 4.10 STEAP2 protein expression and localisation in 3D PC3 cell spheroids by fluorescence microscopy shows even distribution and overexpression throughout the spheroid .....	139
Figure 4.11 Z-stack of 3D PC3 cell spheroids over 50 $\mu$ m depth by fluorescence microscopy showed strong STEAP2 expression throughout the spheroid and good anti-STEAP2 pAb (AB4/ECL3) penetration, which decreased with spheroid depth .....	140
Figure 4.12 No difference in cell viability observed after anti-STEAP2 pAb (AB4/ECL3) treatment in 3D PC3 spheroid cells over 24 h by PI staining and confocal microscopy .....	142
Figure 5.1 Cut of the PDVF-membrane for protein analysis.....	165
Figure 5.2 SEC of the unconjugated anti-STEAP2 pAb (ECL3) .....	168
Figure 5.3 SEC of the commercial anti-STEAP2 pADC (ECL3) .....	169
Figure 5.4 Effect of anti-STEAP2 pADC and pAb on cell viability (PC3 cells) ....	173
Figure 5.5 IC <sub>50</sub> values of the anti-STEAP2 pADC and pAb .....	174
Figure 5.6 Test sera1 – Mouse1 – 4 (linear) assayed against linear STEAP2 antigen .....	176
Figure 5.7 Test sera1 (cyclic) assayed against the cyclic STEAP2 antigen.....	177
Figure 5.8 Test sera2 (linear) recognise the linear STEAP2 antigen.....	179
Figure 5.9 Test sera2 (linear) do not detect the cyclic STEAP2 antigen.....	180
Figure 5.10 Test sera2 (cyclic) recognise the cyclic STEAP2 antigen .....	181
Figure 5.11 Test sera2 (cyclic) do not detect the linear STEAP2 antigen .....	182
Figure 5.12 STEAP2 fluorescent staining by the anti-STEAP2 pAb (AB4/ECL3).....	183
Figure 5.13 Test sera2 (linear) detect native STEAP2 in PC3 cells.....	185
Figure 5.14 Test sera2 (linear) detect lower STEAP2 levels in PNT2 cells .....	186
Figure 5.15 Test sera2 (cyclic) detect native STEAP2 in PC3 cells.....	187
Figure 5.16 Test sera2 (cyclic) detect minimal STEAP2 levels in PNT2 cells .....	188
Figure 5.17 Anti-STEAP2 mAbs recognise the linear STEAP2 antigen .....	191
Figure 5.18 Anti-STEAP2 mAbs contain HC/ LC IgG fragments by Nu-PAGE ..	192
Figure 5.19 Positive controls used for the anti-STEAP2 mAb evaluation .....	194
Figure 5.20 Anti-STEAP2 mAbs do not recognise native STEAP2 in PC3 cells by confocal microscopy .....	195
Figure 5.21 STEAP2 protein analysis using the anti-STEAP2 mAbs .....	197

Figure 5.22 Potential antigen structures for the <i>in-vivo</i> immunisation .....	206
Figure 6.1 Information gained during this thesis qualifies STEAP2 as a suitable drug target to treat prostate cancer.....	217

# LIST OF TABLES

Table 1.1 Prostate cancer grading system for risk stratification according to the International Society of Urological Pathology (ISUP).....	8
Table 1.2 TNM Classification system for cancer staging.....	9
Table 1.3 Overview of the ADCs currently on the market.....	33
Table 1.4 Overview of the current payloads used in the commercial ADCs.....	38
Table 2.1 Reagents used throughout this thesis .....	41
Table 2.2 Material used throughout this thesis. ....	42
Table 2.3 Equipment used throughout this thesis. ....	42
Table 2.4 Buffers and solutions .....	43
Table 2.5 Commercial anti-STEAP2 pAb candidates .....	49
Table 2.6 Gel preparation for the SDS PAGE .....	52
Table 2.7 Channels used for fluorescence microscopy.....	56
Table 2.8 Programs used for analysis. ....	62
Table 3.1 Detailed description of the TMA.....	69
Table 3.2 Semi-quantitative scoring system for the TMA analysis .....	71
Table 3.4 Classification of STEAP2 into structural domains .....	83
Table 3.5 Identified immunogen regions after Ab-ECL mapping .....	88
Table 3.6 Analysed features to compare Peptides1 – 5 .....	94
Table 3.7 STEAP2 expression levels in fold change .....	96
Table 3.8 Differences in scoring systems used for the STEAP2 tissue expression analyses by the HPA and Chapter3 .....	101
Table 3.9 Summary of the anti-STEAP2 Ab panel evaluation .....	111
Table 4.1 Treatments for the cell migration anti-STEAP2 pAb (AB4/ECL3) dose finding assay .....	116
Table 4.2 Treatments to assess the effect on cell migration after the single or dual anti-STEAP2 pAb treatment .....	117
Table 4.3 Treatments for the cell invasion assay to assess the impact of the anti-STEAP2 pAb (AB4/ECL3) on invasive properties in PC3 cells.....	118
Table 4.4 Treatments for the MTT assay to investigate the cell viability of PC3 and PNT2 cells after anti-STEAP2 pAb (AB4/ECL3) drug regimen .....	118
Table 4.5 Treatment to study the receptor internalisation of STEAP2.....	120
Table 4.6 Treatment to study the impact of the anti-STEAP2 pAb (AB4/ECL3) on 3D PC3 spheroids cells after 24 h exposure.....	122
Table 5.1 Treatments to compare the efficiency of the anti-STEAP2 ADC versus the unconjugated anti-STEAP2 pAb in reducing the cell viability .....	161
Table 5.2 Log-scaled doses for the IC <sub>50</sub> assessment .....	162
Table 5.3 Overview of common vaccine adjuvants.....	209

## LIST OF ABBREVIATIONS

aa	Amino acid
Ab	Antibody
ADC	Antibody-Drug Conjugate
ADT	Androgen-Deprivation Therapy
APC	Antigen-Presenting Cell
APS	Ab Production Services
bsAb	Bispecific Ab
CD	Cluster of Differentiation
CTLA4	Cytotoxic T-Lymphocyte-Associated Protein4
ddH <sub>2</sub> O	Double distilled water
GM-CSF	Granulocyte Macrophage Colony-Stimulating Factor
ECM	Extracellular matrix
ECL	Extracellular loop
ELISA	Enzyme-Linked Immunosorbent Assay
ERK	Extracellular Signal-Regulated Kinase
HER2	Human Epidermal Growth Receptor2
HGPRT	Hypoxanthine Guanine Phosphoribosyl-Transferase
HIC	Hydrophobic Interaction Chromatography
hPBMC	Human Peripheral Blood Monocytes
LNCaP	Prostate cancer cells metastatic to the lymph nodes
ICI	Immune-Checkpoint Inhibitor
IgG	Immunoglobulin G
IHC	Immunohistochemistry
IL1 $\beta$	Interleukin1 beta
mCRPC	Metastatic Castration-Resistant Prostate Cancer
mAb	Monoclonal antibody
MAPK	Mitogen-Activated Protein Kinase
MDR	Multi-Drug Resistance
MHC	Major-Histocompatibility Complex
MMAE	Monomethyl-auristatin
MMP	Matrix Metalloprotease
NADH	Nicotinamide Adenine Dinucleotide
NADPH	Nicotinamide Adenine Dinucleotide Phosphate
NCT	National Clinical Trial
NF $\kappa$ B	Nuclear Factor Kappa-Light-Chain-Enhancer of Activated B-cells
OD	Optical Density
pAb	Polyclonal antibody
pADC	Polyclonal anti-STEAP2 Antibody-Drug Conjugate
PAGE	Polyacrylamide Gelelectrophoresis
PC3	Prostate cancer cells metastatic to the bone3
PCR	Polymerase-Chain Reaction

PD1	Programmed Cell Death Protein1
PD-L1	Programmed Death-Ligand1
PNT2	Normal prostate epithelial cells2
PSA	Prostate-Specific Antigen
RT	Room temperature
RNA	Ribonucleic acid
SDS	Sodium-Dodecylsulfate
SEC	Size-Exclusion Chromatography
siRNA	Small interfering RNA
STEAP	Six-Transmembrane Epithelial Antigen of the Prostate
TAA	Tumour-Associated Antigen
TGF $\beta$	Transforming Growth Factor $\beta$
TMA	Tissue-microarray
TNF $\alpha$	Tumour-Necrosis Factor $\alpha$
VEGF	Vascular Endothelial Growth Factor
$\alpha$	alpha
$\beta$	beta
<i>et al.</i>	<i>et al.ii</i>
<i>e.g.</i>	<i>exempli gratia</i>
g	gram
<i>i.e.</i>	<i>id est</i>
h	hour(s)
$\mu$ g	microgram
$\mu$ l	microliter
$\mu$ M	micromolar
mg	milligram
ml	millilitre
mM	millimolar
min	minutes
nM	nanomolar
k	kappa
V	Volt
%	percent
=	equal
$\leq$	less than or equal to
$\geq$	greater than or equal to
®	registered

# 1 General Introduction

## 1.1 The prostate

---

The prostate is a male duct gland, which partakes in the production of prostate fluids, ejaculation and the male hormone metabolism. In healthy, adult men, the gland is approximately as big as a walnut (Dunn & Kazer, 2011; Henry *et al.*, 2018; Hricak & Scardino, 2009). The growth of the prostate starts during puberty and is driven by androgens. The prostate is located below the fundus of the bladder, above the pelvis with the urethra crossing at its centre. Further, the rectum dorsally adjoins the prostate (Henry *et al.*, 2018; Hricak & Scardino, 2009; Mason & Moffat, 2010). The gland is anatomically divided up into three zones (Dunn & Kazer, 2011; Henry *et al.*, 2018; Hricak & Scardino, 2009) (**Figure 1.1**). The transition zone is the smallest zone making up about 5 - 10% of the prostate and surrounds the urethra (**Figure 1.1**). Often, age-dependent benign hyperplasia of the prostate (BPH) occur in the transition zone (Dunn & Kazer, 2011; Henry *et al.*, 2018; Hricak & Scardino, 2009). The central zone makes up about 20 - 25% of the prostate, which is crossed by ejaculatory ducts that lead to the urethra (Dunn & Kazer, 2011; Henry *et al.*, 2018; Hricak & Scardino, 2009). About 70% of the prostate is constituted by the peripheral zone, which surrounds both central and transition zones, where prostate carcinomas are more likely to occur (Lee *et al.*, 2016; Shaikhibrahim *et al.*, 2012) (**Figure 1.1**). The anterior fibromuscular stroma zone is free of prostate glands, however, it is made up of fibrous cells and connective tissue, which surrounds the prostate to form the capsule that support contractile moves for urination or ejaculation (Henry *et al.*, 2018; Hricak & Scardino, 2009) (**Figure 1.1**).

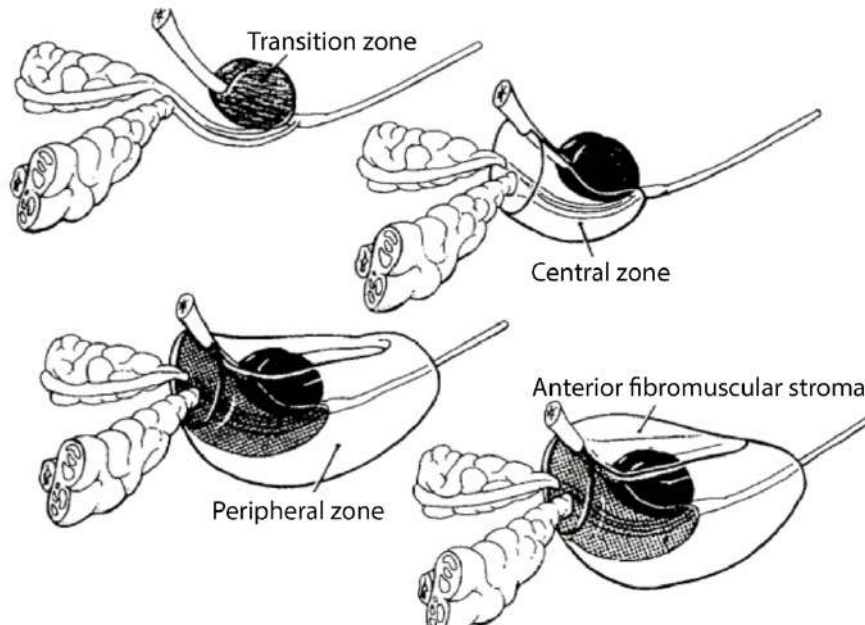


**Figure 1.1 Anatomy of the prostate.** The prostate is made up of the transition zone, the central zone, peripheral zone and the anterior fibromuscular stroma (adapted and modified from Hricak & Scardino, 2009).

The production of prostate fluid begins during puberty and takes place in the prostate as well as in the neighbouring seminal vesicles (Henry *et al.*, 2018; Hricak & Scardino, 2009). The prostate fluid contains a variety of enzymes, for example the acidic prostate phosphatase and Prostate-Specific Antigen (PSA), which serve the mobility of the sperms for fertilisation and provide the sperms with nourishment (Henry *et al.*, 2018; Hricak & Scardino, 2009; Mason & Moffat, 2010). During the process of ejaculation, the sperms are transported from the testicles to the prostate where they are mixed with the prostate fluid from the prostate and the seminal vesicles and enters the urethra for ejaculation via the prostate gland ducts (Henry *et al.*, 2018).

## 1.2 Prostate cancer

---

### 1.2.1 Prevalence

Prostate cancer is the second most frequently occurring male cancer (after lung) worldwide, which accounted for approximately 7.1% of new cancer cases in 2018

globally (WHO, 2019). In 2018, approximately 1.28 million new cases of prostate cancer were reported worldwide (WHO, 2019). Australia and New Zealand showed the highest prevalence for prostate cancer, followed by Europe and North America, while the prevalence is lower in South-Eastern and South-Central Asia (WHO, 2019). Often elderly men of 65 years and older are affected (Cancer Research UK, 2019). Moreover, African-black men are at higher risk of developing prostate cancer than white men; while the lowest prevalence is observed in Asian ethnicities (Cancer Research UK, 2019; WHO, 2019). Despite the high prevalence of prostate cancer, it is generally not life-threatening when diagnosed at an early stage, with localised prostate cancer cases having a 5-year survival rate of approximately 100% (Cancer Research UK, 2019; NIH, 2016). However, the chances of survival for men with advanced and metastatic cancer remain poor with an approximate 30% survival rate within 5 years of diagnosis (Cancer Research UK, 2019; NIH, 2016). Most prostate cancers remain indolent at the early stage and develop asymptotically. However, common symptoms are urination problems as a result of an enlarged prostate which increases the pressure on the urethra, which the prostate surrounds (Dunn & Kazer, 2011; Henry *et al.*, 2018; Hricak & Scardino, 2009; Mason & Moffat, 2003).

### 1.2.2 Prostate cancer types

Approximately 90% of all prostate cancer cases belong to the acinar adenocarcinoma type, which is a cancer that evolves from the epithelial cells of the prostate glandular region, occurring in the peripheral zone of the prostate (**Figure 1.1**) (Hricak & Scardino, 2009; Lee *et al.*, 2016). Other prostate cancer types are more rare, such as squamous cell prostate cancer, which originates from the non-glandular prostate epithelial cells (0.5 - 1.0%) (Cancer Research UK, 2019; Hricak & Scardino, 2009). The prevalence of the neuroendocrine small cell prostate cancer is 0.5 - 2% (Cancer Research UK, 2019; Hricak & Scardino, 2009). Transitional prostate cancer affects the cells in the transition zone of the prostate that surround the urethra (**Figure 1.1**). Its prevalence is also very rare at 0.1 - 1% and often develops from

bladder cancer as secondary tumour (Hricak & Scardino, 2009; Lee *et al.*, 2016). The cancer is localised when the tumour has not spread beyond the prostate gland. Localised prostate cancer accounts for 77% of the diagnosed cases, followed by 13% for locally advanced cancer, where tumour cells are present in the nearby seminal vesicles, bladder, or pelvic lymph nodes, for example (Cancer Research UK, 2019; NIH, 2016). Approximately 6% of the prostate cancers are of metastatic stage, where the tumour has spread to the bone (most commonly), the lymph nodes, lung, and occasionally to the brain (Budnik *et al.*, 2019; Cancer Research UK, 2019; Hatzoglou *et al.*, 2016; NIH, 2016).

### **1.2.3 Diagnosis**

In order to diagnose prostate cancer, a combination of tools is utilised. The current gold standards are the blood-based Prostate-Specific Antigen (PSA) test, the Digital Rectal Examination (DRE) and Transrectal Ultrasound Scan (TRUS)-guided biopsy followed by Gleason and Tumour Lymph Node Metastasis (TNM) staging (Mottet *et al.*, 2018; NCCN, 2018; NICE, 2019).

#### **1.2.3.1 Prostate-Specific Antigen Test**

The PSA test involves the analysis of the Prostate-Specific Antigen (PSA), a blood-based serum biomarker, used alongside the DRE to aid in the diagnosis of prostate cancer (Mottet *et al.*, 2018; NCCN, 2018). PSA is produced specifically by the prostate epithelial cells and is secreted into the lumen of the prostate gland (Henry *et al.*, 2018; Hricak & Scardino, 2009). High PSA levels are therefore likely to indicate the presence of prostate cancer (Cancer Research UK, 2019; Mottet *et al.*, 2018; NCCN, 2018). Generally, an elevated PSA level depends on the patients' age and is considered to increase with age (NCCN, 2018). Thus, elevated PSA levels may start from 3 ng/ml for an age group of 50 – 59, > 4 ng/ml for patients between 60 – 69 years and > 5 ng/ml for patients older than 70 years (NCCN, 2018). PSA screening is highly controversial for many reasons (Boniol *et al.*, 2012). Since benign prostate

diseases (*e.g.* prostatitis and BPH) can lead to elevated PSA levels falsely indicating prostate cancer, PSA screening has led to over-diagnosis and over-treatment in the 1980s (Bonniol *et al.*, 2012; Loeb *et al.*, 2015; Schröder *et al.*, 2009). Further, the PSA test does not accurately discriminate between patients at low- or high-risk of developing advanced prostate cancer (Bonniol *et al.*, 2012; Loeb *et al.*, 2015; Schröder *et al.*, 2009; Velonas *et al.*, 2013).

### **1.2.3.2 Digital Rectal Examination**

During the Digital Rectal Examination (DRE) the physician determines the size and softness of the prostate (Cancer Research UK, 2019; NCCN, 2018). Since the rectum is located dorsally of the prostate, the gland can be assessed by placing the fingers (lat. *digitalis*) into the rectum of the patient (Mason & Moffat, 2003; NCCN, 2018; Tewari, Whelan, & Graham, 2014). The sensitivity of the DRE to correctly diagnose prostate cancer is approximately 20 – 40% (NCCN, 2018). The DRE is useful in practice to assess the enlargement of the prostate (which may be indicative of possible prostate cancer) in patients who suffer urinary issues and which may be reflected by any elevated PSA levels (NCCN, 2018). If the DRE has indicated the potential presence of prostate cancer alongside elevated PSA serum levels, tissue biopsies of the prostate will be collected for further examination (Cancer Research UK, 2019; Mottet *et al.*, 2018; NCCN, 2018).

### **1.2.3.3 Biopsy**

The Transrectal Ultrasound Scan (TRUS)-guided biopsy is the most common technique for the collection of prostate biopsies (Guo *et al.*, 2017; Mottet *et al.*, 2018; NCCN, 2018; Yao *et al.*, 2014). As the name suggests, the prostate is imaged by inserting a TRUS „gun“ into the rectum (NCCN, 2018). The use of ultrasound waves allows the visualisation of the prostate and the seminal vesicles (Mottet *et al.*, 2018; NCCN, 2018). A low echo of the ultrasound may indicate the presence of prostate cancer, blood and liquid, whereas a strong echo usually represents the bone. The

TRUS-guided biopsy provides the advantage of imaging and taking biopsies at desired locations of the prostate at the same time (NCCN, 2018). The “gun” contains needles, in order to take approximately 10 - 12 tissue cores at different locations of the prostate for biopsy analysis (Guo *et al.*, 2017; Yao *et al.*, 2014). A pathologist then evaluates, whether the biopsies are positive, indicating prostate cancer, or negative based on the cell morphology. Biopsies are then categorised according to the Gleason Scoring System (NCCN, 2018). Potential risks are short-term blood in the urine, pain or infection (Kratz *et al.*, 2011; Mottet *et al.*, 2018; NCCN, 2018).

#### **1.2.3.4 Gleason Score**

As approximately 90% of prostate cancers are acinar adenocarcinomas, their malignancy is graded by the Gleason Scoring System (Gordetsky & Epstein, 2016). Grading requires a pathologist to evaluate the prostate cancer tissue biopsies under the microscope (NCCN, 2018). The Gleason Score is utilised to classify (grade) morphological patterns with increasing abnormal prostate cancer cell growth (Chen & Zhou, 2016; Epstein, 2016; Gordetsky & Epstein, 2016; Hricak & Scardino, 2009). The final score is made up by the sum of two separate Gleason grade patterns, which range from 1 – 5 (NCCN, 2018). A high score (*e.g.* Score = 5) describes poorly, clinically less differentiated, more aggressive cells, whereas a low score (*e.g.* Score = 1) represents well differentiated, less aggressive prostate cancer (Chen & Zhou, 2016; Epstein, 2016; Gordetsky & Epstein, 2016; Hricak & Scardino, 2009) (**Figure 1.2**).

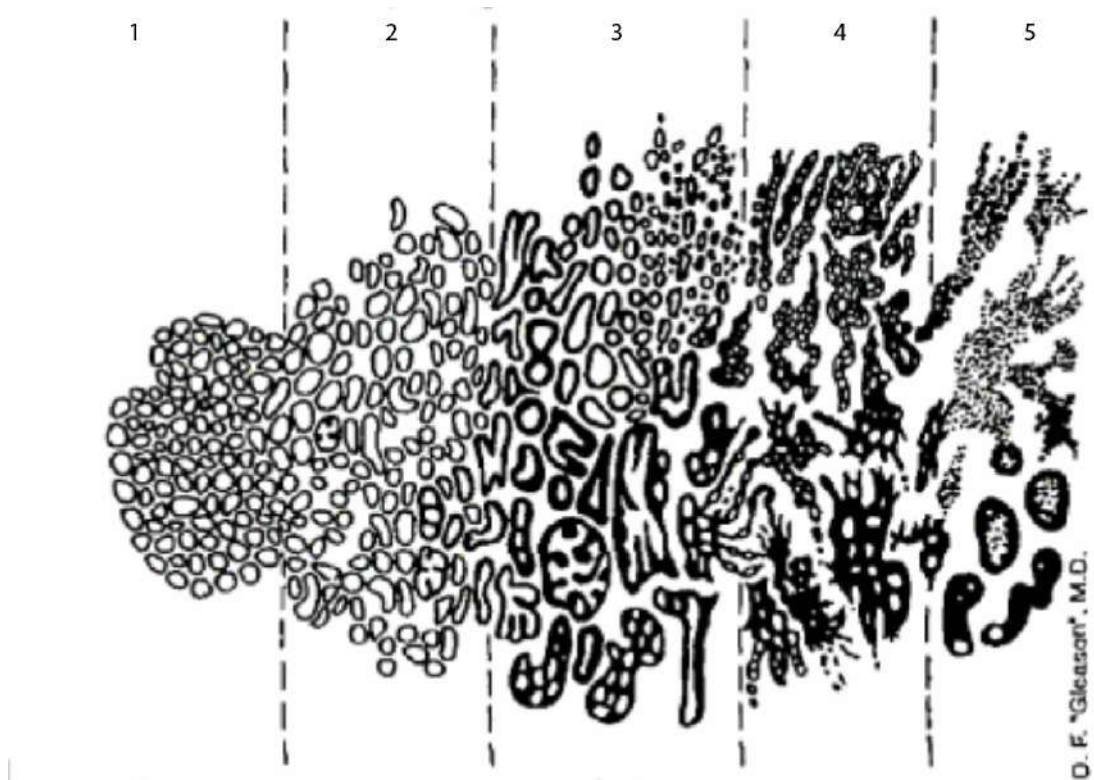


**Figure 1.2 The Gleason pattern grading.** Prostate cancer cells can be scored according to the Gleason score (1 – 5). 1: uniform, well-differentiated prostate glands; 2: less-defined, round-oval cells; 3: variability in gland size, shape elongated; 4: fused, small glands or masses; 5: poorly differentiated masses or sheets of prostate glands (adapted and modified from Hricak & Scardino, 2009, original from D.F. Gleason).

The first Gleason grade pattern is based on the most prevalent observed pattern, while the second grade pattern represents the second most abundant grade found in the biopsy. The final Gleason Score is then summed up by the two individual Gleason Score patterns, which are indicated in brackets after the final Gleason Score (Chen & Zhou, 2016; Gordetsky & Epstein, 2016). For example, if the first Gleason Score is 3 and the second Gleason Score is 2, the final Gleason Score is described as: Gleason Score 5(3+2) (Chen *et al.*, 2016; Gordetsky & Epstein, 2016). Based on the old Gleason Scoring system with the final Gleason Score scale between 2 - 10, a Gleason Score = 6 would suggest patients had an intermediate prostate cancer, although it is considered as low -risk for metastasis (Gordetsky & Epstein, 2016). This approach however, required improvement to better inform clinical management. Therefore, an additional contemporary, simplified grading system was introduced in 2014 for prostate cancer consisting of five categories (Grade 1 - 5): low, intermediate

and three high grade prostate cancer categories, which correlate with increasing Gleason Scores (Epstein, 2016; Gordetsky & Epstein, 2016) (**Table 1.1**).

**Table 1.1 Prostate cancer grading system for risk stratification according to the International Society of Urological Pathology (ISUP).**

Prostate cancer grade	Final Gleason Score
1 = Low grade	2 – 6
2 = Intermediate grade	7a (3+4)
3 = High grade	7b (4+3)
4 = High grade	8 (4+4 or 3+5 or 5+3)
5 = High grade	9 – 10

### 1.2.3.5 TNM Staging

Utilising a combination of TNM staging, PSA level and Gleason Score, prostate cancer can be stratified into specific risk categories important for informing treatment decisions (Mottet *et al.*, 2018; NCCN, 2018). The scope of any type of cancer can be anatomically classified into the extent of the primary tumour (T), if the lymph nodes are affected (N) and if any distant metastasis are present (M); known as the Tumour Node Metastasis (TNM) Staging (Izumi *et al.*, 2015; Mottet *et al.*, 2018; Sobin *et al.*, 2009). The TNM category is divided up into subcategories, that describe the location and spread of the cancer more precisely (Hricak & Scardino, 2009; Mottet *et al.*, 2018; Tewari *et al.*, 2014) (**Table 1.2**). To visualise the extent of the cancer, patients are scanned by Magnetic Resonance Imaging (MRI), Computed Tomography (CT) or Transrectal Ultrasound Scan (TRUS) (Mottet *et al.*, 2018; NCCN, 2018; NICE, 2019).

**Table 1.2 TNM Classification system for cancer staging.** Adapted from NCCN, 2019. The categories are T: primary tumour; N: regional lymph nodes; M: distant metastasis. Categories consist of subcategories, where increasing numbers reflect an increased spread of the cancer.

TNM Clinical Classification	
T – Primary tumour	
T1	Tumour confined to the gland
T2	Larger tumour confined to the gland
T3	Tumour has spread beyond the gland
T4	Tumour has spread to other organs
N – Regional lymph nodes	
NX	Cannot be assessed
N0	No lymph node metastasis
N1	Lymph node metastasis
M – Distant metastasis	
M0	Cannot be assessed
M1	Distant metastasis
M1a	Metastasis in non-regional lymph nodes
M1b	Metastasis in the bone
M1c	Metastasis in other body organs

## 1.2.4 Treatments

Whether and which treatment option is the most suitable depends on the life expectancy, risk group of the patient and, if he will be likely to benefit from the treatment (Mottet *et al.*, 2018; NCCN, 2018; NICE, 2019). The risk groups are based on the TNM staging, Gleason Score and PSA levels of the patient (Mottet *et al.*, 2018; NCCN, 2018; NICE, 2019). For example, there may be little benefit from treating low-risk patients with poor health, if they are likely to suffer more from the treatment side-effects if the cancer is slow-growing and is likely to not cause any problems (NCCN, 2018).

### 1.2.4.1 Active Surveillance

Active surveillance is a treatment-free option for older patients with slow growing, small prostate tumours with a life expectancy of more than 10 years after diagnosis for which the risk of suffering treatment side-effects outweighs the benefits (Cancer Research UK, 2019; NCCN, 2018). Active surveillance is a non-invasive method to monitor the patient, until treatment may be required. This monitoring is achieved by routinely checking the PSA level, biopsies may be taken approximately

every 6 months and the DRE is conducted not more than every 12 months (Mottet *et al.*, 2018; NCCN, 2018).

#### **1.2.4.2 Surgical treatment**

Low-risk prostate cancer patients with a life expectancy of more than 20 years, may prefer to undergo surgery over active surveillance, which has the potential for cure (NCCN, 2018; NICE, 2019; Tewari *et al.*, 2014). During the surgery, known as a prostatectomy, the prostate and the testosterone-producing seminal vesicles are removed. During radical retropubic prostatectomy the prostate is surgically removed via a stomach cut, while radical perineal prostatectomy requires a cut between a scrotum and the anus (NCCN, 2018). Often, older patients are more likely to suffer from surgical side-effects, which are commonly urine incontinence and erectile dysfunction. Also one cannot father children anymore following a prostatectomy (Cancer Research UK, 2019; NCCN, 2018). For those individuals, who are likely and wish to become father of children in the future, sperm banking is an option to collect and cryopreserve the semen, that contains the sperms prior to surgery (NICE, 2019).

#### **1.2.4.3 Radiation therapy**

Radiation therapy is suitable to treat low-risk, favourable or unfavourable intermediate-risk prostate cancers with approximately 10 - 20 years to live after diagnosis (Cancer Research UK, 2019; Mottet *et al.*, 2018; NICE, 2019). It can also be applied in combination with hormone therapy for the treatment of locally advanced and metastatic prostate cancer (NICE, 2019). Traditional radiation therapy is based on the use of x-rays, containing high-energy proton beams generated by a linear accelerator, which results in DNA damage and thereby tumour cell killing (Mottet *et al.*, 2018; NCCN, 2018). One of the most common methods in clinical practice is the so called External Beam Radiation Therapy (EBRT), which takes approximately 8 - 9 weeks (NCCN, 2018). The patient lays on its back when exposed to EBRT. Thus, the location of the prostate is assessed by CT and MRI imaging before EBRT, to

minimise side-effects by reducing the exposed body parts as much as possible (NCCN, 2018). Before EBRT, a treatment plan needs to be implemented. This includes dose finding and determining the number and shapes of beams applied, for which a simulation is run beforehand with the patient (Bakiu *et al.*, 2013). In 3D-conformational radiation therapy (3D-CRT) the location of the prostate is visualised by CT, in order to match the radiation to the tumour-size and to spare healthy tissues (Bakiu *et al.*, 2013). The radiation dose and number and shapes of beams are manually selected by the clinician. The Intensity-Modulated Radiation Therapy (IMRT) is a more advanced EBRT method, that offers more precision to deliver the external beams by using a computer-assisted linear accelerator (Bakiu *et al.*, 2013). During, IMRT the radiation dose can be regulated by using small beams of different radiation strengths to reduce potential side-effects of healthy tissues (Bakiu *et al.*, 2013).

Brachytherapy („seed treatment“) is another method where low dose radioactive iodine ( $^{125}\text{I}$ ) or palladium ( $^{103}\text{Pd}$ ) or high dose, temporary iridium ( $^{192}\text{Ir}$ ) seeds are implanted during an image-guided procedure into the prostate through the peritoneum under anaesthetics (Teixeira Leite *et al.*, 2019; Trindade *et al.*, 2012; Zuber *et al.*, 2015). EBRT is also used in combination with Androgen-Deprivation Therapy (ADT) to treat locally advanced and metastatic prostate cancer (Bolla *et al.*, 2010; Denham *et al.*, 2011; NICE, 2019). Side-effects include the feeling of being sunburned, urination incontinence and haematuria (NCCN, 2018). Bone metastatic prostate cancer is treated with radiopharmaceuticals. Due to the structural similarity to calcium, radium ( $^{223}\text{Ra}$ ) accumulates in the bones, where it exhibits radioactivity to kill the cancer cells. Side-effects include nausea and headaches, for example (NCCN, 2018).

#### 1.2.4.4 Hormone therapy

Initially, prostate cancer growth is driven by androgens (e.g. testosterone and dihydrotestosterone). Therefore, hormone therapy is the favoured treatment modality to treat androgen-sensitive, high-risk localised, advanced and metastatic prostate cancer (Crawford *et al.*, 2018; NCCN, 2018). The goal of hormone therapy is to inhibit tumour growth by reducing the production of androgens or to block the action of testosterone. One can differentiate between surgical and chemical castration (Mottet *et al.*, 2018; NICE, 2019). During bilateral orchiectomy, both of the androgen-producing testicles are removed, while a reduction of androgen production is chemically achieved during Androgen-Deprivation Therapy (ADT) (NCCN, 2018). A successful castration is considered when the serum testosterone level is below 20 – 50 ng/ml requiring the monitoring of serum testosterone to confirm the patient's response to the treatment (Dason *et al.*, 2012; Heidenreich *et al.*, 2014; Klotz *et al.*, 2017; Schulman *et al.*, 2010). During ADT, drugs are applied, that interfere with the hypothalamus-pituitary-gonadal-axis and the Luteinising Hormone-Releasing Hormone Receptor (LHRH receptor) (Mutschler *et al.*, 2012). After continuous administration of LHRH agonist (e.g., Goserelin®), the response of the pituitary gland to LHRH is downregulated via a negative feedback mechanism, which results in a reduced production of androgens (Mutschler *et al.*, 2012; Sipos *et al.*, 2018; Tolkach *et al.*, 2013). Further, LHRH antagonists (e.g. Degarelix®) suppress androgen production by inhibiting LHRH from binding to the LHRH receptor (NCCN, 2018). Other drugs like Finasteride (Proscar®) exhibit their anti-androgenic effect by binding to the enzyme 5 $\alpha$ -reductase required for the conversion of testosterone to dihydrotestosterone (Mutschler *et al.*, 2012; Steinhilber *et al.*, 2012). Side-effects of hormone therapy are erectile dysfunction, reduced libido and osteoporosis (Mottet *et al.*, 2018; Mutschler *et al.*, 2012; NCCN, 2018).

#### 1.2.4.5 Chemotherapy

Chemotherapy is suitable for the treatment of advanced or metastatic castration-resistant prostate cancer (mCRPC), which are no longer sensitive to ADT (Mottet *et al.*, 2018; NCCN, 2018; NICE, 2019). Docetaxel, a semisynthetic analogon of Paclitaxel, is recommended for the first line treatment, which inhibits microtubule depolymerisation (Mottet *et al.*, 2018; NCCN, 2018; Steinhilber *et al.*, 2012). As second line treatment, another taxol derivate, Cabazitaxel is recommended but this has more severe side-effects than Docetaxel (Mottet *et al.*, 2018). In addition, Mitoxanthrone hydrochloride acts as a DNA intercalator, which results in cell killing and is utilised as second line treatment, too. Chemotherapeutics are administered intravenously in cycles and are accompanied with severe side-effects like diarrhoea, fatigue, hair-loss, allergy (NCCN, 2018).

#### 1.2.4.6 Immunotherapy

Sipuleucel-T (Provenge®) was introduced as an immunostimulatory anti-cancer vaccine is used to treat advanced and mCRPC patients (Heidenreich *et al.*, 2014; NCCN, 2018; NICE, 2019; Penson *et al.*, 2012; Schellhammer *et al.*, 2013). It requires the adoptive cell transfer during which patient blood is collected, following leukapheresis for the isolation of peripheral blood monocytes (PBMCs). The PBMCs contain Antigen-Presenting Cells (APCs, e.g. macrophages and dendritic cells). The PBMCs (including APCs) are cultured *ex-vivo* with a fusion protein, consisting of the Granulocyte Macrophage-Simulating Factor (GM-SF) and the prostate cancer tumour antigen Prostate-Acidic Phosphatase (PAP). The PBMCs are then administered to the patients via infusion. GM-SF activates the APCs, in order to kill the PAP-positive prostate cancer cells, which account to approximately 95% of the prostate cancer cells (Graff & Chamberlain, 2014; Penson *et al.*, 2012). Treatment with Sipuleucel-T was shown to increase the overall survival within 36 months by approximately 30% (4.1 months) when compared to the placebo control (Kantoff *et al.*, 2010). However, the

benefit of Sipuleucel-T to improve the time-to-progression is debated, when compared to ADT or chemotherapy (Yi *et al.*, 2016).

In addition, Pembrolizumab (Keytruda®) is a monoclonal Ab, that functions as an Immune-Checkpoint Inhibitor (ICI) of the Programmed-Cell Death Protein-1 (PD-1) (Hansen *et al.*, 2018; MSD, 2019). Binding of the Programmed Death Ligand1 (PD-L1) to its PD-1 receptor turns off the immune response of T-killer cells, which tumour cells employ to escape the immune system (Hansen *et al.*, 2018). Therefore, Pembrolizumab re-activates the anti-tumour immune response of T-killer cells. This treatment modality is suited for patients with solid tumours including mCRPC, who have previously received either chemotherapy or Abiraterone (NCCN, 2018). Recent findings have indicated a small subset (3.1%) of prostate cancers exhibit specific DNA repair mutations of which half benefited from Pembrolizumab treatment (Abida *et al.*, 2019).

### 1.3 Current challenges

---

Advances in analysing the human genome have contributed to a better understanding of the genetic make-up of certain cancers (Schork, 2015). Based on these insights, therapeutic antibodies have proven to be valuable therapy choices for targeted therapies and their clinical application has dramatically expanded during the last two decades (Ryman & Meibohm, 2017). With respect to prostate cancer, current standard treatment options for patients are often accompanied with harsh side-effects, which substantially reduce the well-being of these individuals (Donovan *et al.*, 2019; Mazzola & Mulhall, 2012; Schellhammer *et al.*, 2013). Ongoing research is contributing to great advances in this area, such as the introduction of two new, more patient-tailored immunotherapies, Sipuleucel-T and Pembrolizumab, for mCRPC. However, the clinical benefit of Sipuleucel-T is still under debate when compared to the standard therapy, while Pembrolizumab has been shown to be beneficial for only a narrow subset of patients (Abida *et al.*, 2019; Hansen *et al.*, 2018; Kantoff *et al.*, 2010; Yi *et al.*, 2016). More efficient drugs for treating advanced prostate cancer are lacking, in order to prevent disease progression without compromising patients' quality of life. Therefore, novel medicines for advanced prostate cancer are required to improve options for clinical management of patients.

## 1.4 The STEAP family

The Six-Transmembrane Epithelial Antigen of the Prostate (STEAP) family includes 4 members, which are STEAP1 - 4. As their name suggests, all STEAP proteins comprise six transmembrane helices (Grunewald *et al.*, 2012; Sikkeland *et al.*, 2016).

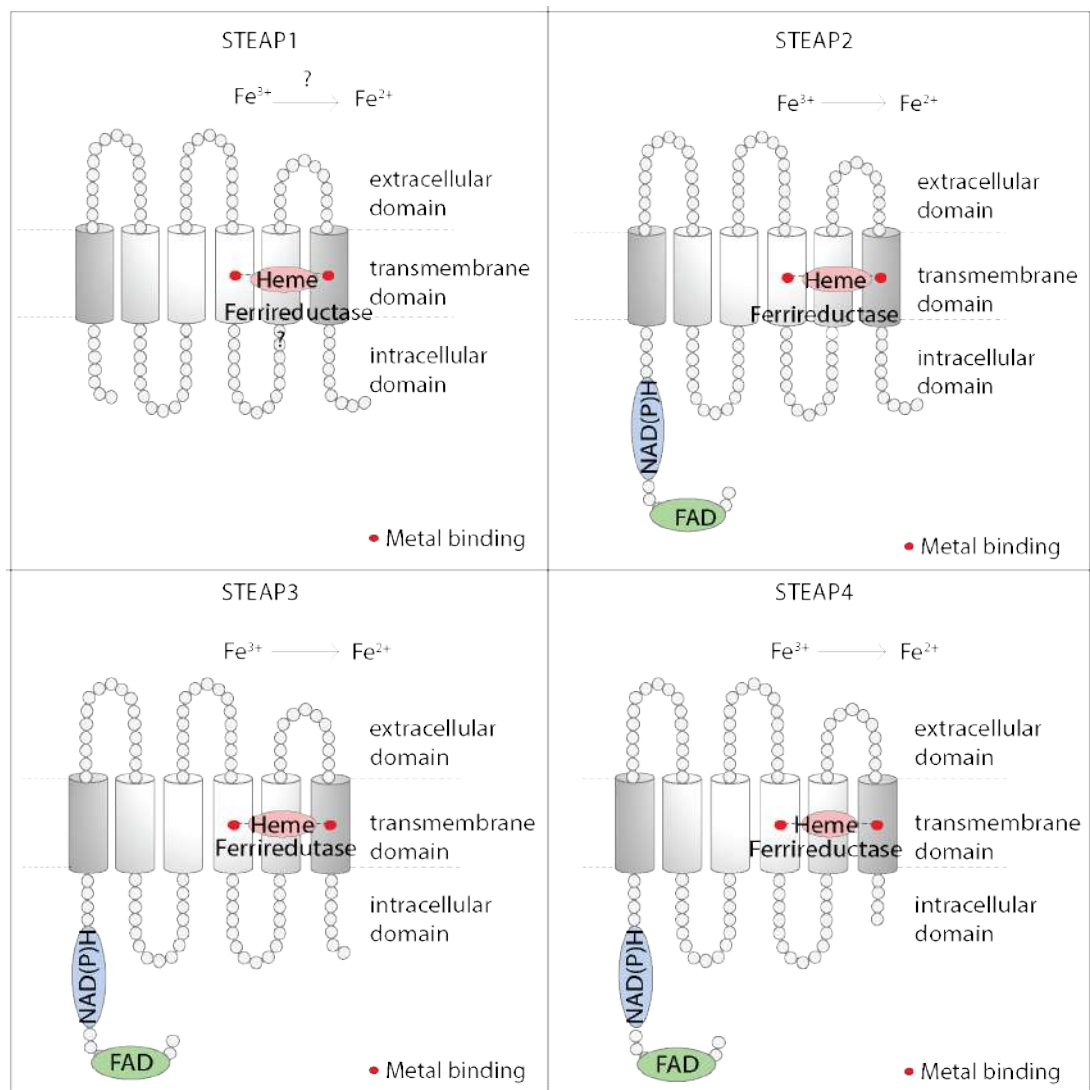


**Figure 1.3 Structural overview of the STEAP family.** The STEAP family of proteins comprises four members: STEAP1, STEAP2, STEAP3 and STEAP4. All STEAP family members comprise six transmembranes and therefore three extracellular loops. A NAD(P)H/FAD domain is located at the N-terminus of STEAP2-4, except STEAP1. STEAP1-4 contain two heme metal binding sites (red dots) where the ferrireductase region is presumably located. The STEAP family of proteins can be categorised into their amino acid (aa) size as follows: STEAP2 (490 aa) < STEAP3 (488 aa) < STEAP4 (459 aa) < STEAP1 (339 aa). Image adapted from (Gauss *et al.*, 2013; Gomes *et al.*, 2012; Grunewald *et al.*, 2012; Sikkeland *et al.*, 2016).

At the N-terminal region, STEAP proteins exhibit structural homology with the archaeal and bacterial F420:NADP<sup>+</sup> oxidoreductase (FNO) binding region, except STEAP1. At their C-terminal region, the STEAP family members contain a yeast homologue ferrireductase domain (FRE). In addition, the Rossman fold, a structural motif for the binding of flavin adenine dinucleotide (FAD) derivatives, is also located at the N-terminal region of the STEAP members (except STEAP1) indicating their potential role in electron transfer (Hubert *et al.*, 1999). Due to the six transmembrane domains, STEAP proteins exhibit structural homology to the eukaryote *NADPH oxidase (NOX)* and bacterial *YedZ* genes, which are both involved in the electron transfer (Ohgami *et al.*, 2006). Moreover, STEAP members contain two conserved histidine residues supposedly for the binding of at least one heme group similar to the *Nox* and *YedZ* genes suggesting their function in the uptake and metabolism of iron and copper (Ohgami *et al.*, 2005; Von Rozycki *et al.*, 2004). The presence of six transmembrane domains containing two distinct histidine residues has been associated with apoptosis and cancer in the past. Therefore, researchers referred to this domain as so called apoptosis, cancer, redox-associated transmembrane proteins (ACRATA) (Sanchez-Pulido *et al.*, 2004). STEAP proteins are found at the plasma membrane and the Golgi apparatus suggesting their potential involvement as receptors and in protein sorting (Hasegawa *et al.*, 2018; Hubert *et al.*, 1999; Korkmaz *et al.*, 2002). In addition, the STEAP2-4 family members co-localise with the Transferrin Receptor1 (TfR1) and the Dimetal Transporter1 (DMT1) in the early endosomes (Lane *et al.*, 2015; Vela, 2018). TfR1 allows the cellular uptake of ferric iron into the endosomes, where it is thought to be reduced by STEAP2-4 to ferrous iron and transported into the cytoplasm via the DMT1, indicating their activity in iron or copper metabolism (Lane *et al.*, 2015; Vela, 2018).

In terms of protein sequence homology, the STEAP family of proteins share some protein sequence identity with STEAP2 (which this thesis focuses on). STEAP3 shares the highest homology to STEAP2, with approximately 52% identical protein sequence. STEAP4 shares the second highest protein sequence similarity with

STEAP2 with approximately 42% identical protein sequence. STEAP1 shares the least protein sequence homology with STEAP2 with approximately 33% identical protein sequence (**Figure 1.4**; for detailed protein sequence alignment between each of the STEAP family of protein members with STEAP2 see Appendix **Figure A1.1 – A1.3**)

Q9UHE8	STEAP1_HUMAN	1	-----	0
Q8NFT2	STEAP2_HUMAN	1	MESISMMSGSPKLSLSETPLPN-----GINGKDKARKVTVGVIKSGDFAKSITRLRLRCGY	54
Q658P3	STEAP3_HUMAN	1	-----MPEEMDKPLISLHLVSDSSSLAKVPDEAPKVGILGSDGFARSLATRLVSGSF	52
Q687X5	STEAP4_HUMAN	1	-----MEKTCI-----DALPLTMNSSEKQETVCIFGTGDGFGRLGLKMLQCGY	43
Q9UHE8	STEAP1_HUMAN	1	-----	0
Q8NFT2	STEAP2_HUMAN	55	HVVIGSRNPKFASEFFPHVVDVTHHEDALTKTNIIFVAIHREHYTSLWDLRHLVKGKILI	114
Q658P3	STEAP3_HUMAN	53	KVVVGSRNPKRTARLFPSSAAQVTFQEEAVSSPEVIFVAVFREHYSSLCSLSDQLACKIIV	112
Q687X5	STEAP4_HUMAN	44	SVVFGSRNPKQTT-LLPSGAEVLSYSEAAKSGIIIIAIREHYDFLTELTEVLNGKILV	102
Q9UHE8	STEAP1_HUMAN	1	-----MERR-----KDIHQEELWKKMPPRN-LEEDDYHKDTG	33
Q8NFT2	STEAP2_HUMAN	115	DVSNMNRIN--QYPPSNAEYLASLFPDSLIVKGFNVVSAWALQGLPKDASRQVYICS---	169
Q658P3	STEAP3_HUMAN	113	DVSNPTEQEHLOHRESNAEYLASLFPDCTVVKAFNVLSAWTQAGPRDGNRCVFCG---	169
Q687X5	STEAP4_HUMAN	103	DISNNLKIN--QYPPSNAEYLAHLVPGAHVVKAFNTISAWALQSGALDASRQVFCG---	157
Q9UHE8	STEAP1_HUMAN	34	ETSMLKRPVLL-----HEHOTAHAEDEDCP-SELQHTQRELEPWHLEIKIAAIASLTFL	87
Q8NFT2	STEAP2_HUMAN	170	NNIQARQQVIELARQLNEIPID-LGSLSSAREIENLPLRFLTLRCPVVAIVASLATFPFL	228
Q658P3	STEAP3_HUMAN	170	DQPEAKRAMSEMALAMGEMVVD-MGSLASAWVEAMPLRLPAWVPTLLALGLFVCFYA	228
Q687X5	STEAP4_HUMAN	158	NDSKAKORVMDIVRNGLTQPMD-QGSLMAAKEIEKYPLQEEPMWRFFEYLSAVLCVLFLEF	216
Q9UHE8	STEAP1_HUMAN	88	YTLIREVHHELATSHQQYFKKIPILVINKVLPVSIHLEALVYLPVIAIVQHNSTRY	147
Q8NFT2	STEAP2_HUMAN	229	YSFVRDVIHEYARNQOQDFYKIPLEIVNKTLDIVAIHLESLVYLAGLAAAYQIYGTKY	288
Q658P3	STEAP3_HUMAN	229	YNFVRDVLQPYVQESONKFKPLPVSIVNTTLCVAYVLESVYLPVIAAALQIRGTKY	288
Q687X5	STEAP4_HUMAN	217	YCVIRDVIYFYVEKKNTRFMATSPNRIFHITALHLEALVYLPVIAAALQIRGTKY	276
Q9UHE8	STEAP1_HUMAN	148	KKPEHNLKDWMLTRKQFGLLSEFFVLAHAIYSLSYEMRERSYKLLNWAYOOVQNKEDA	207
Q8NFT2	STEAP2_HUMAN	289	RRPEPWLLETWLCRRKQGLLSEFFAMVHVAVSLCLPMRSEYVLELNWAYOOVHANIENS	348
Q658P3	STEAP3_HUMAN	289	QRPEPWLDEHLLQHRKQIGLLSEFFCALHALYSEFCLERRAHYDVLNVAVKVLANKSHL	348
Q687X5	STEAP4_HUMAN	277	RRPEPWLDEHMLCRKQIGLVALGFVFLVLYLVIPRIYVYVWRGCLNLTVCAILKKNP	336
Q9UHE8	STEAP1_HUMAN	208	WIEHDVWRMEIIVSLGLVGLAIALLAVTSIPSVSDSLTWRREFFHIQSKLGIIVSLLECI	267
Q8NFT2	STEAP2_HUMAN	349	WNEEEVWRIMETISFGIMSLGLLAVTSIPSVSNALNWRREFFSIQSLGLYVALLISF	408
Q658P3	STEAP3_HUMAN	349	WVEEEVWRMEIIVSLGLVALGTLVSLAVTSIPSVANSNLNWRREFFSVQSSGLFVALVLSL	408
Q687X5	STEAP4_HUMAN	337	FSTSSAWLSDSVVALGILGFLVLLGITSIPSVSNAVNWRREFFVQSKGLYLLTLLCA	396
Q9UHE8	STEAP1_HUMAN	268	HALIFAWNHWIDIKQFVWYTEPTEMLAVFLIVVLIKFSLLFLPCLRKILKIRHGVEDV	327
Q8NFT2	STEAP2_HUMAN	409	HVLIYGWKRAFEEYRYRTEPNFVLAIVLSEIVLIGKIIILFLPCISKRLKIKKQWKS	468
Q658P3	STEAP3_HUMAN	409	HTLTYGWTRAFEEERYRYTEPTEMLAVFLIVVLIKFSLLFLPCLRKILKIRHGVEDV	468
Q687X5	STEAP4_HUMAN	397	HTLVYGGKRFVSPNLRWVLAAYVLLGIIIECTVLIKFLVIMPQVDNLTTRIQGWERN	456

**Figure 1.4 BLAST protein sequence alignment of the STEAP protein family members.** Protein sequences of the STEAP family members (STEAP1 – 4) are displayed as amino acid sequences. Dark grey (highlighted with asterisk): identical amino acids; moderate grey (highlighted with colon): not identical but similar amino acid sequence; light grey: not identical but similar amino acid sequence but less than moderate grey.

Due to the different tissue expression patterns of the STEAP family, it is predicted that each STEAP protein exhibits a distinct, physiological function and their overexpression is linked to cancer, metabolic and inflammatory diseases (Grunewald *et al.*, 2012).

### 1.4.1 STEAP1

The first member of the STEAP family, STEAP1, was discovered in 1999 as a cell surface protein (Hubert *et al.*, 1999). The STEAP1 gene is located on the chromosome 7q21.13 and codes for a 339 amino acid (aa) long protein with a predicted molecular weight of 39.8 kDa. STEAP1 contains two histidine residues on the transmembrane domains 5 and 6, which are predicted to function for the heme binding for electron transfer (Grunewald *et al.*, 2012; Hubert *et al.*, 1999; Sikkeland *et al.*, 2016). In addition, STEAP1 is present at the plasma membrane and endosomes where it co-localises with TfR1 indicating its potential role in iron metabolism. Unlike other STEAP proteins, STEAP1 lacks the FNO-like domain as well as the Rossman motif for the transfer of electrons transfer (Grunewald *et al.*, 2012; Hubert *et al.*, 1999; Sikkeland *et al.*, 2016). Biophysical characterisation of STEAP1 has implied STEAP1 assembles as a homotrimer or heterotrimer with two STEAP2 proteins, in order to exhibit metalloredox activity (Poget *et al.*, 2016). In healthy tissues, the expression of STEAP1 is low, but elevated levels were found at the cell-cell junctions in normal as well as prostate cancer epithelial cells *in-situ* (Challita-Eid *et al.*, 2007; Moreaux *et al.*, 2012; Yamamoto *et al.*, 2013). In addition, STEAP1 was shown to control intracellular communication between prostate cancer and cancer-associated stromal cells important for prostate cancer progression by mediating small, yet unknown molecules (Yamamoto *et al.*, 2013). Further, a monoclonal anti-STEAP1 Ab has been demonstrated to block these intracellular communications *in-vitro* and in prostate cancer xenograft models *in-vivo* (Challita-Eid *et al.*, 2007). Elevated STEAP1 protein levels correlated with an increase in Gleason Scores of malignant prostate cancer tissues and prostatic intraepithelial neoplasia lesions (PIN) *in-situ* when compared to BPH and normal prostate tissues specimens (Burnell *et al.*, 2019; Gomes *et al.*, 2012). Thus, STEAP1 has been put forward as a potential biomarker using immunohistochemistry to discriminate between BPH and PIN versus prostate cancer (Gomes *et al.*, 2012). However, STEAP1 lacks the specificity to distinguish between PIN and prostate cancer *in-situ* (Gomes *et al.*, 2014). There was no

correlation between STEAP1 and other surrogate markers for prostate cancer progression such as PSA levels, age or metastasis (Gomes *et al.*, 2012). Aside from prostate cancer, STEAP1 is significantly overexpressed in 10 other cancer types including breast, bladder, colon, lung, ovarian and Ewing sarcoma (Chen *et al.*, 2019; Grunewald *et al.*, 2012; Hubert *et al.*, 1999; Moreaux *et al.*, 2012). The overexpression of STEAP1 is associated with elevated ROS levels, which were linked to a more aggressive (invasive) phenotype of Ewing sarcoma *in-vitro* as well as in xenograft models *in-vivo* (Grunewald *et al.*, 2012). Knock-down studies of STEAP1 demonstrated a reduction in cell proliferation, invasion and in the colony formation assay. Thus, STEAP1 has been suggested to increase intracellular ROS levels, which regulate pro-invasive genes to drive cancer progression (Grunewald *et al.*, 2012). Moreover, high STEAP1 expression was associated with a poor overall survival in colorectal cancer, large B-cell lymphoma, acute myeloid leukaemia and multiple lymphoma (Moreaux *et al.*, 2012). Together, the data suggests that STEAP1 represents a potential drug target for a variety of solid tumours.

#### **1.4.2 STEAP2**

STEAP2 or Six Transmembrane Protein of Prostate1 (STAMP1) is the second member of the STEAP family and was discovered simultaneously by two independent research groups (Korkmaz *et al.*, 2002; Porkka *et al.*, 2002). Like *STEAP1*, the *STEAP2* gene is located on chromosome 7q21.13 and encodes for a 490 aa long protein with an estimated molecular weight of 56.1 kDa, which represents the canonical isoform1. Fluorescence microscopy analysis has revealed STEAP2 is a cell-surface protein by labelling with Green-Fluorescent Protein (GFP), due to its predominant location at the plasma membrane (Porkka *et al.*, 2002). Time-lapse imaging of GFP-STEAP2 in COS-1 cells has shown STEAP2 shuttles to the Golgi organelle, trans-Golgi network (TGN) suggesting it is involved in protein sorting and secretory pathways (Korkmaz *et al.*, 2002).

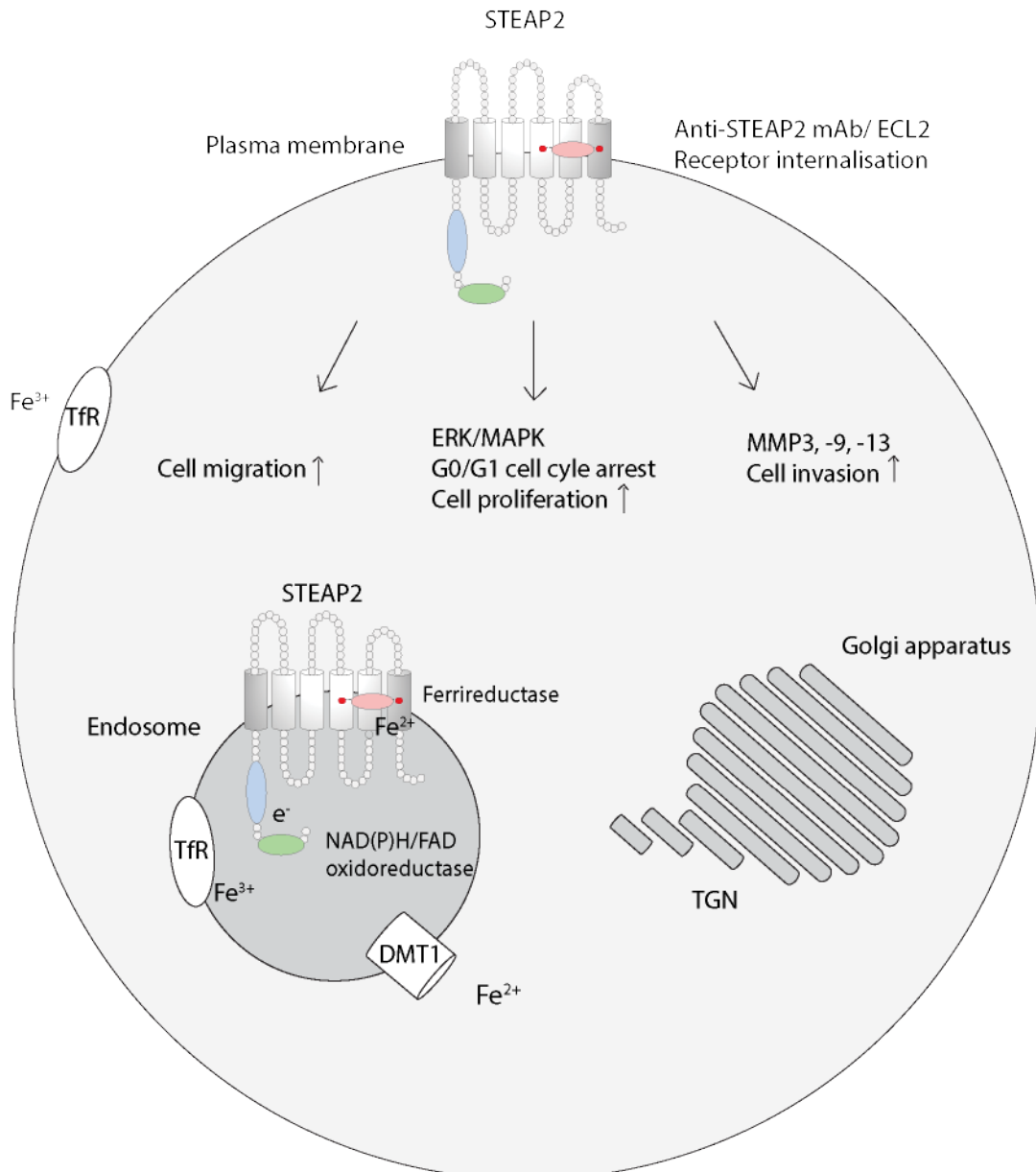


**Figure 1.5 Cellular localisation and function of the STEAP2 protein**

. STEAP2 is predominantly located to the plasma membrane, the Golgi apparatus and the Trans-Golgi Network (TGN) where it is thought to partake in the secretory processing. Antibody targeting of the extracellular loop2 (ECL2) of STEAP2 results in receptor internalisation presumably to the endosomes. The transferrin-receptor (TfR) is known to uptake Fe<sup>3+</sup> and shuttles to the endosomes, where it co-localises with STEAP2. In the endosomes, STEAP2 is presumably exhibits oxidoreductase activity by its NAD(P)H/FAD domain and uses free electrons for its ferrireductase activity to reduce Fe<sup>3+</sup> to Fe<sup>2+</sup>. Reduced Fe<sup>2+</sup> is then transported out of the endosomes into the cytoplasm via the dimetal-transporter1 (DMT1). Overexpressed STEAP2 protein increases cell proliferation via the ERK/MAPK signalling pathway and results in more aggressive cancer phenotypic traits such as cell migration and invasion in-vitro (Figure adapted by Gomes *et al.*, 2012).

In addition, STEAP2 resides in the early endosomes, where it co-localises with the early endosome antigen (EEA) and potentially with TfR1 and DMT1 indicating its

activity in iron or copper metabolism. Given its six transmembrane helices, STEAP2 possesses three extracellular domains (Grunewald *et al.*, 2012). Further, receptor internalisation of STEAP2 using a monoclonal anti-STEAP2 Ab against an epitope on its extracellular loop 2 (ECL2) to the endosomes was shown to be membrane cholesterol-dependent in STEAP2-transfected COS1 cells (Hasegawa *et al.*, 2018). STEAP2 is expressed in significantly lower levels in healthy compared to cancerous prostate specimen tissues (Burnell *et al.*, 2018; Korkmaz *et al.*, 2002). Past research has reported, that the mRNA expression of STEAP2 is androgen-dependent, which requires further validation (Korkmaz *et al.*, 2002). *In-vitro*, STEAP2 protein levels are low in the normal prostate epithelial cell line PNT2 and the prostate confined cancer cell line CA-HPV10 and higher in the advanced, androgen-independent bone metastatic prostate epithelial cell line PC3 and the brain metastatic prostate epithelial cell line DU145 (Burnell *et al.*, 2018; Korkmaz *et al.*, 2002; Whiteland *et al.*, 2014). The highest STEAP2 expression levels were found in the androgen-sensitive lymph node metastatic prostate cancer cell line LNCaP (Burnell *et al.*, 2018; Korkmaz *et al.*, 2002; Porkka *et al.*, 2002; Whiteland *et al.*, 2014). Transfection of PNT2 cells with STEAP2 resulted in a more aggressive PNT2 phenotype with increased invasive properties such as migration and invasion (Whiteland *et al.*, 2014). Conversely, siRNA knock-down of *STEAP2* in PC3 cells led to a reduction in cancer cell migration, invasion and proliferation indicating the role of *STEAP2* in prostate cancer progression (Burnell *et al.*, 2018). In addition, *STEAP2* was identified as survival factor in LNCaP cells as gene knock-down resulted in a reduction in cell proliferation by causing a cell cycle arrest in G0/G1 likely to be mediated via the ERK/MAPK pathway (Wang *et al.*, 2010). The matrix metalloproteases *MMP3*, *MMP9*, the chemokine *IL8* and the *CD82* receptor were identified as genes, which are regulated by *STEAP2* expression (Burnell *et al.*, 2018). A high STEAP2 expression has been shown to drive cancer invasive traits, such as cell invasion (presumably by MMP3, -9 and -13) and migration in PC3 cells (Burnell *et al.*, 2018). *In-silico* analysis of the *STEAP2* gene has shown the presence of 42 non-synonymous Single Nucleotide Polymorphisms (nsSNPs) (Naveed *et al.*, 2016). nsSNP have been hypothesised to

contribute to upregulation of STEAP2 to overcome the malfunctional STEAP2 protein, which may be associated with prostate cancer progression (Naveed *et al.*, 2016). Based on the distinct expression of STEAP2 in advanced prostate cancer cell lines, its overexpression in prostate cancer but not in healthy tissues, STEAP2 represents not only a potential diagnostic biomarker but also an immunotherapeutic drug target for the treatment of advanced prostate cancer (Burnell *et al.*, 2019, 2018; Whiteland *et al.*, 2014). However, further studies are required to determine the effects of an anti-STEAP2 targeted therapeutic on prostate cancer progression *in-vitro* and *in-vivo*.

### 1.4.3 STEAP3

Unlike the rest of the STEAP family members, STEAP3 is located on the chromosome2q14.2. It encodes for a protein with a predicted length of 488 aa and an approximate molecular weight of 54.6 kDa. Alternative names for STEAP3 are the Tumour-Suppressor Apoptosis Protein 6 (TSAP6), dudlin 2 and STAMP3. In rat, *pHyde* was found to be a homologues gene to the human STEAP3 (Zhang *et al.*, 2012). Confocal imaging showed that STEAP3 co-localises with Tfr1 and DMT1 in the endosomes, is present in the Trans-Golgi Network (TGN) and in the endoplasmic reticulum (Amzallag *et al.*, 2004; Gomes *et al.*, 2012; Lespagnol *et al.*, 2008; Ohgami *et al.*, 2005). STEAP3 has been shown to be crucial in the maturation of erythroid cells, the regulation of iron homeostasis and is important for the innate immunity. STEAP3 was found to be highly expressed in the hematopoietic tissues such as the foetal liver, adult bone marrow, placenta and pancreas in embryonic and adult mouse tissues *in-situ* in comparison to low levels in other normal tissues (Gomes *et al.*, 2012; Grunewald *et al.*, 2012; Ohgami *et al.*, 2005). *STEAP3* *-/-* null mice demonstrated, that *STEAP3* is crucial for erythroid maturation as its deficiency resulted in hypochromic anaemia (Ohgami *et al.*, 2005). In 3 human siblings, a heterozygote, non-sense mutation in the *STEAP3* gene led to an anaemic phenotype (Grandchamp *et al.*, 2011). In addition, STEAP3 co-localises with the Tfr1 and DMT1 in the

endosomes and possesses ferrireductase activity; it is therefore proposed to contribute to iron metabolism (Ohgami *et al.*, 2005). *STEAP3* deficient -/- null mice stimulation with Lipopolysaccharides (LPS) led to the accumulation of iron and impaired iron sequestration demonstrated by lower cytosolic iron levels (Zhang *et al.*, 2012). Named as a Tumour-Suppressor Apoptosis Protein 6 (TSAP6), STEAP3 contains a response element in the promotor region for the tumour suppressor protein53 (TP53/p53) (Passer *et al.*, 2003). Therefore, *STEAP3* was hypothesised to partake in cell apoptosis as a downstream signalling gene of p53 (Passer *et al.*, 2003). Knock-down of *STEAP3* by siRNA approaches led to an impaired p53-dependent cell apoptosis *in vitro*. The *Nix* gene, a pro-apoptotic Bcl2 family member, was identified as one binding partner of STEAP3 that induces apoptosis in the mitochondria (Passer *et al.*, 2003). Moreover, STEAP3 associates with the Myt1 kinase, which negatively controls the G2/M Phase of the cell cycle (Passer *et al.*, 2003). However, increased protein levels of STEAP3 were shown to be associated with the disease progression of glioblastoma and high grade serous carcinoma indicating it as a potential prognostic biomarker (Channah *et al.*, 2017; Han *et al.*, 2018).

#### 1.4.4 STEAP4

STEAP4 is the fourth member of the STEAP family and is also known as STAMP2. The gene is situated on chromosome 7q21.12 and is predicted to code for a 459 aa long protein with an approximate molecular weight of 52.0 kDa. STEAP4 is localised at the plasma membrane, the early endosomes, Golgi, the Trans-Golgi Network (TGN), the vesicular tubule structures and the mitochondria (Korkmaz *et al.*, 2005; Xue *et al.*, 2017). The protein is also found in a variety of normal tissues such as the adipose or hepatic tissues (Gomes *et al.*, 2012; Grunewald *et al.*, 2012; Scarl *et al.*, 2018). STEAP4 is considered to partake in iron metabolism and to be responsible for inflammatory as well as metabolic disease (Scarl *et al.*, 2018; Xue *et al.*, 2017). It is alternatively called after its murine homologue the Tumour-Necrosis Factor $\alpha$  Induced Adipose-Related Protein (*TIARP*), which regulates adipogenesis via

TNF $\alpha$ , IL6 and IL1 $\beta$ . Gene knock-down of *STEAP4* was associated with an increased insulin resistance and hyperglycaemia suggesting impaired metabolic regulation that contributes to obesity *in-vitro* and *in-vivo* in both mice and humans (Arner *et al.*, 2008; Kim *et al.*, 2015; Qin *et al.*, 2010; Wellen *et al.*, 2008). *STEAP4* has been identified as a mitochondrial ferrireductase important for iron homeostasis (Xue *et al.*, 2017). When dysregulated, elevated *STEAP4* protein levels contributed to increased iron levels in the mitochondria leading to increased ROS production, colitis and colitis-associated colon cancer (CAC) *in-vivo*, which are major risk factors for developing colorectal cancer (CRC) (Xue *et al.*, 2017). Excessive mitochondrial iron levels were reverted by the addition of iron chelators suggesting *STEAP4* as a potential drug target for CRC (Xue *et al.*, 2017). Moreover, *STEAP4* is considered to be a negative regulator of inflammatory rheumatoid arthritis (RA) *in-vitro* supposedly via a negative regulation of IL6 expression (Qin *et al.*, 2010; Tanaka *et al.*, 2012). *STEAP4* also appears to play a role in prostate cancer as its protein expression was upregulated and correlated with the aggressiveness of human prostate cancer specimens (Jin *et al.*, 2015). High *STEAP4* expression is significantly correlated with prostate cancer relapse indicating patients with higher *STEAP4* expression were more likely to suffer from prostate cancer reoccurrence than patients with low or moderate *STEAP4* levels (Burnell *et al.*, 2019). The finding indicates the potential of *STEAP4* to be used as a prognostic biomarker for prostate cancer reoccurrence (Burnell *et al.*, 2019).

#### **1.4.5 The STEAP family as therapeutic targets**

The *STEAP* family members represent therapeutic drug targets in the future to treat various types of cancer and inflammatory diseases. The distinct overexpression of the *STEAP* proteins in cancerous tissues and their cell surface location makes them promising drug targets with the potential for the application of Ab therapeutics (Grunewald *et al.*, 2012; Ohgami *et al.*, 2006; Sikkeland *et al.*, 2016). One study has demonstrated the therapeutic value of a monoclonal Ab (mAb) against

STEAP1, that resulted in the inhibition of prostate tumour growth *in-vivo* (Challita-Eid *et al.*, 2007). Another study, conducted by Genentech, has developed Antibody-Drug Conjugates (ADCs) against STEAP1, to maximise the Ab efficacy (Boswell *et al.*, 2011). In addition, STEAP2 represents a potential drug target to treat advanced prostate cancer due to its increased expression in high grade Gleason Score prostate cancer specimens but not in normal prostate tissues (Burnell *et al.*, 2018). A patent application was recently filed by Regeneron Pharmaceuticals, which demonstrated the efficiency of STEAP2-targeted mAbs and anti-STEAP2 ADCs in reducing the tumour size in a prostate cancer xenograft mouse model (Patent Application WO-2018058001-A1, 2018). However, the effects of how an anti-STEAP2 mAb modulates the cancer invasive traits such as cell migration and invasion in prostate cancer *in-vitro* remains to be evaluated.

## 1.5 Antibodies and their use as therapeutics

### 1.5.1 Antibody structure

Antibodies are immunoglobulins, which are available in a variety of different formats. The majority of the antibodies found in clinical practice are of the immunoglobulin type IgG format and are of monoclonality as they originate from the same parent cell clone (Grilo, 2019) (**Figure 1.6**).

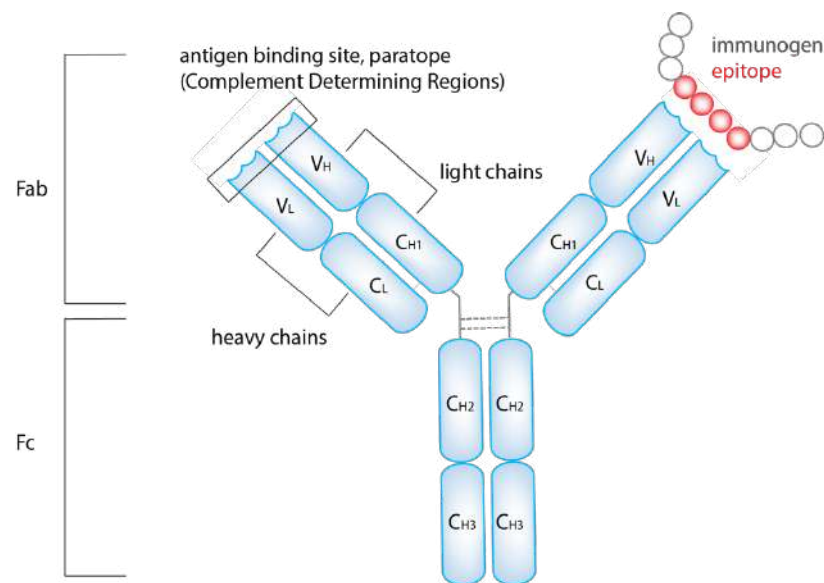


**Figure 1.6 Immunoglobulin G (IgG) Ab structure.** Fab: antigen fragment binding regions; Fc: constant fragment region; <sub>H</sub> and <sub>L</sub>: heavy chain and light chain peptides; V<sub>H</sub> and V<sub>L</sub>: variable heavy and light chain domains; C<sub>H1</sub>, C<sub>H2</sub>, C<sub>H3</sub> and C<sub>L</sub> constant heavy chain and light chain domains. CDR: Complement Determining Regions where the paratope of the Ab binds to the epitope (red) of an immunogen.

Immunoglobulin types originate as result of the immune response to different kinds of immunogen (antigen) exposures (e.g. reaction to specific antigens on allergens). The IgG Ab is „Y-shaped“ and can be distinguished between the constant fragment (Fc-region) and two „arms“ of the antigen-binding fragment (Fab-region) (**Figure 1.6**). As the names suggest, constant regions (C) are consistent in the IgG type, whilst the interaction between the Ab and the host pathogen takes place at the variable domains (V) (**Figure 1.6**). Pathogen exposures triggers the generation of antibodies with unique, variable regions specific to the immunogen regions (antigens) of the pathogen. Immunogens are peptide regions (peptide sequences), which the body

is not familiar with and may cause the body to elicit antibodies as an immune response to fight these pathogens. Immunogens are often interchangeably called antigens (Nelson, 2010; Parren *et al.*, 2017; Schroeder & Cavacini, 2010; Tonegawa *et al.*, 1974). Short immunogen regions with less than 10 aa are also known as epitopes. Here, the variable domains contain the antigen-binding fragments (**Figure 1.6**). Due to the high specificity, development of antibodies as drugs is therefore highly popular through the identification of a disease-specific immunogen, which is targeted against disease-related proteins, that have extracellular domains or “loops” (ECLs) (Gashaw *et al.*, 2012; Grant, 2002; Shih, 2012; Weiner, 2015).

### 1.5.2 Therapeutic antibodies

Ab-based therapeutics have revolutionised cancer treatment over the last two decades (Ryman & Meibohm, 2017). Currently, there are about 80 Food and Drug Administration (FDA) and European Medicines Agency (EMA) approved therapeutic monoclonal antibodies (mAbs) for oncology applications (Carter & Lazar, 2018). mAbs exhibit a high target specificity resulting in fewer side-effects compared to traditional therapies (e.g. chemotherapy) and are used to treat cancer, autoimmune, inflammatory and neurodegenerative diseases. The drug targets of mAbs are mostly overexpressed, disease-associated cell surface receptors (Ducry & Stump, 2010). Depending on the drug target, mAbs exert their therapeutic potential by effecting downstream signalling pathways linked to cell growth, blocking cancer metastasis, cytokines or receptors, that promote angiogenesis or neutralise inflammatory cytokines (Carter & Lazar, 2018; Ducry & Stump, 2010). One blockbuster is Bevacizumab (Avastin®), which targets the Vascular Endothelial Growth Factor (VEGF) molecule, inhibits angiogenesis and is used to treat advanced staged breast, cervix, colon, cervix, lung, kidney and ovarian cancers (Ecker *et al.*, 2015; Grilo, 2019). Another mAb blockbuster, Trastuzumab (Herceptin®), targets the Human Epidermal Growth Receptor2+ (HER2+), which inhibits cell proliferation and is employed in breast cancer patients where HER2+ is overexpressed (Ecker *et al.*, 2015; Grilo, 2019;

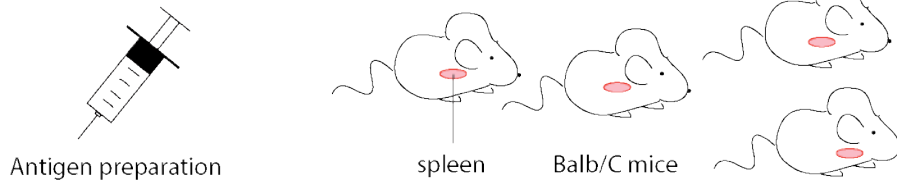
Hudis, 2007). Etanercept (Enbrel®) targets the Tumour-Necrosis Factor $\alpha$  to reduce inflammation, that causes rheumatoid arthritis (Ecker *et al.*, 2015; Grilo, 2019).

### 1.5.3 Monoclonal antibody production (hybridoma technology)

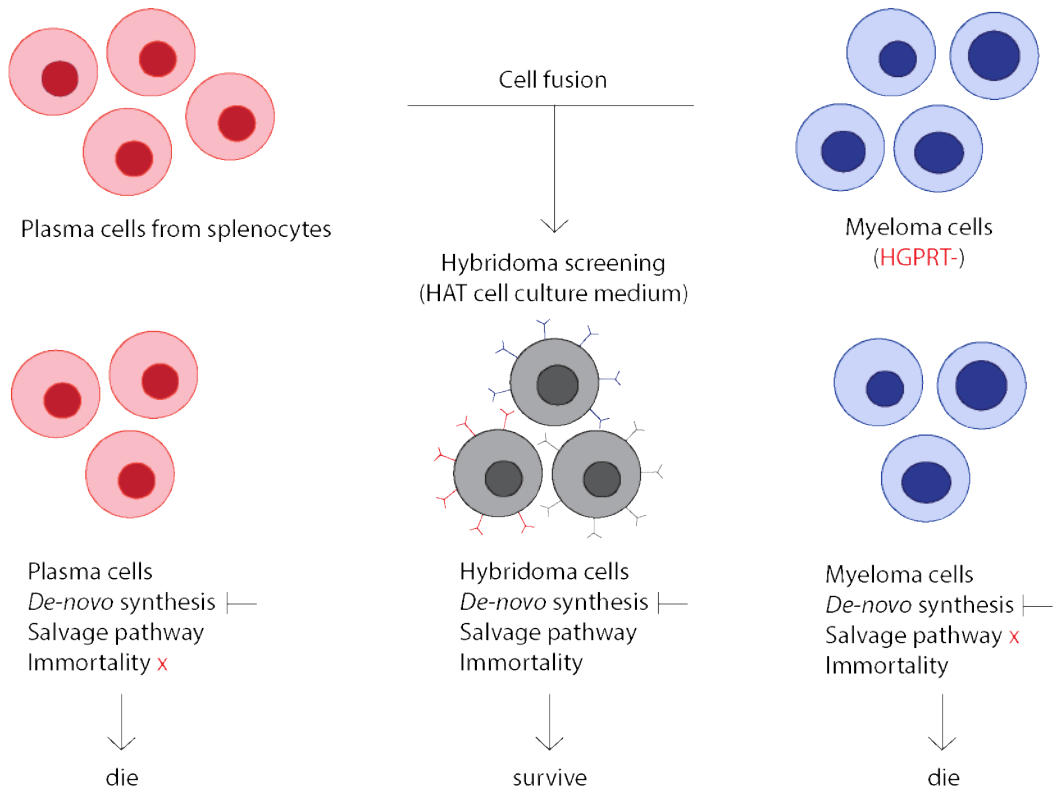
The hybridoma technology dates back to 1975 and was established by Köhler and Milstein. It is the oldest method, which is based on the initial use of host species, typically Balb/C mice, for the generation mAbs (Köhler & Milstein, 1975). The four main stages of the hybridoma mAb development are illustrated in **Figure 1.7**. Prior to Phase I (Immunisation), the antigen (or peptide) is chemically synthesised and then formulated as a vaccine. Balb/C mice are immunised with the antigen (or peptide) of interest, which activates the plasma B-lymphocytes (plasma B-cells) to elicit antibodies against the specific antigen (Pohanka *et al.*, 2016). After Phase I, the splenocytes, containing the plasma B-cells, are harvested and prepared for Phase II. During Phase II, the plasma B-cells are fused with mouse myeloma cells and the successful fusion will yield in the production of hybrid cells (hybridoma cells), that grow in colonies containing the genome of both the plasma B-cells and the myeloma cells. The characteristics of the hybridoma cells are indefinite cell growth inherited from the myeloma cells and the ability to produce antigen-specific antibodies, inherited from the plasma B-cells (Köhler & Milstein, 1975). Mammalian cells can synthesise nucleotides required for replication by either the *de-novo* pathway or the salvage pathway (Greenfield, 2012; Holzlöhner & Hanack, 2017; Pandey, 2010). During the *de-novo* pathway nucleotides are synthesised from scratch, whereas the salvage pathway recycles purine bases and precursors (*e.g.* thymidine and hypoxanthine) to build the nucleotides (Greenfield, 2012; Pandey, 2010). Aminopterin is a drug that inhibits the dihydrofolate-reductase (DHF), which is required for the *de-novo* synthesis (Greenfield, 2012; Pandey, 2010). The Hypoxanthine-Guanine-Phosphoribosyl transferase (HGPTR) is an enzyme, which mammalian cells require to metabolise the purine nucleotide precursors hypoxanthine and thymidine (Greenfield, 2012; Pandey, 2010). For the hybridoma development (Phase II),

HGPTR -deficient myeloma cells are utilised. As the myeloma cell lack HGPTR, they are forced to use the *de-novo* pathway for replication. In contrast, the HGPTR enzyme in B-plasma cells is intact, thus the B-plasma cells can employ both pathways for DNA synthesis. By culturing the cells in a special Hypoxanthine, Thymidine and Aminopterin (HAT) cell culture medium, unfused myeloma cells are unable to replicate because aminopterin inhibits the *de-novo* pathway (Greenfield, 2012; Holzlohner & Hanack, 2017). Unfused plasma and hybridoma cells are able to replicate by using the salvage pathway. However, unlike the myeloma and hybridoma cells, the plasma cell is not immortal and will thus soon die off (Greenfield, 2012; Holzlohner & Hanack, 2017). In Phase III (Limiting Dilution), the hybridoma cell colonies are separated by applying a serial dilution to yield one, single hybridoma cell per well, which are screened by the Enzyme-Linked Immunosorbent Assay (ELISA) for their antigen specificity and affinity (Greenfield, 2012; Holzlohner & Hanack, 2017). Each of the positive hybridoma cells produces and secretes one unique type of mAb against the antigen of interest, which is present in the cell culture supernatant (Greenfield, 2012; Holzlohner & Hanack, 2017; Page & Thorpe, 2009; Pandey, 2010; Tomita & Tsumoto, 2011). During Phase IV (Scale-up), the single hybridoma cells are expanded (cloned) in cell culture from typically 96-/24-well plates to T25 culture flasks and then larger glass roller containers, to obtain large the supernatant of these hybridoma cells, containing the desired mAbs (**Figure 1.7**) (Greenfield, 2012).

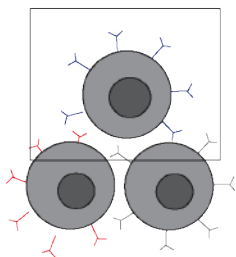
Phase I: Immunisation



Phase II: Hybridoma development



Phase III: Limiting dilution



Phase IV: Scale-up

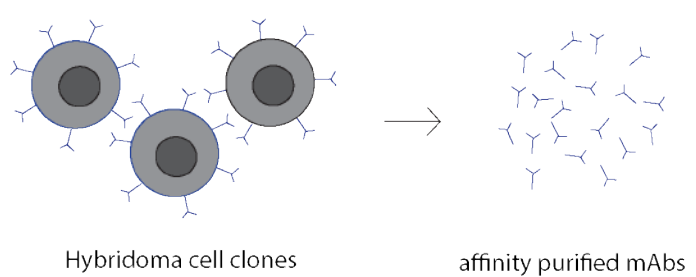


**Figure 1.7 mAb development (hybridoma technology).** HAT: Hypoxanthine-Aminopterin-Thymidine; HGPTR: Hypoxanthine-Guanine-Phosphoribosyl transferase. mAb development can be classified into four stages. Phase I: Balb/C mice are immunised with the antigen of interest to elicit an immune response. Phase II: The splenocytes of the mice is fused with mouse myeloma cells to generate hybridoma cells. Positive hybridoma cells are screened using the HAT selective medium but grow in hybridoma colonies. Phase III: The hybridoma colonies are separated to yield single hybridoma cell clones by a serial dilution. Phase IV: Cell culture expansion of the hybridoma cells to obtain the mAbs.

Hybridoma technology is a powerful and the well-established method for the development of mAbs (Greenfield, 2012; Holzlöhner & Hanack, 2017; Tomita & Tsumoto, 2011; Westerwoudt, 1987). However, one major drawback of the hybridoma technology is the time it takes (approximately 6 - 12 months) to produce the desired antibodies, since animal handling is required for the *in-vivo* purposed immunisation followed by extensive cell culture work (Greenfield, 2012). Further, the success of the mAb production by the hybridoma technology depends on the utilised species, the selected antigen for immunisation, the animals' health and immune response (Greenfield, 2012). Another disadvantage of the hybridoma technology is, that it yields approximately from as little as 5 to 100 positive hybridoma cell clones (Greenfield, 2012). In addition, the produced mAbs require later humanisation, if indicated for the therapeutic use in humans, since they originate from different host species. The advantage of using the hybridoma technology is, that an actual immune response is triggered to produce antibodies including post-translational modifications, which reduce the risk of the Ab failure to detect the desired antigen (Dreyer *et al.*, 2010). Thus, it is considered as the traditional method for the production of mAbs due to its successful use, which generated approximately 80 therapeutic mAbs to date (Kaplun & Reichert, 2018; Sewell *et al.*, 2017).

## 1.6 Antibody-Drug Conjugates

### 1.6.1 ADC structure

An evolving drug class for cancer treatment are Antibody-Drug Conjugates (ADCs). ADCs combine the specificity of the mAb to a tumour-associated cell surface antigen to deliver a highly potent, chemically attached cytotoxin to the cancer cells explicitly while sparing healthy cells (Carter & Senter, 2013). The general structure of an ADC is displayed in **Figure 1.8**. To date, seven ADCs have been approved by the FDA for oncology applications which are summarised below (see **Table 1.3**)

**Table 1.3 Overview of the ADCs currently on the market.** The seven commercially available ADCs were categorised into their names, trade name, drug target, payload and clinical indication. R/R: relapsed or refractory; AML: Acute Myeloid Leukemia; KL: Hodgkin Lymphoma; HER2: Human Epidermal Growth Factor Receptor2; mBC: metastatic Breast Cancer; ALL: Acute Lymphoblastic Leukemia; DLBL: Diffused Large Cell Lymphoma; mUC: Metastatic Urethelial Cancer.

	Trade name	Drug target	Payload	Indication
Gemtuzumab-Ozogamicin	Mylotarg®	CD33	Ozogamicin	AML
Brentuximab-Vedotin	Adcetris®	CD30	MMAE	R/R HL
Ado-Trastuzumab-Emtansine	Kadcyla®	HER2	DM1	HER2+ mBC
Inotuzumab-Ozogamicin	Besponsa®	CD22	Ozogamicin	R/R B-cell precursor ALL
Polatuzumab-Vedotin	Polivy®	CD79b	MMAE	R/R DLBL
Erfortumab-Vedotin	Padcev®	Neotin4	MMAE	mUC
Trastuzumab deruxtecan	Enhertu®	HER2	Deruxtecan	Unresectable HER2+ mBC

For instance, Gemtuzumab Ozogamycin (Mylotarg®) was the first commercial ADC in 2000 but was initially withdrawn to due side-effects (Jen *et al.*, 2018). However, it was reintroduced to the market in 2017 with lowered doses to treat Acute Lymphocytic Leukaemia (Jen *et al.*, 2018). Further, the FDA granted approval in 2011 for Brentuximab Vedotin (Adcetris®), which is used to combat Hodgkin lymphoma and anaplastic large-cell lymphoma, for instance (Gravanis *et al.*, 2016).

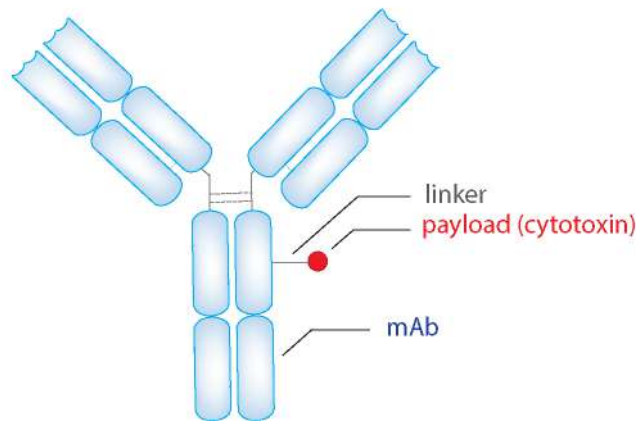


**Figure 1.8 Antibody-Drug Conjugate structure.** A payload is attached via a chemical linker to the monoclonal Ab (mAb). Payloads: drugs which are cytotoxic drugs *e.g.* microtubule inhibitors which cause cancer cell death.

### 1.6.2 ADC receptor internalisation

Receptor internalisation is a cellular process, that allows substrates, hormones or proteins to be taken up by the cells (Christian *et al.*, 2014; Kaksonen & Roux, 2018). After substrate binding to specific cell surface receptors, the plasma membrane buds, in order to form vesicles, that transport the „cargo“ (Christian *et al.*, 2014; Kaksonen & Roux, 2018). Ligand binding to the receptor causes allosteric, conformational change of the receptor by which intracellular adaptor proteins and clathrin proteins are recruited to form the clathrin-coated pits (CCP) (Christian *et al.*, 2014; Popova *et al.*, 2013). These CCP cleave off the plasma membrane by fission proteins such as dynamin to yield the cargo vesicles (Christian *et al.*, 2014; Kaksonen & Roux, 2018; Popova *et al.*, 2013). The clathrin-coated vesicles then uncoats and fuses with the endosome organelle for sorting or recycling the cargo (Christian *et al.*, 2014; Kaksonen & Roux, 2018; Popova *et al.*, 2013). Alternatively, the cargo can be shuttled via the endosomes to the lysosomes, where lysosomal degradation takes places for signal termination (Christian *et al.*, 2014; Popova *et al.*, 2013). The lysosome functions as a waste system and contains an acidic pH (4 - 5), which is maintained by Na<sup>+</sup>/K<sup>+</sup>-ATPases (Hu *et al.*, 2015; Xu & Ren, 2015). Cargo degradation relies on the activity of specific enzymes such as the hydrolase Cathepsin-

B, while other lysosomal enzymes metabolise glycogen into glucose (e.g.  $\alpha$ -glucosidase)(Guha & Padh, 2008; Linke *et al.*, 2002).

The ability of the Ab to bind to a certain tumour-associated antigen (*e.g.* overexpressed receptor) on the cell surface combined with the process of receptor internalisation sets the premise of tumour-cell specific drug delivery by ADCs. Upon binding of the Ab to the cell surface receptor, the ADC-receptor complex is taken up by the cell by the process of receptor internalisation and further shuttles via the endosomes to the lysosomes. Due to the acidic pH in the lysosomal organelle, the ADC-receptor complex is then being degraded into the free Ab, linker and payload. Thereby, lysosomal degradation releases the payload of the ADC into the cytoplasm, where it unleashes its cytotoxic effect (**Figure 1.9**) (Carter & Senter, 2013; Wu & Senter, 2005).

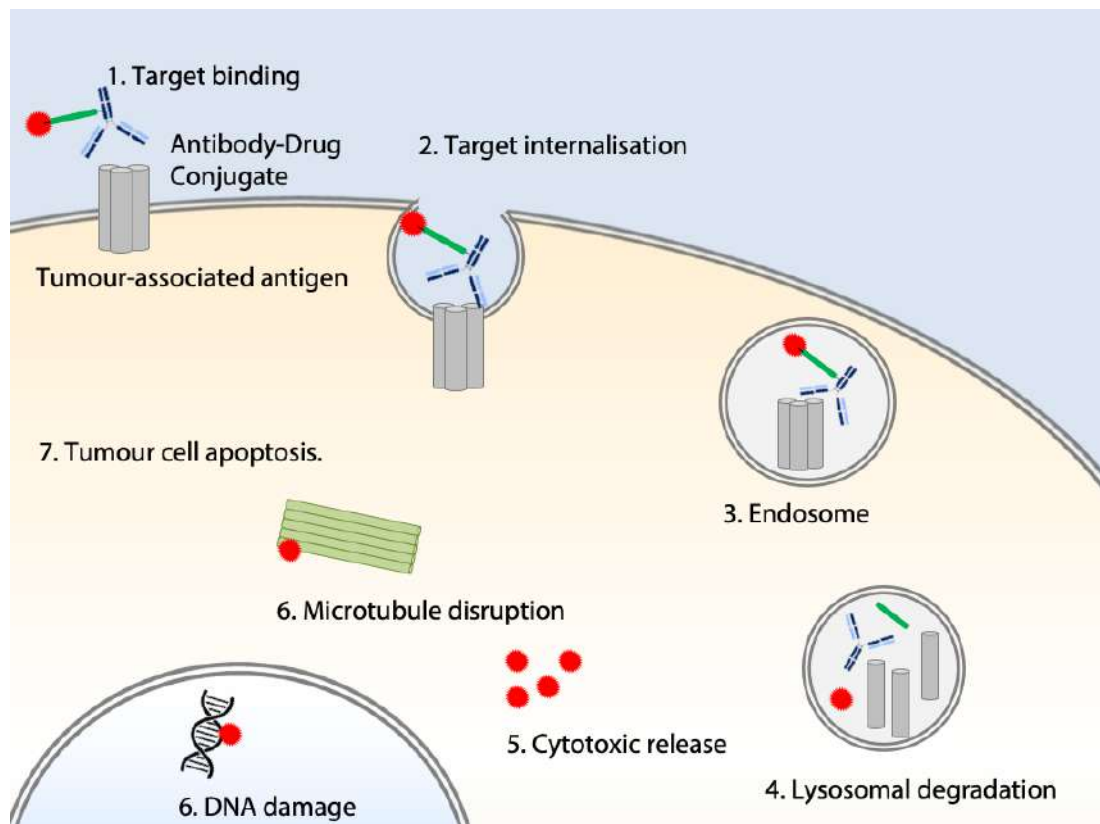


**Figure 1.9 ADC receptor internalisation.** Upon target-binding, the ADC triggers receptor internalisation, shuttles via the endosomes to the lysosomes for the ADC degradation and the cytotoxin release leading to cell apoptosis.

Researchers have exploited the Cathepsin-B-dependent lysosomal degradation for the design of cathepsin-sensitive linkers present in two of the current ADCs for the specific lysosomal release of the cytotoxin (Staudacher & Brown, 2017). Based on this concept, the cytotoxin is released after lysosomal degradation of the ADC, diffuses via the lysosomal plasma membrane to the cytoplasm where it then disrupts the microtubule polymerisation and causes cell death (**Figure 1.9**) (Gravanis *et al.*, 2016).

### 1.6.2.1 ADC linker

The current linkers used for the ADC technology can be classified into cleavable or non-cleavable linkers. Cleavable linkers are sensitive to acidic hydrolases and contain a hydrazine structure. Further, there are protease-sensitive linkers, possessing a disulfide bond that is sensitive to cleavage. The only FDA approved lysosomal proteases sensitive linker (*e.g.* Cathepsin-B) is the dipeptide Valine-Citrulline (VC) (**Figure 1.10**) (Dosio *et al.*, 2011; Jain *et al.*, 2015; Kratz *et al.*, 2011). The VC linker is used in combination with an attachment group (*i.e.* maleimidocaproyl) for Ab linkage. Further, a self-eliminating para-aminobenzyloxycarbonyl (PABC) spacer between the dipeptide VC and the hydroxyaza group of the cytotoxin is incorporated in the VC for the self-immolate cleavage of the PABC, which releases the cytotoxin (**Figure 1.10**) (Kratz *et al.*, 2011).

Non-cleavable linkers, in contrast, require full lysosomal catabolism to degrade the ADC. For instance, a non-cleavable, succinimidyl 4-(N-maleimidomethyl)cyclohexane-1-carboxylate (SMCC) linker is used in the ADC Trastuzumab-Emtansine (Kadcyla®), which is based on a thioether structure making the ADC highly stable in the blood circulation (Verma *et al.*, 2012). An overview of the chemical structure of the linkers used in the present, commercial ADCs is shown in **Figure 1.10** (Dosio *et al.*, 2011; Jain *et al.*, 2015; Kratz *et al.*, 2011).

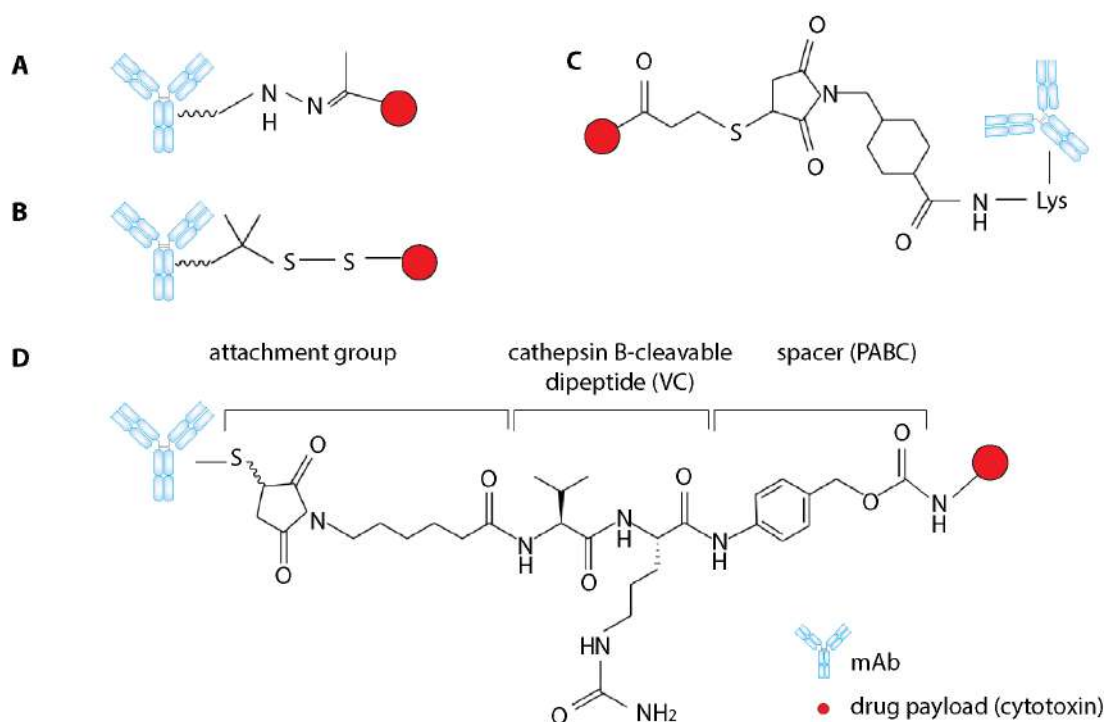


**Figure 1.10 Linkers used in commercial ADCs.** A) Hydrazone linker. B) Disulfide linker. C) thioether linker, 4-(S-maleimidomethyl) cyclohexane-1-carboxylate (SMCC). D) Dipeptide linker, Valine-Citrulline (VC) with self-immolative para-aminobenzyloxycarbonyl (PABC) spacer.

### 1.6.2.2 ADC payloads

ADC payloads are up to 1000-fold more potent than conventional chemotherapeutics, thus they cannot be administered directly as free drug. (Ducry & Stump, 2010). Cytotoxins can act via a number of different modes of action (**Table 1.4**). Maytansinoids (*e.g.* in Trastuzumab Emtansine, Trastuzumab-DM1) are DNA damaging agents. Calicheamicins cause DNA scissions like Ozogamicin (*e.g.* Gemtuzumab Ozogamicin). Others, like Monomethylauristatins act as microtubule inhibitors to induce cell death (*e.g.* Brentuximab Vedotin and Polatuzumab Vedotin, see (**Figure 1.11** and **Table 1.4**) (Jen *et al.*, 2018; Nejadmoghaddam *et al.*, 2019). Currently, DNA intercalators such as Anthracyclines (*e.g.* Doxorubicin) and other DNA damaging agents like Pyrrolobenzodiazepines are under investigation (Dan *et al.*, 2018).

**Table 1.4 Overview of the current payloads used in the commercial ADCs.** Four payload classes (with payload example) are currently in clinical application as ADC warhead and exert their cytotoxic effect by different mode of actions.

Payload class	Payload example	Mode of action
Calicheamicin	Ozogamicin (e.g. Mylotarg®)	Binding of the DNA minor leads to DNA scission
Maytansinoides	Emtansine (e.g. Kadcyla®)	Inhibition of tubulin polymerisation blocks cell division
Dolastins	Monomethylauristatin-E (MMAE) (e.g. Adcetris®)	Inhibition of tubulin polymerisation blocks cell division
Camptothectine-derivates	Deruxtecan (e.g. Enhertu®)	DNA strand breaks by topoisomerase inhibition

Therapeutic antibodies are expected to hold great promise as future medicines to treat cancer, autoimmune and neurogenerative diseases (Lopes dos Santos *et al.*, 2018). The majority of approved mAbs suggest the traditional IgG Ab class will continue to represent the most favoured Ab format (Lopes dos Santos *et al.*, 2018).

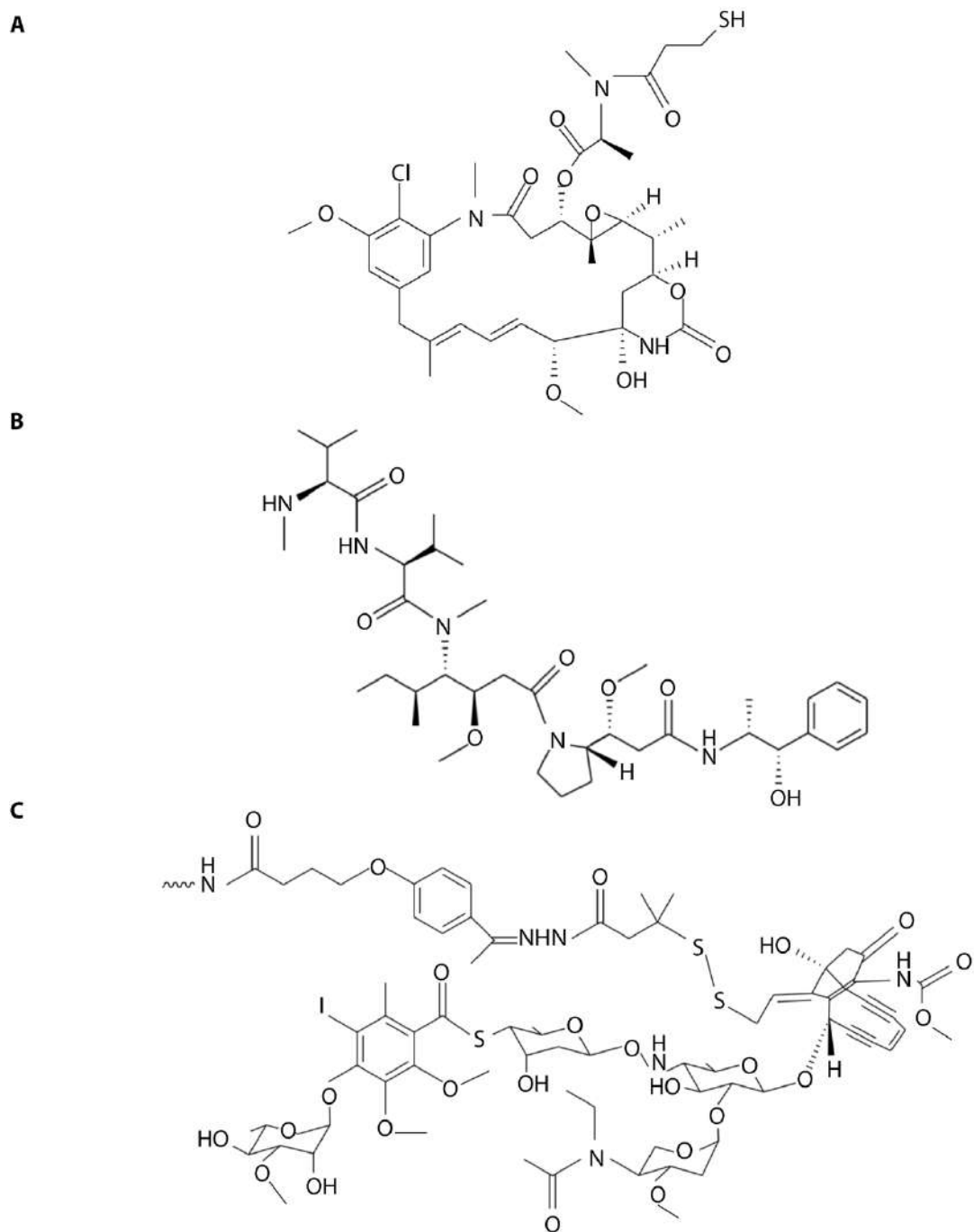


**Figure 1.11 Payloads used in commercial ADCs.** A) Emtansine (DM1), a Maytansine drug. B) Monomethylauristatin-E (MMAE), an Auristatin drug. C) Ozogamicin, a Calicheamicin drug.

## 1.7 Thesis aims

---

Current therapies to treat advanced prostate cancer are accompanied with serious side-effects and compromise patients' quality of life. Thus, more patient-tailored medicines are urgently required to improve their clinical management. STEAP2 is highly expressed in advanced prostate cancer but not in the normal prostate. Elevated STEAP2 protein expression *in-vitro* is significantly linked to an increase in cancer invasive traits, such as cell migration and invasion, associated with prostate cancer progression and correlates with increasing Gleason Scores in patient tissues. Thus, STEAP2 holds the potential as a molecular drug target for Ab-based medicines for the treatment of advanced prostate cancer.

The aim of this thesis was therefore to determine, if STEAP2 qualifies as a viable drug target, specifically focusing on its application as a therapeutic Ab (Ab) and Ab-Drug Conjugate (ADC). Thus, the objectives were to:

- (1) Determine the normal tissue expression profile of STEAP2;
- (2) Identify targetable regions on the extracellular loops (ECLs) of STEAP2 for the application of therapeutic antibodies;
- (3) Select one Ab lead candidate by Ab-STEAP2/ECL mapping, western blotting and confocal microscopy analysis, in order to:
  - (a) The effect of the anti-STEAP2 Ab lead candidate on cancer invasive traits (e.g. cell migration, invasion and viability), and
  - (b) STEAP2 receptor internalisation to assess its suitability for the ADC technology;
- (4) Provide proof-of-concept of STEAP2 as a drug target by studying
  - (a) The effect of the anti-STEAP2 Ab lead candidate on cancer invasive traits (e.g. cell migration, invasion and viability), and
  - (b) STEAP2 receptor internalisation to assess its suitability for the ADC technology;
- (5) Use one identified region on STEAP2 as an antigen for the hybridoma technology-based anti-STEAP2 mAb development, followed by characterisation for their STEAP2-specificity by ELISA, western blotting and confocal microscopy.

## 2 Material and Methods

### 2.1 Material

#### 2.1.1 Reagents

The reagents displayed in **Table 2.1** were used throughout this thesis.

**Table 2.1 Reagents used throughout this thesis.** DAPI: 4'-6' Diamidino-2-Phenylindole; DMEM: Dulbecco's Modified Eagle Medium; MTT: 3-(4,5-Dimethyl-2thiazoyl)-2,5-diphenyl-2H-tetrazolium bromide; TEMED: N, N, N', N' Tetramethylethylenediamine; RPMI-1640: Roswell Memorial Park Medium-1640; SDS: Sodium-Dodecylsulfate; TRIS-base: Tris(hydroxymethyl)aminomethane.

Reagents	Supplier and catalogue number
Acetic acid, glacial (37%)	Sigmaaldrich, UK, #A6283
Acrylamide/ Bis Solution 19:1 (30%)	BioRad, UK, #1610154
Agarose	Sigmaaldrich, UK, #A6013
Ammonium persulfate (APS)	Sigmaaldrich, UK, #A3678
Bovine serum albumin (BSA)	Sigmaaldrich, UK, #A2153
Chemiluminescence reagent (ECL)	BioRad, UK, #170-5060
DAPI-Vectashield	Vectorlabs, UK, #I36933
DMEM, phenolred-free	Life Technologies, UK, #21063029
Fetal bovine serum	Life Technologies, UK, #10271
Formaldehyde, ultra-pure (16%)	Polysciences, USA, #18814-20
Glutamine	Life Technologies, UK, #25030-024
Glycine	Melford, UK, #G36050
Hoechst	Thermofisher, UK, #62249
Image-IT FX Signal Enhancer	Thermofisher, UK, #I26933
Laemmli buffer	Sigmaaldrich, UK, #38733
Monomethylauristatin-E (10mM, 1mL DMSO)	MedChemExpress, Sweden, #HY-15162
MTT	Sigmaaldrich, UK, #T9281
RIPA buffer	Thermofisher, UK, #10017003
Sodium chloride	Sigmaaldrich, UK, #S9888
Sodium bicarbonate	Sigmaaldrich, UK, #S5761
SDS	Sigmaaldrich, UK, #74255
Stripping buffer	Thermofisher, UK, #46430
pHAb Amine Reactive Dye	Promega, UK, #G9845
Phosphate-buffered saline	Life Technologies, UK, #10010023
Propium Iodide	Thermofisher, UK, #P1340MP
RPMI-1640	Life Technologies, UK, #31870025
TEMED	Sigmaaldrich, UK, #T9281
TRIS-base	Melford, UK, #T60040
Triton-X 100	Thermofisher, UK, #T8787
Trypsin-EDTA	Life Technologies, UK, #25300-062
Tween20	Sigmaaldrich, UK, #P1379

### 2.1.2 Material

The reagents displayed in **Table 2.2** were used throughout this thesis.

**Table 2.2** Material used throughout this thesis.

Material	Supplier and catalogue number
Fibre pads	BioRad, UK, #1703922EDU
Filter paper	BioRad, UK, #1702932
Flask, T25	VWR, USA, #82051-070
Flask, T75	VWR, USA, #82050-854
Invasion assay	Merck Millipore, UK, #ECM551
Mini Protean Glass Plates, short	BioRad, UK, #165331
Mini Protean Outer Glass Plates	BioRad, UK, #1651824
Migration culture inserts (2-well)	Ibidi, Germany, #80209
Polyvinylidene fluoride membrane	BioRad, UK, #162-0177
Power Pac300	BioRad, UK, #164-5050
12-well plate	VWR, USA, #82050-928
24-well plate	VWR, USA, #734-2325
96-well plate	VWR, USA, #10861-666
$\mu$ -angiogenesis slides	Ibidi, Germany, #81506
$\mu$ -slide 8-well chambered slides	Ibidi, Germany, #80826

### 2.1.3 Equipment

The equipment used throughout this thesis are displayed in **Table 2.3**

**Table 2.3** Equipment used throughout this thesis.

Equipment	Supplier, model number
Benchtop centrifuge	VWR, USA, Himac CT6E
Cell culture inverted microscope	ZEISS, Germany, AxioCamERC55
Cell culture incubator	MarshallScientific, USA, NU-5510
Centrifuge	ThermoTec, UK, Centra CL3R
Confocal microscope	ZEISS, Germany, LSM710
Laminar airflow	VRW, USA, Scanlaf MRs
Liquid nitrogen container	Thermofisher, UK, Locator JR Plus
Nanodrop spectrophotometer	Thermofisher Scientific, UK, ND-1000
Olympus microscope	Olympus, UK, BX51TF
Plate reader	BMG Labtech, UK, POLARstar
Sonicator	FisherScientific, USA, FB15046
Water bath	Grant, UK, SUB Aqua 18
Western blotting imaging machine	BioRad, UK, ChemiDoc XRS+

### 2.1.4 Buffers and solutions

Buffers used throughout this thesis are displayed in **Table 2.4**.

**Table 2.4 Buffers and solutions.** APS: Ammonium persulfate; BSA: Bovine Serum Albumin; MTT: 3-(4,5-Dimethyl-2thiazoyl)-2,5-diphenyl-2H-tetrazolium bromide, NaCl: Sodium chloride; SDS: Sodium-Dodecylsulfate; PBS: Phosphate-buffered Saline; PFA: Paraformaldehyde, TRIS-base : tris(hydroxymethyl)aminomethane.

TRIS/ Glycine/ SDS 10x	Transfer buffer
30.03 g TRIS-base	100 ml of TRIS/ Glycine/ SDS 10x
144.1. g Glycine	200 ml of methanol
100 ml of 10% SDS	ddH <sub>2</sub> O to 1 L
ddH <sub>2</sub> O to 1 L	Stored at 4°C
TRIS/ Glycine/ SDS 1x	Blocking buffer (5%)
100 ml of TRIS/ Glycine/ SDS 10x	5.0 g BSA
ddH <sub>2</sub> O to 1 L	100 ml of TBST
Stored at 4°C	Stored at 4°C, 0.22 µm filtered
TRIS-buffered saline (TBS) 10x	Blocking buffer (3%)
24.0 g TRIS-base	3.0 g BSA
88.0 g NaCl	100 ml of TBST
ddH <sub>2</sub> O to 1L, stored at 4°C, pH 7.6	Stored at 4°C, 0.22 µm filtered
1.5 M TRIS	TRIS-buffered saline Tween20 1x
45.4 g TRIS-base	100 mL of TBS 10x
ddH <sub>2</sub> O to 250 ml	ddH <sub>2</sub> O to 1 L and 1ml of Tween 20
pH 8.8	Stored at 4°C, pH 7.6
10 % APS	1.0 M TRIS
1 g APS	30.4 g TRIS-base
ddH <sub>2</sub> O to 1 ml	ddH <sub>2</sub> O to 250 ml, pH 6.8
PFA (3.7%)	10 % SDS
9.25 ml of 16% PFA	25.0 g SDS
PBS to 40 ml	ddH <sub>2</sub> O to 250 ml
Stored in aliquots at -20°C	
Triton-X 100 (0.1%)	MTT (5 mg/ml)
0.1 µl of Triton-X 100	1 mg of MTT in 200 ml PBS
PBS to 100 ml	0.22 µm filtered
Stored in aliquots at -20°C	Stored in aliquots at -20°C

### 2.1.5 Cell lines

Three cell lines, normal prostate epithelial cells PNT2, bone metastatic prostate cancer cells PC3 and the human, fibroblast cell line HFF1, were purchased from the American Type Culture Collection (ATCC, USA) (**Figure 2.1**).

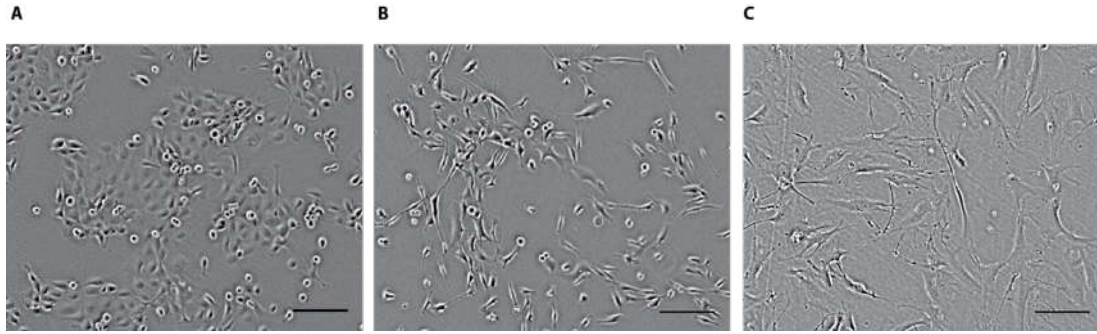


**Figure 2.1** Representatives images of the cell lines used in this thesis. A) Non-cancerous prostate epithelial cells PNT2 was used as a negative control given the low STEAP2 protein expression *in-vitro*. B) Bone metastatic prostate cancer cell line PC3 was used as high expressing STEAP2 positive control cell line; C) Human, normal skin fibroblast cell line HFF1 cell line was used as a negative control given the low STEAP2 protein expression *in-vitro*. Images were acquired with a standard light microscope (AxioCam ERC55, Zeiss, Germany) using a 5x objective. Scale bar = 100  $\mu$ m.

#### 2.1.5.1 PNT2 cell line

Human, normal, epithelial prostate cells (immortalized). Primary cells were obtained from a 33-year old male post-mortem. Cells were sub-cultured in a 1:5 ratio according to the supplier's recommendations in RPMI-1640 supplemented with 10% Fetal Bovine Serum (FBS), 1% Penicillin/ Streptomycin (P/S) and 1% glutamine which were all purchased from Gibco, Life Technologies, UK.

#### 2.1.5.2 PC3 cell line

Human, prostate cancer cells derived from the bone metastatic site originating from a 62-years old male patient with stage 4 prostate cancer. Cells were sub-cultured in a 1:6 ratio according to the supplier's recommendations in RPMI-1640 supplemented with 10% Fetal Bovine Serum (FBS), 1% Penicillin/ Streptomycin (P/S) and 1% glutamine which were all purchased from Gibco, Life Technologies, UK.

#### 2.1.5.3 HFF1 cell line

Human, fibroblast cell line originates from skin cells derived from of a male new-born. Cells were maintained and were sub-cultured according to the supplier's recommendation. Cells were sub-cultured in a 1:10 ratio according to the supplier's

recommendations in DMEM supplemented with 15 % Fetal Bovine Serum (FBS), 1% Penicillin/ Streptomycin (P/S) and 1% glutamine which were all purchased from Gibco, Life Technologies, UK.

## **2.1.6 Cell culture and subculture**

### **2.1.6.1 Monolayer cells (2D)**

Cell culture was conducted in a biological safety cabin with laminar-airflow circulation (Scanlaf Mrs, VWR Internalisation Ltd, UK) to ensure sterility. All items (culture flasks and pipettes, cell culture media, PBS and trypsin) were disinfected with 70% ethanol before use. Cells were grown in an incubator (Nuair™ DHD AUTOFLOW CO<sub>2</sub> Air-Jacketed Incubator) at 37°C/ 5% CO<sub>2</sub>. Cell culture media was obtained from Gibco, Life Technologies, UK. PNT2 and PC3 cells were cultured in Roswell Park Memorial Institute Medium (RPMI 1640 medium, Life Technologies, UK, Cat. 31870025) supplemented with 5% Penicillin/ Streptomycin, 5% glutamine and 10% Fetal Bovine Serum (FBS). The HFF1 cells were cultured in Dulbecco's Modified Eagle Medium (DMEM, Life Technologies, UK, Cat. 10566016) supplemented with 15% FBS, 5% Penicillin/ Streptomycin, 5% glutamine. For microscopical endpoint analysis, cells were cultured in phenol-red free DMEM medium supplemented with 5% Penicillin/ Streptomycin, 5% glutamine and 10% FBS (Life Technologies, UK, Cat. 21063029). Phosphate Buffered Saline (Gibco, Life Technologies, UK, Cat. 10010023) and trypsin-EDTA were pre-warmed prior to use at 37°C in a water bath (SUB Aqua 18, Grant, UK). Briefly, cells were detached by the addition of 3 ml of trypsin and were incubated for 7 min at 37°C in the incubator. Cells were neutralised by the addition of 7 ml of medium, transferred into a 15 ml tube and were spun at 12,000 x g for 3 min using a bench-top centrifuge (VWR, Himac CT6E, UK). Old medium was discarded, cells were resuspended in 10 ml of fresh medium and were split according to the suppliers recommended ratio. Cells were grown to 80% confluency before subculture.

#### **2.1.6.2 Three-dimensional (3D) tumour cell spheroids**

Three-dimensional tumour PC3 cell spheroids were cultured in DMEM phenol red-free medium supplemented with 10% FBS, 5% P/S and 5% glutamine (Life Technologies, UK, Cat. 21063029). Briefly, 10 µl of 1.5% sterile agarose phenol red-free DMEM medium (Sigmaaldrich, UK, Cat. A6013) was added per well of an angiogenesis slide and left to solidify at RT before the addition of 50 µl of 5,000 PC3 cells per well.

#### **2.1.6.3 Cryopreservation**

Cells were cultured in supplemented medium to 80% confluency, following detachment by the addition of 3 ml of trypsin and neutralization by the addition 7 ml of culture medium. Cells were transferred into a 15ml tube and were spun at 12,000 x g for 3 min and old culture medium was then discarded. Cells were resuspended in 3 ml of FBS supplemented with 10% Dimethyl sulfoxide (DMSO) and 1 ml of this cell suspension was added per cryo-preserved vials. These were moved into a cryo-vessel to store at -80°C for 1 day until the cells were transferred to the liquid nitrogen for long-term cryopreservation (Locator JR Plus, Thermofisher Scientific, UK).

#### **2.1.6.4 Determination of cell concentration**

The cell concentration was determined and adjusted by using a hemocytometer. Each hemocytometer contains two big, gridded squares which in turn consist of five smaller, gridded squares. Cells were washed twice in PBS, detached by the addition of 3 ml of trypsin and neutralized by the addition of 7 ml cell culture medium. Cells were centrifuged at 12000 x g for 3 min, old medium was discarded and cells were gently resuspended in 10 ml of fresh medium. From this cell suspension, 10 µl was pipetted onto the hemocytometer via a small notch, covered with a glass slide and transferred to an inverted light microscope (AxioCam ERC55, Zeiss, Germany) to manually count the cells using a cell counter. Each sample was counted once. One square is exemplified

in **Figure 2.2** and consists of 5 additional squares in total of which four corner squares were counted, averaged and further calculated to receive the required cell concentration to prepare for other assays. Only cells touching the top and middle line per corner square were counted.

$$\text{Cell density}_f (\times 10^5 \text{ cells/ml}) \times \text{volume}_f (\text{ml}) / \text{cell density}_i (\times 10^5 \text{ cell/ml})$$

$$= \text{cell suspension (ml)} + [\text{volume}_f (\text{ml}) - \text{cell suspension (ml)}]$$

Where: Cell density<sub>f</sub> = final cell density (x 10<sup>5</sup> cell/ml); Cell density<sub>i</sub> = initial cell density (x 10<sup>5</sup> cell/ml); Volume<sub>f</sub> = final volume (ml)

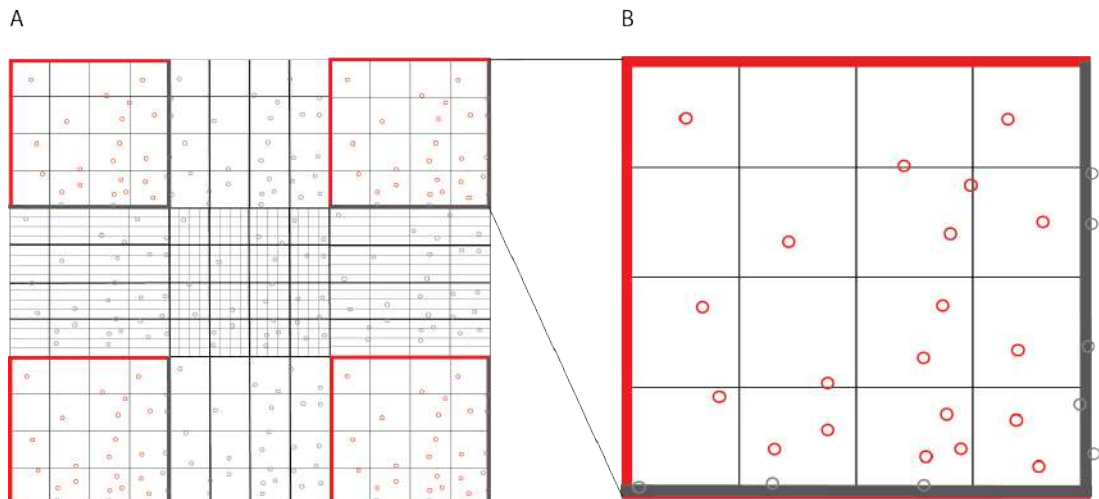


**Figure 2.2 Hemocytometer chamber used for cell counting.** A) Schematic diagram of one chamber on a hemocytometer with 10  $\mu\text{L}$  of cell suspension. The cell number located in four corner squares (thicker strokes) were counted. B) Enlargement of one corner square. Only those cells touching the top and left strokes (red) were scored (red labelled cells).

## 2.2 Methods

### 2.2.1 Immunohistochemistry

To detect STEAP2's expression *in-situ*, immunohistochemistry (IHC) analysis was carried out by the Swansea University Singleton Hospital Histology and Pathology Department. The slides were incubated to enhance the tissue adhesion to the glass. The slides were labelled with a bar code and the IHC staining was conducted using

the automated Ultra VENTANA machine (Roche, Switzerland). The TMA was incubated by EZ prep solution and CC1 (Tris/Borate/EDTA) antigen retrieval buffer (pH 8.0 – 8.5) for 32 min was following the addition of a pre-oxidase inhibitor. The TMA was first incubated with primary rabbit anti-STEAP2 Ab (1:500) (see Table 2.5 Ab3 specific to ECL1) for 36 min (Abcam, UK). The STEAP2 expression was detected using the OptiView DAB IHC Detection Kit (Roche, Switzerland). The secondary anti-IgG HP-linked Ab was added, following the addition of an anti-HQ HRP-linked multimer. The slides were then incubated with 3,3'Diaminobenzidine Tetrahydrochloride (DAB) chromogen substrate and H<sub>2</sub>O<sub>2</sub> following the addition of copper. Nuclei were counterstained with hematoxylin.

### **2.2.2 Structural analysis of the human STEAP2 protein**

Ab targetable extracellular domains were identified using UniProt and SwissProt. Briefly, the amino acid sequence (FASTA format) for the full-length human STEAP2 protein was retrieved from Uniprot (UniProt ID: Q8FNT-2, entry name: HU\_STEAP2, canonical isoform a). Further, structural analysis was conducted to characterise selected peptide regions of interest for their hydrophobicity, structural conservation or similarity to other species, uniqueness, immunogenicity, topology, post-translational modifications, ligand binding sites and single nucleotide polymorphisms using the AbDesigner tool. The protein's FASTA format was used and the following default settings were applied: peptide length = 15 amino acids, epitope length = 7 amino acids.

#### **2.2.2.1 Immunogen region identification by Ab mapping**

A list of commercially available anti-STEAP2 antibodies was manually created. The number of antibodies was narrowed down by selecting those antibodies with known amino acid sequences for immunogen region (amino acid sequence) the antibodies have been raised against only. These immunogen regions were mapped and overlapped

with the previously identified protein's ECLs (**Section 2.2.2**). The overlapping amino acid regions ultimately formed the final, four immunogen regions (Immunogen1 – 4).

### 2.2.2.2 Classification of the immunogen regions into peptide sequences

The identified immunogen regions (Immunogen1 – 4) were divided up into 15 amino acid long peptide sequences according to the default settings of AbDesigner (**Table 2.5**).

**Table 2.5 Commercial anti-STEAP2 pAb candidates.** AB: antibodies; Immun. (aa): amino acid sequence of immunogen; Supplier, Cat.: Supplier catalogue number. Applications recommended by the manufacturer: WB: western blotting; IF: Immunofluorescence microscopy; IHC: Immunohistochemistry; ELISA: Enzyme-Linked Immunosorbent Assay; FC: Flow Cytometry; Concentration: Stock concentration in mg/ml.

AB name	Clonality	Application	Concentration	Immun. (aa)	Supplier, Cat.
Ab1	Polyclonal	WB, IHC, ELISA	0.5	226 – 253	Avivasystems, # OAAB02995
Ab2	Polyclonal	FC, IHC, WB	1.0	226 – 253	LifeSpan Bio, # LS-C161555
Ab3	Polyclonal	FC, IHC, WB	1.0	233 – 262	Abcam, # ab174978
Ab4	Polyclonal	IF, IHC, ELISA	1.0	400 – 480	Avivasystems, # OASG06901

### 2.2.2.3 Peptide sequence analysis by AbDesigner

The identified peptide sequences from **Section 2.2.2.2** were analysed for their conservation (%), similarity (%), uniqueness (%) and immunogenicity (%) based on the AbDesigner tool's data output.

## 2.2.3 Western blotting

### 2.2.3.1 Protein extraction

Cells were grown to 80% confluency, trypsinised and neutralised with RPMI 1640 as described in the **Section 2.1.6.1 and 2.1.6.4** following a centrifugation and resuspension step in fresh RPMI media following the determination of cell concentration. If protein of several technical replicates was to be extracted, the cell concentration was adjusted for each replicate to the one with the lowest cell seeding

density amongst the replicates. Cells were washed twice with ice-cold PBS, spun at 12000 x g for 8 min at 4°C (Centra CL3R, ThermoIEC, Thermo Electron Corporation, USA). Cell pellets were resuspended in 200 µl of ice-cold RIPA buffer (Pierce™ RIPA buffer, Thermofisher Scientific, UK) supplemented with 1% protease-inhibitor cocktail (Sigma Aldrich, UK), transferred to pre-cooled micro-centrifuge tubes and incubated for 10 min on ice. Cells were lysed by a 10 s vortex and centrifuged at 12000 x g for 10 min at 4°C (Centrifuge 5415 R, Eppendorf, UK). Sample supernatants were collected in pre-chilled, fresh micro-centrifuge tubes and stored in 1:1 Laemmli buffer after thorough mixture until ready to use at -80°C.

### 2.2.3.2 Protein quantification

Protein quantification was carried out in a 96-well plate using the Pierce™ BCA Protein Assay Kit (Thermofisher Scientific, UK) according to the manufacturer's instructions with 10 µl of protein per sample in triplicate alongside an albumin standard series (0 – 2,500 µg/ml) outlined in **Figure 2.3**.

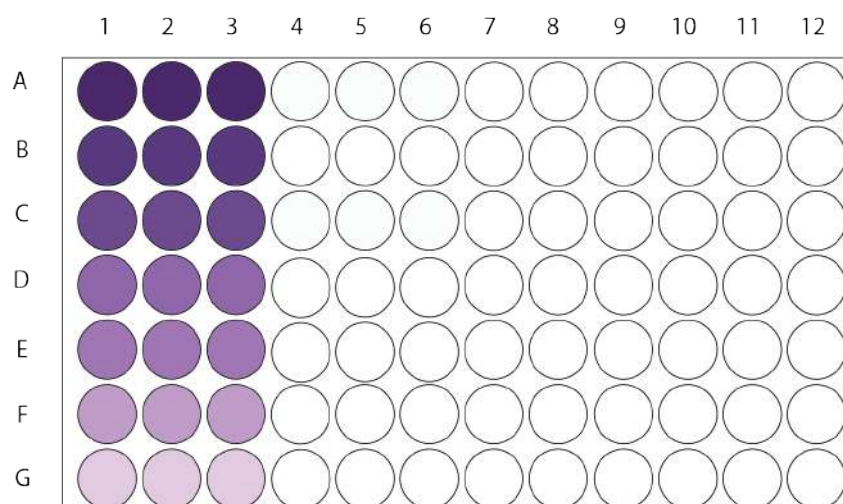


**Figure 2.3 The BCA assay for protein quantification.** A 96-well plate containing the protein standard (albumin) with a known concentration range (0 – 2,500 µg/ml) illustrated in purple. Each standard concentration was loaded in triplicate horizontally from the highest (2,500 µg/ml at A 1 – A 3) to the lowest concentration (0 µg/ml, A 4 – A 6).

The albumin standard was prepared according to the manufacturer's recommendation. Absorbance was measured at  $\lambda = 562$  nm to establish the protein concentration using a fluorescence plate reader (POLARstar, BMG Labtech Ltd., UK). Protein standard curve of known concentration plotted against the measured absorbance for which the mathematical equation ( $y = mx + c$ ) was displayed and used to calculate the sample loading. A line of best fit using the protein standard was created and was accepted with at least  $r^2 \geq 0.95$  to calculate the final protein loading concentration of 30  $\mu\text{g}$  (**Figure 2.3** and **Figure 2.4**).

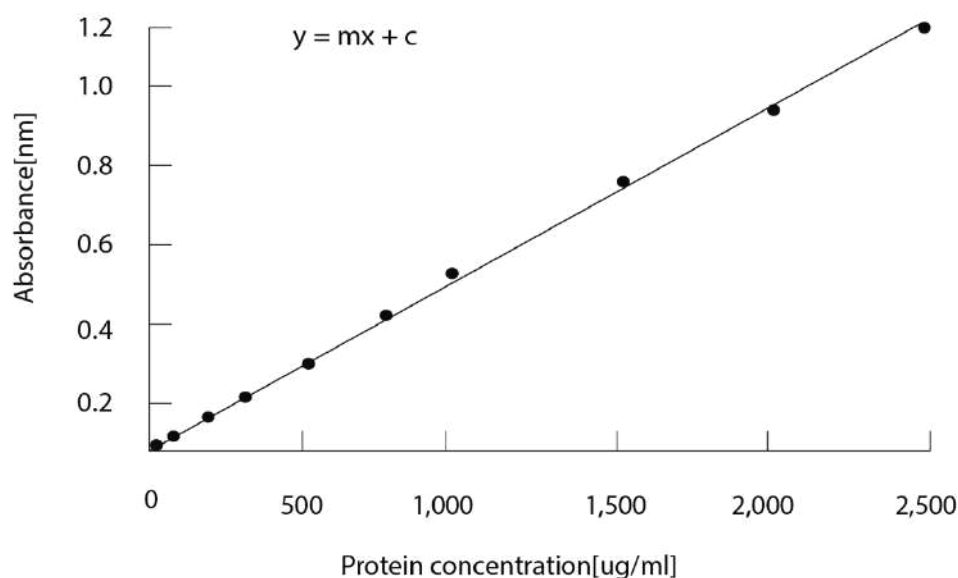


**Figure 2.4 Protein standard curve against the absorbance (nm).** Protein standard curve of known concentration 0 – 2,500  $\mu\text{g}/\text{ml}$  was plotted against the measured absorbance at  $\lambda = 562$  nm for which the equation  $y = mx + c$  was displayed.

### 2.2.3.3 Molecular weight ladders

Two molecular weight ladders were used: a pre-stained ladder; Dual Color Precision Plus Standard (Bio-Rad Laboratories, UK) and an unstained ladder (Biotinylated Detection Pack, Cell Signaling Technologies, UK). The pre-stained ladder (15  $\mu\text{l}$ ) was loaded into well number 1 of the gel. The pre-stained ladder was added into well number 2 (7.5  $\mu\text{l}$ ).

#### 2.2.3.4 Sodium-Dodecylsulfate-Polyacrylamide Gel preparation

Polyacrylamide gel was prepared as illustrated in **Table 2.6**. Glass-plates and well-combs were wiped with 70% ethanol and dried before they were assembled into the cast-stand. First, the resolving gel was added until the bottom of the green line 2 cm below the top of the glass-plates. A 1 cm thick layer of isopropanol was added on top of the resolving gel. After 30 min when the resolving gel has polymerized, the gel was washed with water to remove residual isopropanol. The stacking gel was prepared freshly and added on top of it. Combs were carefully inserted from left to right to avoid bubble formation. The gel was left to polymerise for another 15 min. When required, gels were wrapped in moist blue kitchen roll and cling film foil and stored at 8°C in the fridge prior to use. Gels were used within 3 days of preparation.

**Table 2.6 Gel preparation for the SDS PAGE.** A 10% resolving and 4% stacking gel was prepared. Constituents used for each gel are itemised above components with their respective volume [ $\mu$ l] required to create a 4% stacking or 10% resolving gel for 2 or 4 gels at the same time.

Components	Stacking gel 4% [ $\mu$ l]		Resolving gel 10% [ $\mu$ l]	
	2 gels	4 gels	2 gels	4 gels
30% Acrylamide	150	1,300	5,000	10,000
ddH <sub>2</sub> O	3,000	6,000	6,000	12,000
1.5 M Tris	1,250	-	3,750	7,500
1.0 M Tris	50	2,500	-	-
10% SDS	50	100	150	300
10% APS	25	50	75	150
TEMED	5	10	15	30
Isopropanol	-	-	until top	until top

#### 2.2.3.5 Sodium-Dodecylsulfate-Polyacrylamide Gel-Electrophoresis

Protein was thawed on ice, quickly spun with a bench-top centrifuge, sonicated 3x 10 s at level 2 (Fisher Scientific, FB15046UK), spun again and samples denatured for 5 min (3 min for the biotinylated ladder) at 90°C on a heating block (Techne, USA). The combs were carefully removed from the casted gel before the assembly in the electrophoresis-cassette. The cassette was kept cool in a with ice-filled polystyrene box. Two pairs of glass plate, which were wiped clean with 70% ethanol, were placed into the clip to form the cassette. A buffer damn was added when only one gel was run as a balance. First, the running buffer 1x was slowly added to the cassette middle

to remove all the bubbles trapped in the gel-well followed by the rest of the cassette. Protein sample and the molecular weight ladders were loaded onto the gel. Any empty wells were filled with 10  $\mu$ l of Laemmli buffer only to avoid unequal running of the gel. The SDS-PAGE was run at 120 V for 20 min until the protein samples were stacked to one horizontal line. Once the protein samples have hit the end of the stacking gel, the voltage was increased to 150 V for 150 min.

#### **2.2.3.6 Electro-blotting**

An Immuno-Blot Polyvinylidene Difluoride (PVDF) Membrane for Protein Blotting was manually cut to the required size (Bio-Rad Laboratories, UK). Into a small box, a sufficient amount of 100% methanol was filled and the PVDF membrane activated prior to protein transfer. To do so, the box was placed onto a platform shaker and gently agitated for 5 min (Innova 2100, New Brunswick Scientific, UK). In the meantime, two fibre pads per gel and two Mini Trans-Blot filter paper, were transferred into a small box containing pre-chilled transfer buffer and were left at 4°C to equilibrate prior to the transfer (Bio-Rad Laboratories, UK). The membrane was incubated in a separate box containing transfer buffer. The box was cleaned with 70% ethanol beforehand. The transfer cassette, glass-plate opener and a tweezer were wiped with 70% ethanol. The transfer cassette was then assembled as illustrated (**Figure 2.5**). Before closing the cassette, a roller was used to remove all bubbles formed and the cassette was placed in the polystyrene box. After the SDS-PAGE, the gel was quickly placed into pre-chilled 1x TBST to cool down for 10 s immediately before setting up the transfer cassette. The protein transfer was carried out at 400 mA for 100 min at 4°C (Powerpack Basic<sup>TM</sup>, Bio-Rad Laboratories, UK).

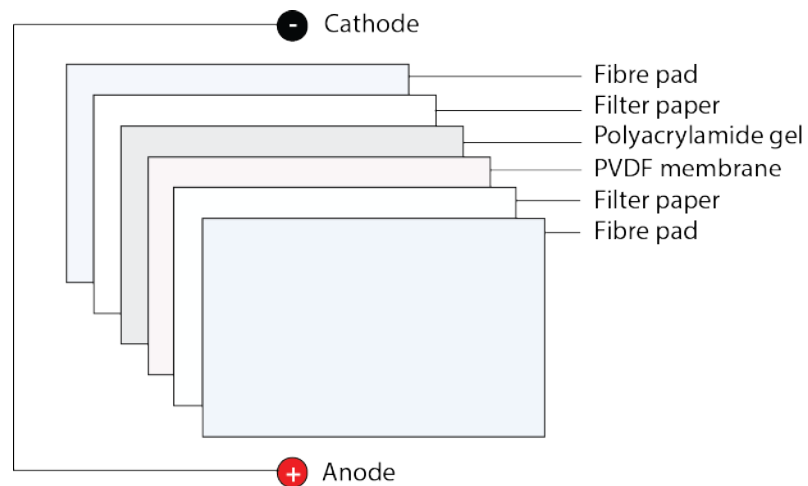


**Figure 2.5 Material assembly prior to electro blotting.** From bottom to top (cathode to anode): One fibre pad lays at the bottom of the blotting sandwich, followed by a filter paper, polyacrylamide gel, the PVDF membrane, another filter paper and a fibre pad on top.

### 2.2.3.7 Cutting the PVDF Membrane

After the electro-blotting, the unstained ladder was separated from the rest of the PVDF membrane by cutting the centre of the pre-stained ladder vertically as presented in **Figure 2.6**.

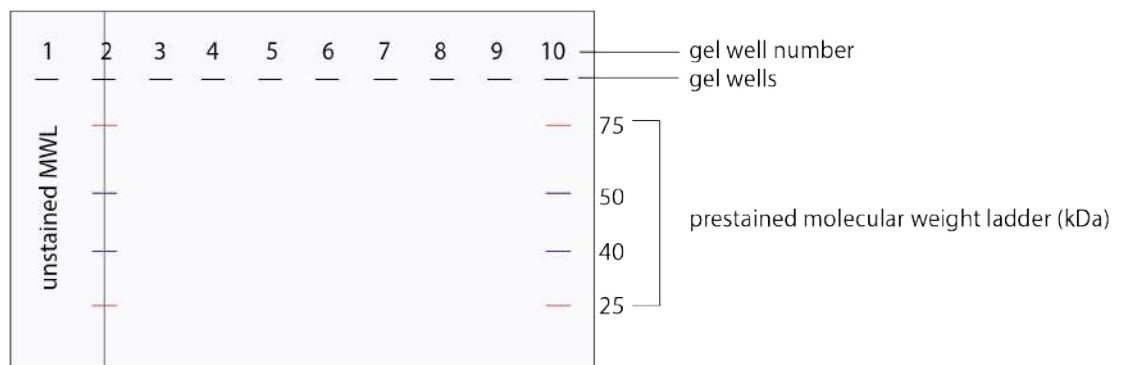


**Figure 2.6 PVDF membrane cut.** Vertical, short lines: gel wells; numbers: number of gel wells; well 1: unstained, biotinylated molecular weight ladder (MWL), well 2 + 10: pre-stained dual colour precision MWL (kDa) with red and blue short, vertical lines, which represent the relevant molecular weight bands for this study. Vertically line (alongside well 2) indicates the cut containing the unstained MWL and half of one of the pre-stained MWL.

This was done to avoid cross reaction with the secondary polyclonal anti-IgG Horse-Radish-Peroxidase (HRP)-linked detection Ab. If the membrane was cut differently, the detailed description can be read in the respective chapters.

#### **2.2.3.8 Blocking and Ab incubations**

After the transfer, the membrane was washed with 1x TBST to remove any transfer buffer, transferred to a plate containing 7.5% blocking buffer BSA/ TBS-T for 1 h to reduce unspecific binding of the primary Ab. The membrane washed 3x 5 min with 1x TBST and incubated with the primary Ab overnight at 4°C on a platform rocker with gentle agitation (Platform Rocker, STR6, Stuart-equipment, UK). The next day, the membrane was washed with 1x TBST 3x 5 min with strong agitation on a platform rocker (Innova 2100, New Brunswick Scientific, UK). Following incubation with the secondary anti-IgG HRP-linked Ab (Abcam, UK) or anti-biotinylated HRP-linked Ab (Cell Signaling Technology, UK) for 1 h at RT with gentle agitation after which it was washed 3x 10 min in 1x TBST with strong agitation.

#### **2.2.3.9 Stripping the PDVF membrane for re-probing**

The membrane was washed 3x 5 min in TBST, following incubation in Restore™ PLUS Western Blot Stripping buffer (ThermoFisher Scientific, UK). After a 3x 5 min wash in TBST, the membrane was ready to be re-probed. The membrane was only stripped and re-probed once. The membrane was probed for the house-keeping gene first, stripped and re-probed for STEAP2.

#### **2.2.3.10 Protein detection and analysis**

The ECL reagent (Bio-Rad Laboratories, UK) was prepared according to the manufacturer's instructions. The membranes were incubated in ECL (500µl) for 10s before placing them onto the Chemisorbs tray. For image acquisition and densitometry analysis, the ChemiDocXRS and ImageLab software, Version 5.2.1 were used (ChemiDocXRS, Bio-Rad Laboratories, UK). Saturated pixels were highlighted,

in order to avoid overexposure. If required, a linear regression analysis was conducted to confirm the molecular weight of the detected protein. The experiment was conducted in triplicate, if not otherwise stated.

## 2.2.4 Fluorescence microscopy

### 2.2.4.1 Slide preparation and staining

Approximately  $2.5 \times 10^4$  cells were grown for 48 h, washed 2x with PBS, fixed with PFA, washed 2x with PBS and blocked in 3% BSA/PBS for 1 h at RT. Cells were incubated with primary Ab diluted (concentration was Ab dependent) in blocking buffer overnight at 4°C. The next day, cells were washed 3x with PBS, incubated with polyclonal secondary anti-IgG Alexa Fluor-488 Ab (Abcam, UK) for 1 h at RT in the dark. Cells were washed 10x with PBS, 5x with ddH<sub>2</sub>O and counterstained the nuclear stain 4',6-Diamidino-2-Phenylindole (DAPI Vectashield Antifade Mounting Medium, Vector Laboratories, UK) or Hoechst (Thermofisher Scientific, UK) incubated at 37°C/ 5% CO<sub>2</sub> following image analysis.

### 2.2.4.2 Fluorescence microscopical imaging

The settings employed during confocal laser scanning microscopy analysis are displayed below in **Table 2.7**.

**Table 2.7 Channels used for fluorescence microscopy.** Ex.: excitation wavelength (nm), Em.: emission wavelength (nm); DAPI: 4'-6' Diamidino-2-Phenylindole; FITC: Fluorescein isothiocyanate.

Channel	Ex. (nm)	Em.(nm)	Em. colour	Light source
DAPI	405	461	Blue	Diode
FITC	488	527	Green	Argon/ mercury
Rhodamine	532	553	Orange	Helium neon

### 2.2.4.3 Image analysis

Fluorescent images which were taken with the confocal microscope (Confocal Laser Scanning Microscope 710, ZEISS, Germany) and the ZEN software Version 10 were processed and analysed using ImageJ Version FIJI Is Just another version of ImageJ

(FIJI, USA) into separate channels (blue, green, red, brightfield, merged composition). Scale bars were based on the known microscope pixel sizes ( $\mu\text{m}$ ) for each objective and microscope used as illustrated. To display coloured images, the Red-Blue-Green (RBG) setting was selected. In addition, any images which were taken with the standard light microscope (AxioCam ERC55, ZEISS, Germany) were displayed in brightfield. Images for the migration assay were converted into 8-bit files beforehand, in order to apply a standard bypass-filter. All images were assembled using Adobe Illustrator CS6, USA, Version 16.0.3

## **2.2.5 Anti-STEAP2 Ab effects *in-vitro***

### **2.2.5.1 Cell migration**

After cells have reached 80% confluence, medium was replaced for 24 h with serum-starved RPMI 1640 medium. The next day, cells were detached and resuspended and adjusted to a desired cell concentration. Each silicone insert was placed into one well of a 12-well plate (Ibidi, Germany, Cat. 80209). The cell suspension was first added into each chamber and then to the surrounding well. After 24 h of incubation at 37°C% 5%CO<sub>2</sub>, the inserts were removed and cell migration was monitored by taking images every 4 h for a total of 12 h with an inverted light microscope (AxioCamERC55, ZEISS, Germany). The experiment was conducted in duplicate if not otherwise indicated.

### **2.2.5.2 Cell invasion**

The cell invasion kit was obtained from Merck Millipore, UK (Cat. ECM 550). Cells were grown to 80% confluence and serum-starved in RPMI medium containing 0.5% FBS. The next day, inserts and a 24-well plate were allowed to equilibrate to RT as well as the FBS-free RPMI medium. The inserts were moisturised with FBS-free RPMI while cells washed in PBS, trypsinised, neutralised with FBS-free RPMI and resuspended in fresh FBS-free RPMI. The desired cell concentration was adjusted.

500  $\mu$ L of FBS was added as a chemoattractant per well, where required. Cells were treated with control or sample Ab and were carefully mixed and added into the inserts and incubated for 48 h at 37°C/ 5% CO<sub>2</sub>. The treatment was removed, the insert was stained with staining solution, washed and cotton-swabbed. Images were taken if necessary (AxioCamERC55, Zeiss, Germany). Cells were air-dried and placed into 200  $\mu$ L of extraction buffer and the absorbance was read at  $\lambda = 490$  nm using the POLARstar plate reader (POLARstar, BMG Labtech, UK). The experiment was conducted in triplicate.

### **2.2.5.3 Cell viability**

In a 96-well plate, cells were seeded per well and were left to grow until 70% confluence was reached. The next day, the cell culture medium was aspirated and replaced with treatment for 24 h, following the addition of 20  $\mu$ l of 3-(4,5-Dimethyl-2-thiazolyl)-2,5-diphenyl-2H-tetrazolium bromide (MTT) stock solution (5 mg/ml) (Sigmaaldrich, UK, Cat. M2128) and the incubation at 37°C/ 5% CO<sub>2</sub> in the dark. Medium was aspirated, cells were washed twice with PBS, 200  $\mu$ L of DMSO was added and the absorbance was read at  $\lambda = 570$  nm using a fluorescence plate reader (POLARstar, BMG Labtech, UK). The experiment was conducted in triplicate.

### **2.2.5.4 Receptor internalisation**

In an 8-well chamber slide (Ibidi, Germany), cells were grown for 48 h at 37°C/ 5% CO<sub>2</sub> before receptor internalisation was carried out. On the analysis day, old medium was discarded and the treatment was added quickly. To allow Ab cell surface binding (0min time point) the chamber was transferred to 4°C, washed with PBS and fixed with PFA (Polysciences, USA, Cat. 18814-20). For any other time point, the cells were shifted from 4°C to 37°C and incubated for the desired time, point to allow receptor internalisation, following PBS wash, fixation, and signal quenching using Image IT FX Signal Enhancer (Thermofisher Scientific, UK, Cat. I36933), blocking with BSA (Sigmaaldrich, UK, Cat. A2153), PBS washes and permeabilisation with

0.1 % Triton-X 100 (Sigmaaldrich, UK, Cat. T8787) Cells were washed in PBS and nuclei were counterstained with DAPI (Vectorlabs, UK, Cat. H-1200). Images were acquired with the confocal LSM 710 microscope (Zeiss, Germany) at a 63x zoom magnification. The experiment was conducted in duplicate.

### **2.2.6 Anti-STEAP2 ADC development (CellMosaic)**

Commercial polyclonal anti-STEAP2 Ab specific to ECL3 (Insightbiotechnology, UK) was purchased by CellMosaic, USA. The ADC development was carried out by CellMosaic using the PerKit™ Ab MMAE Conjugation Kit (CM11409x3, CellMosaic, USA) and all necessary reagents and buffers were provided by CellMosaic. The disulfide bonds of the commercial Ab were reduced by the addition of a reducing buffer containing solution A and Reagent A and was incubated at 37°C for . The Ab solution was then cooled to 2 - 8°C for 5 min in the refrigerator. Next, the Ab solution was transferred to the filter device and spun at 14,000 x g for 8 min and 8°C for purification and concentration yielding < 100 µl and was collected in a fresh tube. The labelling buffer was prepared to a total volume of 500 µl and added into a fresh filter device and concentrated at 14,000 x g for 8 min and 8°C, following repetition of the process. The labelling buffer was added to the Ab solution to make up approximately 640 µl, vortexed and spun down quickly. The MC-VC-PAB-MMAE was defrosted, then added to the Ab labelling buffer solution and mixed for 1 h at RT. A fresh filter device was equilibrated with PBS buffer 3x by gravity flow. The MMAE labelled Ab solution was then transferred into the pre-equilibrated filter device, 1.25 ml of PBS buffer was added. The solution was allowed to pass the gel bed of the filter device by gravity flow before collection in a fresh tube and stored at 4°C.

#### **2.2.6.1 Size-Exclusion Chromatography (CellMosaic)**

SEC analysis was conducted to assess the Drug-to-Ab Ratio (DAR). A UV-detector was used and absorbance was measured at  $\lambda = 280$  nm (protein and IgG),  $\lambda = 240$

nm (MMAE) and  $\lambda = 220$  nm (peptides). The unconjugated, polyclonal anti-STEAP2 Ab (Insightbiotechnology, UK) was included as negative control, whereas purified anti-mouse anti-IgG monoclonal Ab was used as positive control (provided by CellMosaic).

#### **2.2.6.2 Hydrophobic Interaction Chromatography (CellMosaic)**

HIC analysis was performed to determine the ADC product aggregation. A UV-detector was used and absorbance was measured at  $\lambda = 280$  nm (protein and IgG) and  $\lambda = 240$  nm (MMAE).

### **2.2.7 Monoclonal anti-STEAP2 development (APS)**

#### **2.2.7.1 Immunogen synthesis**

The 14 amino acid long peptide sequence „GWKRAFEEEEYYRFY “ situated on STEAP2/ECL3 was utilised as antigen for *in-vivo* immunisation for Ab development using the hybridoma technology. Two approaches for the peptide synthesis were utilised: a linear, free peptide (referred as „linear peptide“) and a multiple antigen-branched peptide (MAP, referred as „cyclic peptide“). The synthesis of both peptides was carried out by Ab Production Services (APS, UK).

#### **2.2.7.2 Animals**

Eight Balb/ C mice were grown by the animal facility of APS. Four mice per set of either linear or cyclic STEAP2 peptide and were used and were routinely checked and were of appropriate health condition at the time point of immunisation. The use of mice granted ethical approval by both Ethics Committees of Swansea University and APS.

### **2.2.7.3 Hybridoma development**

Four Balb/C mice were subjected to immunisation per set of anti-STEAP2 peptide (antigen). Mice were sacrificed following spleen preparation and cell fusion with mouse myeloma cells. Cells were cultured in 96-well plates and their supernatants were screened by indirect ELISA for positive hybridoma cell colonies. Positive hybridoma cell colonies were separated by using three rounds of limiting dilution (serial dilution) to obtain single hybridoma cell clones. Identified hybridoma cell clones were cultured in 24 well plates, expanded and affinity purified using a Protein-G column yielding mouse monoclonal anti-STEAP2 Ab diluted in PBS. For more information about the hybridoma development, please see Chapter 5, **Section 5.2.6**.

### **2.2.7.4 Antibody sample retrieval for the screening and storage**

Samples (approximately 10 - 20  $\mu$ l) from Test Sera1 and 2 containing polyclonal mouse anti-STEAP2 Abs were retrieved from the tail of the mice during the immunisation step (Phase I). Test Sera1 was provided after 3 immunisations and Test Sera2 after the fourth immunisation, respectively. A fifth immunisation was given before Phase II. Approximately 1 ml of hybridoma colony supernatant containing a heterogenous pool of mouse monoclonal anti-STEAP2 Abs was provided for testing (Phase III). Approximately 1.5 - 5 ml of purified mouse monoclonal anti-STEAP2 Abs originating from single hybridoma cell clones were provided for screening (Phase IV). Test samples were shipped on dry ice or cool packages by APS to Swansea University and were stored at 4°C when ready to use or at -20°C in aliquots for long-term storage.

### **2.2.7.5 Antibody screening technique**

#### **2.2.7.5.1 Indirect Enzyme-Linked Immunosorbent Assay (APS)**

The ELISAs were carried out by APS according to the Standard Operating Procedure SOP CC13. Maxisorp Nunc plates (ThermoFisher, UK) were coated with either cyclic or the free linear STEAP2 peptide beforehand at 1  $\mu$ g/ml in bicarbonate/carbonate

antigen-coating solution. Antigen was blocked with 0.2% gelatine/ PBS following washes with PBST (0.01%) and the addition of the test sera at a serial dilution from 1:100 - 1:204,800. Samples were washed and incubated with secondary goat anti-mouse anti-IgG (Fc-specific)-HRP conjugate at 1:2,000 (Sigmaaldrich, UK). Next, samples were incubated with 3,3',5,5'- tetramethylbenzidine, peroxidase substrate (TMP) and the reaction was stopped by the addition of 2 M sulfuric acid. Absorbance was read at  $A = 450$  nm (Cheshire Scientific, UK). Serum from mice prior to immunisation (pre-immunised sera) was included as negative control when available due to limited volume. The experiment was conducted in technical duplicate.

## 2.2.8 Programs

The programs used for analysis are displayed in **Table 2.8**.

**Table 2.8 Programs used for analysis.**

Programs	Supplier and version
AbDesigner	National Heart Lung Blood Institute, USA
Adobe Illustrator CSA	Adobe, USA, Version 16.0.3.
ChemDraw	Free online version (access date:09/2019)
GraphPad Prism	GraphPad Prism, USA, Version 8
ImageJ	ImageJ, USA, Version FIJI 2.0.0.
ImageLab	BioRad, UK, Version 6.0.1
SWISS-MODEL	Biozentrum Basel, Switzerland
Zen Software	ZEISS, Germany, Version 10

## 2.2.9 Statistical analysis

Results were statistically analysed with GraphPad Prism (Version 8, USA). Normality analysis was assessed by using the Shapiro-Wilk test (when  $N < 10$ ). A p-value  $< 0.05$  for each sample indicated the data was not normally distributed, whereas a p-value  $> 0.05$  suggested the data was normally distributed. If the data was considered as normally distributed, an ANOVA *post hoc*-Dunnnett test was employed to compare multiple samples, while a student t-test (two tailed) was applied for the comparison of two different groups. If the data was not normally distributed, a non-parametric ANOVA *post-hoc* Kruskis-Wallis test was applied to compare multiple groups,

whereas a student t-test (two tailed) *post-hoc* Mann-Whitney test was utilised to compare two different groups. Data was considered as statistically significant when p-value of  $\leq 0.05$  (\*), p-value  $\leq 0.01$  (\*\*) or a p-value of  $\leq 0.001$  (\*\*\*) or p-value  $\leq 0.0001$  (\*\*\*\*) and were annotated with in the respective figures.

## 3 “Evaluation of STEAP2 as a drug target.”

### 3.1 Introduction

---

Past *STEAP2* functional characterization and drug target assessments by gene-knock down and transfection studies have demonstrated, that it represents a potential molecular drug target for locally advanced prostate cancer (Burnell *et al.*, 2018; Korkmaz *et al.*, 2002; Ohgami *et al.*, 2006; Wang *et al.*, 2010; Whiteland *et al.*, 2014). High protein levels are known to be present in cancerous bone cells PC3 and lymph node metastatic LNCaP cells, whereas lower expression levels were reported for normal epithelial prostate cells PNT2 (Burnell *et al.*, 2018; Whiteland *et al.*, 2014). Previous findings have implied that high STEAP2 levels resulted in more aggressive cancer phenotypic outcomes such as cell migration, invasion and proliferation and therefore may promote prostate cancer progression (Burnell *et al.*, 2018; Wang *et al.*, 2010; Whiteland *et al.*, 2014).

Monoclonal antibodies (mAbs) have been successfully developed as anti-cancer drugs, cancer immunotherapy or to treat autoimmune diseases (Gashaw *et al.*, 2012; Hughes *et al.*, 2011). Given their specificity, Ab-based therapeutics have proven to be great therapy options with little side-effects and display a great alternative to conventional drugs in clinical practice. In order to evaluate STEAP2 as a viable drug target for circulating drugs, such as Abs and ADCs, three major features need to be taken into account: the drug target characterisation (assessment), tissue specificity, and Ab accessibility (**Figure 3.1**) (Gashaw *et al.*, 2012; Hughes *et al.*, 2011). Ideally, STEAP2’s tissue distribution should be low in normal, healthy tissues to ensure damaging effects associated with side-effects of Ab treatment are kept to a minimum. In the target tissues, such as tumours located in the prostate, or at metastatic (secondary) sites, higher STEAP2 expression levels need to be more abundant compared to healthy tissues to ensure Ab specificity and minimal off-target side-

effects (Gashaw *et al.*, 2012; Grant, 2002; Hughes *et al.*, 2011; Sauter *et al.*, 2003). To employ an Ab therapeutic as a drug, high tumour-tissue specific Ab-STEAP2 binding ability is required. Peptide sequences located at the cell surface are often considered as the peptide sequence of choice primarily due to their Ab accessible domains (Gashaw *et al.*, 2012; Grant, 2002; Shih, 2012; Strebhardt & Ullrich, 2008; Weiner, 2015).

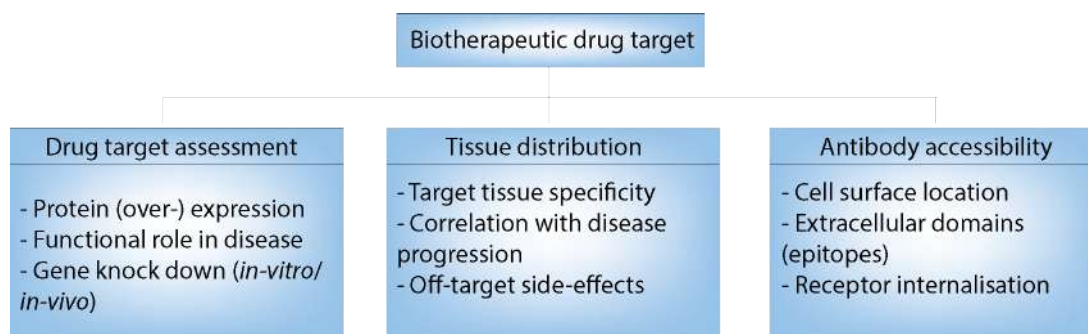


**Figure 3.1 Drug target properties to consider for Ab drug development.** Drug target overexpression in a certain disease (stage) must be assessed (e.g. by protein expression, functional role and gene knock-down analysis) to ensure target tissue or disease (stage) specificity. Tissue distribution in normal as well as diseased tissues must be determined to ensure targeted drug delivery and reduce undesired off-target side-effects. Ab accessibility must be investigated to identify targetable, extracellular and immunogenic domains (peptide sequences or epitopes). Adapted from (Gashaw *et al.*, 2012).

Short immunogen regions with less than 10 amino acids (aa) are also known as epitopes. Here, the variable domains contain the antigen-binding fragments. Due to the high specificity, development of Abs as drugs is therefore highly popular through the identification a disease-specific immunogen, which is targeted against tumour-associated antigens (TAA), that possess extracellular loops (ECLs) (Gashaw *et al.*, 2012; Grant, 2002; Shih, 2012; Weiner, 2015). For example, Bevacizumab (Avastin®) is used for the treatment of a variety of cancers (*e.g.* cervix, colon, lung and kidney and ovarian cancers) by targeting the Vascular Endothelial Growth Factor (VEGF) molecule, which results in the inhibition of angiogenesis (Ecker *et al.*, 2015; Grilo, 2019). Further, Trastuzumab (Herceptin®) has been successfully used to treat Human Epidermal Growth Receptor2+ (HER2+) overexpressed breast cancer, which blocks cell proliferation (Ecker *et al.*, 2015; Grilo, 2019; Hudis, 2007). Another example is Etanercept (Enbrel®) which is clinically applied to treat rheumatoid

arthritis and targets the Tumour-Necrosis Factor to reduce inflammation (Ecker *et al.*, 2015; Grilo, 2019).

Several open access tools exist to facilitate the prediction of peptide sequences for immunogen design to assist in the Ab development. One of the oldest methods is the so called hydropathy model. It analyses a protein for hydrophilic and hydrophobic elements based on the hydrophilicity of the protein's aa composition. Hydrophilic regions are water-soluble, they are more likely to be found in the extracellular domains, whereas hydrophobic regions located within the transmembrane domains of the biphospholipid cell membrane (Hopp & Woods, 1981). Another method is to assess the secondary structure of peptide sequences including the alpha-helix, beta-sheet or beta-turnover structures. Beta-sheets are thought to be more exposed to the cell surface and are therefore more accessible compared to alpha-helices, which are more likely to be found within the transmembrane based on their hydrophobic aa constitution (Chou & Fasman, 1974). The AbDesigner tool aligns a variety of pre-established protein propensity models, which are used to analyse the Ab drug target for the following properties: hydropathy, immunogenicity, uniqueness, similarity, conservation, topology, ligand binding domains, single nucleotide polymorphisms (SNPs) and splicing variants (Pisitkun *et al.*, 2014). Researchers have used these models for the prediction and the selection of the right peptide sequences for Ab-based therapies. Ideally, these peptide sequences possess an extracellular location to ensure Ab accessibility, high immunogenicity to elicit a sufficient Ab generation with low similarity to other proteins to avoid undesired side-effects (Gashaw *et al.*, 2012; Grant, 2002; Shih, 2012; Strebhardt & Ullrich, 2008; Weiner, 2015). Proteins or peptide sequences must be checked for their uniqueness. By aligning the target peptide sequence with any other desired species, the AbDesigner tool indicates a uniqueness score (Pisitkun *et al.*, 2014).. If a very similar protein exists, a similarity percentage and the species are depicted alongside the uniqueness core (Pisitkun *et al.*, 2014).. The name of the similar protein or peptide is provided, which is important for the evaluation to avoid damaging off-target effects (Pisitkun *et al.*, 2014).. If a protein is

not highly conserved, it may be present in other species. The conservation of the peptide can be checked through alignment of the peptide sequence with other species (Pisitkun *et al.*, 2014). Information about the topology is retrieved based on the hydrophilicity of the protein's aa sequence and divides the protein sequence into the transmembrane or non-transmembrane domains (Pisitkun *et al.*, 2014). To further evaluate extracellular domains, the protein can be visualized in a 2D or 3D model by plotting its aa sequence using Swissprot, for instance. AbDesigner supports the identification of putative splicing variants and Single Nucleotide Polymorphisms (SNPs) (Pisitkun *et al.*, 2014). This is to avoid the selection of peptide sequences of a different peptide length as a result of alternative splicing or those sequences including a SNP, that may alter protein function, which could impact the favourable attributes of the original immunogen (Pisitkun *et al.*, 2014).

The aim of the present chapter was to identify, if STEAP2 is a viable drug target for circulating therapeutics, such as Abs. The objectives were thus to:

- (1) Identify STEAP2's normal tissue distribution by tissue-microarray/immunohistochemistry analysis to predict off-target side-effects in healthy tissues;
- (2) Determine a suitable peptide sequence (immunogen), that can be used as antigen (vaccine) for the development of an anti-STEAP2 mAb;
- (3) Map commercial Abs to identify immunogens for future target characterisation studies by comparing a panel of commercial Abs for their STEAP2 binding ability using fluorescence microscopy and western blotting.

## 3.2 Material and methods

---

### 3.2.1 Tissue micro-array (TMA) description

Commercial tissue-microarrays were obtained from Proteinbiotechnologies (#TMA1205, Proteinbiotechnologies, USA) in technical duplicate. Each TMA comprised a total of 96 normal (disease-free), human tissue cores with a diameter = 1.5 mm and thickness = 4  $\mu$ m per tissue core. Each tissue core was assigned a specific array position (*e.g.* A 1) consisting of a word (A - H) and a number (1 - 12; **Figure 3.2** and **Table 3.1**).

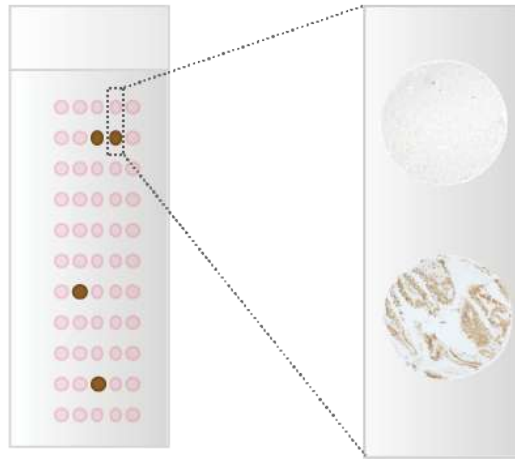


**Figure 3.2 Example TMA layout with IHC staining.** Brown tissue cores: high protein expression. The zoom demonstrates examples of a target protein low (upper) or high expressing (lower, brown) tissues.

Tissue biopsies originated from normal (non-diseased) female as well as male donors aged 1 - 82 years. Of these tissues, 25 were taken from donors who had passed away indicated with an asterisk (\*) in **Table 3.1**. Two tissue cores were of abnormal origin (D11 = swelling liver and E10 = adenoma parathyroid). The tissue cores per TMA slide represented biological replicates as each originated from individual donors.

**Table 3.1 Detailed description of the TMA**

. Each TMA contained 96 cores originating from biopsies from normal (un-diseased, healthy) tissues of human donors if not else specified in 3.2.1. Tissue: the tissue origin is itemised by its name. The TMA slide was categorized into words (A - H) and numbers (1 - 12), which specified each individual tissue core's position on each slide („ID“). Replicates: most of the tissues were provided in biological replicates. The number of biological replicates is displayed in the order of their number of replicates. N: number of replicates. Tissues labelled with asterisks (\*): tissues were taken from donor biopsies who passed away.

Tissue	Position on TMA (“ID”)	Replicates
Bone marrow*	A 7	N = 1
Parathyroid	E 10	N = 1
Eye*	A 8 – A 9	N = 2
Pituitary gland*	E 11 – E 12	N = 2
Skin	F 7- F 8	N = 2
Spinal cord*	F 9 – F 10	N = 2
Spleen	F 11 – F 12	N = 2
Adrenal gland*	A 1 – A 3	N = 3
Bladder	A 4 – A 6	N = 3
Breast	A 10 – A 12	N = 3
Cerebellum*	B 1 – B 3	N = 3
Cerebral cortex*	B 4 – B 6	N = 3
Fallopian tube	B 7 – B 9	N = 3
GI-Oesophagus	B 10 – B 12	N = 3
GI-stomach	C 1 – C 3	N = 3
GI-small intestine	C 4 – C 6	N = 3
GI-colon	C 7 – C 9	N = 3
GI-rectum	C 10 – C 12	N = 3
Heart*	D 1 – D 3	N = 3
Liver	D 10 – D 12	N = 3
Lung	E 1 – E 3	N = 3
Ovary	E 4 – E 6	N = 3
Pancreas*	E 7 – E 9	N = 3
Placenta	F 1 – F 3	N = 3
Prostate	F 4 – F 6	N = 3
Striated muscle*	G 1 – G 3	N = 3
Testis	G 4 – G 6	N = 3
Thymus*	G 7 – G 9	N = 3
Thyroid	G 10 – G 12	N = 3
Tonsil	H 1 – H 3	N = 3
Ureter	H 4 – H 6	N = 3
Uterus-cervix	H 7 – H 9	N = 3
Uterus-endometrium	H 10 – H 12	N = 3
Kidney	D 4 – D 9	N = 6

On the first TMA, the following tissue cores were excluded from analysis: A1 = adrenal gland\*, A5: bladder, B4: cerebral cortex\*, B8: fallopian tube, G9: thymus\*, G11: thyroid with > 50% of the total tissue core missing; misfolded tissue cores were B3: cerebellum\*, B5: cerebral cortex, F4: prostate and G10: thyroid and E10: parathyroid with no additional technical replicate available, which were also excluded (N = 1) (see **Table 3.1**). Thus, a total of 85 (of 96) tissue cores were analysed on the first TMA. On the second TMA, the following tissue cores were excluded from

analysis: B4: cerebral cortex, B8: fallopian tube, F4: prostate as > 50% of the total tissue core was missing and E10: parathyroid due to misfolding (see **Table 3.1**). Thus, a total of 92 (of 96 tissue cores) were analysed on the second TMA. Therefore, a total of 177 (of 192) tissue cores were included into the analysis. Images were taken from each tissue core with the 4x objective using a light microscope Olympus microscope BX51TF (Olympus, UK) after IHC staining of the TMAs.

### **3.2.2 Immunohistochemistry of the tissue-microarray**

To detect STEAP2's expression *in-situ*, immunohistochemistry (IHC) analysis was carried out by the Samantha Spencer and Kate Murphy from the Swansea University Singleton Hospital Histology and Pathology Department. The slides were incubated for 1 h at 60°C to enhance the tissue adhesion to the glass. The slides were labelled with a bar code and the IHC staining was conducted using the automated Ultra VENTANA machine (Roche, Switzerland). The TMA was incubated by EZ prep solution at 72°C. For antigen retrieval, a CC1 antigen retrieval buffer (pH 8.0 – 8.5) was utilized at 98°C for 32 min following the addition of a pre-oxidase inhibitor at 36°C for 4 min. The TMA was first incubated with primary rabbit anti-STEAP2 Ab at 36°C for 36 min (Ab2/ ECL1 aa 233 – 262, 1:50, Abcam, UK). The STEAP2 expression was detected using the OptiView 3,3'Diaminobenzidine Tetrahydrochloride (DAB) IHC Detection Kit (Roche, Switzerland). In brief, a secondary anti-IgG HRP-linked Ab was added, following the addition of an anti-HQ HRP-linked multimer. The slides were then incubated with DAB chromogen substrate and H<sub>2</sub>O<sub>2</sub> for 8 min following the addition of copper for 4 min. Nuclei were counterstained with hematoxylin for 8 min.

### **3.2.3 TMA semi-quantitative scoring system and statistical analysis**

Each tissue core was manually scored for the staining intensity and staining distribution per tissue core by two trained scientists using a light microscope (Olympus, UK) which was compared to the positive control of high grade prostate

cancer tissues (provided by Burnell *et. al*). The intensity score describes the depth of colour of the STEAP2 expressing tissues and ranged from 0 – 3 (with 0 = not present and 3 = very strong) (**Table 3.2**).The staining distribution score describes the proportion (distribution) of the core expressing STEAP2 protein in the cells (%), where the scores ranged from 0 - 4 (with 0 = absent and 4 = 100%) (**Table 3.2**).The intensity score was then multiplied by the staining distribution score; thus, the minimum final score was 0 and the maximum final score was 12 ((**Table 3.2**).Reference high grade prostate cancer (PCA) tissues with Gleason Scores 8 - 10 were used as the positive control with STEAP2 expression set as „very strong“ (maximum score = 12) (provided by Burnell *et. al*). When the final score was assigned, the tissues were divided up into four categories: score 0 - 3 = low expression, score 4 - 6 = medium expression, score 7 - 9 = strong expression and score 10 - 12 = very strong expression (**Table 3.2**).

**Table 3.2 Semi-quantitative scoring system for the TMA analysis.** Each tissue core was individually assigned an intensity score, proportion of cells with STEAP2 signal (%) score as well as a descriptive expression, respectively, compared to the positive, high grade prostate cancer tissue controls. The highest final score represents very strong STEAP2 expression based on the positive control of high grade (aggressive) prostate cancer tissues.

Expression	Intensity (%)	Intensity score
negative	0	0
weak	< 25	1
moderate	26 – 50	2
strong	> 75	3
Expression	STEAP2 distribution per core (%)	Staining distribution score
negative	0	0
weak	< 25	1
moderate	26 – 50	2
strong	> 51 – 75	3
very strong	> 75	4
Expression	Final score (= intensity score x staining distribution score)	
negative	0	
weak	1 – 3	
moderate	4 – 6	
strong	7 – 9	
very strong	10 - 12	

### **3.2.4 Structural analysis of the human STEAP2 protein**

#### **3.2.4.1 Identification of extracellular domains by UniProt and SwissProt**

The amino acid (aa) sequence for the full-length human STEAP2 protein was retrieved in FASTA format from UniProt (UniProt ID: Q8FNT-2, entry name: HU\_STEAP2, canonical isoform a). The aa sequences of the six transmembrane domains were also provided specifically by UniProt. The protein's FASTA format was inserted into SwissProt to receive the 2D structural model as data output, which visually displayed the STEAP2 protein into its transmembrane (TM), intracellular (ICLs) and extracellular domains (ECLs) categorised with detailed aa sequences. A table containing STEAP2's number of TM, ICLs, and ECLs with individual aa sequences was subsequently created for a detailed overview based on the SwissProt output and the known TM domain sequences from UniProt. A 3D STEAP2 protein structure was provided by clicking on the SwissProt link at the UniProt website, which indicated NADPH, FAD binding and transmembrane domains as a colour code.

#### **3.2.4.2 Full length human STEAP2 protein structural analysis by AbDesigner**

The AbDesigner tool was used for STEAP2's protein structural analysis (website: <http://helixweb.nih.gov/AbDesigner/>). STEAP2's FASTA format was inserted into AbDesigner's „protein of interest“ field with the following settings: peptide length = 15 aa; epitope length = 7 aa (chosen by default). The protein was analysed for its hydropathy (Kyte and Doolittle algorithm with turquoise colour code: bright turquoise: hydrophilic; dark turquoise: hydrophobic), structural conservation (%; red colour code, bright red: highly unique; moderate red: moderately unique; dark red: less unique), uniqueness (%; yellow colour code; bright yellow: highly unique; moderate yellow: moderately unique; dark yellow: less unique), similarity to species (%; high percentage: high similarity; low percentage: low similarity), immunogenicity

score (Ig-score, green colour code; bright green: highly immunogenic; moderate green: moderately immunogenic; dark green: low immunogenic), topology (transmembrane, intracellular and extracellular domains), post-translational modification (PTM), splicing variants, single-nucleotide polymorphisms (SNP) and ligand binding sites.

#### **3.2.4.3 Immunogen region identification by Ab-STEAP2 ECL mapping to create the anti-STEAP2 pAb lead candidate panel**

A list of commercial polyclonal anti-STEAP2 antibodies (anti-STEAP2 pAbs) was manually created (date:03/ 2016) and classified into the following categories: Ab clonality, Ab name, species, target-species, immunogen region and respective aa residue (aa), supplier and catalogue number based on the supplier's datasheet (Appendix, **Table A1.2** ). Next, a table containing STEAP2's ECLs domains plus respective aa sequences was designed. Available aa sequences of the Ab immunogen regions of the commercial Ab were identified from the list and overlapped with the known ECL aa sequences to determine STEAP2's final immunogen regions (Immunogen1 - Immunogen4). Mapped commercial Abs were given the names Ab1, Ab2, Ab3 and Ab4. These formed the polyclonal commercial Ab panel for later evaluation of STEAP2 binding ability (see **Table 2.5**).

#### **3.2.4.4 Classification of immunogen regions into peptide sequences**

Immunogens1 – 4, which were identified by previous commercial anti-STEAP2 pAb - ECL mapping were divided up into 15 aa long peptides according to the AbDesigner default settings. These formed a panel of 5 peptide sequences (Peptide1, Peptide2, Peptide3, Peptide4 and Peptide5). Immunogen1 (ECL1) aa sequence was divided up into two 15 aa long peptide sequences (Peptide1 and Peptide2). Immunogen2 (ECL2) was divided up into two 15 aa long peptide sequences (Peptide3 and Peptide4). Immunogen3 (ECL3) was divided up into one 15 aa long peptide sequence (Peptide5).

#### **3.2.4.5 Ranking of immunogenic peptide sequences by AbDesigner**

Each peptide sequence was further separately analysed for the following AbDesigner parameters: conservation (%), similarity (%), uniqueness (%) and immunogenicity. The Ig-scores were ranked from the highest to lowest immunogenic sequence based on the additional tabular AbDesigner output. This tabular Ig-score output presented individual immunogenicity scores for the full-length STEAP2 protein, which was divided up into 15 aa long peptide sequences.

#### **3.2.5 Polyclonal, commercial lead anti-STEAP2 pAb candidates**

Commercial lead Ab candidates were of polyclonal origin and shown in **Table 2.5**.

#### **3.2.6 Protein extraction**

Protein was extracted as described in Chapter2, **Section 2.2.3.1**.

#### **3.2.7 Western blotting**

##### **3.2.7.1 SDS-PAGE and Electro-Blotting**

Samples were loaded onto a 10-well gel (10%) in the following order: well 1: unstained molecular weight ladder, well 2: pre-stained molecular weight ladder, well 3 - 5: protein lysate from PNT2 cells, well 6 - 9: protein lysate from PC3 cells, well 10: visible molecular weight ladder (**Figure 3.3**). SDS PAGE was run as described in Chapter2, **Section 2.2.3.5** and electro-blotting was carried out as described in Chapter2, **Section 2.2.3.6**.

##### **3.2.7.2 PVDF-membrane cutting**

The PVDF-membrane was cut after the electro-blotting. The unstained molecular weight ladder was loaded into well-1 following the pre-stained molecular weight ladder, vertically cut off by cutting the pre-stained molecular weight ladder into two halves to avoid cross-reaction with the secondary detection Ab (**Figure 3.3**).

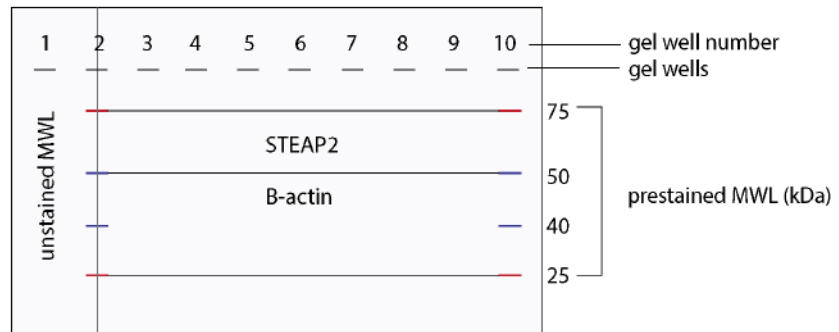


**Figure 3.3 PVDF membrane cut after electro-blotting.** A) Samples were loaded onto a 10-well polyacrylamide gel (10%); the well numbers represent individual wells, which were numbered as follows: 1 – 10 (from left to right). Vertical black lines below each number represent the wells. 1: unstained, biotinylated molecular weight ladder (MWL); 2: pre-stained molecular weight ladder (red and blue vertical lines), 3 – 10 = wells for protein samples, where 3 – 5: PNT2 cell lysates and 6 – 8: PC3 cell lysates. B) Schematic illustration of how the PDVF membrane was cut. Pre-stained MWL: four coloured, vertical lines were of importance for PVDF membrane cutting; 75 kDa (red), 50 kDa (blue), 40 kDa (blue) and 25 kDa (red). Grey thin lines indicate where the PVDF was cut: two horizontal cuts resulted in two membranes containing STEAP2 (upper, 50 – 75 kDa) and B-actin (lower, 40 – 50 kDa) each. One vertically cut in the middle of the pre-stained ladder at the well position 2, resulted in a separate membrane containing the unstained, biotinylated MWL only.

This enabled correct alignment of the two membranes for analysis. Further, the membrane containing the protein of interest, was horizontally cut between the 25 kDa – 50 kDa and the 50 – 75 kDa range of pre-stained molecular weight ladder for simultaneous incubation of STEAP2 and Beta-actin (housekeeper) Ab two allow rapid screening of the Ab panel. A total of three PDVF membrane parts were thereby created: one containing the unstained molecular weight ladder (with no horizontal cutting), a membrane of 25 – 50 kDa range containing the house-keeping protein Beta-actin and a membrane containing the 50 – 75 kDa range within which the STEAP2 protein was located (**Figure 3.3**).

### 3.2.7.3 Ab incubations and analysis

Concentrations of the primary rabbit anti-STEAP2 pAbs were: Ab1 (1:500, Insightbiotechnology, UK), Ab2 (1:500, Life Span Bio Source, UK), Ab3 (1:500, Abcam, UK) and Ab4 (1:250, Insightbiotechnology, UK). The antibodies were diluted in 7.5% BSA/ TBS-T and incubated with the membrane overnight at 4°C

with gentle agitation. The membranes were then washed 3x 5min with TBS-T and incubated with the secondary polyclonal goat anti-rabbit anti-IgG HRP-linked Ab (1:10,000, Abcam, UK) diluted in 7.5% BSA/ TBS-T for 1 h at RT with gentle agitation on a plate shaker. Analysis was carried out as described in Chapter2, **Section 2.2.3.8 - Section 2.2.3.10**. The experiment was conducted in triplicate.

### **3.2.8 Fluorescence Microscopy**

#### **3.2.8.1 Slide preparation and staining**

Cells were cultured on 8-well chambered slides (Ibidi, Germany) as described in Chapter2, **Section 2.2.4.1**. Cells were incubated with 200 µl of primary rabbit anti-STEAP2 pAb diluted in 3% BSA blocking buffer (Ab1, 1:20; Ab2, 1:20; Ab3, 1:20; Ab4, 1:200), sealed with parafilm and incubated ON at 4°C. The next day, cells were prepared for fluorescence microscopy analysis as described in **Section 2.2.4.1**. The experiment was conducted in triplicate.

#### **3.2.8.2 Fluorescent imaging analysis and image processing**

Image analysis was conducted using the LSM 710, Zeiss, Germany as described in Chapter2, **Section 2.2.4.1 – Section 2.2.4.3**. The lasers used were the 405 (blue channel) and the 488 (green channel). The test was carried out in triplicate. Three different field of views per test sample were applied to acquired three images for qualitative analysis per replicate with a 63x zoom objective.

#### **3.2.8.3 Statistical analysis**

The data generated from the tissue-microarrays was analysed using GraphPad Prism. A non-parametric, one-way ANOVA, *post-hoc* Kruskal-Wallis test was used to compare the mean scores to the positive control tissues. A student t-test was used to assess the statistical significance of STEAP2 expression during western blotting analysis.

Data was considered as statistically significant when p-value of  $\leq 0.05$  (\*), p-value  $\leq 0.01$  (\*\*) or a p-value of  $\leq 0.001$  (\*\*\*) or p-value  $\leq 0.0001$  (\*\*\*\*) and were annotated with in the respective figures.

### 3.3 Results

#### 3.3.1 STEAP2 is expressed at minimal levels in over 33 normal tissues across the human body

To determine STEAP2's tissue distribution *in-situ*, a normal TMA was analysed by IHC. High grade PCA tissue was used as a positive control for very strong STEAP2 expression. PCA tissues of a Gleason Score 8, 9 and 10, were all assigned a final score of 12 given their strong STEAP2 expression (**Figure 3.4**). The three, high grade (aggressive) prostate cancer tissues very heavily stained for STEAP2 throughout the tissue cores. Thus, they were assigned the maximum intensity score of 3. Moreover, the proportion of STEAP2 stained cells was allocated the maximum score of 4 given the cancer tissue cores were strongly stained within the entire core (**Figure 3.4**). Therefore, the cancerous prostate tissues were assigned the maximum score of 12.

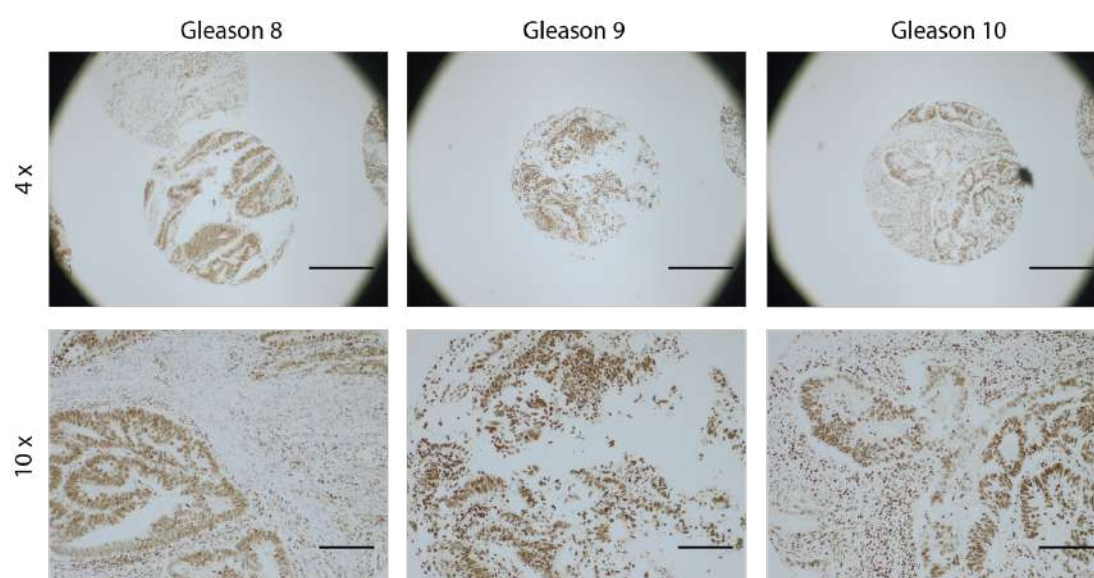


**Figure 3.4 STEAP2 expression in high grade prostate cancer tissues.** PCA: Prostate cancer. PCA tissues were provided by Burnell *et al.*, 2018. All high grade PCA tissues (Gleason 8 – 10) were assigned the maximum final score of 12 and were used as a positive control for a very strong STEAP2 expression. Images were acquired with a 4x and 10x objectives using the Olympus microscope model BX51TF, UK. Scale bar = 50  $\mu$ m.

Upon analysis of the normal-tissue TMA, 67% (22 of 33 tissues organs) of the tissues exhibited substantially lower levels of STEAP2 expression (final score < 3) compared to the high grade PCA tissues (**Figure 3.5**). All of the tissues showed a very low staining intensity as well as staining level compared to the high grade PCA tissues visually. Approximately 45.45% of all tissues (15/33 tissue organs) significantly expressed STEAP2 in lower levels compared to the high grade prostate cancer tissue specimen (an overview of all p-values is displayed in the appendix **Table A1.1**). The highest STEAP2 expression levels were observed in the GI-rectum and GI-small intestine closely followed by the spleen. A mean expression score of 2.3 (out of 12) was assigned to both the GI-rectum and GI-small intestine whereas the mean expression score for the spleen was slightly lower (2.0 out of 12). Although these three tissues demonstrated the highest STEAP2 protein levels amongst all the tissues, they were nonetheless considered to be in the low expression range. Low STEAP2 levels were predominantly observed in the glandular cells of the fallopian tube, breast and thyroid tissues. Further, no substantial STEAP2 expression was present in 33% (11 of 33 tissues organs) of the tissues which include: bladder, cerebral cortex, prostate, pancreas, skin, spinal cord, testis, thymus, thyroid, tonsil and the uterus-endometrium. The majority of these tissues showed blue nuclei staining pattern and were therefore assigned a score of 0 (low expression) (see **Figure 3.5** and **Figure 3.6**). The IHC analysis of a normal TMA demonstrates, STEAP2 is minimally expressed in 33 tissues from across the human body, which implies it could be a viable drug target specific for prostate cancer.

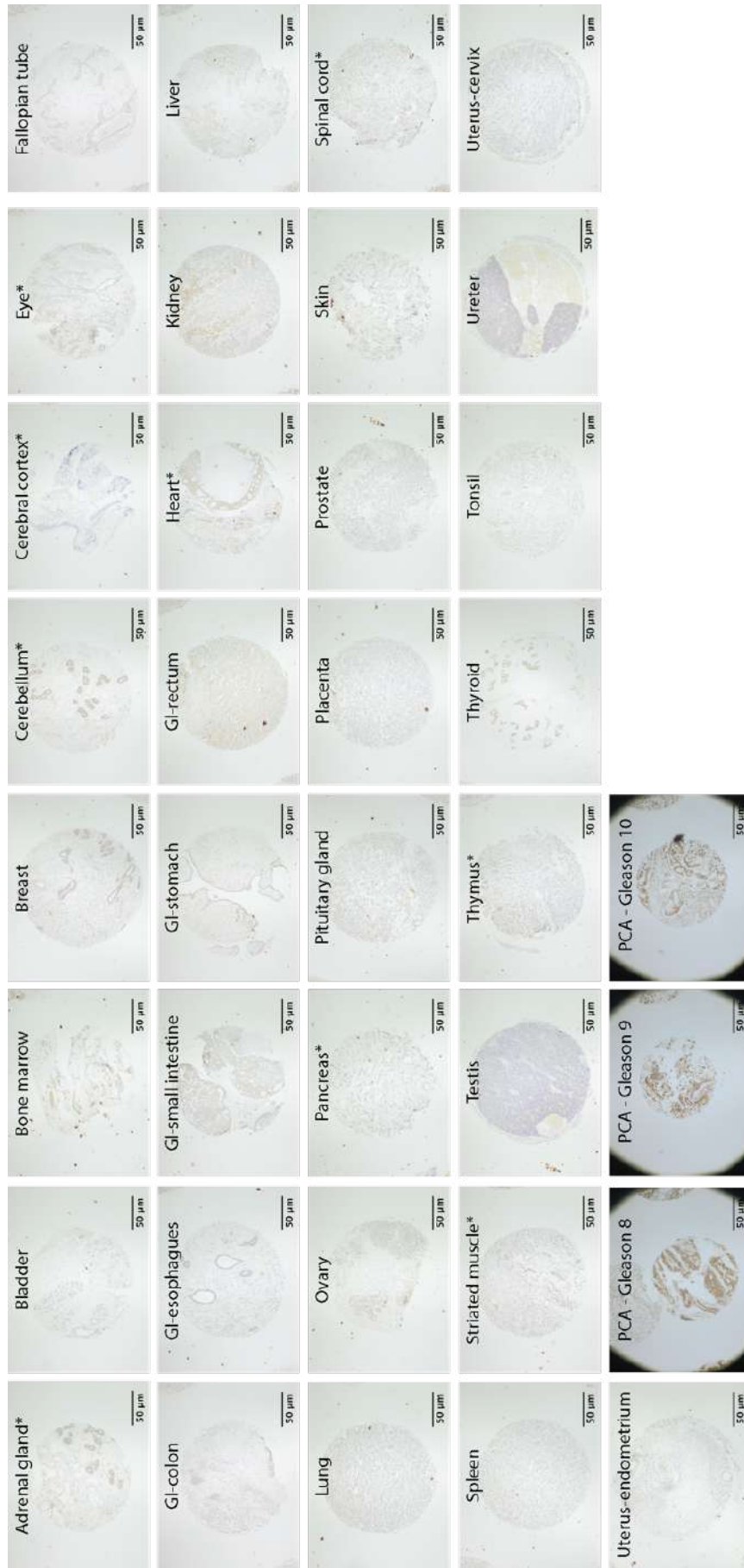


**Figure 3.5 Tissue profile of STEAP2 in 33 human tissues by IHC/TMA**

. High grade prostate cancer tissues show strong STEAP2 staining intensity and staining levels compared to its low expression in all of the normal tissues across the human body. For each tissue, the most representative image was selected for illustration. Prostate cancer tissue originated from a custom designed tissue-microarray (provided by Burnell *et. al.*, 2016) hence the tissue cores are minor compared to the normal tissue cores. All images displayed were taken on a 4 x objective with the Olympus light microscope model BX51TF (Olympus, UK). Scale bar = 50 µm.

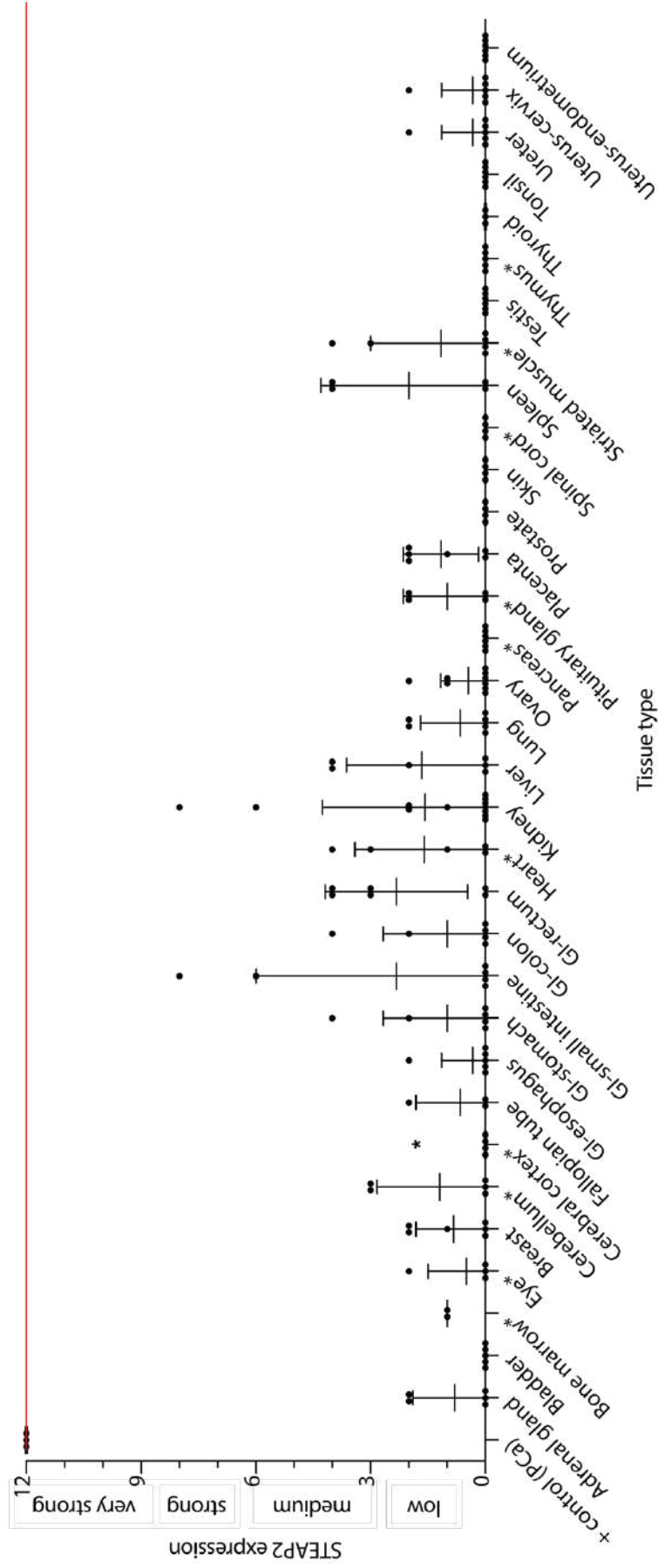


**Figure 3.6 Tissue expression of STEAP2 in 33 human tissues by IHC/TMA**

. 33 different tissues across the human body in alphabetical order. STEAP2 expression is shown as descriptive expression (low, medium, strong and very strong) with respective mean final scores (0 – 12) Horizontal red line indicates the mean score value of the high grade prostate cancer tissues utilised as reference positive control tissues of "very strong" STEAP2 expression (corresponding a maximum score: 12). A non-parametric, one-way ANOVA, *post-hoc* Kruskal-Wallis test was used to compare the mean scores to the positive control tissues. p-value  $\leq$  0.01 (\*\*).

### 3.3.2 Structural analysis of the human STEAP2 protein revealed three Ab-accessible extracellular loops (ECLS)

The structural analysis aimed to generate an overview of the structure and topology of the human STEAP2 protein to identify targetable, extracellular domains accessible for Ab drugs. STEAP2's aa sequence was retrieved from the database UniProt for the visualization of the 2D and 3D STEAP2 protein structure using SwissProt. Structural protein modelling revealed six transmembrane domains (TM) and 4 intracellular loops (ICLs). Moreover, 3 extracellular loops (ECLs) were identified, which were important as accessible regions for the future design of anti-STEAP2 Ab therapeutics (**Figure 3.7 A**). The 3D protein model of STEAP2 was also retrieved by SwissProt and provides additional ligand binding sites as depicted by the colour code (**Figure 3.7 B**).

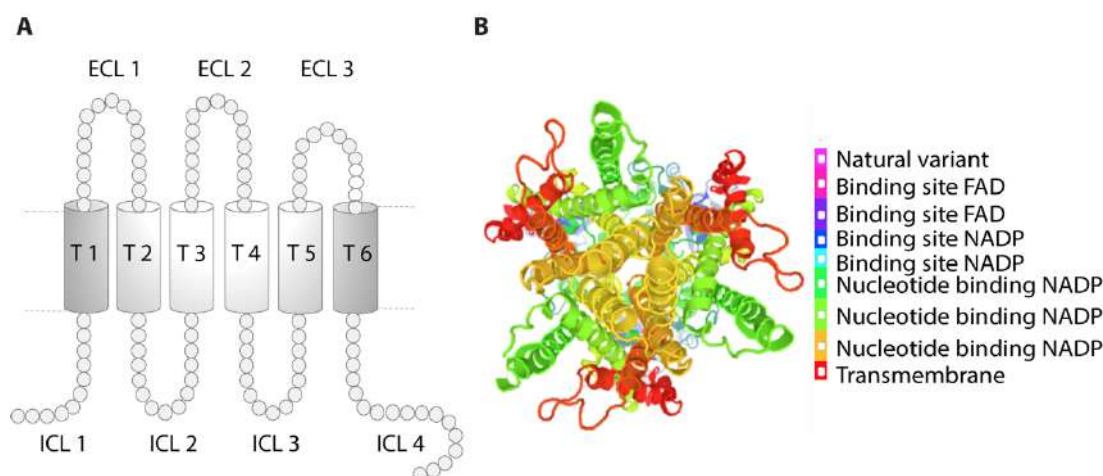


**Figure 3.7 2D and 3D structures of STEAP2.** A) STEAP2's 2D structure was re-designed based on the SwissProt output. Three extracellular loops (ECLs 1 - 3), four intracellular loops (ICLs 1 - 4) and six transmembrane domains (TM 1 - 6) are displayed. B) Original crystallographic 3D structure of STEAP2 (isoform a) was retrieved from SWISSModel provided on the UniProt website (date: 04/2019). The colour code indicates different binding sites, natural variants or transmembrane domains.

The exact aa sequences of the six transmembrane domains were provided by UniProt prior to the structural modelling, which allowed the specification and categorization of the human STEAP2 protein according to its TM, ICL and ECLs aa sequences after 2D modelling (shown in **Table 3.3**). By doing so, the specific aa

sequences located to the ECLs 1 - 3 were identified as accessible regions for the design of potential Ab therapeutics suggesting STEAP2 presents a viable drug target.

**Table 3.3 Classification of STEAP2 into structural domains**

. Domain categories transmembrane domains (TM), intracellular domains (ICLs) and extracellular domains (ECLs). Three ECLs (ECL1 - 3), four ICLs (ICL 1 - 4) and six TM were identified (TM 1 - 6). Numbers indicate the domain number as they structurally appear. aa sequence: amino acid sequence of the individual domains after alignment with known aa sequences of the TM domains from UniProt; aa position (numbers): position of the amino acid sequences for each determined domain.

Domain	aa sequence	aa position
ECL1	YSFVRDVIHPYARNQQSDFYKIPIEIVNKT	229 – 258
ECL2	RRSERYLFLNMAYQQVHANIENSWNEEE VWRIE	326 – 358
ECL3	GWKRAFEETYYRFYTPPN	414 – 431
ICL 1	MESISMMGSPKSLSETFLPNGINGIKDAR KVTVGVIKSGDFAKSLTIRLIRCGYHVIG SRNPKFASEFFPHVVDVTHHEDALTKTN IIFVAIHREHYTSLWDLRHVVLGKILIDVSS MRINQYPESNAEYLASLFPDSLIVKGFNV VSAAWALQLGPKDASRQVYICSNNIQAR QQVIELARQLNFIPIDLGLSSAREIENLP LR	1 – 207
ICL 2	YQLYYGTYRRFPPWLETWLQ	280 – 304
ICL 3	PSVSNALNWREFS	380 – 392
ICL 4	PCISRKLKRIKKGWEKSFLEEGMGGTI PHVSPERVTVM	452 – 490
TM 1	LFTLWRGPVVAISLATFFFL	208 – 228
TM 2	LPIVAITLLSLVYLAGLLAAA	259 – 279
TM 3	LGLLSFFFAMVHVAYSCLLPM	305 – 325
TM 4	MYISFGIMSLGLLSLLAVTSI	359 – 379
TM 5	FIQSTLGYVALLISTFHVLIY	393 – 413
TM 6	FVLALVLPISVILGKIILF	432 - 452

STEAP2 was then analysed for additional protein propensities, which are commonly used to predict immunogenic regions to generate mAbs. AbDesigner provides a visual output after analysis, which was employed to evaluate the human STEAP2 protein based upon the following parameters: topology (*i.e.* ECLs, ICLs and TMs), splicing variants (isoforms), conservation, hydrophathy, uniqueness, immunogenicity, any post-translational modifications (PTM), or SNPs and its metal binding sites. The AbDesigner's data output for the full length human STEAP2 protein is represented in **Figure 3.8**. Its topology domains were observed as follows: six red TMs, four grey ICLs and three blue ECLs. This analysis revealed, that STEAP2 is a 490 aa long protein, representing the first and canonical isoform 1, which

further analysis focused on. The canonical STEAP2 isoform 1 showed low conservation as demonstrated by a 90% similarity in 128 different species including the bovine, chimpanzee, guinea pig, monkey, mouse and rat.

Based on the hydropathy plot, more hydrophilic regions were allocated to both the ECLs and ICLs. This suggested, that these regions were more exposed to the intracellular or extracellular site of the cell membrane due to their higher content in hydrophilic aa. In contrast, more hydrophobic regions were assigned to all six TMs shown by the dark turquoise designation in **Figure 3.8**. This implied, that a higher content of hydrophobic aa may be ascribed to the TM regions. Moreover, hydrophilic regions such as the ECLs and ICLs were classified as moderate to high immunogenic domains. This was observed by an alignment of the hydropathy plot data with the immunogenicity plot for each individual topology region. Interestingly, the most immunogenic residues were observed for ICL1 and ICL4. These were not further analysed for their Immunogenicity-score (Ig-score), due to their inaccessibility. Low immunogenic domains were identified for more hydrophobic residues like the TMs as demonstrated by the dark green coloured regions **Figure 3.8**.

Moving on to the additional protein parameters evaluated, STEAP2's ferrireductase activity spanned between the ICL2 to the TM5 shown by the yellow column between the aa position 259 - 407. Two vertical, black lines were observed in the metal binding plot indicating STEAP2 possesses two binding sites for heme ligands at the aa position 316 - 409 residing at TM4. Further, 5 natural variants have been observed within the canonical STEAP2 isoform 1 indicated by 5 vertically coloured lines within the variant plot. The first Single-Nucleotide Polymorphism (SNP) was found on ICL1, the second SNPs was identified on ICL2 and the third SNP was located at TM1. The fourth and fifth SNPs were assigned to ICL6. This suggests, that STEAP2 has several natural Single-Nucleotide mutations with exception for its ECLs. Given the absence of the SNP from the ECLs of STEAP2, any future design of potential immunogens situated on the extracellular site of the

protein were not affected. Based on the UniProt's information, one post-translational modification (PTM) has been identified at the ICL6 near the C-terminus indicating a phosphorylation at the aa position 483. Again, this was irrelevant regarding potential immunogen regions, since it was not located at the protein's ECLs (see **Figure 3.8**).

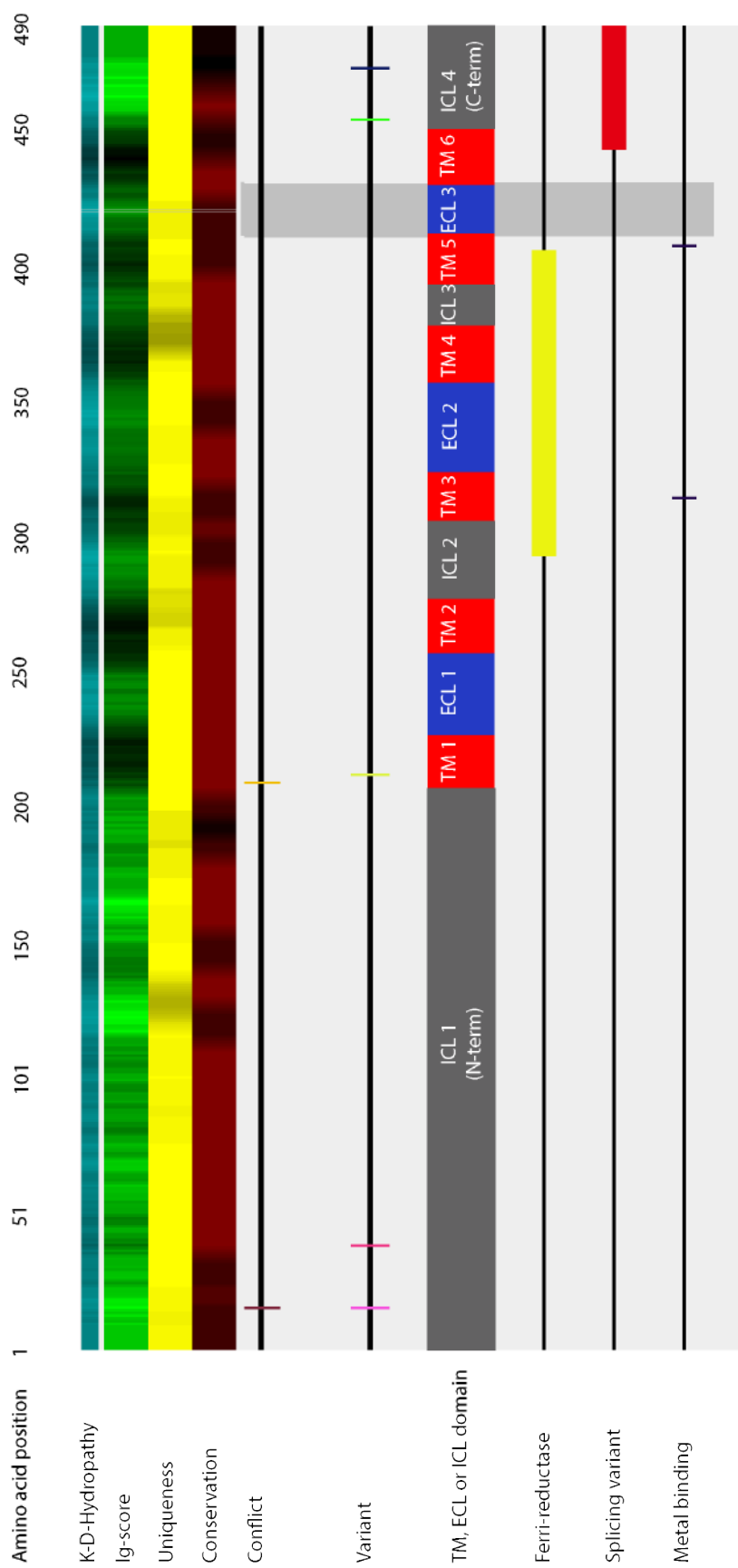


**Figure 3.8 AbDesigner output for STEAP2 protein**

. Amino acid sequence of STEAP2 was retrieved from UniProtKB - Q8NFT2, STEA2\_HUMAN). The protein amino acid sequence positions are indicated as numbers in the top row. The target protein was analysed for the following parameters: Chou-Fasman : secondary structure; K-D-Hydrophathy: Hydrophathy plot; Ig-score: Immunogenicity-score (green colour code); Uniqueness (yellow colour code); Conservation: protein conservation (%; red colour code); conflict (based on any literature linked to the UniProt database); variants: based on single nucleotide polymorphisms (SNP, pink, vertical lines); topology: transmembrane (TM, red), extracellular loop (ECL, blue) or intracellular loop (ICL, grey); ferri-reductase activity (yellow); splicing variants: other existing isoforms; metal binding site (vertical, short lines). Output was provided by AbDesigner and modified illustration

### **3.3.3 Ab mapping to STEAP2's ECLs suggested three targetable immunogens leading to selection of four commercial Abs**

After having identified three ECLs within the STEAP2 protein, coupled to isolation of their respective aa sequences, the next step was to specify the most promising immunogen region. This was addressed by creating a commercial anti-STEAP2 Ab list of which known (available) immunogen regions were mapped to the protein's ECLs (based on the datasheet information of the Abs) to determine the final immunogen sequence. The objective was to identify the most promising commercial Ab candidate for future proof-of-concept studies by evaluating its STEAP2 binding ability using western blotting and fluorescence microscopy. In total, 46 commercial, polyclonal anti-STEAP2 Ab (anti-STEAP2 pAb) suppliers were identified (Appendix 1, **Table A1.1**). The number of anti-STEAP2 pAbs was reduced down to a total of four commercial, anti-STEAP2 pAb lead candidates by the identification of their known aa sequences for the immunogen regions they have been raised against. This set of Abs formed the Ab panel (Ab1- 4) and were the only Abs identified, which targeted the ECLs regions on STEAP2 (**Table 2.5**). Therefore, they were evaluated for the best STEAP2 binding ability (Chapter3, **Section 3.3.5**). The known commercial anti-STEAP2 pAbs' immunogen regions overlapped with individual aa sequences of the ECLs on STEAP2 resulting in four final immunogens (Immunogen1 - 4) (**Table 3.4**). Immunogen1 and 2 were identified for STEAP2/ECL1 and differed in 7 aa. While Immunogen1 region began at the aa position of 226, Immunogen2 started at the aa position 233. No ECL2 matching anti-STEAP2 pAb was available. However, its known aa sequence formed the third Immunogen3. Moreover, Immunogen4 was exclusively located at STEAP2/ECL3 (**Table 3.4 and Figure 3.9**). Having identified four immunogenic regions on STEAP2's ECLs, these regions were narrowed down to shorter peptide sequences to ensure high specificity for the Ab development. In order to identify more specific, targetable peptides (immunogens) on STEAP2's ECLs, a default peptide length of 15 aa was pre-set for the analysis using AbDesigner (as recommended by the supplier).

**Table 3.4 Identified immunogen regions after Ab-ECL mapping**

. ECL: extracellular loop 1 - 3 (ECL1 - 3); Immunogen and aa sequence: Ab's immunogen region with respective amino acid sequence; aa position: number indicates the exact amino acid position within the STEAP2 protein; N/A: not available.

ECL - AB	aa sequence	aa position
ECL1	YSFVRDVIHPYARNQQSDFYKIPIEIVNKT	229 – 258
AB1 - Immunogen	FFLYSFVRDVIHPYARNQQSDFYKI	226 – 253
AB2- Immunogen	FFLYSFVRDVIHPYARNQQSDFYKI	226 – 253
Immunogen1	YSFVRDVIHPYARNQQSDFYKI	229 - 253
ECL1	YSFVRDVIHPYARNQQSDFYKIPIEIVNKTR	229 – 258
AB3- Immunogen	DVIHPYARNQQSDFYKIPIEIVNKTLPIV	233 – 262
Immunogen2	RDVIHPYARNQQSDFYKIPIEIVNKT	233 – 258
ECL2	RRSERYLFLNMAYQQVHANIENSWNEEE VWRIE	326 – 358
AB - Immunogen N/A	N/A	N/A
Immunogen3	RRSERYLFLNMAYQQVHANIENSWNEEE VWRIE	326 – 358
ECL3	GWKRAFEEYYRFYTPPN	414 – 431
AB4 - Immunogen	VALLISTFHVLIYGWKRAFEEYYRFTPPN FVLALVLPISIVLGGKILFLPCISRKLKRIKKG WEKSQFLEEEMGGTIP	400 – 480
Immunogen4	GWKRAFEEYYRFYTPPN	414 – 431

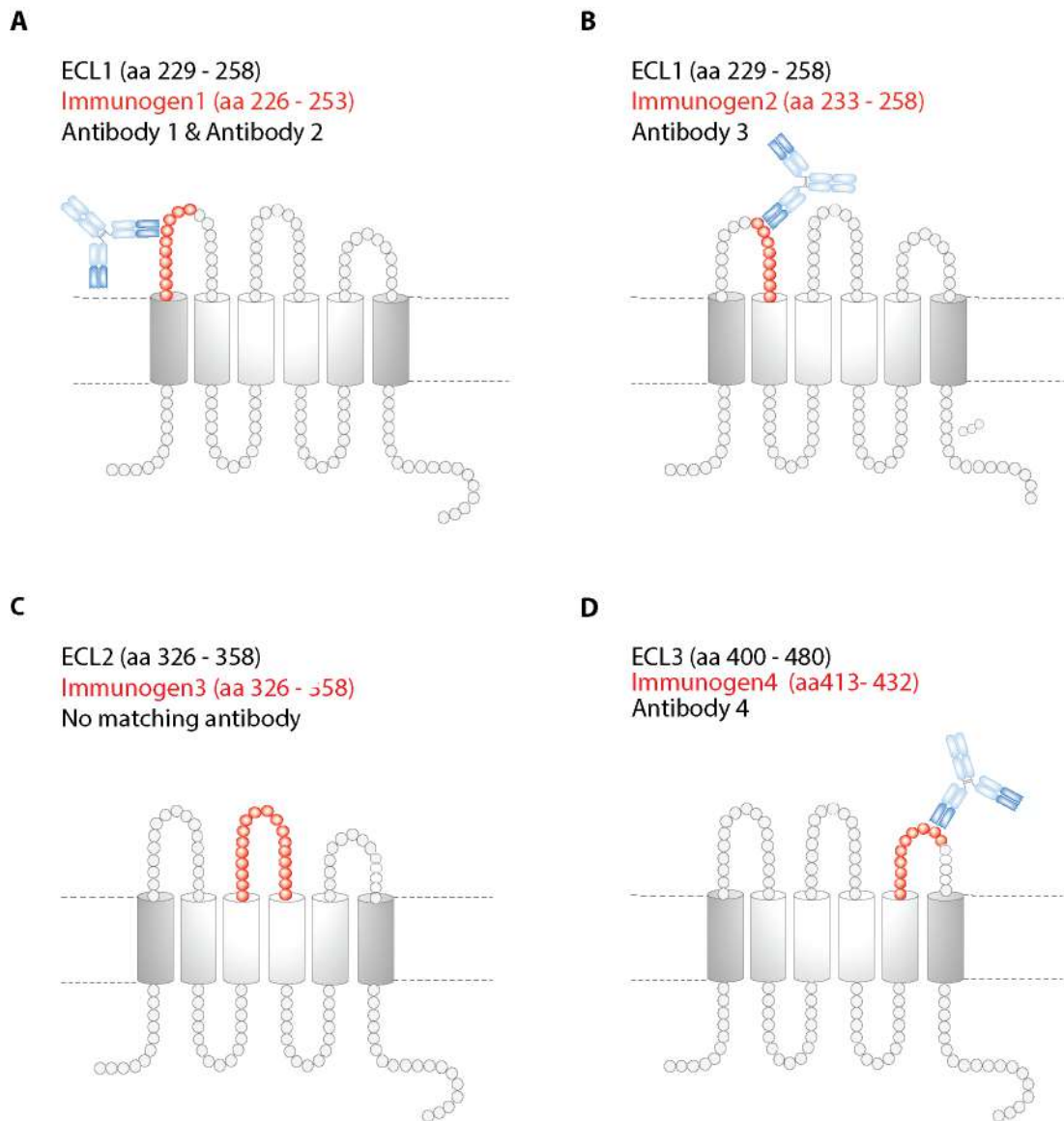


**Figure 3.9 Identified immunogen regions on the ECLs of STEAP2.** The immunogen regions are displayed with their respective amino acid sequence position within the full-length protein and matching commercial anti-STEAP2 antibodies. A) Immunogen1 is located on STEAP2/ECL1 and is targeted by two Abs, Ab1 and Ab2. B) Immunogen2 is located to STEAP2/ECL1 and being targeted by Ab2 and begins 7 amino acids later compared to Immunogen1. C) Immunogen3 is located to STEAP2/ECL2 with no matching commercial anti-STEAP2 Ab currently available. D) Immunogen4 is located to STEAP2/ECL3 and is targeted by Ab4. aa: amino acid position within the full-length human STEAP2 protein. Blue: IgG Ab; red: immunogen region; grey: human STEAP2 protein; dashed lines: categorization to extracellular (upper), trans-membranous (middle) or intracellular domains (lower).

### 3.3.4 Peptide5 is the most suitable peptide sequence for immunogen design for hybridoma Ab development

The four identified immunogen regions (**Table 3.4** and **Figure 3.9**) were investigated for three relevant properties for Ab development, which were: immunogenicity, conservation and uniqueness. The immunogenicity of a peptide plays a crucial role in generating a high immune response in species for *in-vivo* Ab production. Therefore, the immunogenicity score (Ig-score) of each ECL was further analysed to select an appropriate peptide with sufficient immunogenicity (antigenicity). The lower the Ig-score, the higher its predicted immunogenicity. The conservation was also taken into account to determine the cross-reaction of the peptides, present in any other species. Vice-versa, the uniqueness score represents the similarity of the peptide to any other existing protein (peptide). The lower the uniqueness-score, the more likely the probability, that there was no other protein. This was important to determine for any cross-reactions and to predict unwanted off-target side-effects. **Figure 3.10**, **Figure 3.11** **Figure 3.12** represent AbDesigner's output for Immunogen1 – 4. In total, five peptides were identified with a pre-set peptide length of 15 aa. This resulted in two unique peptides for both ECL1 and ECL2, whereas only one peptide was identified for ECL3 (**Figure 3.10**, **Figure 3.11** and **Figure 3.12**, ).

In **Figure 3.10**, the first 15-mer Peptide1 „YSFVRDVIHPYARNQ” was selected as one potential peptide situated at the beginning of ECL1 with an Ig-score of 247, which implied moderate immunogenicity. The peptide was well conserved as indicated by the bright red conservation region with a 100% overlap in mouse and was allocated a uniqueness score of 160. These results suggested this peptide was of moderate immunogenicity, well conserved in mice, although unique as with no indicated similar proteins. The second Peptide2 „QSDFYKIPIEIVNKT“ was positioned at the end of ECL1. This peptide showed an Ig-score of 289, a uniqueness-score of 183 and 100% conservation in mice. This implies it was of moderate

immunogenicity, well conserved in mice with no other known similar proteins and therefore considered as quite unique (**Figure 3.10**).

Peptide3 „RRSERYLFLNMAYQQ“ was chosen for ECL2, which was located at the beginning of the loop. Here, an Ig-score of 235 and a uniqueness-score of 330 were indicated. Again, this suggested the peptide was moderately immunogenic. However, the low-moderate uniqueness-score indicated a 15% similarity to another protein (CD1E). Peptide4 „VHANIENSWENEEEV“, located on the ECL2, demonstrated an Ig-score of 234 and a uniqueness-score of 152. Therefore, a moderate immunogenicity was considered. The low-moderate low uniqueness score indicated that this peptide may of greater uniqueness than Peptide3. Dark red/black coloured conservation region implied, that the peptide was not well-conserved with only 22% presence in mice (**Figure 3.11**). As identified by „GWKRAFEEEEYYRFY“, Peptide5 was located to ECL3 to which an Ig-score of 203 and a uniqueness-score of 390 were ascribed indicating moderate immunogenicity with less uniqueness. It showed an 11% similarity to two other proteins (K175 and MOCOS). The conservation region was dark-red/black indicating the peptide was of low conservation with a 22% similarity in mice species (**Figure 3.12**).

Taken together, all Ig-scores were considered as moderately immunogenic suggesting all identified peptides may be employed as peptides for Ab generation. However, the peptides were ranked for their immunogenicity from the highest to the lowest as follows: Peptide5 > Peptide3 > Peptide4 > Peptide1 > Peptide2 (**Table 3.7**) Based on the desired three properties for the peptide design, Peptide5/ECL3 was considered as the most immunogenic peptide, and therefore selected as a suitable immunogen peptide for future mAb development.

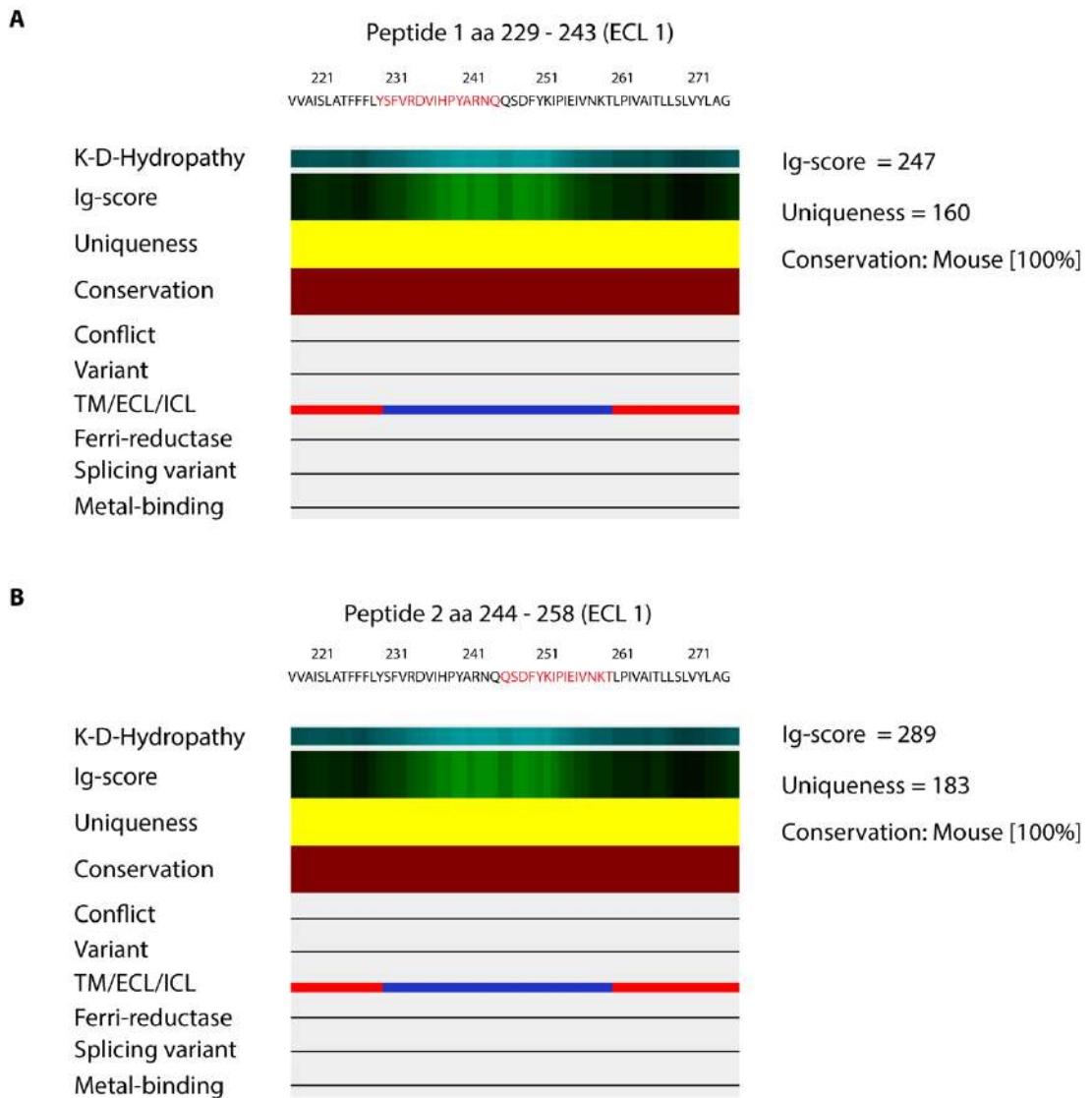


**Figure 3.10 AbDesigner output for Peptide1 and 2 (STEAP2/ECL1).** The analysed peptide of interest (amino acid sequence) is highlighted in red. A) Peptide1 is positioned at aa 229 - 243 (ECL1) and shows slightly higher immunogenicity and higher immunogenicity than Peptide2. B) Peptide2 is positioned at aa 244 - 258 (ECL1). The peptides were analysed for the following protein features by AbDesigner protein databases. Hydrophathy (K-D-Hydrophathy); Immunogenicity (Ig-score); uniqueness (yellow colour code, where bright yellow is highly unique and dark yellow is less unique); peptide conservation (red colour code; bright red is a highly conserved region and dark red is a less conserved region); conflict: any conflicts with protein databases; variants: evolving by single nucleotide polymorphism (SNP); topology classified in transmembrane (TM in red), extracellular (ECLs in blue) and intracellular domains (ICLs in grey); ferri-reductase activity; splicing variants and metal binding sites (black dot); aa: amino acid position within the STEAP2 protein. Output was provided by AbDesigner and modified for graphical illustration.

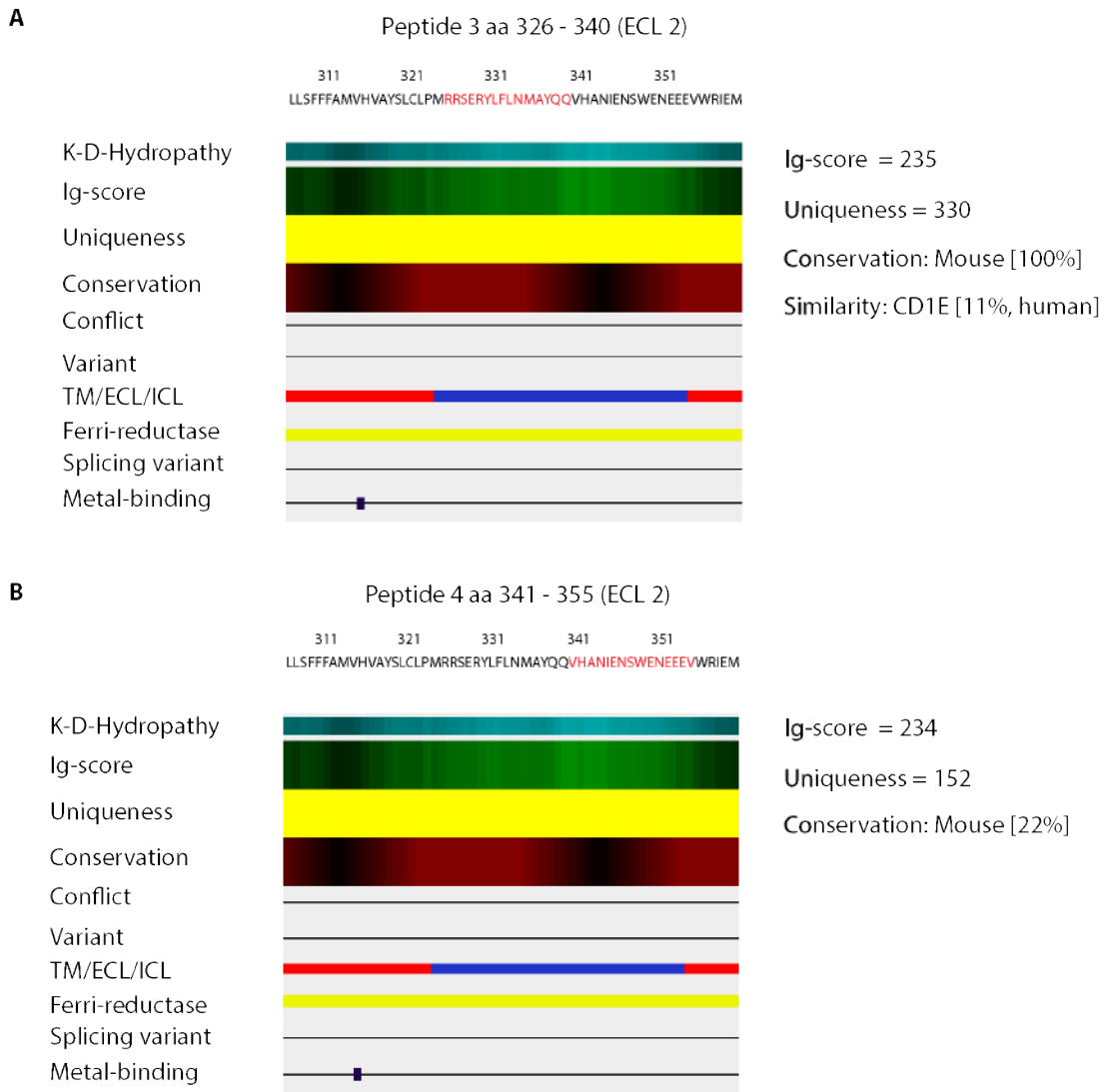


**Figure 3.11 AbDesigner output for Peptide3 and4 (STEAP2/ECL2).** The analysed peptide of interest (amino acid sequence) is highlighted in red. A) Peptide3 is positioned at aa 326 - 340 (ECL1) and shows very similar moderate immunogenicity to Peptide4. B) Peptide4 is positioned at amino acid 341 - 351 (ECL1) but demonstrates higher uniqueness than Peptide3. The peptides were analysed for the following protein features by AbDesigner. Hydrophathy (K-D-Hydrophathy); Immunogenicity (Ig-score); uniqueness (yellow colour code where bright yellow is highly unique and dark yellow is less unique); peptide conservation (red colour code; bright red is a highly conserved region and dark red is a less conserved region); conflict: any conflicts with protein databases; variants: evolving by single nucleotide polymorphism (SNP); topology classified in transmembrane (TM in red), extracellular (ECLs in blue) and intracellular domains (ICLs in grey); ferri-reductase activity; splicing variants and metal binding sites (black dot). aa: amino acid position within the STEAP2 protein. Output was provided by AbDesigner and modified for graphical illustration.

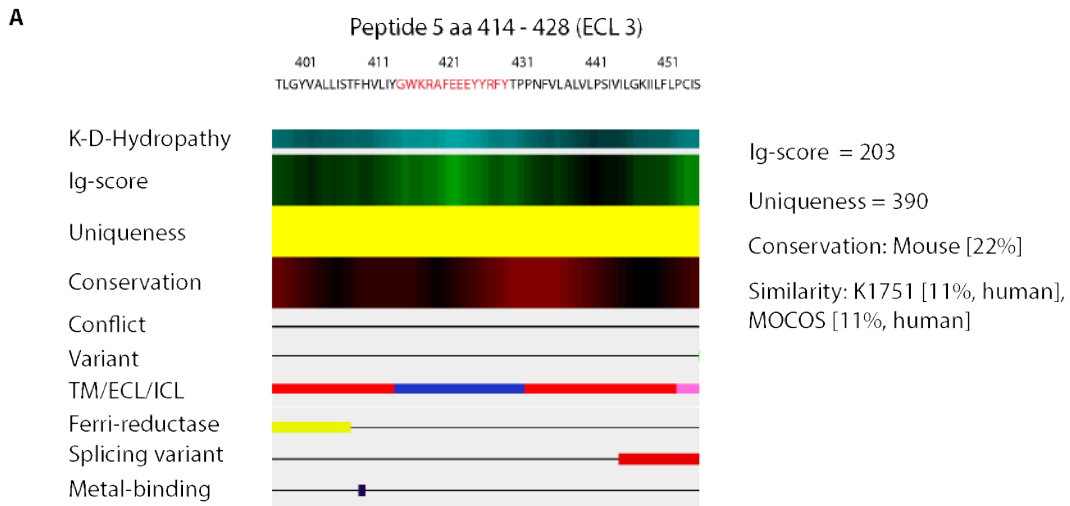


**Figure 3.12 AbDesigner output for Peptide5 (STEAP2/ECL3).** The analysed peptide of interest (amino acid sequence) is highlighted in red. A) Peptide5 is positioned at aa 414 - 428 (ECL3) and shows moderate immunogenicity. The peptide was analysed for the following protein features by AbDesigner: Hydropathy (K-D-Hydropathy); Immunogenicity (Ig-score); uniqueness (yellow colour code where bright yellow is highly unique and dark yellow is less unique); peptide conservation (red colour code; bright red is a highly conserved region and dark red is a less conserved region); conflict: any conflicts with protein databases; variants: evolving by single nucleotide polymorphism (SNP); topology classified in transmembrane (TM in red), extracellular (ECLs in blue) and intracellular domains (ICLs in grey); ferri-reductase activity; splicing variants and metal binding sites (black dot). aa: amino acid position within the STEAP2 protein. Output was provided by AbDesigner and modified for graphical illustration.

**Table 3.5 Analysed features to compare Peptides1 – 5.** Individual peptides with matching extracellular domains (ECL1 - 3) are illustrated with respective amino acid position (aa pos.) within the full length STEAP2 amino acid sequence. Ig: immunogenicity score (indicated by number, green colour code where dark green is highly immunogenic, moderate green is moderately immunogenic and light green is lower immunogenic). Peptide conservation indicated in percentage (%) and the presence in other species (red colour code; bright red is a highly conserved region and dark red is a less conserved region); U: uniqueness (numbers indicate uniqueness rank, blue colour code; bright blue is highly unique, moderate blue is moderately unique and dark blue is less unique); S: similarity of the peptide sequence to other human proteins indicated as percentage (%); CD1E: T-Cell Surface Glycoprotein; K1751: cilia and flagella-associated protein; MOCOS: Molybdenum Cofactor Sulfurase; Pep1 – 5: Peptide1 - 5; ECL1 – 3: extracellular loop1 – 3; Ms: Mouse species.

Pep/ ECL	aa pos.	Ig	Conservation	Uniqueness	Similarity
Pep1/ECL1	229 – 243	247 <span style="color: green;">■</span>	Ms, 100%	160 <span style="color: blue;">■</span>	
Pep2/ECL1	244 – 258	289 <span style="color: lightgreen;">■</span>	Ms, 100%	183 <span style="color: blue;">■</span>	
Pep3/ ECL2	326 – 340	235 <span style="color: green;">■</span>	Ms, 100%	330 <span style="color: lightblue;">■</span>	CD1E, 11%
Pep4/ ECL2	341 – 358	234 <span style="color: green;">■</span>	Ms, 22%	152 <span style="color: blue;">■</span>	
Pep5/ ECL3	414 – 428	203 <span style="color: green;">■</span>	Ms, 22%	390 <span style="color: lightblue;">■</span>	K1751, 11% MOCOS, 11%

### 3.3.5 Ab panel detected overexpressed STEAP2 in PC3 cells and low expression levels in PNT2 cells

After one unique Peptide5 was determined for the potential anti-STEAP2 mAb production, it was of great interest to characterize the previously identified commercial anti-STEAP2 pAbs (Ab1 – 4) for their linear STEAP2 protein binding ability by Western blotting. In cancerous PC3 cells, substantially increased STEAP2 protein levels were detected by Ab1 - 4 opposed to lower protein levels in normal PNT2 cells (**Figure 3.13** and **Table 3.6**). These were clearly demonstrated by the visible bands located at molecular size of STEAP2 at approximately 56kDa (**Figure 3.13**).

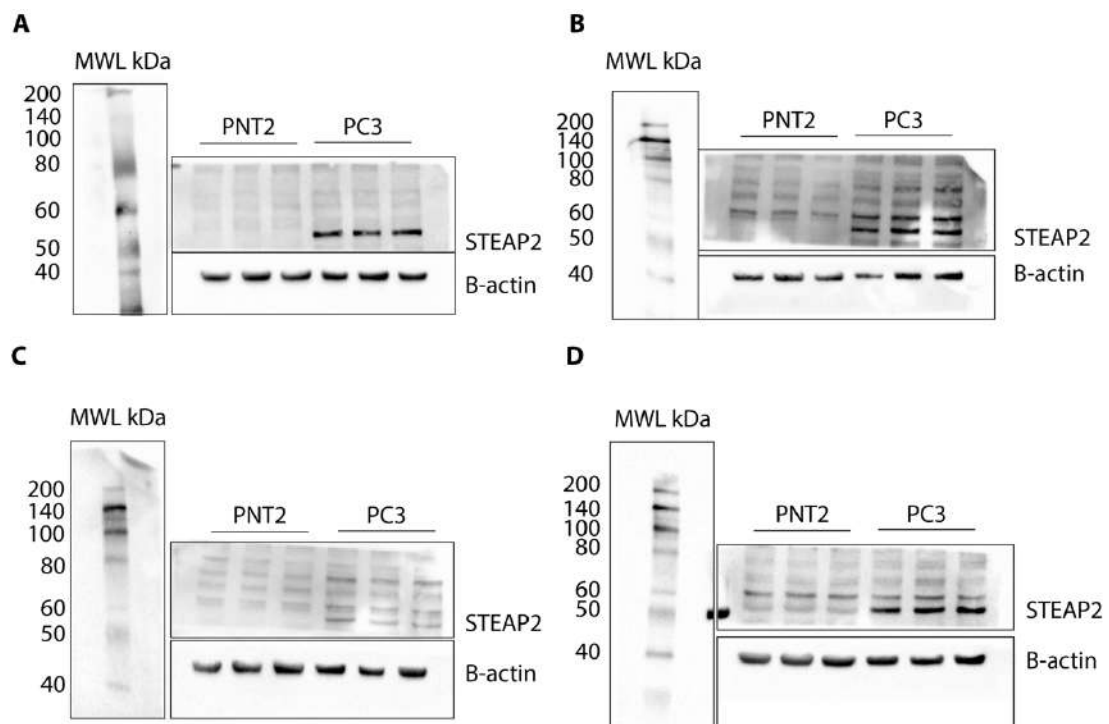


**Figure 3.13 STEAP2 protein analysis using the anti-STEAP2 pAb panel.** Four commercial, polyclonal anti-STEAP2 antibodies “Ab1 – 4” were utilised to study the protein expression of STEAP2 (56 kDa) by Western blotting. The normal PNT2 and cancerous PC3 cells were included in technical triplicate per cell line per blot. Each blot illustrates the biotinylated molecular weight ladder (MWL in kDa, left). The PNT2 cells show lower and the PC3 cells express higher STEAP2 protein levels. A) Ab1/ECL1. B) Ab2/ECL1. C) Ab3/ECL1. D) Ab4/ECL3. Rectangular boxes show where the blot was cut and re-assembled for densitometry analysis (N = 3).

The greatest significant difference in the STEAP2 protein expression was observed for Ab2 with a fold increase of 17.26 (p-value = 0.001), while Ab4 ranked second with a 11.75-fold change (p-value = 0.001), respectively. It is, however, notable that both Ab2 and 4 demonstrated the highest non-specific background noise, with many additional bands. Ab1 and Ab3 substantially expressed higher STEAP2 protein levels compared to the normal PNT2 cells with a 8.319 fold change (p-value = 0.005) and 7.178 fold change (p-value = 0.012), respectively (**Table 3.6**). Based on the fold change in protein expression, the antibodies were further ranked for their STEAP2 binding ability from the highest to the lowest (poorest) as follows: Ab2 < Ab4 < Ab1 < Ab3. To conclude, the antibodies have performed differently in their capacity to detect linear STEAP2 protein. However, each individual Ab was considered to be of good quality and suitable for the western blotting technique.

**Table 3.6 STEAP2 expression levels in fold change.** The fold change was measured by comparing of the expression levels in PC3 cells opposed to normal PNT2 cells using the commercial polyclonal anti-STEAP2 Ab panel. Upregulation: +; p-value: where  $p^* < 0.05$ ,  $p^{**} < 0.01$  and  $p^{***} < 0.001$  (N=3).

Ab	Fold-change	P-value
Ab1	+8.319	0.005**
Ab2	+17.26	0.001**
Ab3	+7.178	0.012*
Ab4	+11.75	0.001**

### 3.3.6 Ab panel detected intracellular STEAP2, whilst Ab4 demonstrated exclusive cell surface location

The anti-STEAP2 pAb panel was assessed for their STEAP2 binding quality by fluorescence microscopy to investigate their ability to recognise STEAP2 in a 3D conformational like structure. In PC3 cells, staining of STEAP2 resulted in a strong fluorescent signal using Ab1 – 4 (**Figure 3.14**). In contrast, low fluorescent signal was observed in healthy PNT2 cells (**Figure 3.15**). Ab4 detected STEAP2 prominently at the cell-surface in PC3 cells shown by an accumulation of fluorescent signal at the cell periphery, indicating plasma membrane localisation besides the presence of intracellular punctuates. In contrast, the Ab1 – 3 exhibited a fluorescent

signal as clustered punctuates suggesting intracellular presence such as in the Golgi apparatus. Ab1, Ab2 and Ab3 demonstrated a strong fluorescent signal throughout the cell, albeit no cell membrane specific fluorescence was observed (**Figure 3.14**). Therefore, Ab4 exhibited the best STEAP2 binding by fluorescence microscopy as it demonstrated both intracellular as well as cell surface STEAP2 protein in PC3 cells. In healthy PNT2 cells, medium-sized fluorescent agglomerates at lower fluorescent signal intensity was a common staining pattern compared to the PC3 cells. This implied a significantly lower STEAP2 expression when using all Abs compared to the stronger fluorescent signal in STEAP2 overexpressing PC3 cells. These small fluorescent punctuates are likely to represent an intracellular localisation such as the Golgi apparatus (**Figure 3.15**).

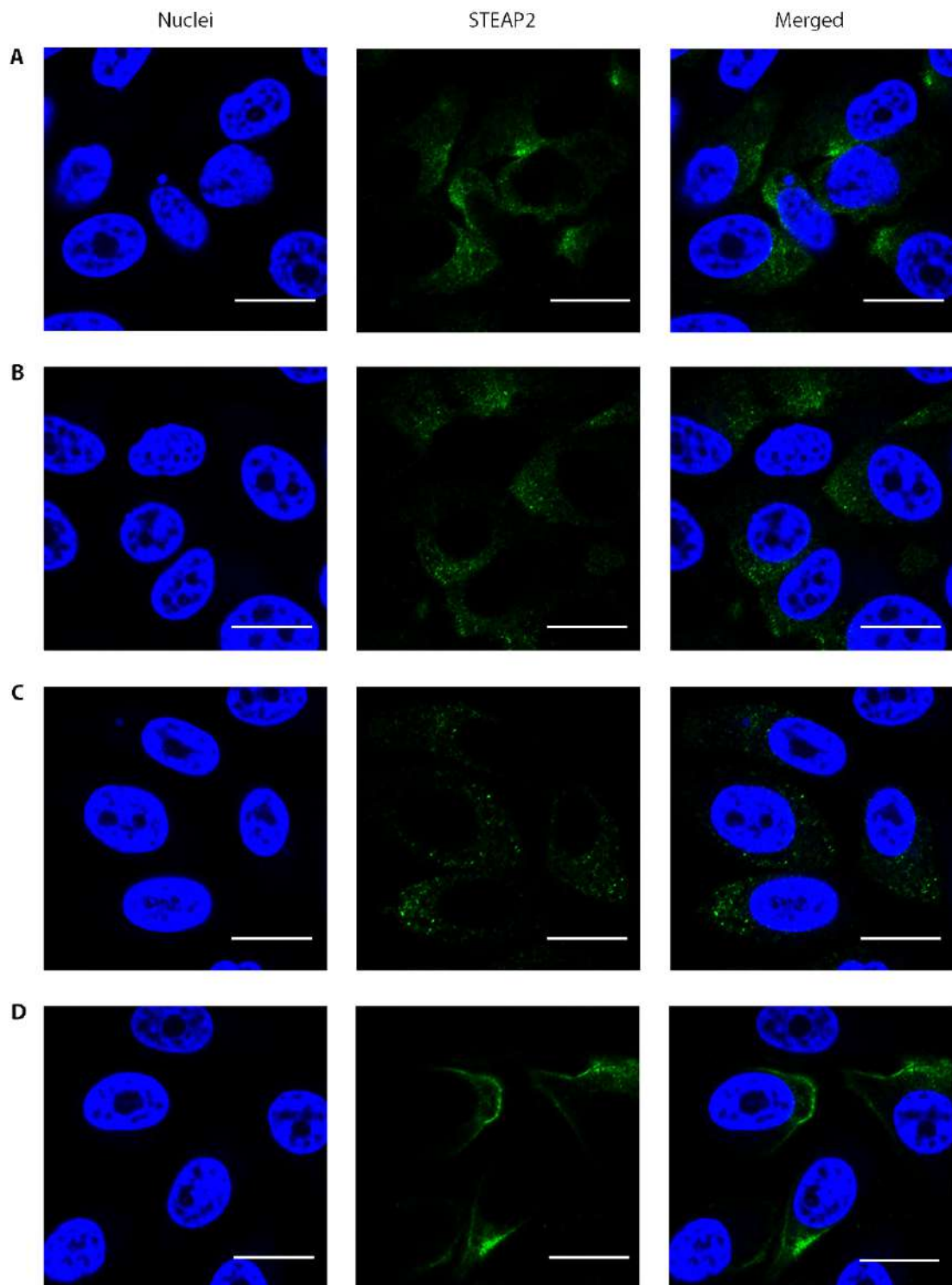


**Figure 3.14 Higher STEAP2 expression in PC3 cells by confocal microscopy.** Ab panel: A – D. A – C) Ab1, 2, 3 (STEAP2/ECL1); D) Ab4 (STEAP2/ECL3). Nuclei: blue; STEAP2: green; merged: overlap of blue and green channel. Images were acquired with a 63x objective zoom of a Confocal Laser Scanning Microscope (LSM 710, Zeiss, Germany). Scale bar = 20 $\mu$ m (N = 3).

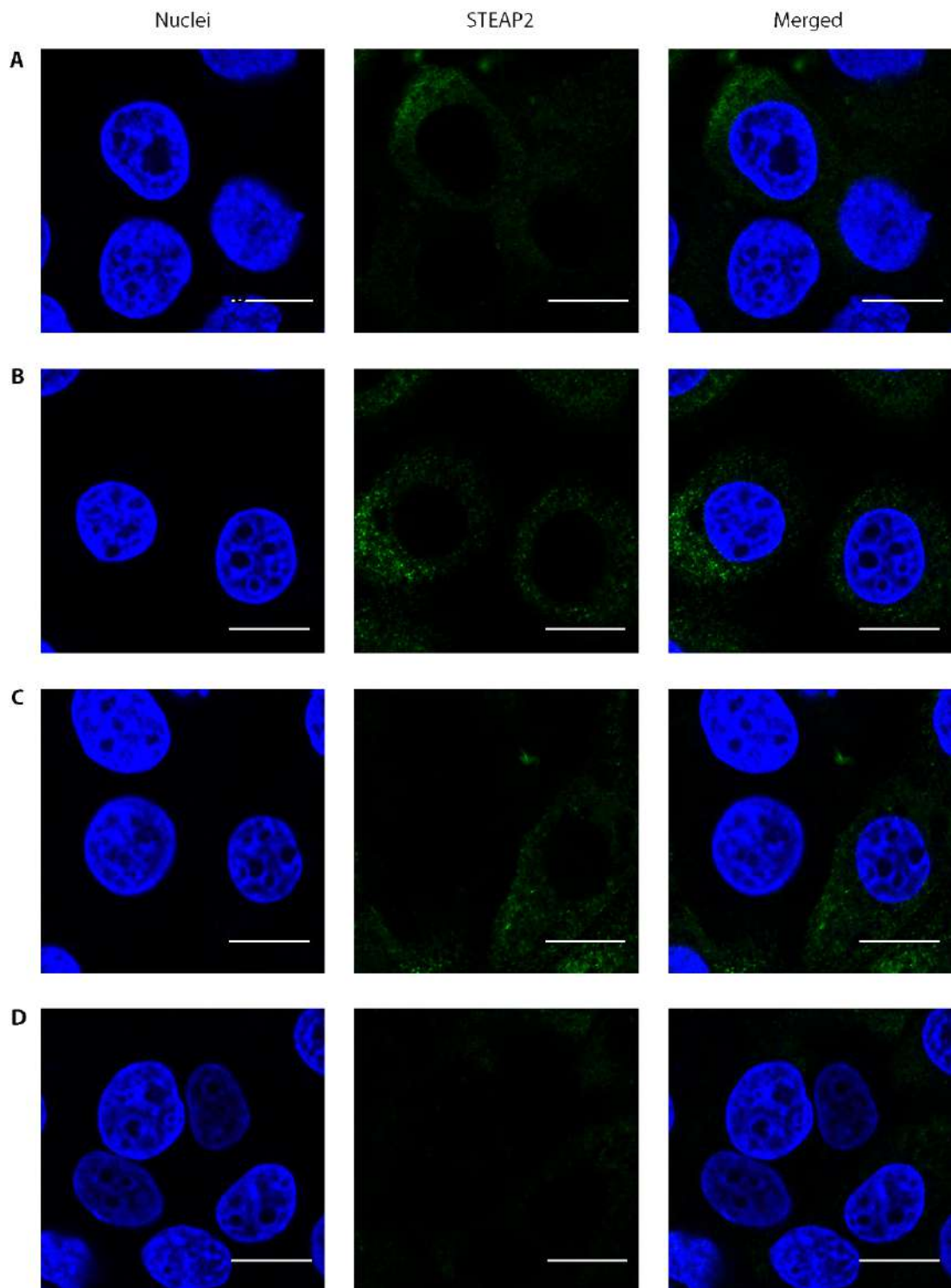


**Figure 3.15 Lower STEAP2 expression in PNT2 cells by confocal microscopy.** IF: immunofluorescence microscopy analysis. Ab panel: A - D. A - C) Ab1, 2, 3 (STEAP2/ECL1); D) Ab4 (STEAP2/ECL3). Nuclei: blue; STEAP2: green; merged: overlap of blue and green channel. Images were acquired with a 63x objective zoom of a Confocal Laser Scanning Microscope (LSM 710, Zeiss, Germany). Scale bar = 20 $\mu$ m (N = 3).

## 3.4 Discussion

---

### 3.4.1 Normal tissue distribution of STEAP2

This chapter aimed to investigate, if STEAP2 was a viable biotherapeutic molecular drug target. Therefore, STEAP2's normal tissue distribution was studied by IHC of TMAs containing 33 different normal (disease-free) human tissues. This present study has used high grade PCA tissues of known STEAP2 expression as appropriate positive controls to compare to STEAP2's expression in normal tissues (Burnell *et al.*, 2018). Moreover, the anti-STEAP2 Ab used for IHC analyses in this study has been previously validated by a past study for IHC studies (Burnell *et al.*, 2018).

The first normal tissue distribution analysis of STEAP2 was demonstrated by the Human Protein Atlas (HPA) (Uhlen *et al.*) Two approaches were common when comparing the HPA and the present study: the number of scientists, that analysed the tissues and the scoring system. First, the tissues were analysed by two trained scientists, contained biological replicates from individual samples (HPA minimum of  $N = 3$ ; this study minimum of  $N = 2$ ) per tissue. Additionally, this study analysed a second normal TMA as technical replicates. Further, the TMAs were analysed based on a semi-quantitative scoring system in both studies. Thereby, all tissues were scored for both staining intensity as well as staining level. Based on the HPA's information about IHC and annotation, it remains unclear, if the HPA allocated a numerical system according to their given staining intensity descriptive and staining level percentages. **Table 3.7** outlines the differences in the scoring systems in detail.

**Table 3.7 Differences in scoring systems used for the STEAP2 tissue expression analyses by the HPA and Chapter3.** HPA: Human Protein Atlas (Uhlen *et. al*). Both studies scored tissues for both staining intensity and staining level of different definitions for each range. STEAP2 expression descriptive range from negative (= neg), weak, moderate and strong. Staining level percentage was separated into four categories in both studies, however showing different percentage ranges. N/A: corresponding descriptive or scores not available. Information about the scoring system used for the HPA was retrieved March/2019 from: <https://www.proteinatlas.org/about/assays+annotation#ihk>.

Staining intensity				Staining distribution			
HPA		Chapter3		HPA		Chapter3	
Descrip.	Score	Descrip.	Score	%	Descrip-	Descrip	Sore
neg	N/A	neg - weak	1	N/A	Rare	< 25%	1
weak	N/A	medium	2	< 25%	N/A	>25 - 50%	2
moderate	N/A	strong	3	25 – 75	N/A	> 50 - 75%	3
strong	N/A			> 75%	N/A	> 75%)	4

The HPA examined 44 different tissues and reported medium STEAP2 expression for the majority of the tissues. Both studies analysed 28 common tissues of which only three tissues (*i.e.* ovary, skeletal muscle and spleen) were in accordance, demonstrating low STEAP2 expression. Of this common pool of tissues, the HPA reported medium expression for 25 tissues, as opposed to a low expression determined in Chapter3 within this thesis. Moreover, the HPA reported medium STEAP2 protein expression for an additional 16 tissues, which were not available in this study. However, the data presented in this Chapter reports low STEAP2 protein expression for an additional five tissues, which were not analysed in the HPA investigation

**Figure 3.16.**

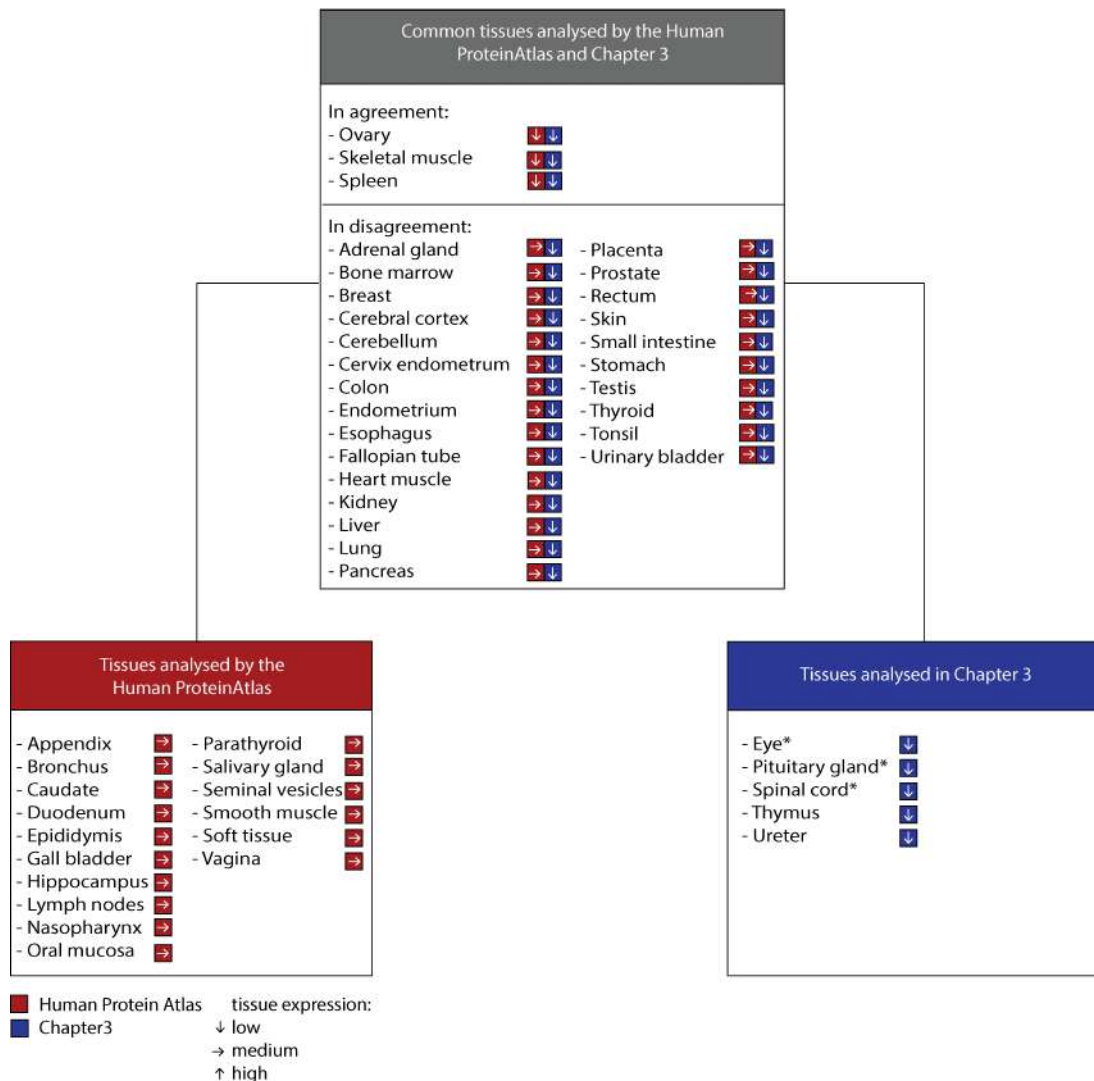


**Figure 3.16 Differences in the tissue profile of STEAP2 by the HPA/ Chapter3.** Red box: tissues which were analysed by Uhlen *et. al* but missing in the present study; blue box = tissue overview which were analysed by Nguyen Chi *et. al* but missing in Uhlen *et. al.*'s study; grey box: tissues analysed by both studies, horizontal grey line indicating tissues with identical STEAP2 expression (= in agreement) or a different STEAP2 expression (= in disagreement) found by both studies. STEAP2 's tissue expression is indicated by coloured boxes in red (Uhlen *et. al*) or blue (Chapter3). Arrow directions in the boxes display STEAP2's expression as follows: ↑: high expression; →: medium expression; ↓: low expression.

The major differences between the two studies were the Ab supplier, immunogen region (antigen) and the Ab validation process. Both applied Abs were suitable and validated for IHC analysis, but they were obtained from different suppliers (HPA -Sigmaaldrich; the present study - Abcam). Moreover, the Ab validation processes were different from each other. The HPA anti-STEAP2 Ab was validated by an antigen-microarray (containing 384 different antigens) showing a

single peak and thereby high specificity to the immunogen region. However, the reliability score is currently classified as „uncertain“ based on “consistency between Ab staining pattern, available RNA sequence, gene and protein characterisation data as well as independent Ab targeting the same protein“. Additional Western blotting data provided by the HPA implies, that the utilised Ab does not detect STEAP2 with high specificity. The HPA reported intracellular location to vesicles for STEAP2 but also states, that its location is not consistent with its protein expression data shown by fluorescent staining. Further, a different cell line (A549) was used for fluorescent microscopy than the PC3 and PNT3 cells in the present Chapter3. The Chapter3 data has used an anti-STEAP2 pAb, which has been previously validated and a clear association was demonstrated between increasing STEAP2 expression and prostate cancer aggressiveness by IHC/TMA (Burnell *et al.*, 2018). Moreover, Chapter3 has confirmed, that this anti-STEAP2 pAb used by Burnell *et. al* is able to detect STEAP2 by Western blotting in the higher STEAP2 expressing cell line PC3 compared to normal PNT2 cells as control. Importantly, the two anti-STEAP2 Abs utilised by the HPA and Chapter3 target different immunogen regions (antigens). The HPA used an anti-STEAP2 Ab, which was specifically designed for the IHC application using a protein signature-tagged Ab (Zeiler *et al.*, 2012). Thereby, this anti-STEAP2 Ab targets an immunogen region located to 131 - 212 aa on STEAP2/ICL1 (, while this Chapter3 uses an anti-STEAP2 pAb specific to the 233 - 262 aa on STEAP2/ ECL1. This is very important to consider as although these anti-STEAP2 Abs bind the same target protein, this can result in a substantially different performance in Ab target binding affinity (Goldstein *et al.*, 2007; Kim *et al.*, 2016; Lin & Chen, 2014).

Lastly, as shown in the present Chapter3, all tissues exhibited very low STEAP2 protein levels compared to the PCA positive control tissues and they were all given a score of < 3 of 12 (low expression). Thus, the data indicates little off-target side-effects are likely to occur in these low STEAP2 expressing tissues. To conclude, a STEAP2 normal tissue distribution compared to high grade PCA tissue is provided

by the present Chapter3. Low STEAP2 expression was observed in 33 different tissues across the human body. Thereby, this study supports the hypothesis, that STEAP2 may be a viable target for drug delivery by Ab-based treatments, which may provide a benefit of little side-effects compared to conventional prostate cancer treatment.

### **3.4.2 Structural modelling of STEAP2 to identify targetable peptide sequences for immunogen design to generate mAbs**

A key aim of this Chapter3 was to identify a suitable peptide sequence (immunogen) on STEAP2 for future mAb production and to determine, if a commercial Ab with sufficient STEAP2 binding specificity was available for proof-of-concept studies. The objective was to identify accessible domains on the ECLs of STEAP2 and to narrow these down to shorter peptide sequences, which should exhibit sufficient immunogenicity. Structural analysis was performed using AbDesigner. Moreover, a list of all commercially available STEAP2 Abs was created following Ab mapping to STEAP2's ECL domains. This resulted in an anti-STEAP2 Ab panel, which was evaluated by fluorescence microscopy and Western blotting for their naïve and linear STEAP2 binding ability. There are different methods available to identify targetable peptide regions on a protein of interest such as an Ab-dependent method by Ab mapping or protein homology modelling approaches. Homology modelling describes the approach to virtually design a target protein's 3D conformation based on the availability of aa sequences that code for genes of the human genome with specifically high similarity (homology) to the protein of interest (Clementi *et al.*, 2013). This enables the modelling of ligand–protein complexes often used for drug development and this concept has been widely developed for small molecules. For example, a small molecule generally binds to a target protein by fitting into a very specific “pocket”. To model the ligand–protein interaction site, the aa sequences must be known for both the ligand and the target protein (Clementi *et al.*, 2013). For this approach, the Ab's Complementary Determining Regions (CDRs) would have represented the ligand. The disadvantage of using commercial pAbs was the difficulty

in obtaining the CDRs' sequences because pAbs detect multiple, heterogeneous epitopes (Stills, 2012). Hence, this method was excluded and not further considered.

The data obtained in this Chapter3 was thus based on the Ab-dependent aa based method with an additional fully integrated protein structural analysis by AbDesigner tool. The full length human STEAP2 protein's aa sequence was retrieved from the database UniProt, a consortium which hosts comprehensive descriptive information about existing (human) proteins. UniProt makes all sequenced proteins available online, providing basic information such as the aa sequence of a given protein, its isoforms and existing natural ligands (Holgerson *et al.*, 2010; Uhlén *et al.*, 2005). Following 2D modelling by SwissProt, mapping of commercial anti-STEAP2 pAbs with known immunogen regions to the three ECLs of STEAP2 enabled the prediction of Ab-dependent immunogens on the protein. This demonstrated, that STEAP2 possessed three accessible ECLs (ECL1, ECL2 and ECL3). Moreover, five unique peptides sequences were determined to reside on these ECLs (Peptide1, Peptide2, Peptide3, Peptide4 and Peptide5) with the highest immunogenicity observed for Peptide5, albeit moderate. After mapping, the anti-STEAP2 Ab list to the ECLs, it was narrowed down to four commercial anti-STEAP2 pAbs (Ab1, Ab2, Ab3 and Ab4) of which Ab4 exhibited the most favourable ability of binding and detecting STEAP2 in both naive and linear (denatured) protein structure using Western blotting and confocal microscopy. Therefore, Peptide5 located on STEAP2/ECL3, was considered as the most suitable peptide region for future mAb development.

The use of the AbDesigner tool provided a robust approach for the screening for suitable peptide sequences as immunogens on STEAP2 for Ab development. It was easy to use and only requires the protein sequence input (*e.g.* FASTA format) of the target protein, which can be accessed by common databases (*e.g.* UniProt and SwissProt) The data output was visualised, which is a unique service only provided by AbDesigner. The analysis combined many protein propensity factors, that

determine a successful immunogen, which was supported by a visual output as an overview. AbDesigner was created to support the prediction of immunogens with consecutive aa, called linear peptides (or epitopes if  $< 15$  aa). To begin with, the peptide length was therefore pre-set to 15 aa before the data input as recommended by AbDesigner. To ensure the target specificity, it is recommended to keep the peptide sequence short (Abcam, 2019; Grant, 2002).

Currently, one conventional peptide design option for mAbs is to use a short linear peptide sequence in contrast to the full-length protein. The advantage is the limited peptide length, typically about 10-20 aa long, which are in linear order (Abcam, 2019; Grant, 2002). A 15 aa long peptide was chosen by the default recommendation by AbDesigner. The topology results have shown, that STEAP2 possesses three ECLs containing four possible immunogens in total. These immunogens were analysed for immunogenic peptides with the pre-set peptide length resulting in give individual peptide sequences. Given the short, pre-set peptide sequence, the similarity of linear peptides to other proteins was considered as very low. The reason for the use of linear peptides is, that they may be more unique to a certain protein in order to raise an Ab with high target specificity. Linear peptides may also be more advantageous to reduce potential cross-reactions, while the likelihood for full-length proteins is higher as they contain far more immunogen regions (Abcam, 2019; Grant, 2002). Thereby, the resultant Ab may recognise several other immunogens besides the original peptide sequences, which may thereby increase the chances of cross-reactions. Shorter peptides are considered as low immunogenic, whereas higher immunogenicity is described for full-length proteins as they contain a far larger amount of potentially immunogenic peptides. The downside may be, that conformational immunogens (epitopes), which evolve by the protein's 3D structure, may be missed out. However, predicting for conformational immunogens represents a major challenge in peptide design and was not approached in this study (PacificImmunology, 2019). Further, full-length proteins may better represent 3D conformational immunogens, which mimic the actual target protein. However, full-

length proteins can be more difficult to synthesise versus shorter peptides (Grant, 2002; PacificImmunology, 2019). Full-length proteins display a greater risk of instability once they degrade. Therefore, linear peptides are more popular as antigens for the mAb production as scientists are able to design them with ease, while keeping costs at bay (Grant, 2002). To increase the immunogenicity of linear peptides, they are frequently being chemically modified by the addition of the Keyhole Limpet Hemocyanin carrier protein (KLH), which ensures sufficient immune response in the species due to its size (Di Pasquale *et al.*, 2015; Yang & Kim, 2015). To elicit a desired immune response in animal species to produce Abs, the immunogen needs to have sufficient immunogenicity. It is commonly anticipated, that peptides with higher immunogenicity may increase the immune response in animal species to produce a higher Ab titre (Di Pasquale *et al.*, 2015; Grant, 2002; Junutula *et al.*, 2008). Therefore, the identified ECLs have been analysed and ranked for their immunogenicity-score (Ig-score) from highest to the lowest immunogenic peptide. The peptide sequences were all of moderate immunogenicity including the highest ranked Peptide5. Higher immunogenicity has been shown not to ultimately guarantee the success of Ab generation (Pisitkun *et al.*, 2014). This was confirmed in the past by the generation of a human anti-Podocin Ab using a moderately immunogenic peptide (Ig-value 55). The target specificity of the Ab was confirmed by using a blocking peptide of different concentrations by fluorescence imaging (Pisitkun *et al.*, 2014). Taken this data into account, Peptide5 was ultimately selected based on its Ig-score, albeit with moderate immunogenicity.

Furthermore, AbDesigner's outputs takes the protein's hydrophathy, conservation, uniqueness and similarity to other proteins into account for the analysis. Hydrophathy analysis separates the protein into hydrophilic, amphiphilic and lipophilic parts and historically dates back to an established mathematical algorithm (Hopp & Woods, 1981). This gives information about where the protein is located within a cell (topology). This is important as it facilitates the identification of potential immunogens on the extracellular site (*e.g.* ECLs). Thereby, the accessibility of the

drug target was included by AbDesigner to increase the tool's power (Grant, 2002). Interestingly, the hydrophilic regions were identified for ECLs and ICLs, which were of moderate immunogenicity suggesting these regions contain a higher number in hydrophilic amino acids. Further, information was provided on the protein's conservation indicating its likelihood to be present in other species and thereby to cross-react. The data has shown that STEAP2 is not highly conserved and is present in more than 128 species. However, as this study has focused on identifying a short peptide as an immunogen, their conservation has been evaluated in further depth to reduce the probability of cross-reactivity. It can also be used to deliberately choose a cross-reactive Ab, which is often used in secondary fluorophore-labelled Abs to allow the application of primary Abs from different species. Moreover, information about a peptide or protein's conservation can be advantageous to selectively narrow down the species of interest in which the Ab therapeutic shall be therapeutically active or not. Peptide1, Peptide2 and Peptide3 were fully conserved (100%) in mice indicating that cross-reactions are likely to occur in this species. A lower conservation (22%) in mice, was observed for Peptide4 and Peptide5 suggesting the chances these peptide sequences may cross-react in mice are much lower compared to Peptide1 – 3. This Chapter3 data implied, that STEAP2 targeted Ab drugs are likely to cross-react with a few proteins in mice species. Moreover, the similarity score reflects the probability (%) of a selected peptide region to be present as a similar peptide or protein and can also be used to mirror the Ab's cross-reaction. Peptide3 was observed to share low structural similarity (11%) to the human CD1E protein. Its gene codes for the T-cell surface glycoproteins membrane associated form, which is required to accurately present glycolipid antigens on the cells' surface. However, this form is not active and only present in the intracellular compartment such as the Golgi apparatus, endosomes and lysosomes (see UniProtKB: P15812; Entry name: CD1E\_HUMAN). For Peptide5, two proteins were identified with low similarity (11%). One was the K1751 protein, which is a cilia and flagella-associated protein which is involved in the cilium movement (see UniProtKB: Q9C0B2; Entry name: CFA74\_HUMAN). The second protein, MOCOS, is the Molybdenum Co-factor Sulfurase. MOCOS partakes in

metabolic activity; however, little information is provided on the databases (see UniProtKB: Q96EN8; Entry name: MOCOS\_HUMAN). The similarity of the identified proteins with STEAP2 peptides needs to be addressed by future *in-vivo* studies to prevent potential off-target side-effects. Important post-translational modifications (PTM), splicing variants (isoforms) and single-nucleotide polymorphisms (SNPs, variants) were also considered. If the splicing position affects any of the identified targetable regions, it may be pertinent to omit these regions to avoid undesired peptide modification (*e.g.* shortening) (Van Eyk & Stastna, 2012). This may equally result by aa residue phosphorylation, leading to masking of the target peptide sequence. Although STEAP2 showed 2 additional splicing variants, the identified alternative splicing positions implied the ECLs remained unaffected. Thus, all Peptides1-5 on ECL1-3 are theoretically suitable to be used as antigens to produce anti-STEAP2 mAbs. SNPs were also taken into account, which showed STEAP2 (isoform a) possessed four SNPs. This is in line with a past finding that reported over 44 non-synonymous SNPs (nsSNPs) (Naveed *et al.*, 2016). The study indicated, that alterations in STEAP2 protein function as a result of the SNPs may led to more aggressive cancer phenotypic outcomes (Naveed *et al.*, 2016). It is however notable, that none of the SNPs identified in this study were present at STEAP2/ ECL3 which thus did not raise concern for the selection of Peptide 5. This demonstrates the peptide design approach using AbDesigner may require complementary literature research on the target protein given its limited SNP detection. In summary, the data highlights AbDesigner as a powerful tool to screen for desired peptide sequences, that may represent immunogens within a target protein for mAb development.

### **3.4.3 Ab panel evaluation and candidate selection**

The commercial anti-STEAP2 pAb lead candidates were analysed for their binding ability for linear and naïve STEAP2 protein. Therefore, fluorescence microscopy and Western blotting were conducted. Fluorescent staining using the commercial anti-STEAP2 pAbs, Ab1, 2 and 3, did not show sufficient detection of

any cell membranous STEAP2 protein in PC3 cells. The fluorescent signal for STEAP2 was present throughout intracellular compartments in PC3 and PNT2 cells. This signal pattern may suggest Golgi localisation or endosomal/ lysosomal co-localisation, which has been previously shown for STEAP2 by *STEAP2*-transfected HEK-293T cells (Hasegawa *et al.*, 2018; Korkmaz *et al.*, 2002; Ohgami *et al.*, 2006). However, fluorescent staining of STEAP2 using Ab4 showed cell membranous specific localisation alongside staining of the intracellular punctuates. Recently, an anti-STEAP2 mAb against the ECL2 was developed, which also showed a strong cell membranous location by fluorescent staining (Hasegawa *et al.*, 2018) supporting the hypothesis of STEAP2 as a protein to shuttle between the plasma membrane to the trans-Golgi network (Korkmaz *et al.*, 2005; Ohgami *et al.*, 2006). In contrast, Abs of polyclonal origin were used in the present study, which naturally bind to a heterogenous immunogen pool, as opposed to the anti-STEAP2 mAb highly specific to one, single immunogen region in ECL2 (Hasegawa *et al.*, 2018; Stills, 2012). However, the Chapter3 results demonstrated, that STEAP2's ECL3 represents an accessible domain for Abdrugs besides ECL2.

Moreover, STEAP2's cell membranous epitopes may have been masked after cell fixation, which is a widely known problem. Cell fixation may have also formed minor holes in the cell membrane, that provided Ab access to the intracellular site. This may explain why a Golgi-like fluorescence staining pattern can be observed especially in the PNT2 cell line without cell permeabilisation. This pattern was also present in PC3 cells using Ab1 – 4 in alignment with previous reports about its intracellular presence such as in the Golgi (Korkmaz *et al.*, 2005; Ohgami *et al.*, 2006). Thus, this study suggests Ab1, 2 and 3 are more suitable to detect intracellular STEAP2 protein by fluorescence staining but not cell membranous staining compared to Ab4. For Western blotting, a linear, denatured protein structure - different to its natural 3D conformation – is required. Normally, this protein originates from denatured cell lysates, a linear protein extract, that does not distinguish between the ECLs and ICLs (Forsström *et al.*, 2015; Taylor *et al.*, 2013). Western blotting was

more suitable as semi-quantitative analysis of the Ab panel to recognize linear STEAP2 protein, which was complemented by a more qualitative analysis for the sub-cellular localisation by fluorescence staining. All anti-STEAP2 Abs showed higher STEAP2 expression in cancerous PC3 cells compared to normal PNT2 cells in accordance with previous findings using Western blotting, albeit with different specificity to STEAP2 (Burnell *et al.*, 2018; Whiteland *et al.*, 2014). Ab2 and 4 demonstrated superior STEAP2 binding ability followed by Ab1 and Ab3 with the poorest binding ability. Ab1, Ab2 and Ab3 were recommended for Western blotting, whereas Ab4 was determined as unsuitable for this application by the supplier. Yet, Ab4 showed excellent target specificity, albeit with higher background associated with non-specific bands in Western blotting. In contrast, Ab3 detected STEAP2 in western blotting poorly, despite being suitable for the application by the supplier.

To conclude, Ab4 and performed well in both methods (**Table 3.8**, details are provided in **Table 2.5**. Further, Ab4 was the only antibody which showed excellent ability to detect the membrane location of STEAP2 and was thus selected as the Ab lead-candidate to take forward for *in-vitro* proof-of-concept studies.

**Table 3.8 Summary of the anti-STEAP2 Ab panel evaluation.** The antibodies were rated according to their performance in western blotting and fluorescence microscopy which resulted in Ab4 as the Ab lead candidate. Ab/ECL: Antibodies1 - 4 (AB1 - 4) with respective extracellular loops (ECLs). Applications used for the evaluation of the anti-STEAP2 Ab panel: WB: western blot, IF: Immunofluorescence microscopy. ELISA: Enzyme-Linked Immunosorbent Assay; FC: Flow Cytometry; Yes: good performance, no: poor performance. The conclusion was either "not selected" or "selected" for further studies.

Ab/ECL	WB	IF	Conclusion
AB1/ECL1	yes	no	not selected
AB2/ECL1	yes	no	not selected
AB3/ECL1	yes	no	not selected
AB4/ECL3	yes	yes	selected

### 3.5 Conclusion

---

The data generated in the current Chapter3 confirms STEAP2 is a viable drug target for Ab-based therapies. STEAP2 was shown to be higher expressed in prostate cancer tissues and only expressed at lower protein levels for a wide range of undiseased, human tissues meaning severe-side effects are unlikely to occur (by using Ab2 specific to ECL1 (aa 233 – 262)). Protein analysis of STEAP2 confirmed to be high in prostate cancer cells PC3 but low in normal PNT2 cells by western blotting strengthening the hypothesis of STEAP2 as a suitable therapeutic drug target for Abs to treat advanced prostate cancer. Structural protein analysis indicated the 14 amino acid long Peptide5 („GWKRAFEEYRFFY“) on STEAP2/ECL3 as the most immunogenic peptide region within STEAP2 suggesting it represents a promising antigen for future mAb generation. Analysis of a panel of commercial anti-STEAP2 pAbs by confocal microscopy showed anti-STEAP2 pAb targeting an immunogen on ECL3 detected cell surface STEAP2, one important prerequisite for Ab therapeutics. Since the anti-STEAP2 pAb (Ab4/ECL3) targets an immunogen region on STEAP2/ECL3 and is highly specific to cell-membranous STEAP2 it has been selected as the antibody lead candidate to take forward for proof-of-concept studies.

## 4 “Impact of an anti-STEAP2 Ab on invasive properties of prostate cancer cells *in-vitro*.”

### 4.1 Introduction

---

Data until date, including the previous Chapter3, have implied STEAP2 as a viable drug target. STEAP2 is abundant in advanced-staged prostate cancer tissues, while it is only present in lower levels in over 33 organs across the human body (see Chapter3, **Section 3.3.1**). Moreover, STEAP2 promotes cancer invasive properties such as cell migration and invasion *in-vitro* underlying cancer cell metastasis (Burnell *et al.*, 2018; Whiteland *et al.*, 2014). The previous Chapter3 has identified one commercial anti-STEAP2 pAb lead candidate (AB4/ECL3), which recognises both linear and naïve STEAP2 protein (Chapter3, **Section 3.3.3** and **3.3.4**). This insight raised the question, if advanced staged prostate cancer patients may profit from Ab-based therapies against STEAP2 overexpressing tumour cells. Thereby, the tumour cell killing specificity would be increased, while healthy cells can be spared to reduce adverse side-effects unlike the current treatments.

For example, the ADC technology may provide a benefit by increasing the tumour cell killing efficacy. Not only do ADCs rely on the ability of mAbs to specifically recognise tumour-specific, cell surface biomarkers, but ADCs safely shuttle a highly potent toxin into the cells via the attached mAb. Therefore, the Ab must bind STEAP2 with high specificity and trigger receptor internalisation for drug delivery. The ADC-receptor complex then shuttles to the lysosomes where the ADC is being degraded by lysosomal enzymes, thereby releasing the payload, which results in cancer specific cell killing (Carter & Senter, 2013; Chari, Miller, & Widdison, 2014; Drachman & Senter, 2013; Ducry & Stump, 2010; Senter & Sievers, 2012; Wu & Senter, 2005). Researchers commonly apply the indirect immunofluorescent method

by confocal microscopy or flow cytometry to study receptor internalisation. To visualise cell surface receptor, the primary Ab must be incubated at 4°C, while receptor internalisation is being initiated once the temperature is raised to 37°C (Cheng *et al.*, 2011; Vainshtein *et al.*, 2015). After this, a secondary detection Ab is being added. Given the multiple steps being applied, this method is not only time-consuming but also requires co-staining of the cell compartments to accurately determine the cell localisation. Recently, Promega has designed a kit to study receptor internalisation without co-staining additional organelles. It requires the alteration of the pH, since the Ab is being conjugated to a fluorophore dye, which is only active at the acidic pH 5 (Nath *et al.*, 2016). Thus, any observed fluorescence can be related to the localisation of the Ab to the acidic organelles such as the lysosomes (pH 4.5 – 5.5) and endosomes (pH 5.5 - 6.5) (Diering *et al.*, 2014; Hu *et al.*, 2015; Ishida *et al.*, 2013; Ritchie *et al.*, 2013). However, it demands a change to an acidic pH to localise the Ab-receptor complex before it has reached the acidic organelles, for instance at the cell surface (Nath *et al.*, 2016). STEAP2 resides in the Golgi, in the early endosomes and at the plasma membrane (Grunewald *et al.*, 2012; Hasegawa *et al.*, 2018; Korkmaz *et al.*, 2005; Ohgami *et al.*, 2006; Porkka *et al.*, 2002). Yet, it is uncertain if the ADC technology qualifies to target STEAP2 because it is unknown, if STEAP2 internalises and localises to the lysosomes after Ab binding.

Further, it is unknown, if the use of anti-STEAP2 Abs have an effect on the cancer invasive properties in prostate cancer cells in 2D monolayer cells and 3D spheroid cells. 2D cells are routinely used during the early drug development phase due to their cost-effectiveness and simplicity to culture to receive preliminary results (Hoarau-Véchet *et al.*, 2018; Huang & Gao, 2018). However, 2D cells lack more *in-vivo* like features to better physiologically represent the tumour tissue. Due to their monolayered cell arrangement 2D cells are directly exposed to drug treatments, which does not truly represent the drug penetration of tumours *in-vivo* (Hoarau-Véchet *et al.*, 2018; Huang & Gao, 2018). The use of 3D cells has bridged the gap between 2D *in-vitro* and *in-vivo* studies given their spheroidal architecture, which better mimics

a more physiological cell-cell interaction (Hoarau-Véchet *et al.*, 2018; Huang & Gao, 2018). The advantage of 3D cells include a better reflection of the structural heterogeneity of the tumour and its gene/ protein expression profile (Costa *et al.*, 2016; Hirschhaeuser *et al.*, 2010; Nunes *et al.*, 2019; Weiswald *et al.*, 2010). These properties make 3D cells powerful during the screening and selection process of drug candidates, tumour penetration and drug efficacy testing including Ab-based therapies (Edmondson *et al.*, 2014; Malandrino *et al.*, 2018; Phung *et al.*, 2011; Sant & Johnston, 2017; Zanoni *et al.*, 2016).

In order to shed light on these questions this chapter aimed to:

- (1) Assess the suitability of the ADC technology for the potential development of Ab-based drugs specific against STEAP2;
- (2) Evaluate the impact of the commercial anti-STEAP2 pAb lead candidate (AB4/ECL3) on the cancer invasive properties in prostate cancer cells.

Therefore, the objectives were to investigate the effect of the anti-STEAP2 pAb lead candidate (AB4/ECL3), previously identified in Chapter3, on cell migration, cell invasion and receptor internalisation. In addition, the effect of the anti-STEAP2 pAb lead candidate (AB4/ECL3) on cell viability was studied in both 2D and 3D cells.

## 4.2 Methods

---

### 4.2.1 Cell culture

#### 4.2.1.1 2D monolayer cells

The three cell lines PNT2, PC3 and HFF1 (Chapter2, Section 2.1) were routinely cultured as described in Chapter2, **Section 2.1.6.1**. For microscopy or absorbance-dependent endpoint analyses, cells were grown in DMEM phenol red-free, supplemented medium (Thermofisher Scientific, UK).

#### 4.2.1.2 3D PC3 spheroid cells

Approximately 5,000 PC3 cells were cultured and prepared as described in Chapter2, **Section 2.1.6.2**.

### 4.2.2 Assays to study the Ab's effect on cancer invasive traits

#### 4.2.2.1 Cell migration

Approximately 25,000 cells were prepared as described in Chapter2, **Section 2.1.6.4**. For the anti-STEAP2 pAb (AB4/ECL3) (Insightbiotechnology, UK) dose finding, PC3 cells were treated as summarised in **Table 4.1**.

**Table 4.1 Treatments for the cell migration anti-STEAP2 pAb (AB4/ECL3) dose finding assay**

Treatments are listed in the left column; brackets indicate Ab dose [ $\mu\text{g}/\text{ml}$ ]; +ctrl (untreat): positive control PC3 cells (untreated); +ctrl (IgG): positive control, anti-IgG isotype Ab treated PC3 cells; AB4: commercial, polyclonal anti-STEAP2 Ab directed against an epitope on its ECL3, Cell susp. [ $\mu\text{l}$ ]: volume of PC3 cells suspension used, Treat vol. [ $\mu\text{l}$ ]: treatment volume, Medium [ $\mu\text{l}$ ]: volume of cell culture medium required, Volume<sub>f</sub> [ $\mu\text{l}$ ]: total final volume.

Treatment [ $\mu\text{g}/\text{ml}$ ]	Cell susp. [ $\mu\text{l}$ ]	Treat vol. [ $\mu\text{l}$ ]	Medium [ $\mu\text{l}$ ]	Volume <sub>f</sub> [ $\mu\text{l}$ ]
+ctrl (untreat)	384	-	16	400
+ctrl IgG (20)	384	4.7	11.3	400
AB4 (5)	384	2.5	13.5	400
AB4 (10)	384	5	11	400
AB4 (20)	384	10	6	400

The dose finding experiment was conducted as a one-off test. For cell migration studies using single anti-STEAP2 pAb treatments, Ab1 (STEAP2/ECL1, stock concentration: 0.5 mg/ml, Insightbiotechnology, UK) or Ab4 (STEAP2/ECL3, stock concentration 1 mg/ml) were employed. For the dual Ab treatment a combination of both Ab1 and Ab4 was utilised. Positive controls used were untreated cells and cells treated with an anti-IgG isotype Ab (stock concentration: 1.7 mg/ml, Thermofisher, UK), which was unspecific to STEAP2. The single and dual Ab treatment preparations are summarised in **Table 4.2**. The analysis was carried out according to **Section 2.2.5.1** and the experiments were conducted in duplicate.

**Table 4.2 Treatments to assess the effect on cell migration after the single or dual anti-STEAP2 pAb treatment**

. Treatments are listed in the far-left column; brackets indicate Ab dose [ $\mu\text{g/ml}$ ]; +ctrl (untreat): positive control, untreated PC3 cells used to demonstrate their migratory property; +ctrl (IgG): positive control, anti-IgG isotype Ab treated PC3 cells; AB: antibodies; AB1: commercial, polyclonal anti-STEAP2 Ab directed against an epitope on its ECL1; AB4: commercial, polyclonal anti-STEAP2 Ab directed against an epitope on its ECL3; AB1+AB4: dual Ab treatment targeting ECL1 and ECL3, Cell susp. [ $\mu\text{l}$ ]: volume of PC3 cells suspension needed, Treat vol. [ $\mu\text{l}$ ]: treatment volume, Medium [ $\mu\text{l}$ ]: volume of cell culture medium required, Volume<sub>f</sub> [ $\mu\text{l}$ ]: final volume in total.

Treatment [ $\mu\text{g/ml}$ ]	Cell susp. [ $\mu\text{l}$ ]	Treat vol. [ $\mu\text{l}$ ]	Medium [ $\mu\text{l}$ ]	Volume <sub>f</sub> [ $\mu\text{l}$ ]
+ctrl (untreat)	384	-	16	400
+ctrl IgG (20)	384	4.7	11.3	400
AB1 (20)	384	16	-	400
AB4 (20)	384	8	8	400
AB1+AB4 (20)	384	12	4	400

#### 4.2.2.2 Cell invasion

Approximately 25,000 cells were prepared as described in Chapter2, **Section 2.1.6.4**. As positive controls, untreated PC3 cells or anti-IgG isotype Ab (Thermofisher, UK) treated PC3 cells were used with chemoattractant (20% FBS). As negative controls, PNT2 cells (with 20% FBS) and PC3 cells (without 20% FBS) were employed. Cells were treated as summarised in **Table 4.3**. The assay was conducted according to **Section 2.2.5.2** and was performed in triplicate.

**Table 4.3 Treatments for the cell invasion assay to assess the impact of the anti-STEAP2 pAb (AB4/ECL3) on invasive properties in PC3 cells.** Treatments are listed in the left column. +ctrl (untreat): positive control PC3 cells, untreated to demonstrate their migratory properties; +ctrl (IgG) (20 µg/ml): anti-IgG isotype Ab treated PC3 cells used as positive control; AB4 (20 µg/ml): commercial, polyclonal anti-STEAP2 Ab directed against an epitope on its ECL3; Cell susp. [µl]: volume of PC3 cells suspension needed; Treat vol. [µl]: treatment volume; Medium [µl]: volume of cell culture medium required; Volume<sub>f</sub> [µl]: final volume in total.

Treatment [µg/ml]	Cell susp. [µl]	Treat vol. [µl]	Medium [µl]	Volume <sub>f</sub> [µl]
+ctrl (untreat)	245	-	5	250
+ctrl IgG (20)	245	2.9	2.1	250
AB4 (20)	245	5	-	250

#### 4.2.2.3 Cell viability (2D monolayer cells)

Approximately 10,000 cells per well in a 96-well were cultured for 24 h before 24 h exposure to the treatment (**Table 4.4**). First, 50 µl of the old culture medium was replaced with 50 µl of the treatment and incubated for 24 h. The cell viability was assessed as described in Chapter2, **Section 2.2.5.3**. Absorbance was read at A = 570 nm using a fluorescence plate reader (POLARstar, BMG Labtech, UK). The cell viability experiments were conducted in triplicate.

**Table 4.4 Treatments for the MTT assay to investigate the cell viability of PC3 and PNT2 cells after anti-STEAP2 pAb (AB4/ECL3) drug regimen.** Treatments are listed in the far-left column; +ctrl (untreat): positive control, PC3 cells, untreated to demonstrate their migratory properties. +ctrl (IgG): PC3 cells treated with the max. dose of anti-IgG isotype Ab used as a positive control; AB4: commercial, polyclonal anti-STEAP2 Ab directed against an epitope on its ECL3; Final [µg/ml]: final Ab dose. Ab vol. [µl]: Treatment volume with control medium, control IgG Ab or anti-STEAP2 Ab, Medium [µl]: volume of cell culture medium required.

Treatment	Final [µg/ml]	Ab [µl]	Medium [µl]
+ctrl (untreated)	25	-	500
	50	-	500
	75	-	500
+ctrl IgG	75	42	458
AB4	25	25	475
	50	50	450
	75	75	425

#### 4.2.3 Fluorescence microscopy

For the fluorescence microscopical analysis, the confocal laser scanning microscope (LSM710, ZEISS, Germany) was utilized (**Section 2.2.4.2**). The analysed channels and emission wavelengths (nm) were blue (405 nm) for the nuclei, green (488 nm) for

STEAP2 with the primary rabbit polyclonal anti-STEAP2 Ab (1:200, Insightbiotechnology, UK) or the Golgi organelle with the primary mouse monoclonal anti-golgin97 Ab (1:1,000, Invitrogen, UK), red (543 nm) for internalised STEAP2-receptor Ab complex and transmitted light (brightfield). The secondary goat anti-rabbit anti-IgG (1:1,000, Abcam, UK) or secondary goat anti-mouse anti-IgG antibodies (1:1,000, Invitrogen, UK) were utilised to detect the primary antibodies.

#### **4.2.3.1 Ab pHAb Amine Reactive Dye Conjugates preparation**

The Ab-pHAb Amine Reactive Dye conjugation was carried out as recommended by Promega, UK. The storage buffer of the Zeba Desalting Spin Columns (ThermoFisher Scientific, UK) with a 40 kDa molecular weight cut-off was removed by a quick spin and equilibrated with amine conjugation buffer (0.84g Sodium Bicarbonate dissolved in 100 ml ddH<sub>2</sub>O, pH 8.5) by 3x 12000 x g for 1min each spin. The pHAb Amine Reactive Dye was dissolved in 25  $\mu$ l of 1:1 DMSO:H<sub>2</sub>O, vortexed and left for 15 min at RT for the dye to dissolve completely. In a 1.5 ml Eppendorf tube, 1.2  $\mu$ l of dye was added to 100  $\mu$ g of Ab to make a 20 Molar excess of dye and mixed every 10 min for 1 h at RT in the dark. Unconjugated dye was removed using the Zeba Desalting Spin Column, which was equilibrated with amine conjugation buffer beforehand. The Ab-pHAb Amine Reactive Dye conjugate was collected in a fresh Eppendorf tube and was kept in the dark at 4°C wrapped in aluminium foil until ready to be used.

#### **4.2.3.2 Drug-to-Antibody-Ratio (DAR)**

The absorbances were measured at  $A = 280$  nm (proteins including antibodies) and  $A = 253$  nm (pHAb Amine Reactive Dye) using the Nanodrop (ND-1000 Spectrophotometer, ThermoFisher Scientific, UK). The software Nanodrop version 3.1.2 was used to measure the absorbance by selecting the UV/Vis option. The DAR was used as a quality control where a DAR of 1 – 8 was considered as optimal and was calculated according to the manufacturer (Promega, UK) as follows:

$$\text{Ab concentration [mg/ml]} = \text{A280} - (\text{A532} \times 0.256) / 1.4$$

$$\text{Dye-to-Ab-Ratio} = (\text{A532} \times 150,000) / (\text{Ab concentration [mg/ml]} \times 75,000)$$

Where: Molecular weight of Ab = 150,000 Da; Extinction coefficient of pHAb Amine Reactive Dye = 0.256

#### 4.2.3.3 Receptor internalisation

In an 8-well chamber slide (Ibidi, Germany), 25,000 cells were grown for 48 h at 37°C/5% CO<sub>2</sub> before receptor internalisation was carried out. The Ab-fluorophore conjugation was carried out as recommended by Promega, UK. On the analysis day, the chamber slides were cooled on ice, while old medium replaced with treatment was added quickly (**Table 4.5**).

**Table 4.5 Treatment to study the receptor internalisation of STEAP2**

. Treatments are illustrated in the far-left column; +ctrl (untreat): positive control PC3 cells, untreated to demonstrate their migratory properties; +ctrl IgG: anti-IgG isotype Ab treated PC3 cells, vehicle, positive control, AB4: commercial, polyclonal anti-STEAP2 Ab directed against an epitope on its ECL3; Ab vol. [μl]: Treatment volume with control medium, control IgG Ab or anti-STEAP2 Ab; Medium [μl]: volume of cell culture medium required. The final concentration of the Ab conjugates applied was 100 μg/ml.

Treatment [μg/ml]	Medium [μl]	Blocking [μl]	Ab [μl]	Volume <sub>r</sub> [μl]
+ctrl (untreat)	208.4	41.6	-	250
+ctrl IgG (100)	193.7	41.6	14.7	250
AB4 (100)	183.4	41.6	25.0	250

Cells were washed with PBS and 100 μg/ml of anti-STEAP2 or anti-IgG Ab pHAb Amine Reactive Dye Conjugates was applied. The chamber slides were sealed with parafilm, incubated at 4°C for 30 min to allow even Ab cell surface binding (0 min time point), the cells were washed free of Ab with PBS and fixed with PFA for 5 min at RT. For any other time point, the cells were shifted from 4°C to 37°C, incubated for the desired time to allow receptor internalisation, following PBS washes, fixation, PBS washes, 30 min signal quenching using Image iT Signal Enhancer® (Thermofisher Scientific, UK), 30 min blocking with 3% BSA, PBS washes and 10min permeabilization with 0.1% Triton-X 100. Cells were washed with PBS and ddH<sub>2</sub>O, nuclei were counterstained with DAPI (15 μg/ml final concentration) for 15 min at

37°C, following 1x PBS wash immediately before image analysis. The pH 5 solution was added prior to analysis to detect cell surface STEAP2. As controls, PC3 cells were incubated with the anti-IgG pHAb Amine Reactive Dye conjugate isotype Ab conjugate (Thermofisher, UK) or HFF1 cells treated with anti-STEAP2 Ab pHAb Amine Reactive Dye Ab conjugate at 0 min, 15 min, 30 min and 240 min. To visualise cell surface STEAP2 at 0 min, the fluorescence of the anti-STEAP2 pHAb Amine Reactive Dye was activated using a pH5 solution. For co-localisation studies of STEAP2 with the Golgi organelle, cells were blocked for 30 min in 3%BSA, incubated with primary goat anti-mouse anti-golgin97 monoclonal Ab (1:1000, Invitrogen, UK) for 1h at RT after receptor internalisation, washed with PBS and incubated with goat anti-mouse anti-IgG-Alexa488 Ab (1:1000, Invitrogen, UK) for 1 h at RT following PBS washes and analysis. Experiments were conducted in duplicate.

#### **4.2.4 Cell surface STEAP2 staining of 3D PC3 spheroid cells**

Approximately 10,000 PC3 cells were prepared to form spheroids over night as described in Chapter2, **Section 2.1.6.2**. 3D PC3 spheroid cells were fixed in 3% PFA/Triton (0.01%) for 3h at 4°C and washed 4 x 15 min PBS. 3D PC3 spheroid cells were then exposed to an increasing and decreasing methanol/ddH<sub>2</sub>O series (10%, 20%, 30%, 40%, 50%, 60%, 80%, 90%, 100%) for dehydration for 15 min each. 3D PC3 spheroid cells were then treated with rabbit anti-STEAP2 Ab (Ab4/ECL3, 1:50, Insightbiotechnology, UK) for 48 h at 4°C. As a negative control, anti-IgG isotype (Thermofisher, UK) treated PC3 spheroid cells (1:50) was used. Cells were then washed 4x in PBS for 30 min each and incubated with secondary goat anti-rabbit anti-IgG Alexa-488 Ab (1:200, Abcam, UK) for 24 h at RT protected from light. Nuclei were counterstained with Hoechst (10 µg/ml) for 15 min at 37°C/ 5% CO<sub>2</sub>. 3D PC3 spheroid cells were collected and mounted onto a glass slide using a pre-cut 200 µl tip. Two double layers of autoclave tape were placed on each slide to create a spacer beforehand. A coverslip was added and sealed with nail polish. Experiment procedure was adapted from Weiswald *et. al*, 2010 and conducted in duplicate.

#### 4.2.5 Cell viability (3D PC3 spheroid cells)

Spheroids were treated for 24 h with 75 µg/ml of anti-STEAP2 pAb (Ab4/ECL3, Insightbiotechnology, UK) or anti-IgG isotype control Ab (Thermofisher, UK) on day 1 or were left untreated one day after cell spheroid preparation (**Table 4.6**). Cells were stained simultaneously with of Hoechst (10 µg/ml) and PI (10 µg/ml) for 15 min at 37°C/ 5% CO<sub>2</sub>, following 3x PBS washes before live imaging using the confocal LSM 710 microscope (ZEISS, Germany) with a 10x objective. The experiment was conducted in duplicate.

**Table 4.6 Treatment to study the impact of the anti-STEAP2 pAb (AB4/ECL3) on 3D PC3 spheroids cells after 24 h exposure.** Treatments are illustrated in the far left column; +ctrl (untreat): positive control PC3 cells, untreated to demonstrate their migratory properties; +ctrl (IgG) = anti-IgG isotype Ab treated PC3 cells, positive control; AB4: commercial, polyclonal anti-STEAP2 Ab directed against an epitope on its ECL3; Final [µg/ml]: treatments were prepared at their double concentration which was diluted 1:1 with the remaining cell culture medium per well to make the final concentrations of 75 µg/ml of Ab; Ab vol. [µl]: Treatment volume with control medium, control IgG Ab or anti-STEAP2 Ab; Medium [µl]: volume of cell culture medium required.

Treatment [µg/ml]	Ab [µl]	Medium [µl]	Final dose [µg/ml]
+ctrl (untreated)	-	500	75
+ctrl IgG (75)	42	458	75
AB4 (75)	75	425	75

#### 4.2.6 Statistical analysis

Normality of the data was assessed by the Shapiro-Wilk test (as  $N < 10$ ). Data was normally distributed and statistical analysis was therefore carried out using the one-way ANOVA *post-hoc* Dunnett test for the cell viability and cell invasion data. Results were considered as statistically significant as follows: p-value  $< 0.05$  (\*), p-value  $< 0.01$  (\*\*), p-value  $< 0.001$  (\*\*\*) and p-value  $< 0.0001$  (\*\*\*\*). Confocal microscopy and the cell migration analysis were conducted in duplicate. Confocal microscopy for receptor internalisation studies and STEAP2 expression in spheroid 3D PC3 cells were conducted by acquiring three images of three different fields of view per test sample at a 63x zoom objective as qualitative analysis. During cell migration analysis, three images per time point and test sample were acquired.

## 4.3 Results

---

The aim of this chapter was to evaluate the impact of a commercial, anti-STEAP2 pAb (AB4/ECL3) on the invasive properties of PC3 cells and to examine, if the ADC technology qualifies as a potential therapeutic option for patients with prostate cancer. The aim was addressed by evaluating the following properties in PC3 cells following exposure to anti-STEAP2 pAb (AB4/ECL3): cell migration, cell invasion, receptor internalisation and cell viability (in both cells cultured in 2D and 3D format).

### 4.3.1 Anti-STEAP2 pAbs exposure substantially inhibit cancer cell migration in PC3 cells

In order to evaluate the potential of the commercial anti-STEAP2 polyclonal Ab (pAb), Ab4 (ECL3), to reduce invasive cancer cell traits, the cell migration assay was performed. Initially, three doses ranging from 5, 10 and 20  $\mu\text{g}/\text{ml}$  of Ab4 (ECL3) were applied to PC3 cells over 12 h as a one-off test to establish the effective Ab dose to completely inhibit cancer cell migration (**Figure 4.1**). After 12 h, the wound gap was fully closed in the untreated and IgG control treated PC3 cells, which demonstrated their migratory capacity. In contrast, a dose-dependent inhibition in cell migration was observed in PC3 cells after Ab4 (ECL3) treatment (**Figure 4.1**). At 5  $\mu\text{g}/\text{ml}$  of Ab4 (ECL3), the wound gap did not appear to differ from both the untreated and IgG Ab treated controls. However, at 10  $\mu\text{g}/\text{ml}$  the wound gap was prevented from closing over the 12 h time period. Importantly, PC3 cells exposed to the maximum dose of 20  $\mu\text{g}/\text{ml}$  of Ab4 (ECL3) showed no difference in the wound gap size as compared to the initial starting point 0 h. Therefore, Ab4 (ECL3) treatment led to a substantial blockage of the cancer migratory capacity of the PC3 cells (**Figure 4.1**).

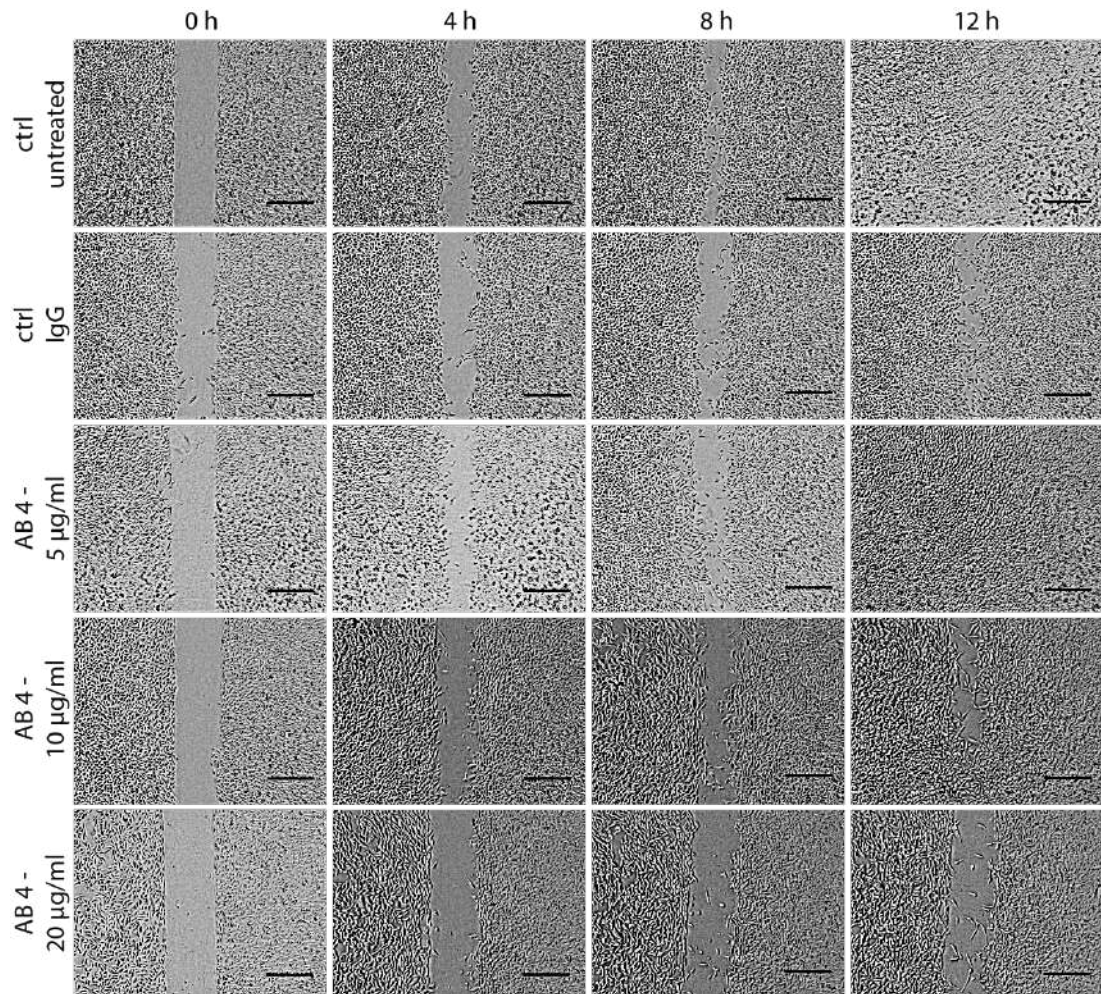


**Figure 4.1 Anti-STEAP2 pAb (AB4/ECL3) inhibits cell migration of PC3 cells in a dose-dependent manner.** Time points at which the images were taken: 0h, 4h, 8h and 12h; +ctrl untreated: PC3 cells; + ctrl IgG: PC3 cells treated with anti-IgG isotype Ab (20 µg/ml); AB4: Ab4 (commercial anti-STEAP2 Ab specific against ECL3) with a dose range of 5 µg/ml, 10 µg/ml and 20 µg/ml. Images were acquired using an inverted light microscope with a 5x objective (AxioCam ERC5s, ZEISS, Germany). Scale bar = 500 µm (N = 1).

In order to evaluate, if targeting two unique epitopes on STEAP2 resulted in a stronger inhibitory effect on cell migration, PC3 cells were subjected to two single Ab treatments, each of which bind to different ECLs. Initially, Ab1 (ECL1) and Ab4 (ECL3) were employed individually as a comparison, then a dual Ab treatment was performed. The wound gap closed fully in both the untreated and IgG Ab treated controls over a 12 h period (**Figure 4.2**, where representative images are illustrated; images from the additional replicate can be found in Annex 2, **Figure A2. 1**).

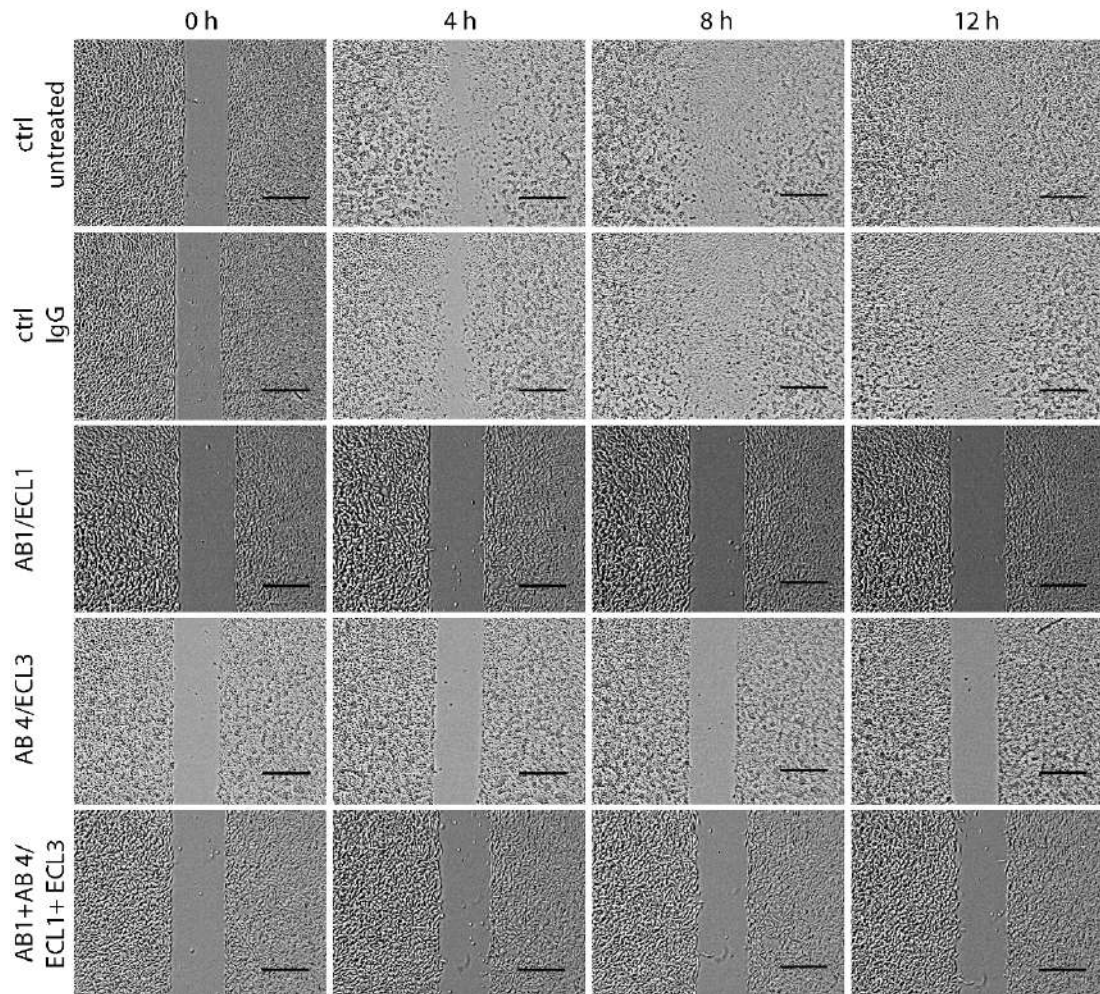
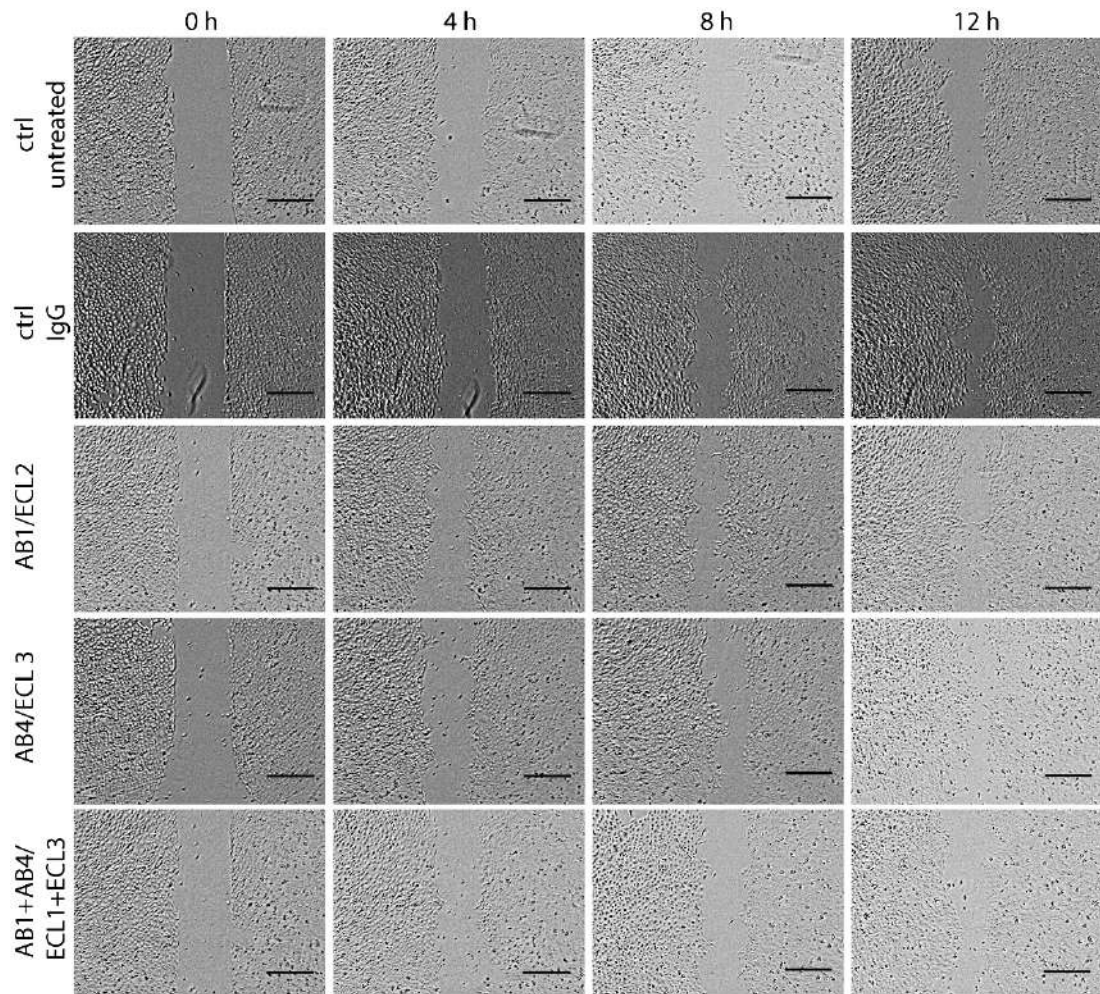


**Figure 4.2 Single and dual anti-STEAP2 pAb exposure block cell migration in PC3 cells.** Time points at which the images were taken: 0h, 4h, 8h and 12h; +ctrl, untreated PC3 cells; + ctrl IgG: PC3 cells treated with anti-IgG isotype Ab (20  $\mu\text{g}/\text{ml}$ ); AB1/ECL1: single anti-STEAP2 Ab targeting an epitope of the ECL1 (20  $\mu\text{g}/\text{ml}$ ); AB4/ECL3: single anti-STEAP2 Ab targeting an epitope of the ECL3 (20  $\mu\text{g}/\text{ml}$ ); AB1+AB4/ECL1+ECL3: dual anti-STEAP2 Ab targeting of two unique epitopes on ECL1 and ECL3. Images were acquired using an inverted light microscope with a 5x objective (AxioCam ERC5s, ZEISS, Germany). Scale bar = 500  $\mu\text{m}$  (N = 2).

Interestingly, the wound gaps remained wide open after single Ab treatment at all given time points, irrespective of the targeted ECL, with no difference as compared to the size of the 0 h wound gaps (**Figure 4.2**). This indicates that the cell migration was blocked when applying the maximum Ab dose of 20  $\mu\text{g}/\text{ml}$ . It further suggests, that Ab1 and Ab4 were equally capable of inhibiting cell migration and, that both immunogens on ECL1 and ECL3 represent targetable regions on STEAP2. The dual Ab treatment (ECL1+ECL3) showed an open wound gap up until 12 h post-treatment. The wound gap was wide open with no evidence of cell migration as

seen at the 0 h starting point (**Figure 4.2**). In addition, the wound gap opening was very similar to the observations when the single Ab treatments had been applied, at all given time points (**Figure 4.2**, where representative images are illustrated; images from the additional replicates can be found in Annex 2, **Figure A2. 1**). Therefore, this data demonstrated there was no stronger effect in reducing the cancer cell migration in PC3 cells by the combined Ab treatment as compared to the single Ab treatments.

The cell migration assay was also conducted with non-cancerous prostate PNT2 cells as a negative control cell line given their low STEAP2 expression. The results demonstrated, that the PNT2 cells slowly migrated across the wound gaps irrespective of the employed Ab treatments (**Figure 4.3**). This finding suggests the PNT2 cells were not responsive to the anti-STEAP2 regimens where representative images are illustrated in **Figure 4.3**; images from the additional replicate can be found in **Annex 2, Figure A2. 2**). To conclude, Ab4 treatment (ECL3) resulted in a dose-dependent reduction in cell migration in the PC3 cells, which was marginally as equally efficient as Ab1 (ECL1). The use of the dual Ab treatment (ECL1+ECL3) against STEAP2, induced a similar inhibiting effect on cell migration. Therefore, Ab4 (ECL3) was selected for further studies given its strong cancer cell migration inhibition capabilities combined with its suitability for imaging purposes, while the use of Ab1 (ECL1) was discontinued.

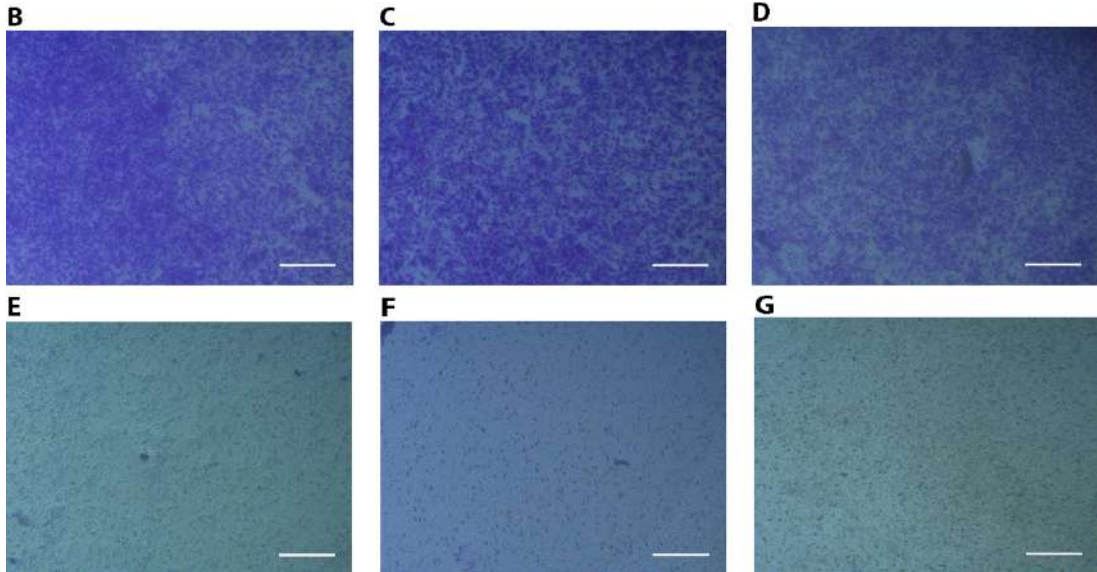
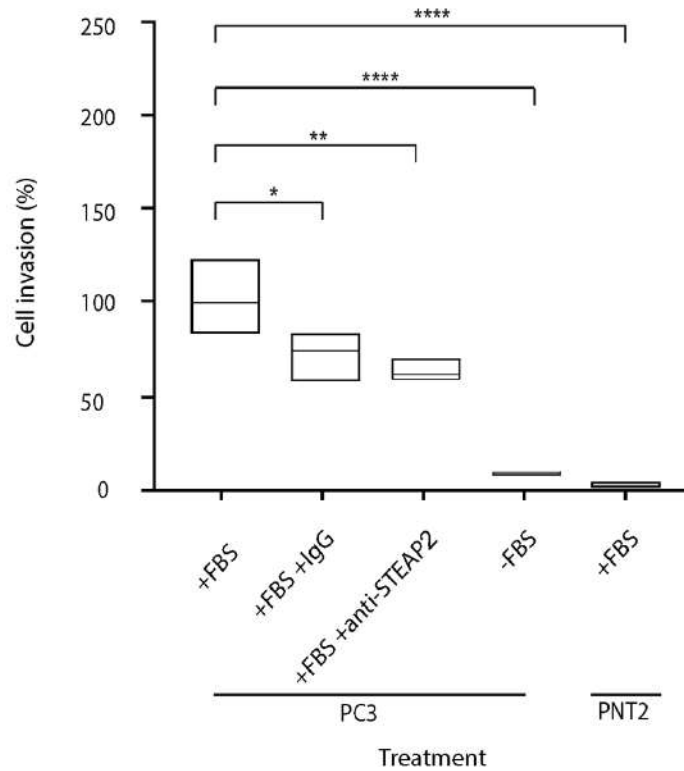


**Figure 4.3 Anti-STEAP2 pAb (AB4/ECL3) does not affect the cell migration in PNT2 cells.** Time points at which the images were taken: 0h, 4h, 8h and 12h; +ctrl, untreated PNT2 cells; + ctrl IgG: PNT2 cells treated with anti-IgG isotype Ab (20 µg/ml); AB1/ECL1: single anti-STEAP2 Ab targeting an epitope of the ECL1 (20 µg/ml); AB4/ECL3: single anti-STEAP2 Ab targeting an epitope of the ECL3 (20 µg/ml); AB1+AB4/ECL1+ECL3: dual anti-STEAP2 Ab targeting of two unique epitopes on ECL1 and ECL3. Images were acquired using an inverted light microscope with a 5x objective (AxioCam ERC5s, ZEISS, Germany). Scale bar = 500 µm (N = 2).

#### 4.3.2 Anti-STEAP2 pAb (ECL3) reduced cell invasion in PC3 cells

The cell invasion assay was conducted to evaluate, if targeting STEAP2 using the commercial pAb, Ab4 (ECL3), had an effect on inhibiting cancer cell invasion underlying cancer cell metastatic properties. Thus, the cell invasion assay was performed, where the bottom of a culture plate-insert was coated with ECM (by the manufacturer) and FBS served as a chemoattractant to stimulate the ability of the tumour cells to invade through the ECM. As the cells were grown on top of the insert chamber, only those cells with invasive capacity are capable of crossing the ECM

barrier. The Ab dose applied, 20  $\mu\text{g}/\text{ml}$  of Ab4 (ECL3), was based on the most effective dose used in the cell migration assay in **Section 4.3.2**. The result illustrated in **Figure 4.4** demonstrate, that 100% (SD = 17.61%) of the untreated PC3 cells invaded through the ECM in the presence of the chemoattractant (FBS), which illustrates their aggressive, invasive capacity (**Figure 4.4 A** and **Figure 4.4 B**). The IgG isotype control treated PC3 cells showed a minor, but significant decrease in cell invasion to 77.82% (SD = 10.89%,  $p = 0.0376$ ) suggesting the IgG isotype Ab had an effect on altering the invasive properties of these cells (**Figure 4.4 A** and **Figure 4.4C**). However, it was notable, that the anti-STEAP2 pAb (ECL3) exposure in PC3 cells led to a stronger and significant reduction in cell invasion to 68.80% (SD= 4.88%,  $p = 0.0082$ , **Figure 4.4 A** and **Figure 4.4 D**). Without chemoattractant, only 10.86% (SD = 0.94%,  $p < 0.0001$ ) of the PC3 cells invaded through the ECM (**Figure 4.4A** and **Figure 4.4 E**), highlighting the importance of the chemoattractant to facilitate the interpretation of this cell invasion assay. PNT2 were also included in the analysis as they are a non-cancerous prostate cell line. In contrast to PC3 cells, only 2.96% (SD = 1.14%,  $p < 0.0001$ ) of the normal PNT2 cells were shown to penetrate the ECM in the presence of chemoattractant (**Figure 4.4 A** and **Figure 4.4 F**).

**A**

**Figure 4.4 Anti-STEAP2 pAb (AB4/ECL3) reduces cancer cell invasion of PC3 cells**

. A) Colorimetric analysis of the cell invasion after 48 h Ab treatment. B) untreated PC3 cells to show the invasive properties. C) PC3 cells treated with isotype control anti-IgG Ab. D) Anti-STEAP2 Ab treated PC3 cells (Ab4/ECL3). E) PC3 cells without FBS, F) Healthy PNT2 cells with FBS showing minimal invasive capacity, G) ECM. Statistical analysis was conducted using an ANOVA *post-hoc* Dunnett test. P-value < 0.05 (\*), p-value < 0.01 (\*\*) and p-value < 0.0001 (\*\*\*\*) (N = 3). Images (N = 1) were taken with an inverted light microscope at a 5x objective (AxioCamERC5s, ZEISS, Germany). Scale bar = 500  $\mu$ m, (N = 3).

### 4.3.3 Receptor internalisation was triggered by anti-STEAP2 pAb (AB4/ECL3) and indicates acidic organelle localisation

To visualise cell-surface STEAP2 prior to evaluating its capacity for receptor internalisation, the fluorescent signal of the anti-STEAP2 pHAb Amine Reactive Dye conjugate was activated by the addition of acid (pH 5) (**Figure 4.5 A**, where representative images are illustrated; images from the additional replicate can be found in Appendix 2, **Figure A2. 3**). This represented the time point 0 min. An anti-IgG pHAb Amine Reactive Dye Ab fluorophore conjugate (non-specific to STEAP2) was applied alongside in PC3 cells as Ab isotype control (**Figure 4.5 B**). The low STEAP2 expressing HFF1 cell line was also included as a negative control and was incubated with the anti-STEAP2 pHAb Amine Reactive Dye conjugate (**Figure 4.5 C**). The addition of the acidic solution (pH 5) resulted in an enhanced fluorescent signal of the anti-STEAP2 pHAb Amine Reactive Dye conjugate. The fluorescence was observed at the cell surface of the PC3 cells suggesting STEAP2 was present at the plasma membrane. Minimal fluorescence signal was visible in the low STEAP2 expressing HFF1 cell line with no specific cell localisation, despite the addition of the acid solution. This indicated there was no evident cell surface STEAP2 present (**Figure 4.5 B**) in the HFF cells. Further, the PC3 cells incubated with anti-IgG pHAb Amine isotype Ab control exhibited a similar, low fluorescence with no specific STEAP2 cell surface localisation (**Figure 4.5 C**). This confirmed, that any observed effect was due to the specificity of the anti-STEAP2 Ab but not to the generic, unspecific anti-IgG Ab. Thus, the anti-IgG Ab qualifies as a suitable isotype control Ab.

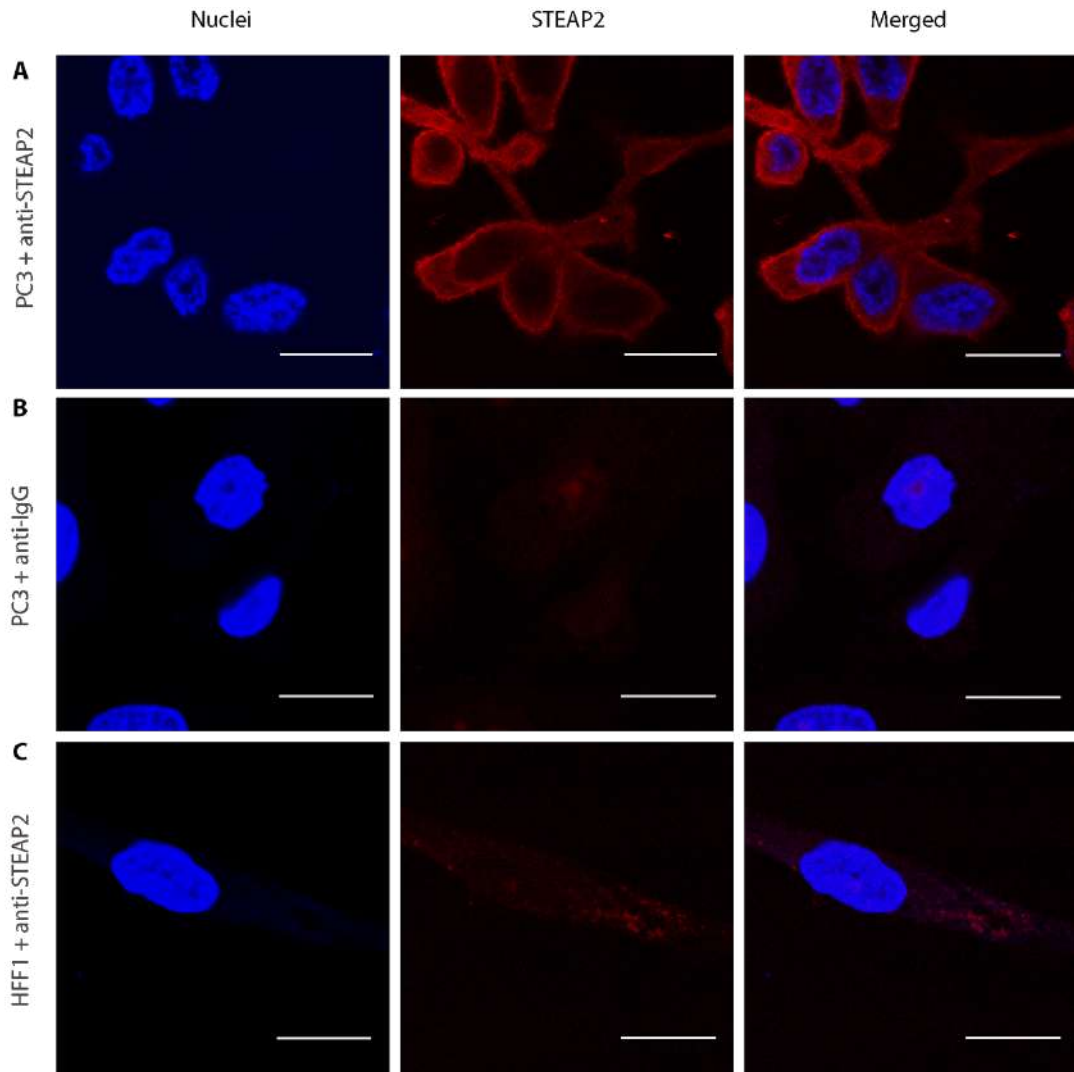
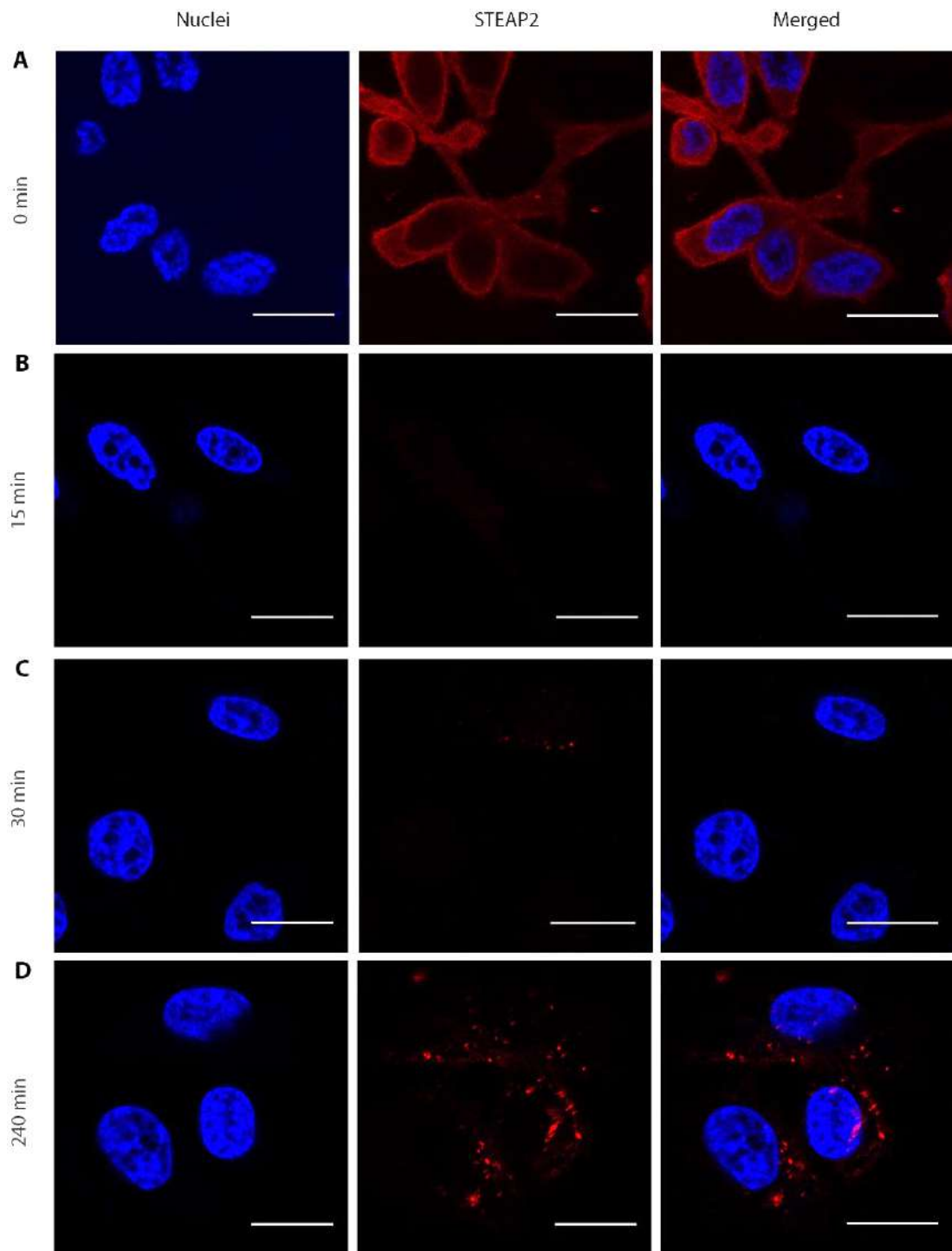


**Figure 4.5 STEAP2 is located to the cell membrane prior to receptor internalisation in cancerous PC3 cells but not in HFF cells.** A) PC3 + anti-STEAP2 pHAb Amine Reactive Dye Conjugate showing cell surface STEAP2. B) PC3 + anti-IgG pHAb Amine Reactive Dye Conjugate: Ab isotype control unspecific to STEAP2 with no cell-surface fluorescence observed. C) HFF1 + anti-STEAP2 pHAb Amine Reactive Dye Conjugate, a STEAP2 low expressing used as negative control cell line showing low fluorescence without cell-surface staining. Blue: nuclei; red: STEAP2. Images were acquired with the Confocal LSM 710 (ZEISS, Germany) at a 63x zoom objective. Scale bar = 20  $\mu$ m (N = 2).

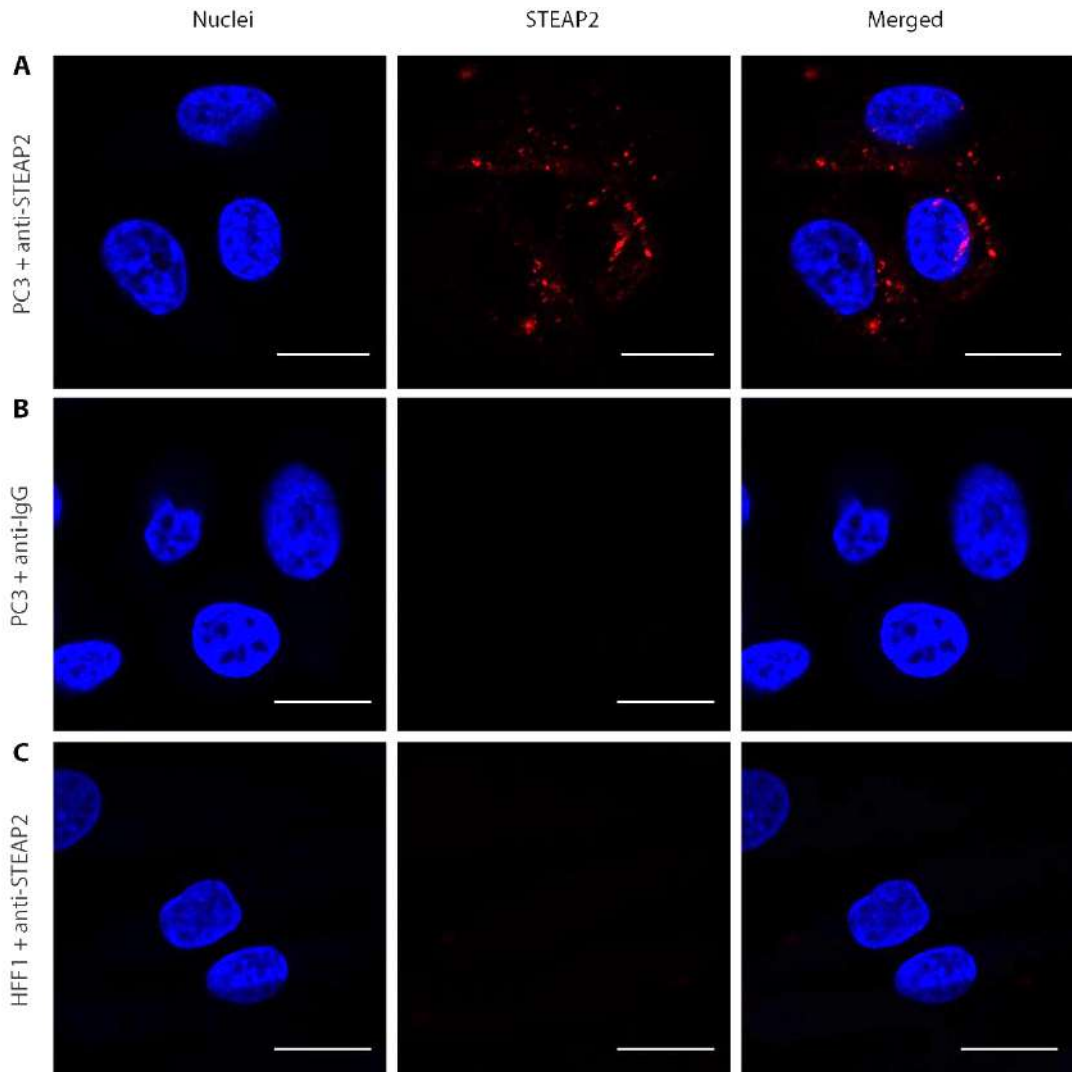
With increasing incubation time with the anti-STEAP2 Ab pHAb Amine conjugate, intracellular puncta became more evident in the PC3 cells starting from as little as 30 min post incubation, suggesting time-dependent internalisation of the anti-STEAP2 Ab pHAb Amine conjugate-STEAP2 receptor complex (**Figure 4.6 A – E** and **Figure 4.7**, where representative images are illustrated; images from the additional replicate can be found in Appendix 2, **Figure A2. 4** and **Figure A2. 5**). At 240 min, prominent, red puncta were evenly distributed throughout the cell but

not present at the cell-periphery of the PC3 cells. This data indicates the STEAP2 receptor has been specifically triggered upon the binding of the low-pH sensitive anti-STEAP2 Ab pHAb Amine conjugate, became internalised and was subsequently localised within the acidic cell compartments such as the endosomes and lysosomes (**Figure 4.7**, where representative images are illustrated; images from the additional replicate can be found in Appendix 2, **Figure A2. 4** and **Figure A2. 5**).

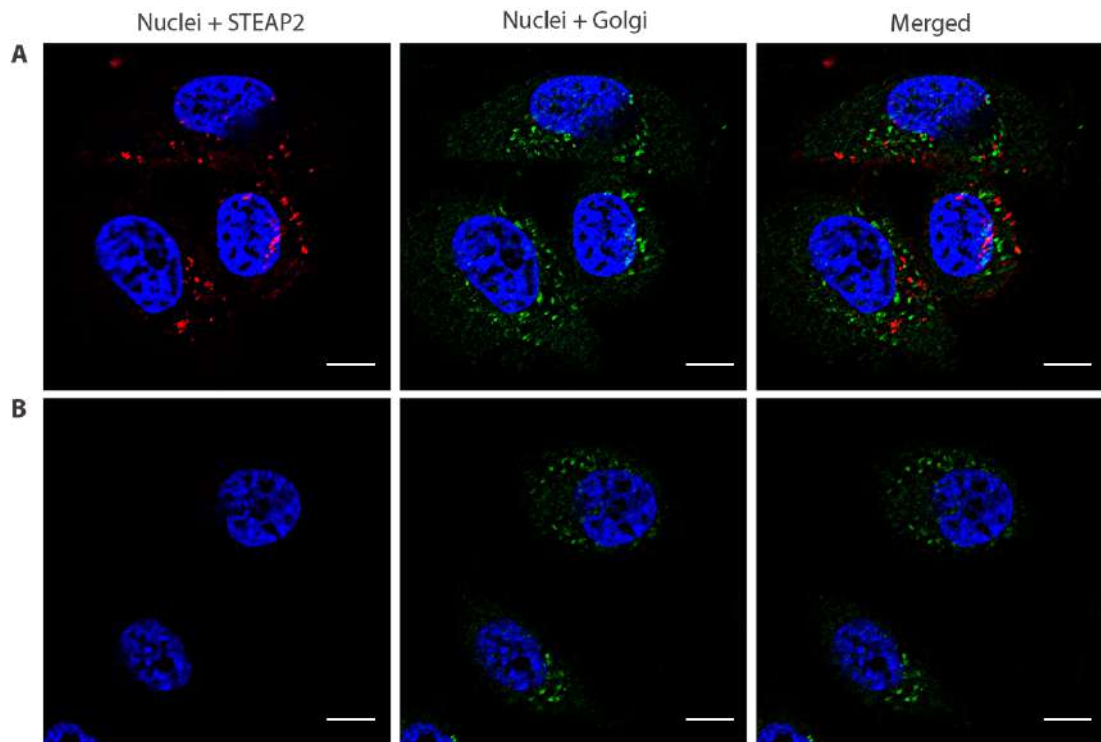
In order to confirm the localisation of the internalised anti-STEAP2 Ab pHAb Amine conjugate-STEAP2 receptor complex was in acid cellular compartments (of pH 5 – 6.5), and not within the Golgi apparatus (pH 7), receptor internalisation was conducted alongside a Golgi-specific Ab. After 240 min, strong, green fluorescent puncta were evident as a Golgi organelle-like structure indicating a Golgi-specific staining (**Figure 4.8**, where representative images are illustrated; images from the additional replicate can be found in Appendix 2, **Figure A2. 6**). However, the green Golgi staining was clearly distinguishable from the red puncta exhibited by the Ab-STEAP2 complex (**Figure 4.8**). This suggested the STEAP2 receptor internalisation was triggered upon an anti-STEAP2 Ab pHAb Amine conjugate binding and accumulated in acidic organelles but not in the Golgi apparatus after 240 min.



**Figure 4.6 STEAP2 receptor internalisation was triggered after anti-STEAP2 pAb pHAb Amine Reactive Dye Conjugate (ECL3) binding.** A) 0 min: cell surface STEAP2 was visualised by the addition of acid (pH 5.0) before receptor internalisation. B) 15 min: receptor internalisation was initiated. C) 30 min: first evident internalised cell surface STEAP2. (D) 240 min: fully internalised STEAP2 shown as red puncta. Blue: nuclei; red: STEAP2. Images were acquired with a Confocal LSM 710 with a 63x zoom objective (ZEISS, Germany). Scale bar = 20  $\mu\text{m}$  (N = 2).



**Figure 4.7** STEAP2's is localised in the endosomal/lysosomal organelles after 240 min of receptor internalisation in PC3 cells but is absent in HFF1 cells. A) PC3 + anti-STEAP2 pHAb Amine Reactive Dye Conjugate Ab (ECL3). B) PC3 + anti-IgG pHAb Amine Reactive Dye Conjugate Ab isotype control. C) STEAP2 low expressing negative control cell line HFF1 + anti-STEAP2 pHAb Amine Reactive Dye Conjugate (ECL3). Blue: nuclei; red: internalised STEAP2. Images were acquired with the Confocal LSM 710 with a 63x zoom objective (ZEISS, Germany). Scale bar = 20  $\mu$ m (N = 2).

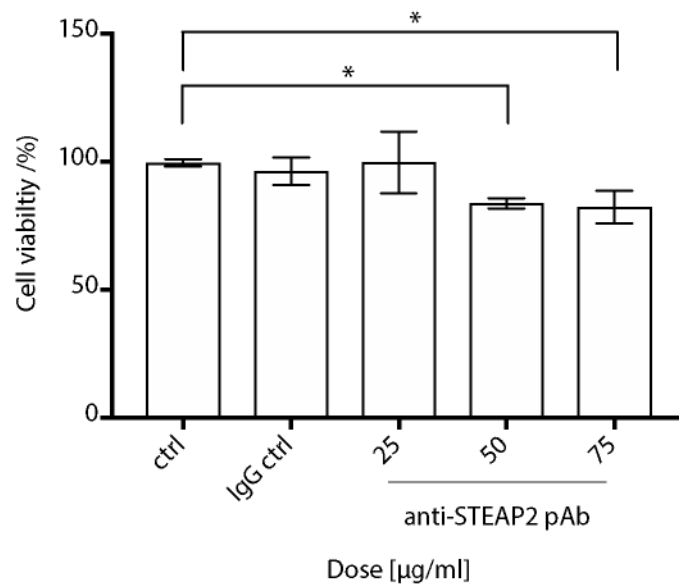
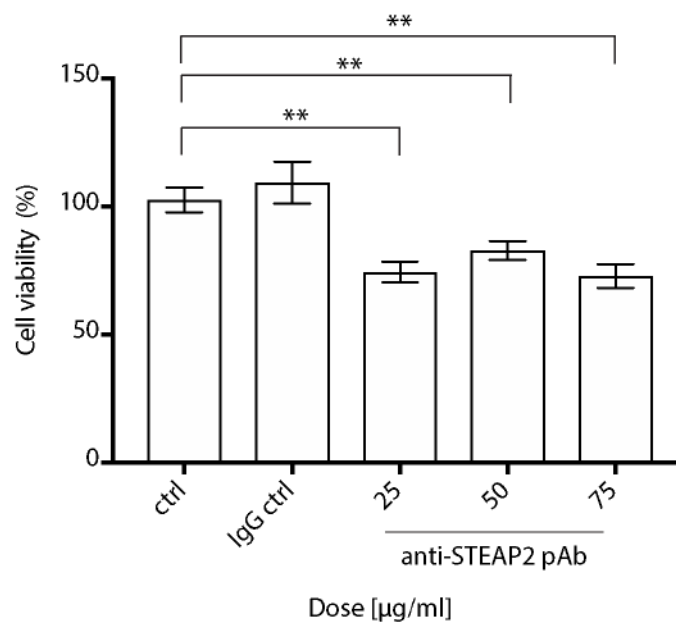


**Figure 4.8 Internalised STEAP2 does not co-localise with the Golgi apparatus indicating endosomal/ lysosomal accumulation after 240 min time point in PC3 cells.** A) PC3 cells + anti-STEAP2 pHAb Amine Reactive Dye Conjugate Ab (ECL3). B) PC3 cells + anti-IgG pHAb Amine Reactive Dye Conjugate isotype control Ab. Blue: nuclei; red: internalised STEAP2; green: Golgi. Images were acquired with the Confocal LSM 710 with a 63x zoom objective (ZEISS, Germany). Scale bar = 10  $\mu\text{m}$  (N = 2).

#### 4.3.4 Anti-STEAP2 pAb (Ab4/ECL3) exposure reduces cell viability

The impact of the commercial anti-STEAP2 pAb (Ab4/ECL3) on the cell viability of 2D PC3 prostate cancer and PNT2 normal cells was assessed by the MTT assay. Two controls, an untreated control, an anti-IgG isotype control Ab and three different anti-STEAP2 pAb doses (Ab4/ECL3) were applied.

In PC3 cells, no significant decrease in cell viability was observed after 24 h treatment with IgG control (96.25%, SD= 5.14%) compared to untreated PC3 cells (99.49 %, SD = 1.13%; **Figure 4.9 A**). PC3 cells treated with 25 µg/ml of anti-STEAP2 pAb also remained viable (99.56%, SD = 8.89%; **Figure 4.9 A**). However, treatment with 50 µg/ml and 75 µg/ml of anti-STEAP2 pAb led to a significant reduction in cell viability in PC3 cells (83.66%, SD= 2.21%,  $p = 0.048$  and 82.21%, SD= 5.38%,  $p = 0.0311$  respectively), with the dose effect plateauing at 50 µg/ml (**Figure 4.9 A**). When PNT2 cells were treated with 25 µg/ml, 50 µg/ml and 75 µg/ml of anti-STEAP2 pAb, a significant reduction in cell viability was also observed: 74.20% (SD = 3.32%,  $p = 0.0003$ ), 82.7% (SD = 3.02%,  $p = 0.0037$ ) and 72.77% (SD = 2.77%,  $p = 0.0002$ ), respectively (**Figure 4.9 B**). This reduction in viability was specific to the anti-STEAP2 pAb, since PNT2 cells exposed to the anti-IgG isotype pAb exhibited no reduction in cell viability (**Figure 4.9 B**). This data suggests the normal PNT2 cells are slightly more sensitive to the Ab exposure.

**A****B**

**Figure 4.9 Anti-STEAP2 pAb (AB4/ECL3) reduces cell viability after 24 h exposure in PC3 and PNT2 cells.** A) Cell viability after Ab exposure in cancerous PC3 cells, B) Cell viability after Ab exposure in normal PNT2 cells. Ctrl: untreated cells; anti-STEAP2 pAb (AB4/ECL3 at 25, 50 and 75 µg/ml dose); ctrl pAb: anti-IgG isotype control Ab unspecific to STEAP2 (75 µg/ml). An ANOVA *post-hoc* Dunnett test was performed for statistical analysis. p-value < 0.05 (\*), p-value < 0.01 (\*\*) (N = 3).

#### 4.3.5 STEAP2 is overexpressed in 3D PC3 cells

To evaluate the impact of the anti-STEAP2 pAb exposure on prostate cancer tumour spheroids, the STEAP2 expression and cellular distribution was first evaluated in PC3 cells cultured in a 3D spheroid format. This 3D prostate cancer spheroid cell model has been previously established within the group (Wang *et. al*, to be published).

Confocal microscopy demonstrated STEAP2 as a strong, green fluorescent signal which was evenly distributed throughout the 3D PC3 spheroid (**Figure 4.10**, where representative images are illustrated; images from the additional replicate can be found in Appendix 2, **Figure A2. 7**). STEAP2 was found to be located at the cell periphery as well as in the cytoplasm (**Figure 4.10 A – C**). A z-stack of the 3D PC3 spheroid cells by confocal microscopy confirmed the spherical morphology of the cells throughout the spheroid, which had an overall diameter of approximately 700  $\mu\text{m}$ . The fluorescence signal for STEAP2 was evenly distributed throughout the spheroid as demonstrated by the z-stacks indicating an overexpression of STEAP2 in the 3D PC3 spheroid cells (**Figure 4.11 A – F**, where representative images are illustrated; images from the additional replicate can be found in Appendix 2, **Figure A2. 8**). However, the fluorescent signal became fainter with increasing spheroid depth indicating less anti-STEAP2 pAb (AB4/ECL3) has penetrated the thick spheroid structure (**Figure 4.11 G – I**). Nonetheless, the localisation of the STEAP2 protein could be clearly visualised and was strongly expressed by most cells within the structure.

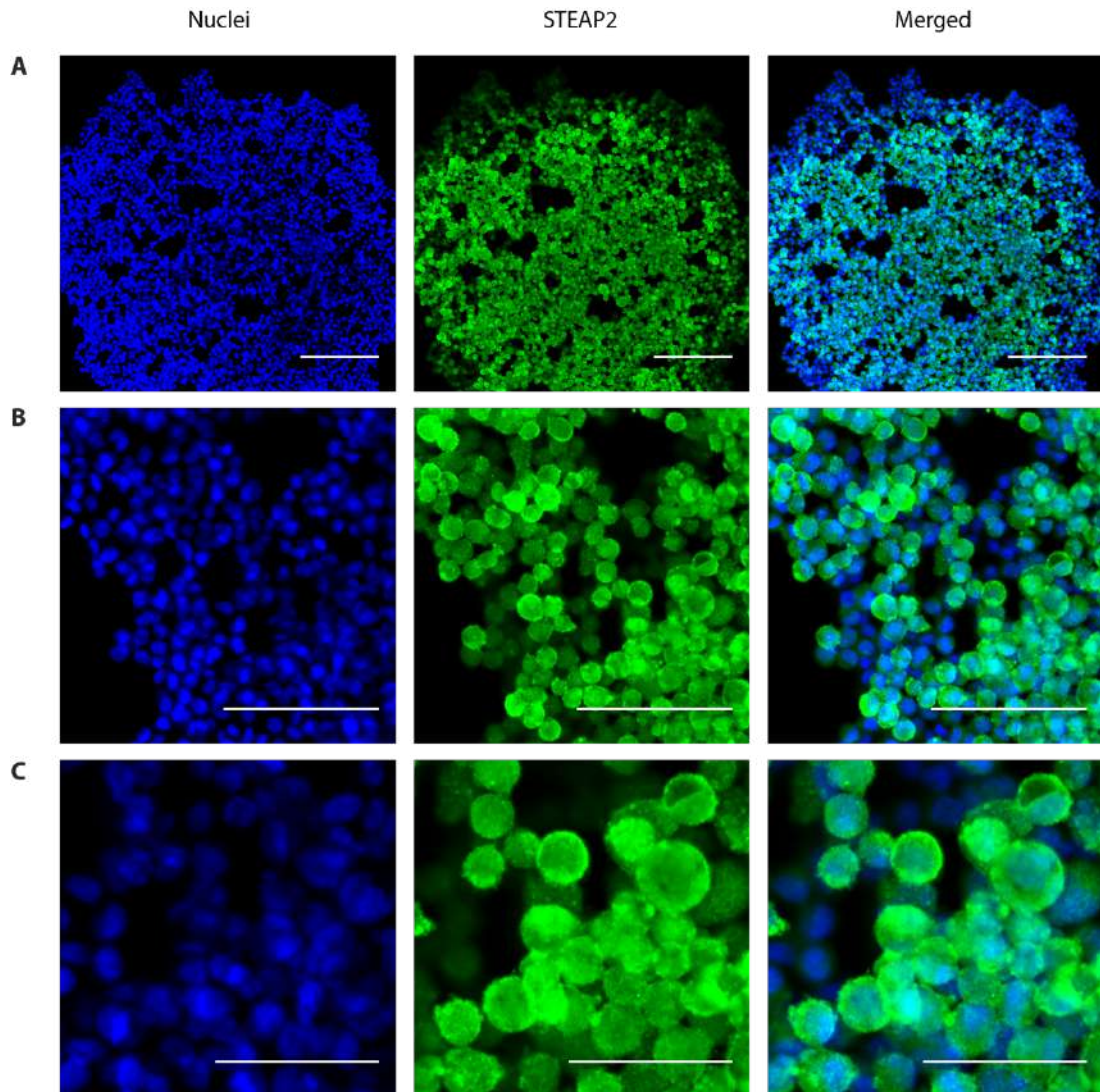


**Figure 4.10 STEAP2 protein expression and localisation in 3D PC3 cell spheroids by fluorescence microscopy shows even distribution and overexpression throughout the spheroid.** A) Protein expression of STEAP2 in 3D PC3 spheroid cells at 10x magnification showing the full spheroid. Scale bar = 200  $\mu\text{m}$ . B) Protein expression of STEAP2 in 3D PC3 spheroid cells at 10x magnification with 1x standard zoom application showing a strong, evenly distributed protein expression evident both intracellular as well as at the cell membrane. Scale bar = 100  $\mu\text{m}$ . C) STEAP2's protein expression in 3D PC3 cell spheroids at 10x magnification showing the full spheroid with 2x standard zoom application. Scale bar = 50  $\mu\text{m}$ . Blue: nuclei; green: STEAP2 protein expression. Images were acquired with the Confocal LSM 710 (ZEISS, Germany) (N = 2).

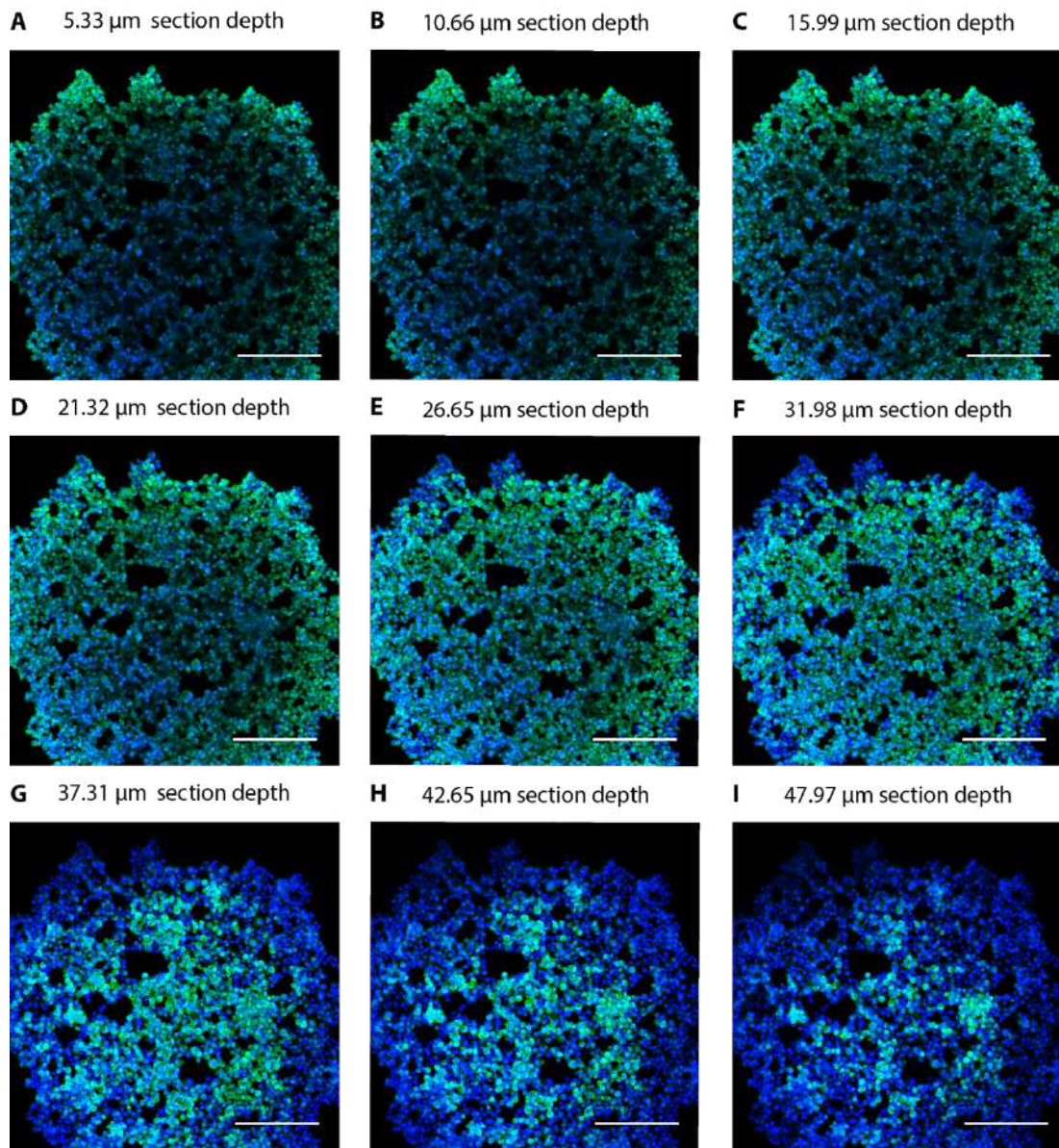


**Figure 4.11 Z-stack of 3D PC3 cell spheroids over 50  $\mu\text{m}$  depth by fluorescence microscopy showed strong STEAP2 expression throughout the spheroid and good anti-STEAP2 pAb (AB4/ECL3) penetration, which decreased with spheroid depth.** A) 5.33  $\mu\text{m}$  section depth, starting point of the z-stack. B) 10.66  $\mu\text{m}$  section depth. C) 15.99  $\mu\text{m}$  section depth. D) 21.32  $\mu\text{m}$  section depth. E) 26.65  $\mu\text{m}$  section depth. F) 31.98  $\mu\text{m}$  section depth. G) 37.31  $\mu\text{m}$  section depth. H) 42.647  $\mu\text{m}$  section depth. I) 47.97  $\mu\text{m}$  section depth, final z-stack. Blue: nuclei; green: STEAP2 protein expression. Images were acquired with the Confocal LSM 710 with a 10x objective (ZEISS, Germany). The z-stack was taken over a 50  $\mu\text{m}$  depth with 5  $\mu\text{m}$  interval slices. Scale bar = 200  $\mu\text{m}$  (N = 2).

#### **4.3.6 The anti-STEAP2 pAb (AB4/ECL3) has no significant effect on reducing the cell viability in 3D PC3 spheroid cells**

Based on the decreased penetration of the anti-STEAP2 pAb (ECL3) (**Section 4.3.5**) with increasing 3D PC3 spheroid depth together with the cell viability results in the 2D PC3 cells (**Section 4.3.4**), the maximum dose, 75 µg/ml was selected to evaluate its impact in reducing the cell viability of PC3 3D spheroids.

The 3D spheroids were treated for 24 h with 75 µg/mL of anti-STEAP2 pAb (ECL3), anti-IgG pAb isotype control or were left untreated. The 3D PC3 spheroid cells treated with anti-IgG isotype control Ab were employed as a negative control, in order to confirm, that any observed effect was due to the specificity of the anti-STEAP2 pAb (ECL3) to STEAP2. Initial experiments were conducted to evaluate the utility of the Propidium Iodide (PI) stain in the 3D system following fixation as a positive control for dead cells (**Figure 4.12 A**, where representative images are illustrated; images from the additional replicates can be found in Appendix 2, **Figure A2. 9**). The fixed cell spheroids strongly exhibited red, fluorescent staining, while the untreated (and non-fixed) 3D PC3 spheroid cells demonstrated some red clusters with random location within the 3D PC3 spheroid (**Figure 4.12 A**, **Figure 4.12 B**, **Figure 4.12 C**, where representative images are illustrated; images from the additional replicate can be found in Appendix 2, **Figure A2.9**) Similarly to the untreated negative control spheroids, some red, fluorescent clusters were observable after the exposure with the anti-IgG pAb isotype control. Therefore, this confirmed, that any observed effect was due to the specificity of the anti-STEAP2 pAb (ECL3) but not to a generic, unspecific Ab. Thus, this anti-IgG Ab qualifies as a suitable isotype control Ab (**Figure 4.12 C**). Moreover, minimal fluorescent clusters were present after the anti-STEAP2 pAb (ECL3) exposure of the 3D PC3 spheroid (**Figure 4.12 D**, where representative images are illustrated; images from the additional replicates can be found in Appendix 2, **Figure A2. 9**).

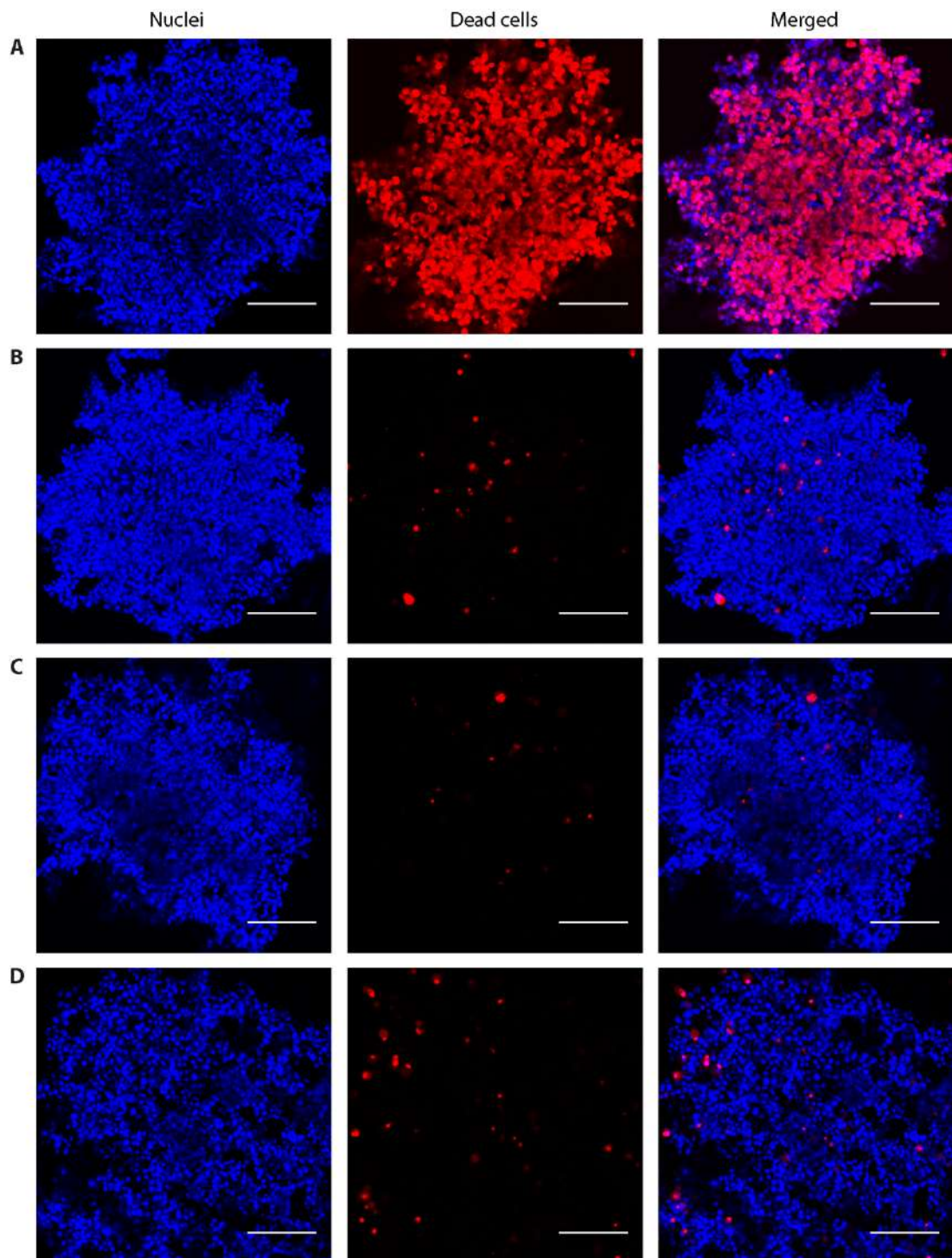


**Figure 4.12 No difference in cell viability observed after anti-STEAP2 pAb (AB4/ECL3) treatment in 3D PC3 spheroid cells over 24 h by PI staining and confocal microscopy**

. A) Fixed 3D PC3 spheroid cells to demonstrate dead cells stained with Propium Iodide (PI.) B) Untreated 3D PC3 spheroid cells, negative control. C) 3D PC3 spheroid cells treated with anti-IgG isotype control Ab. D) 3D PC3 spheroid cells treated with 75  $\mu\text{g}/\text{ml}$  of anti-STEAP2 pAb (AB4/ECL3 specific). Blue: nuclei; red: PI, dead cells. Images were acquired with the Confocal LSM 710 with a 10x objective (ZEISS, Germany). Scale bar = 200  $\mu\text{m}$  (N = 2).

## 4.4 Discussion

---

This Chapter aimed to determine, if STEAP2 internalises into acidic organelles, which is a key property, that underpins its utility in ADC technology. Additionally, the Chapter aimed to study the effect of an anti-STEAP2 pAb (AB4/ECL3) on the invasive properties in PC3 cells, by evaluating the response of the prostate cancer cells treated with anti-STEAP2 pAb (AB4/ECL3) on cell migration, cell invasion and cell viability. To examine the impact of the anti-STEAP2 pAb (AB4/ECL3) on cell viability in a more physiologically relevant prostate cancer model, PC3 cells cultured in 3D spheroid format were employed. The results demonstrated the commercial anti-STEAP2 pAb (AB4/ECL3) significantly reduced cell migration, cell invasion and cell viability in the PC3 cells cultured in 2D format. However, no significant impact on the cell viability was achieved by the anti-STEAP2 pAb (AB4/ECL3) exposed to 3D PC3 cell spheroids. Moreover, receptor internalisation of cell surface STEAP2 was triggered upon anti-STEAP2 pAb (AB4/ECL3) binding. Therefore, STEAP2 represents an attractive target for the design of Ab-based therapeutics, including ADCs, to potentially prevent localised prostate cancer from spreading and may support the clinical management of locally advanced and metastatic prostate cancer.

### 4.4.1 Cell migration

Increased cell migration is an essential mechanism for cancer cells to develop within the metastatic cascade. Cell migration enables them to move from the primary tumour site, in order to establish secondary tumours (Clark & Vignjevic, 2015; Krakhmal *et al.*, 2015; Stoletov *et al.*, 2010). To examine, if STEAP2 Ab targeting has an effect on blocking cancer cell migratory properties, the cell migration assay was employed. Single anti-STEAP2 pAb treatment (ECL1 or ECL3 of STEAP2) demonstrated an inhibitory effect on cell migration irrespective of the targeted ECLs. Importantly, the study demonstrates, that the anti-STEAP2 pAbs were capable of

completely blocking the cell migration in PC3 prostate cancer cells at the maximum dose (20 µg/ml). No synergistic effect on inhibiting the cell migration was observed by the dual Ab treatment (AB1+AB4/ECL1+ECL3), which is therefore less favourable for the design of therapeutic antibodies. However, both immunogens located on the ECL1 or ECL3 qualify as potential target regions for the design of STEAP2 directed Ab therapeutics. The data confirms previous findings about STEAP2 being involved in promoting cancer cell migration and thereby enhancing prostate cancer progression (Burnell *et al.*, 2018; Whiteland *et al.*, 2014). Burnell and colleagues used the siRNA technology to knock-down the gene expression of STEAP2 in PC3 cells, which resulted in a significant decrease in the cell migratory capacity (Burnell *et al.*, 2018). Moreover, when normal PNT2 cells were transfected with STEAP2 vectors to increase expression, they gained an increased ability to migrate compared to non-transfected cells (Whiteland *et al.*, 2014). In the past, several researchers have suggested STEAP2 as a drug target (Burnell *et al.*, 2018; Grunewald *et al.*, 2012; Korkmaz *et al.*, 2002; Porkka *et al.*, 2002; Wang *et al.*, 2010). Based on this chapter's data, anti-STEAP2 antibodies are hypothesized to hold potential as anti-metastatic therapeutic intervention by inhibiting cancer cell migration. For example, antibodies may be employed as adjuvant therapy during Active Surveillance of localised or locally advanced prostate cancer (Palmer *et al.*, 2011). Antibodies may also be used for preventing cancer metastasis from becoming more systemic (Palmer *et al.*, 2011).

The key to the successful clinical application for mAbs has been their evidence to reduce both cell motility (e.g., cell migration and invasion) and cell growth (cell proliferation, cell viability) (Corraliza-Gorjon *et al.*, 2017; Palmer *et al.*, 2011). One FDA approved migration inhibitor is Trastuzumab (Herceptin®), a “blockbuster” mAb specific against the HER2+, which is overexpressed HER2+ breast cancer (Hudis, 2007; Panowski *et al.*, 2014; Verma *et al.*, 2012). Bevacizumab (Avastin®) blocks the formation of new blood vessels required for cancer cell invasion by targeting the Vascular Endothelial Growth Factor (VEGF) (Keating, 2014). In addition,

Dasatinib and Bosutinib are both mAbs specific to the Src tyrosine kinase for the treatment of several cancer (Roskoski Jr., 2015). The Src protein is activated via a number of surface receptors which further affects downstream signaling pathways that affect cell motility, proliferation and angiogenesis (Roskoski Jr., 2015). Another popular drug target under investigation is the cytokine Transforming Growth Factor $\beta$  (TGF $\beta$ ) (Connolly *et al.*, 2012; Neuzillet *et al.*, 2015; Palmer *et al.*, 2011). In cancer, TGF $\beta$  promotes cell growth and cancer invasion by angiogenesis (Connolly *et al.*, 2012; Neuzillet *et al.*, 2015). Thus, scientists have worked on the development of TGF $\beta$  ligand neutralising antibodies.

The key mechanism underlying how the anti-STEAP2 pAb (ECL3) inhibited cancer cell migration specifically remains unknown. The cell migration was blocked irrespective of the targeted ECL on STEAP2. Thus, it is likely that cell surface STEAP2 may be hindered from its physiological function as a receptor for iron and copper uptake/metabolism by anti-STEAP2 pAb (ECL3) binding (Grunewald *et al.*, 2012; Korkmaz *et al.*, 2005; Ohgami *et al.*, 2005; Porkka *et al.*, 2002). In this context, anti-STEAP2 pAb (ECL3) treatment may have compromised STEAP2 ligands, such as iron or copper, from binding to STEAP2. Thereby, a cascade of intracellular signaling pathways, including the MAPK/ERK signaling pathway, may have been suppressed. Two studies have hypothesized that *STEAP2* may affect cell cycle regulation and thereby cell proliferation via the MAPK/ERK signaling pathway (Burnell *et al.*, 2018; Wang *et al.*, 2010). The gene knock-down of *STEAP2* has resulted in cell cycle arrest by a G0/G1 phase block in both LNCaP and PC3 cells (Burnell *et al.*, 2018; Wang *et al.*, 2010). The MAPK/ERK pathway has been shown to regulate the LIMP pathway, which controls the expression of key determinant genes responsible for cell motility and mitosis (*e.g.*, Cofilin) (Ohashi, 2015; Pritchard *et al.*, 2004). High levels of Cofilin have been reported to be significantly linked to cancer (Coumans *et al.*, 2018; Maimaiti *et al.*, 2017; Shishkin *et al.*, 2016). Phosphorylated Cofilin, its activated form, contributes to the formation invadopodia cell structures, which are associated to cancer cell invasion (Bravo-Cordero *et al.*,

2014). Invadopodia is an actin rich cell type, which is capable to mediate ECM disruption and cancer invasion given its ability to structurally elongate and its cellular neighbourhood to the ECM (Leong *et al.*, 2014; Lohmer *et al.*, 2014; Murphy & Courtneidge, 2012). To evaluate, if *STEAP2* is associated with these pathways and results in enhanced cell migration, it would be exciting to study the gene and protein expression of phosphorylated Cofilin and MAPK/ERK by Western blotting after the gene knock-down of *STEAP2*. To determine the rate of (inhibited) cell migration after anti-STEAP2 pAb (ECL3) treatment more accurately in the future, real time monitoring using a suitable microscope (e.g. Juli microscope) is necessary. This allows the observation of the cell migration of one sample at a time for a desired time period. However, this requires a larger Ab volume and a lower number of samples, which can be visualized simultaneously (Grada *et al.*, 2018; Jonkman *et al.*, 2014). This chapter's data has provided evidence for the potential use of STEAP2 targeted antibodies to block of cancer cell migration.

#### 4.4.2 Cell invasion

The cell invasion assay was performed to assess, if the anti-STEAP2 pAb (ECL3) had an impact on the other key feature associated with cancer cell motility. The analysis conducted in this Chapter4 confirmed, that anti-STEAP2 pAb (ECL3) treatment resulted in a significant reduction in the invasive capacity of PC3 cells. The data supports past findings of the scientific literature, which showed, that the gene knock-down of *STEAP2* substantially decreased cancer cell invasion in PC3 cells (Burnell *et al.*, 2018). Additionally, Whiteland *et. al* has previously highlighted, that normal prostate epithelial cells (PNT2) gained the ability to invade the ECM after they have been transfected with a *STEAP2* plasmid, that resulted in overexpression of the gene (Whiteland *et al.*, 2014). Therefore, this chapter's data confirms the hypothesis, that STEAP2 is involved in promoting cancer invasion underlying prostate cancer progression. The exact mechanism of how increased STEAP2 levels drive cancer cell invasion is not well understood, yet. Burnell *et. al* has demonstrated,

that the gene knock down of *STEAP2* led to a significant reduction in *MMP* expression, which is required to degrade the ECM and therefore aids cancer cell invasion (Burnell *et al.*, 2018). However, there is evidence, that prostate cancer progression may be associated with an increased *MMP* expression by the NFkB signaling pathway (Chen *et al.*, 2013; Nguyen *et al.*, 2014). In addition, advanced stage prostate cancer may be ascribed to a constitutively active *NFkB* as found in the bone metastatic prostate cancer cell line PC3 (Gasparian *et al.*, 2002). Further, the NFkB signaling pathway may contribute to the overexpression of the gene *RANKL*, which is associated with cancer invasion, thereby enhancing prostate bone metastatic formation by osteoclastogenesis (Chen *et al.*, 2013; Jin *et al.*, 2015; Nguyen *et al.*, 2014). Future work may study how the gene knock-down of *STEAP2* alters the NFkB expression on a gene and protein level by PCR or Western blot following cell invasion tests.

A surprising result was, that the IgG isotype control Ab also slightly reduced the ability of PC3 cells to invade the ECM. The constant region of an immunoglobulin (Fc region of IgG) is a known binding region for the Fc-receptor. Subtypes of the Fc-receptor are mostly found on the cell surface of immune cells for host pathogen elimination or the placenta for nutrient supply (Li *et al.*, 2007, 2017; Van der Poel *et al.*, 2011). The IgG - Fc-receptor binding aids the recognition of pathogen-marked cells by natural killer cells (NK) and promotes the Ab-Dependent Cellular-mediated Cytotoxicity (ADCC) (Li *et al.*, 2017; Van der Poel *et al.*, 2011; Yamashita *et al.*, 2016). To which extent the Fc-receptor is expressed in the prostate or malignant prostate tissue remains to be elucidated. However, one research group has shown that silencing a specific immunoglobulin gene subtype, *IgG1*, significantly reduced the cell survival, cell cycle progression, cell migration and invasion of LNCaP cells (Xu *et al.*, 2016). Recent Ab based drug development include enhancing the tumour cell killing via ADCC (Yamashita *et al.*, 2016). In order to test, if the ADCC can be facilitated by *STEAP2* Ab targeting, PC3 cells could be subjected to anti-*STEAP2* pAb (ECL3) exposure. After the anti-*STEAP2* pAb (ECL3) exposure, the PC3 cells may be

incubated with human Peripheral Blood Monocyte Cells (hPBMC) from healthy or diseased donor blood to study the ADCC by flow cytometry (Yamashita *et al.*, 2016). The effects of the anti-STEAP2 pAb (ECL3) on cancer invasive properties combined with the ability to cause ADCC could increase the therapeutic efficiency of the drug in the future.

#### 4.4.3 Receptor internalisation

STEAP2 receptor internalisation was triggered upon the anti-STEAP2 pAb (ECL3) binding, thus the data confirmed STEAP2-Ab receptor complex trafficked to the acidic cell compartments. Research findings (including Chapter3, Section 3.3.5) has implied several, cellular distributions for STEAP2. Fluorescence microscopy has demonstrated, that STEAP2 resides at the plasma membrane, the Golgi and the early endosomes (Korkmaz *et al.*, 2005; Ohgami *et al.*, 2006; Porkka *et al.*, 2002). Based on its broad, cellular distribution and its metalloredutase activity, researchers have suggested STEAP2 partakes in the iron metabolism (Korkmaz *et al.*, 2005; Ohgami *et al.*, 2006; Porkka *et al.*, 2002). Cell surface STEAP2 may serve the uptake (internalisation) of metal containing molecules such as heme, iron or copper to maintain the physiological functions of the cell. After receptor internalisation, it is postulated, that STEAP2 shuttles via the Golgi organelle to the endosomes where the Tfr1 and the DMT1 proteins co-localise. These two proteins, Tfr1 and DMT1, are involved in the iron metabolism (Bogdan *et al.*, 2016; Korkmaz *et al.*, 2005; Ohgami *et al.*, 2006; Porkka *et al.*, 2002). The Tfr1 is known for the uptake of ferric iron, which is metabolised by STEAP2 to ferrous iron in the endosomes. From the endosomes, ferrous iron is exported by the DMT1 to the labile iron pool and distributed to the mitochondria (Bogdan *et al.*, 2016; Bradbury *et al.*, 2018; Gozzelino & Arosio, 2016; Soto-Herederero *et al.*, 2017). This chapter's data thus supports previous findings about STEAP2 to shuttle to the endosomes (Korkmaz *et al.*, 2005; Ohgami *et al.*, 2006; Porkka *et al.*, 2002). Recently, a mAb against the ECL2 of STEAP2 has been developed to study its plasma membrane cholesterol-dependent

receptor internalisation in *STEAP2* transfected HEK cells (Hasegawa *et al.*, 2018). The study has detected juxtannuclear puncta after the activation of the receptor internalisation using an anti-STEAP2 mAb (ECL2) and has also suggested an endosomal localisation of the protein (Hasegawa *et al.*, 2018).

Besides the endosomes, the chapter's findings further indicates STEAP2 to be present in the lysosome organelle based on the use of Promega's proprietary technology to design Ab pHAb Amine Reactive Dye Conjugates (Nath *et al.*, 2016). In the lysosomes, the presence of proton pumps creates the acidic environment (pH 4.5 – 5.5) where endocytosed macromolecules are being degraded (Nath *et al.*, 2016). The specific function of STEAP2 in the lysosomes remains unknown. Yet, kinetic analysis of STEAP4, a member of the STEAP family, exhibited metal-specific, low pH dependent reductase activity demonstrated by a kinetic analysis (Gauss *et al.*, 2013). The protein showed maximum ferrireductase activity at the acidic pH (pH 5.0 – 6.5) but not at basic pH levels (pH > 6.5) (Gauss *et al.*, 2013). Therefore, this chapter's finding confirms, that the ferrireductase activity of STEAP2 is dependent on acidic pH which is found in both the endosomal and lysosomal compartments (Gauss *et al.*, 2013). In this context, STEAP2 may responsible for the metabolism of released ferric iron in the acidic organelles. For example, STEAP2 may be involved in processing intracellular ferric iron from molecules such as ferritin. Ferritin is a molecule that carries and stores intracellular, ferric iron ( $\text{Fe}^{3+}$ ) and thus contributes to the maintenance of the iron homeostasis (Lane *et al.*, 2015). However, ferric iron may be released by ferritin upon lysosomal degradation (Lane *et al.*, 2015). In this context, STEAP2 may be involved in the iron homeostasis given its ferrireductase capacity to metabolise the released ferric ( $\text{Fe}^{3+}$ ) to ferrous iron ( $\text{Fe}^{2+}$ ). Taken together these novel insights about the trafficking of STEAP2, its lysosomal localisation sets the rationale to develop more efficient STEAP2 directed Ab drugs, such as ADCs. Future analysis could study kinetics of the receptor internalisation of STEAP2 STEAP2 over a desired time period. This can be achieved by live confocal imaging of PC3 cells and the anti-STEAP2 pHAb Amine Reactive Dye Conjugate (ECL3)

technology (Liao-*chan et al.*, 2015). The major disadvantage with live confocal imaging is, however, that cell surface STEAP2 cannot be visualised by the addition of acid because this would then be indistinguishable from the acidic organelle visualisation. Another technique, that provides more quantitative data about the receptor internalisation kinetics is flow cytometry analysis (Rigo & Vinante, 2017; Vainshtein *et al.*, 2015). Flow cytometry analysis allows rapid receptor visualisation studies due to the fast sample preparation time (Rigo & Vinante, 2017; Vainshtein *et al.*, 2015). However, this method is restricted to the visualisation of cell surface STEAP2.

#### 4.4.4 Cell viability

Treatment with the commercial anti-STEAP2 pAb (ECL3), at the 50 µg/ml and 75 µg/ml doses resulted in a decreased cell viability in 2D PC3 cells. After exposing the normal PNT2 cells to the anti-STEAP2 pAb (ECL3), a significant reduction in cell viability was observed indicating the PNT2 cells were more sensitive to the drug regimen than PC3 cells. It also implies, that the anti-STEAP2 pAb (ECL3), was cytotoxic to both PC3 and PNT2 cells at higher doses (50 – 75 µg/ml). In 3D PC3 spheroid cells, anti-STEAP2 pAb (ECL3) drug exposure (75 µg/ml) did not result in a significant effect on the cell viability. This suggests, that higher anti-STEAP2 pAb (ECL3) doses may be required to achieve a cytotoxic effect in these complex culture models, that are more representative of the tissue barriers that occur *in vivo*.

Antibody-STEAP2 targeting could have reduced the cell viability of PC3 and PNT2 cells by inhibiting the ERK/MAPK signalling pathway thereby compromising cell proliferation. In prostate cancer tissue specimen, increasing pERK expression has been shown to substantially correlate with increasing Gleason Scores indicating overexpressed MAPK/ERK is linked to prostate cancer progression (Gioeli *et al.*, 1999). With regards to STEAP2, Wang *et al.* have suggested it is involved in cell

proliferation, while preventing cells from apoptosis via the ERK/MAPK signalling (Wang *et al.*, 2010). When LNCaP cells were stimulated with Epidermal Growth Factor (EGF) increased pERK expression was observed compared to short hairpin-RNA (sh-RNA) LNCaP cells with STEAP2 knock-down (Wang *et al.*, 2010). Further, siRNA knock-down of STEAP2 gene expression in LNCaP cells resulted in a G0-G1 cell cycle arrest compared to the control by flow cytometry analysis which is presumably regulated by affecting cell-cycle genes (e.g. Ki67) (Wang *et al.*, 2010). Moreover, when STEAP2-siRNA LNCaP cells were treated with an apoptosis-inducing drug (e.g. TRAIL) a significant increase in apoptosis versus the non-silenced control was observed by TUNEL analysis suggesting STEAP2 to possess anti-apoptotic properties (Wang *et al.*, 2010). Based on these insights, it is concluded that antibody-targeting of STEAP2 reduces ERK-mediated cell proliferation/ cell viability of PC3 cells *in-vitro*. In order to confirm this hypothesis, PC3 cells could be treated with anti-STEAP2 antibody (Ab4/ECL3) (with or without EGF) following protein analysis of pERK/ERK by western blotting similar to Wang *et al.* and compared to untreated cells and siRNA STEAP2 PC3 cells.

STEAP2 is a transmembrane protein and its antibody binding may have triggered its conformational change, in order to allow the ion exchange or for intracellular signaling after ligand binding. Thus, it may be likely, that Ab binding to STEAP2/ECL3 may have sterically hindered binding of endogenous STEAP2 ligands (such as the NAD(P)H and heme) or inhibited its change to its active conformation leading to compromised physiological functions, which have been reflected by the decrease in cell viability (Gauss *et al.*, 2013; Gomes, Maia, & Santos, 2012; Korkmaz *et al.*, 2005; Ohgami *et al.*, 2006; Porkka *et al.*, 2002; Sikkeland, Sheng, Jin, & Saatcioglu, 2016). The MTT assay measures the viability of cells based on the quantification of their metabolic activity (Carneiro Borra *et al.*, 2009; Riss *et al.*, 2016; Stoddart, 2011). The MTT assay is based on a NAD(P)H dependent reduction of the tetrazolium salt to produce formazan, the absorbance of which can be measured. The absorbance value is often indirectly considered as proportional to the viability of

the cells (Carneiro Borra *et al.*, 2009; Riss *et al.*, 2016; Stoddart, 2011). The NAD(P)H enzyme is present in macrophages where it is responsible for induction of ROS by oxygen metabolism, in order to ensure pathogen killing (Alberts, 2015). Moreover, NAD(P)H is involved in the mitochondrial respiration process for energy production based on its oxidoreductase activity, which is used for the transport of electrons (Alberts, 2015).-Homology analysis of *STEAP2* has shown remote similarity with the *FAD420:NADH*, *NOX* and *Yedz* genes (Gomes *et al.*, 2012; C. G. Korkmaz *et al.*, 2005; Ohgami *et al.*, 2006; Sikkeland, Sheng, Jin, & Saatcioglu, 2016). The *FAD* gene exhibits NADPH oxidoreductase-like features (Challita-Eid *et al.*, 2007; Gauss *et al.*, 2013; Gomes *et al.*, 2012). The *NOX* gene has two binding sites for one FAD and one NAD(P)H molecule and is linked to increased ROS production (Challita-Eid *et al.*, 2007; Gauss *et al.*, 2013; Gomes *et al.*, 2012). The *Yedz* gene is thought to be responsible for the electron transfer via one single heme binding (Challita-Eid *et al.*, 2007; Gauss *et al.*, 2013; Gomes *et al.*, 2012). Based on the similarity to both the *NOX* and *Yedz* genes, *STEAP2* may be likely to exhibit NAD(P)H oxidoreductase-like properties (Challita-Eid *et al.*, 2007; Gauss *et al.*, 2013; Gomes *et al.*, 2012). Therefore, it is hypothesized, that a functional *STEAP2* protein is vital to retain the viability of the cells by partaking in redox reactions. The commercial anti-*STEAP2* pAb (ECL3) used in this study specifically targets a unique immunogen region on the ECL3 of *STEAP2* (aa 413 - 432). This immunogen region is in structural proximity to two FAD binding sites on the protein (aa 378 and aa 395) (see Chapter3, **Section 3.3.3**, **Table 3.4** and **Figure 3.9**, UniProt: Q8NFT2\_STEA2\_HUMAN). The anti-*STEAP2* pAb (ECL3) binding may have sterically compromised the FAD binding of *STEAP2*, leading to a dose-dependent decrease in its FAD/NAD(P)H oxidoreductase capacity. Subsequently, a reduction in oxidoreductase activity of *STEAP2* may have resulted in a decrease in cell viability.

In addition, molecular cloning and protein analysis of *STEAP2* (included in Chapter3) has provided evidence of two heme and two iron binding sites close the ECL2 and ECL3 positions of the protein (Korkmaz *et al.*, 2005; Ohgami *et al.*, 2005).

Iron and cupric reductase activity tests have confirmed STEAP2 as a metalloreductase (Ohgami *et al.*, 2006). The target immunogen region of the anti-STEAP2 pAb (ECL3), is situated on the ECL3 of STEAP2 (which spans the aa 413 - 432) and is closely located to the second iron binding site (predicted aa 409) (see Chapter3, **Section 3.3.3**, **Table 3.5** and **Table 3.6**, UniProt: Q8NFT2\_STEA2\_HUMAN). Thus, another explanation for the reduction in cell viability may be due the additionally compromised ferri/cupric metalloreductase activity of STEAP2 as a result of anti-STEAP2 pAb (ECL3) binding. STEAP2 shares endosomal localisation with the transferrin receptor and is capable of taking up ferric iron itself or from the transferrin receptor for iron metabolism (Ohgami *et al.*, 2005). STEAP2 is able to take up ferric iron ( $\text{Fe}^{3+}$ ) following the reduction to ferrous iron ( $\text{Fe}^{2+}$ ) in the endosomes. DMT1 is then responsible for the release of ferric iron into cytoplasm to store ferric iron in the labile iron pool (Bogdan *et al.*, 2016; Vela, 2018; Wang *et al.*, 2019). Iron is essential for the regulation of the cell cycle, cell proliferation and for DNA damage repair (Bogdan *et al.*, 2016; Gozzelino & Arosio, 2016). Furthermore, iron is utilised in the mitochondria for heme synthesis, an essential co-factor for red blood cells to carry oxygen (Barupala *et al.*, 2017; Stehling & Lill, 2013; Webert *et al.*, 2014). Thus, iron homeostasis is vital for physiological functions and the viability of the cells (Bogdan *et al.*, 2016; Gozzelino & Arosio, 2016). However, STEAP2 may be hindered from changing its protein conformation for the ferric iron uptake when the anti-STEAP2 pAb (ECL3) is bound to extracellular STEAP2 domains. Non-functional STEAP2 may have disrupted the iron metabolism in the endosome organelle. STEAP3 is also involved in iron transport via endosomal - mitochondria interaction which may serve the mitochondrial respiration (Yoo *et al.*, 2014). As a member of the STEAP family, a crosstalk between endosomal STEAP2 and the mitochondria may also exist. Ab STEAP2 binding may have therefore impaired both the metalloreductase and the oxidoreductase activity leading to insufficient iron and NAD(P)H supply for the mitochondria. Thus, the lack iron may have compromised the mitochondria's function, while the insufficient availability of NAD(P)H may explain the decreased capacity (viability) of the cells. To understand

the role of STEAP2 in these processes in greater detail, future studies should therefore investigate metalloredox activity utilising methods as described by Gauss *et al* after anti-STEAP2 pAb (ECL3) treatment (Gauss *et al.*, 2013). Interestingly, the PNT2 cells showed a significant reduction in cell viability at all given doses (25 µg/ml, 50 µg/ml and 75 µg/ml), as opposed to the PC3 cells, which exhibited a decrease in cell viability only at the 50 µg/ml and 75 µg/ml doses. This result suggests the PNT2 cells were more susceptible to anti-STEAP2 pAb (ECL3) drug treatment. The difference in STEAP2 expression pattern, higher STEAP2 presence in PC3 cells and lower STEAP2 protein in PNT2 cells, may provide an explanation for this observation. Thus, physiological functions, such as the NAD(P)H-like oxidoreductase activity and ion metabolism may be more sensitive for disruption based on the lower cell-surface STEAP2 availability in the PNT2 cells. The lower STEAP2 expression in PNT2 cells may explain why only 1/3 (25 µg/ml) of the maximum Ab dose (75 µg/ml) was required to reduce the cell viability. In comparison, the PC3 cells may have required at least double the Ab dose (50 µg/ml) to cause a reduction in cell viability because of the greater abundance of STEAP2 protein in these cells. Although the anti-STEAP2 pAb (ECL3) was cytotoxic to both normal prostate (PNT2) and prostate cancer (PC3) cells *in-vitro*, its maximum dose (75 µg/ml) did not substantially affect the cell migration of the normal PNT2 cells. Together, this would suggest undesired side-effects may occur in other low STEAP2 expressing tissues, should an Ab-based treatment approach be used clinically. However, it suggests cancerous PC3 cells are more likely to be blocked from cell migration than normal PNT2 cells. Given the cytotoxicity of the anti-STEAP2 pAb (ECL3) to both normal PNT2 and cancerous PC3 cells, the design of anti-STEAP2 ADC may be of advantage to improve the tumour cell killing-targeted approach.

#### 4.4.5 STEAP2 cell-surface expression and cell viability assessment after anti-STEAP2 pAb (AB4/ECL3) treatment in 3D PC3 spheroid cells

Often drugs fail to pass pre-clinical or clinical drug development due to lack of drug efficacy. 3D spheroid models represent an excellent *in-vitro* system to preliminarily evaluate drug potency (Huang & Gao, 2018). As only the two higher doses showed an effective reduction in cell viability in 2D monolayer PC3 cells, the highest dose (75 µg/ml) was selected to further study the impact of anti-STEAP2 pAb (ECL3) treatment on 3D spheroid cells. A z-stack of fluorescent-labelled STEAP2 in 3D PC3 cells demonstrated a strong fluorescent staining with increasing depth, indicating excellent Ab spheroid penetration and a homogenous STEAP2 expression throughout the spheroid. Thus, the pre-established 3D PC3 model was considered as suitable *in-vitro* drug screening model to assess cell viability after anti-STEAP2 pAb (ECL3) exposure.

Interestingly, the total section depth of the spheroids was approximately 14-fold less than the diameter. A methanol dehydration step was included in the staining protocol, to allow efficient Ab penetration and target binding. This is a common technique for antigen detection and Ab staining in tissue analysis (Miller, 2014; Troiana *et al.*, 2010). Thereby, any water content is removed and replaced with organic methanol (Weiswald *et al.*, 2010). The spheroids may collapse indicated by the formation of a rather epileptic instead of spheroid architecture as observed during our study (Weiswald *et al.*, 2010). Yet, no disaggregated spheroid parts were observed suggesting, that the spheroid maintained its integrity with only minor alterations in its original spherical structure. Thus, the 3D PC3 cells represent well the overexpression of STEAP2 in prostate-cancer *in-vitro* and was suitable for anti-STEAP2 pAb (ECL3) drug evaluation. The PI staining of the 3D PC3 cells after anti-STEAP2 pAb (ECL3) treatment (24 h) showed, that the highest Ab dose did not significantly lead to a difference in cell viability compared to the untreated and IgG

controls. This result suggested higher anti-STEAP2 pAb (ECL3) doses or longer exposure times (72 – 96 h) are required to impact the cell viability of 3D PC3 cells. This result is not unsurprising given that past research have reported substantial higher doses (up to 100-fold) are required to cause cytotoxicity in 3D spheroid cells compared to 2D monolayer cells for chemotherapeutic drugs (*e.g.* for Doxorubicin and Paclitaxel), while efficacy can be enhanced by extending the treatment time (Gong *et al.*, 2015; Nicholson *et al.*, 1997). Some spheroids become more compact over the time, form necrotic cores (Hirschhaeuser *et al.*, 2010; Hoarau-Véchet *et al.*, 2018; Huang & Gao, 2018). Thus, growth characteristics such as shape and diameter were monitored over a 14 days by Wang *et. al* (work within the group, unpublished). Wang *et. al* reported, that 3D PC3 cells reached its maximum cell viability within 72 h after seeding and a decrease in cell viability after this time point by PI staining. This study included untreated and IgG controls to take into account the base level of dead cells. Therefore, the PI staining allowed an effective Ab drug screening in 3D PC3 cells and the 24 h treatment time was selected to prevent false positive dead cells.

Future work may apply the CelltiterGlo test (Promega) for a more quantitative assessment. This assay correlates the absorbance with the cell viability by using a simple add and read format. Concludingly, the 3D PC3 cells are an excellent *in-vitro* drug screening prostate cancer model, which may be employed prior to pre-clinical testing. Future studies may require higher anti-STEAP2 pAb (ECL3) doses to achieve tumour cell killing effects in 3D PC3 spheroids to calculate effective doses (and IC<sub>50</sub> values).

## 4.5 Conclusion

---

The data generated in this chapter provides strong evidence for the therapeutic value of a STEAP2-targeted pAb (ECL3) for the future clinical translation, potentially as a mAb or ADC. Targeting the ECL3 appears to be promising as the anti-STEAP2 pAb lead candidate suppressed the ability of PC3 cells to display invasive properties, reduced their motility and promoted cytotoxicity in standard 2D culture. Thus, the anti-STEAP2 pAb lead candidate (ECL3) holds potential for the treatment of unfavourable localised or locally advanced prostate cancer to possibly prevent cancer metastasis *in-vivo*.

## 5 “Generation and *in-vitro* assessment of anti-STEAP2 antibodies.”

### 5.1 Introduction

---

Past insights into carcinogenesis on a molecular level have contributed to the identification of tumour specific biomarkers, which has driven the establishment of more targeted treatments (Schork, 2015). Examples of which include therapeutic antibodies, such as monoclonal antibodies (mAbs) or Antibody-Drug Conjugates (ADCs) (Carter & Senter, 2013; Chari *et al.*, 2014; Siew & Garofalo, 2015). The most common approach to produce mAbs is the hybridoma-based technology (Köhler & Milstein, 2019). The hybridoma technology demands the *in-vivo* immunisation (vaccination) of animal species with a specific antigen, which then elicits the Ab production of plasma B-cells *in-vivo*. The spleen cells, containing the Ab-producing plasma B-cells, are then harvested and fused with myeloma cells to generate hybrid cells (hybridoma cell clones), that each produce a unique mAb (Greenfield, 2012; Holzlöhner & Hanack, 2017; Köhler & Milstein, 2019; Pandey, 2010). Linear peptide sequences conjugated to the Keyhole Limpet Hemocyanin (KLH) protein are commonly used as antigens to increase the antigen’s immunogenicity (Swaminathan *et al.*, 2014; Wimmers *et al.*, 2017; Zivny *et al.*, 2011). Another way to enhance the immunogenicity of the antigens is to use a multiple branched antigen (MAP or cyclic antigen), which is made up of several molecules of the linear antigen (Basak *et al.*, 1995; Ganeshrao & Vikas, 2013). Progress in Ab discovery have contributed to a variety of novel Ab formats including ADCs. The mechanism of action of the ADC demands the ADC receptor internalisation by the tumour-antigen associated (TAA) cancer cells to release the cytotoxin upon lysosomal degradation (Chalouni & Doll, 2018; Drachman & Senter, 2013; Peters & Brown, 2015). The well-studied cytotoxin Monomethylauristatin-E (MMAE) is a microtubule inhibitor, that blocks the microtubule polymerisation, thereby preventing cancer cell division and growth (Chen

*et al.*, 2017; Johansson *et al.*, 2017; Kratschmer & Levy, 2018). MMAE is a cytotoxin commonly used in the ADC technology and is utilised in the FDA approved ADC Brentuximab Vedotin (Adcetris®). Brentuximab Vedotin specifically targets CD30 and is used to treat lymphoma (Gravanis *et al.*, 2016). Besides STEAP2, prostate-specific drug targets including the Prostate-Specific Membrane Antigen (PSMA) and STEAP1 are currently investigated for the development of Ab therapeutics to treat metastatic prostate cancer (Boswell *et al.*, 2011; Hofman *et al.*, 2018; Patent Application No. 1/2019/500603, 2018; Petrylak *et al.*, 2019; Wang *et al.*, 2011). However, there is no commercial mAb or ADC available on the market, yet, which can be used to treat men with advanced prostate cancer specifically. Previous findings have demonstrated the role of STEAP2 in driving cancer invasive and migratory properties *in-vitro* underlying prostate cancer progression (Burnell *et al.*, 2018; Wang *et al.*, 2010; Whiteland *et al.*, 2014). The previous Chapter4 has also highlighted the potential of a commercial, polyclonal anti-STEAP2 Ab (anti-STEAP2 pAb/ECL3) to block cancer invasive properties, plus the ability to trigger STEAP2 receptor internalisation in the cancerous PC3 cell line.

The aims of this Chapter were therefore to:

- (1) Develop a monoclonal anti-STEAP2 Ab (ECL3);
- (2) Fabricate a polyclonal anti-STEAP2-MMAE ADC (ECL3) and to evaluate its impact on reducing the cell viability versus the unconjugated anti-STEAP2 pAb (ECL3) in the cancerous PC3 cells.

## 5.2 Material and methods

---

### 5.2.1 Cell lines

The cell lines utilised throughout the present chapter are described in Chapter2, **Section 2.1.5**.

### 5.2.2 Cell culture

Cell culture was maintained as described in Chapter2, **Section 2.1.6**.

### 5.2.3 Polyclonal anti-STEAP2-MMAE ADC generation

The ADC development was carried out by CellMosaic using the PerKit™ Ab MMAE Conjugation Kit and the Maleimidocaproyl-Valine-Citrulline Para-amino benzoylcarbonyl (MC-VC-PABC) linker (Cell Mosaic, USA, Cat. No. CM11409x3). All necessary reagents and buffers were provided by CellMosaic. The disulphide bonds of 3.0 mg of the commercial anti-STEAP2 pAb (AB4/ECL3) (Insightbiotechnology, UK) were reduced and conjugated to VC-PABC MMAE as described in Chapter2, **Section 2.2.6** and stored at 4°C until ready for use.

### 5.2.4 Polyclonal anti-STEAP2 ADC quality control

Quality controls were conducted by CellMosaic to assess the anti-STEAP2 pADC were Size Exclusion Chromatography and the Hydrophobic Interaction Chromatography.

#### 5.2.4.1 Size-Exclusion Chromatography (SEC)

SEC analysis was conducted as described in Chapter2, **Section 2.2.6.1** to assess the Drug-to-Ab Ratio (DAR). The unconjugated anti-STEAP2 pAb (ECL3) (Insightbiotechnology, UK) and the free MMAE payload (provided by CellMosaic) were included as positive controls. As a positive control for highly purified Ab, an anti-mouse anti-IgG monoclonal Ab was used (Thermofisher, UK). Absorbances were

measured at A = 280 nm (protein e.g. IgG), A = 248 nm (MMAE) and A = 220 (amide bonds of proteins or peptides). The DAR of 3:1 was calculated and provided by CellMosaic according to the Area Under the Curve (AUC) of the samples during SEC analysis. Test was run once by CellMosaic.

#### 5.2.4.2 Hydrophobic Interaction Chromatography (HIC)

HIC analysis was performed as described in Chapter2, **Section 2.2.6.2**. Three graphs are presented in the data, which show the absorbances measured at A = 280 nm (protein e.g. IgG), A = 248 nm (MMAE) and A = 220 (amide bonds of proteins or peptides) (Appendix 3, **Figure A3. 1 - Figure A3. 3**). Test was run once by CellMosaic.

#### 5.2.5 Cell viability assay

Approximately 2,000 cells were cultured per well of a 96-well plate and left to adhere for 24 h. The next day, cells were exposed to 0.01, 0.1, 1.0, 10.0, 100.0 and 200.0 µg/ml of either anti-STEAP2 pAb (ECL3) (stock concentration: 1.0 mg/ml), anti-STEAP2 pADC (stock concentration: 1.24 mg/ml), anti-IgG pAb (stock concentration: 1.7mg/ml), MMAE (stock concentration: 10 mM) or 0.1% Triton for 72 h ( **Table 5.1**) before analysis was carried out in triplicate according to Chapter2, **Section 2.2.5.3**.

**Table 5.1 Treatments to compare the efficiency of the anti-STEAP2 ADC versus the unconjugated anti-STEAP2 pAb in reducing the cell viability**  
. MMAE doses were prepared in the ng/ml range equivalent to the MMAE molecules each anti-STEAP2 pADC contained with a DAR of 3:1. \*: excluding the anti-STEAP2 pADC.

pADC, pAb, IgG – dose [µg/ml]	MMAE - dose [ng/ml]
200.0* (excluding pADC)	1,423.0
100.0	142.3
10.0	14.23
1.0	1.423
0.1	0.1423
0.01	0.0001423

The negative controls used were untreated cells and a STEAP2-non-specific anti-IgG isotype Ab. Positive controls for cell viability reducing agents (cell killing) were the free cytotoxin MMAE (MedChemExpress, Sweden) and 0.1% Triton-X 100. During the dose finding experiments, the presence of the cells was checked under after 72 h using the AxioCam ERC55 (ZEISS, Germany). During optimisation studies using the dose range 0.01 – 100 µg/ml, no cells were evident under the microscope at 100 µg/ml after the anti-STEAP2 pADC treatment (data not shown). Therefore, the maximum anti-STEAP2 pADC dose was 100 µg/ml, whereas the maximum dose for the other treatments was increased to 200 µg/ml. The MMAE doses were prepared in the ng/ml range equivalent to the MMAE molecules (DAR), which each of the anti-STEAP2 pADC doses contained (see Appendix 3, **Table A3. 1**).

#### 5.2.5.1 Minimal inhibiting concentration (IC<sub>50</sub>)

Based on the data obtained from Chapter 5, **Section 5.2.5**, a log-scaled dose-response curve was generated for the anti-STEAP2 pADC and anti-STEAP2 pAb following a dose-response-inhibition four-parameter variable slope analysis by GraphPad. Increasing dose points were added to extrapolate the data points (grey in **Table 5.2**), in order to determine the IC<sub>50</sub> value. Analysis was conducted using GraphPad's dose-response-inhibition four-parameter variable slope analysis (**Table 5.2**).

**Table 5.2 Log-scaled doses for the IC<sub>50</sub> assessment**

. Grey: extrapolated doses.

Dose [µg/ml]	Log dose pADC	Log dose pAb
0.01	-2	-2
0.1	-1	-1
1	0	0
10	1	1
100	2	2
200	2.3	2.3
1,000	3	3
10,000	4	4
100,000	5	5

### **5.2.6 Monoclonal anti-STEAP2 Ab development at APS**

The monoclonal anti-STEAP2 Ab development was undertaken by Ab Production Services (APS), UK. Both the linear and cyclic antigen syntheses was carried out by APS. Eight Balb/C mice (four Balb/C mice per type of antigen) were utilised for the anti-STEAP2 mAb development in total, which was carried out at Ab Production Services, UK (Chapter 2, **Section 2.2.7.3**). The four Balb/C mice received 5 immunisations in total with either linear or cyclic STEAP2 antigen and a final booster 3 days before the fusion (Phase I). Test sera 1 and 2 (Phase I) were retrieved from the tail of the Balb/C mice for verification during. Balb/C mice were sacrificed and their spleens were harvested and prepared for Phase II. The hybridoma development (cell fusion, Phase II) was carried out by the fusion of the mouse spleen cells with mouse myeloma cells by Polyethylenglycol (PEG) and the initial hybridoma cell colonies cells were cultured (Phase II). Then, the cell culture supernatant was screened in 96-well plates for STEAP2-positive, single mouse cell hybridoma clone by a serial dilution (1:100 – 1:204,800) and indirect ELISA during the Limiting Dilution step (Phase III). Positive mouse monoclonal anti-STEAP2 antibodies 1 – 4 were scaled up in 24-well plates following affinity purification by Protein-G (Phase IV). The final Ab concentration in the cell culture supernatant was measured by UV-VIS ( $A = 280 \text{ nm}$ ) by APS. M1 CB12 H7 F7 was referred as anti-STEAP2 mAb1 (linear) with a concentration of 2.0 mg/ml, M 1DG5 1 B9 A9 F7 was referred as anti-STEAP2 mAb2 (linear) with a concentration of 1.3 mg/ml, M1 FC7 B9 D12 was referred to anti-STEAP2 mAb3 (linear) with a concentration of 1.8 mg/ml and M4 JA12 B9 1 D12 was referred as anti-STEAP2 mAb4 (cyclic) with a concentration of 2.1 mg/ml. Names were given by APS.

#### **5.2.6.1.1.1 Nu-PAGE analysis (APS)**

2  $\mu\text{g}$  of Protein-G affinity purified monoclonal anti-STEAP2 Ab was loaded per 4 - 12% Bis-Tris gel (denaturing/ reducing conditions) provided by APS. As a negative

control PBS was run. The visible SeeBlue Plus2 provided by APS was used as a molecular weight marker. Nu-PAGE analysis was carried out by APS once.

#### **5.2.6.2 Shipping and storage of the Ab containing samples**

Test samples from Phase I – IV of the monoclonal anti-STEAP2 Ab development were shipped on dry ice from APS (Slough, UK) to Swansea University and stored at -20°C.

### **5.2.7 Ab screening methods**

#### **5.2.7.1 Indirect Enzyme-Linked Immunosorbent Assay (ELISA)**

The ELISAs were carried out by APS as described in Chapter2, **Section 2.2.7.5.1** while additional data analysis was conducted during this thesis. An OD  $\geq 1.0$ mg/ml at 1:10,000 was determined as ideal reference point for a sufficient Ab titre (to move on to Phase II). As a second reference point, the ratio (cut-off point) of OD (sample): OD (negative control)  $\geq 2$  was considered as a sufficient reference. Serum from Balb/C mice prior to the immunisation (pre-immunised sera) was included as negative control during Phase I, when available due to limited volume. Test sera1 samples were evaluated against the type of STEAP2 antigen they were raised against. Test sera2 was assessed for both linear and cyclic STEAP2 peptides. The anti-STEAP2 mAbs were assayed against the linear STEAP2 peptide. Tests were conducted in technical duplicate at APS.

#### **5.2.7.2 Western blotting**

Western blotting was conducted as described in Chapter2, **Section 2.2.3**. After electro-blotting, the membrane was cut into 4 pieces (**Figure 5.1**).

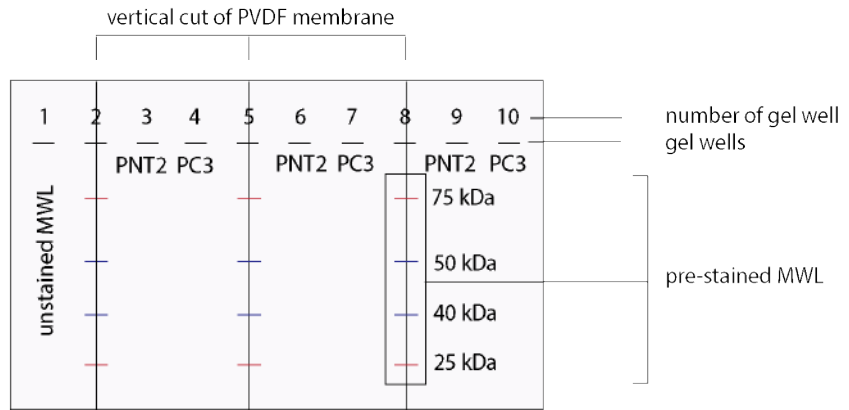


**Figure 5.1 Cut of the PDVF-membrane for protein analysis.** Membrane was cut into four pieces indicated by the vertical lines. Cell lysates from the PNT2 (low STEAP2 expression) and PC3 (higher STEAP2 expression) cell lines were utilised. 1:Unstained molecular weight ladder; 2: pre-stained dual colour molecular weight marker; 3, 6, 9: technical triplicate of PNT2 cell lysate; 4, 7, 10: technical triplicate of PC3 cell lysate.

Each of the membranes was first probed over night at 4°C with mouse (testing samples) or rabbit primary anti-beta-actin (1:1,000, CST, UK). After 3x TBST washes, the secondary goat anti-mouse or rabbit anti-IgG-HRP linked Ab and the anti-biotin-HRP-linked Ab were applied at 1:10,000 for 1 h at RT. The secondary goat anti-rabbit anti-IgG Ab (Abcam, UK) was applied to detect the commercial primary rabbit anti-STEAP2 pAb (ECL3) used as a positive control Ab for STEAP2 protein expression. The secondary goat anti-mouse anti-IgG Ab (Abcam, UK) was applied to detect the testing primary mouse anti-STEAP2 antibodies (from the Test sera2, supernatant of the hybridoma cell colonies or monoclonal anti-STEAP2 antibodies). The membranes were washed 3x TBST, stripped, washed 3x TBST and blocked for 1 h in 7.5 % BSA (Chapter2, **Section 2.2.3.8** and **Section 2.2.3.9**). Membranes were re-probed with test sera (1:250), Ab supernatant from hybridoma colonies (1:100) or mouse monoclonal anti-STEAP2 Ab (1:100) over night at 4°C. First, a colorimetric image was acquired to demonstrate the membranes with pre-stained molecular weight marker and to indicate where the membranes were cut exactly. Then a chemiluminescent image was acquired without moving the membranes and merged with the colorimetric image using the equipment described in Chapter2, **Section 2.1.3**.

### 5.2.7.3 Fluorescence microscopy

Cells were prepared as described in Chapter 2, **Section 2.2.4.1**. Cells were incubated overnight at 4°C with either Test sera2 (1:200, Phase I, N = 1), supernatant from hybridoma colonies (undiluted, Phase II, N = 1) or the purified mAbs obtained from the single hybridoma cell clones (undiluted, Phase IV, N = 3) or commercial polyclonal primary rabbit anti-STEAP2 pAb (ECL3) (1:200, Insightbiotechnology, UK) as a positive control. The next day, cells were washed with PBS before the addition of secondary polyclonal goat anti-mouse anti-IgG-Alexa Fluor-488 Ab (1:1,000, Invitrogen, UK) to the testing samples for 1 h at RT. The polyclonal goat anti-rabbit anti-IgG-AlexaFluor-488 Ab (1:1,000, Abcam, UK) was used to detect the commercial primary rabbit anti-STEAP2 pAb(ECL3) control for 1h at RT. The primary mouse monoclonal anti-golgin97 Ab (1:100, Invitrogen, UK) was used as a positive control for the secondary polyclonal goat anti-mouse anti-IgG-AlexaFluor-488 Ab and was exclusively included during the mAbs (Phase IV). Samples were further prepared for analysis as described in Chapter 2, **Section 2.2.4.1 - 2.2.4.3**. Images with three different fields of view with a 63x zoom objective were acquired per test sample for qualitative analysis.

### 5.2.8 Statistical analysis

Results were statistically analysed with GraphPad Prism (Version 8, USA). Normality of the data was evaluated by the Shapiro-Wilk test ( $N < 10$ ). Cell viability data was analysed by using the one-way ANOVA *post-hoc* Dunnett test. A student t-test was used to assess the statistical significance of STEAP2 expression between the PNT2 and PC3 cell lines during western blotting analysis. Data was considered as statistically significant when p-value of  $\leq 0.05$  (\*), p-value  $\leq 0.01$  (\*\*), a p-value of  $\leq 0.001$  (\*\*\*) or p-value  $\leq 0.0001$  (\*\*\*\*) were annotated with in the respective figures.

## 5.3 Results

---

In order to compare the impact of the polyclonal anti-STEAP2-MMAE Ab-Drug Conjugate (anti-STEAP2 pADC) and the commercial polyclonal anti-STEAP2 Ab (anti-STEAP2 pAb/ECL3) on reducing the cell viability, the MTT assay was performed using the prostate cancer PC3 cells. Further, the monoclonal anti-STEAP2 Ab (anti-STEAP2 mAb/ECL3) development was carried out in collaboration with Ab Production Services (APS, UK). Test samples were screened for the presence of anti-STEAP2 mAbs during Phase I, after Phase III and after Phase IV using ELISA (carried out by APS and analysed at Swansea University), confocal microscopy and Western blotting.

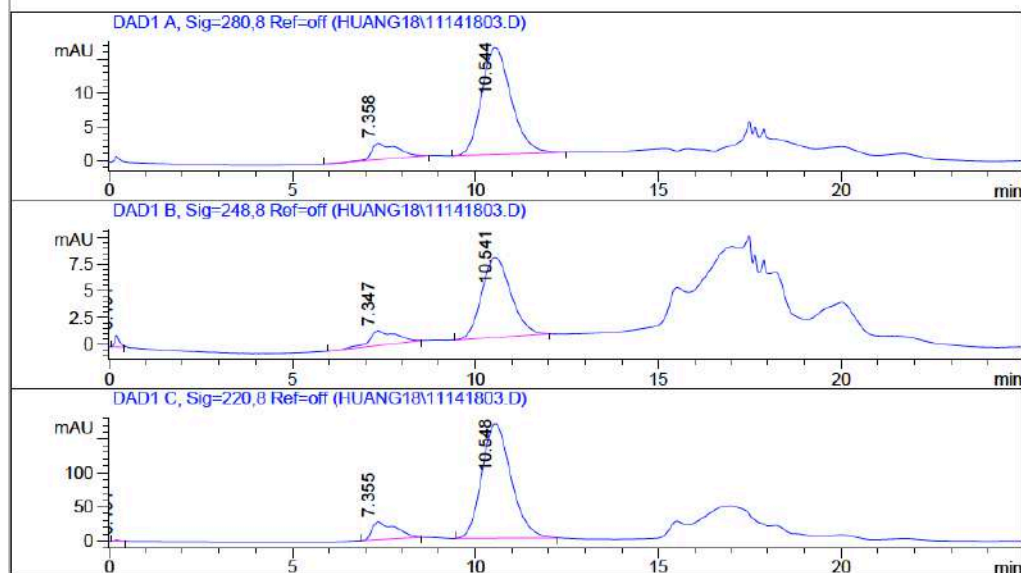
### 5.3.1 SEC to determine the DAR of the anti-STEAP2 pADC

The SEC analysis of the unconjugated, commercial anti-STEAP2 pAb (ECL3) showed two distinct peaks at approximately 7.3 min and 10 min (**Figure 5.2**). The first peak (at 7 min) indicates, that smaller molecules, such as salts like PBS or glycine, may be present in the formulation of the anti-STEAP2 pAb (ECL3), which elute first given their small molecular size (**Figure 5.2**). The major peak at 10 min suggests the later elution of the anti-STEAP2 pAb (ECL3) based on its larger molecular weight than the salts (**Figure 5.2**). The SEC analysis of the anti-STEAP2 pADC showed three distinct peaks. The first two most abundant molecules eluted after 7.3 and 7.7 min (**Figure 5.3**). The first peak (at 7.3 min) may suggest the presence of smaller molecules like PBS or glycine in the formulation of the anti-STEAP2 pADC, which elute first given their small molecular size (**Figure 5.3**). This is in alignment with the SEC data using the unconjugated, commercial anti-STEAP2 pAb (ECL3) (**Figure 5.3**).

HPLC Data Analysis

Data File name: C:\HPCHEM\1\DATA\HUANG18\11141803.D  
 Method name: TSK-L5.M  
 Injection Time: 9:33:58 AM **SEC HPLC of STEAP Antibody Alone**  
 Injection Date: 11/14/2018

CellMosaic, Inc. Injection Volume: 20.000  
 Instrument 1 Sequence Name:  
 Data Acquired By: CellMosaic QA Pressure (bar) : 67.440  
 Location: Vial 51 Flow (mL/min) : 0.750  
 Sample Name: steap2 Temp (C) : 24.980



#	Meas.RT	Main Peak Area	Main Peak Area %	Main Peak Height
1	0.191	17.229	0.163	1.860
2	7.355	1163.892	10.984	26.529
3	10.548	9414.980	88.853	168.219
Total				

**Figure 5.2 SEC of the unconjugated anti-STEAP2 pAb (ECL3).** The data provided by CellMosaic shows two distinct peaks. The three graphs represent the absorbances measured at A 280 nm: protein (IgG) (top); A 248 nm: MMAE (middle); A 220 nm: amide bonds of proteins or peptides (bottom) (N = 1).

The second peak (at 7.7 min) may indicate the presence of free MMAE molecules, which possess a larger molecular size than the salts but is not larger than the anti-STEAP2 pADC (**Figure 5.3**). Therefore, the third and major peak at approximately 10 mins, may be ascribed to the anti-STEAP2 pADC, given its larger molecular weight. Moreover, the 94.13% main peak area implies a successful ADC development with little remaining, free MMAE (**Figure 5.3**).

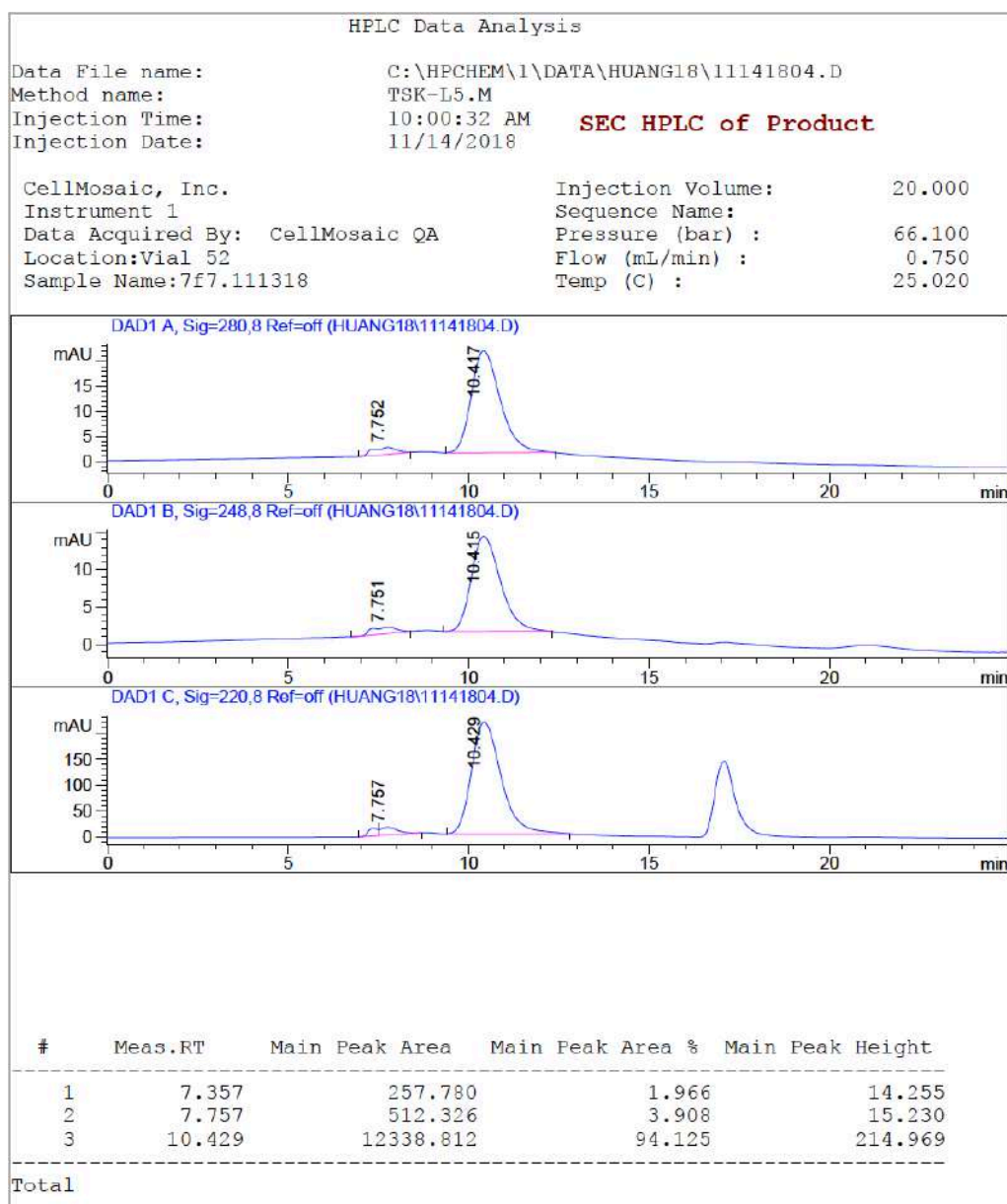


**Figure 5.3 SEC of the commercial anti-STEAP2 pADC (ECL3).** The data shows two distinct peaks provided by CellMosaic. The three graphs represent the absorbances measured at A 280 nm: protein (IgG) (top); A 248 nm: MMAE (middle); A 220 nm: amide bonds of proteins or peptides (bottom) (N = 1).

The DAR of the anti-STEAP2 pADC was calculated based on the R-value (A248 nm/A280 nm) of the maximum product peak at 10.24 min as follows by CellMosaic:  $DAR = (21 \times 0.63 - 9) : (1.615 - 0.1425 \times R) = 2.77 \sim 3$ ; Where: A248 nm = 721.2; A280 nm = 1142.7; R = 0.63. Thus, 1 molecule of anti-STEAP2 pADC contained about 3 MMAE molecules.

### 5.3.2 Poor anti-STEAP2 pADC cell killing efficiency in PC3 cells

To evaluate, if the anti-STEAP2 pADC was more efficient to specifically reduce the cell viability of the PC3 cells more efficiently than the commercial anti-STEAP2 pAb, the MTT assay was applied.

At a dose of 0.01  $\mu\text{g}/\text{ml}$  of drug regimen, cancerous PC3 cells exposed to MMAE showed a significant decrease in cell viability of 37.41% (SD = 7.9%) compared to all other treatments. These were the untreated control with a cell viability of 102.3 % (SD = 1.81%, p-value = 0.003), PC3 anti-IgG antibody treated cells with a cell viability of 109.13% (SD = 5.18%, p-value = 0.009), anti-STEAP2 pAb treated PC3 cells with a cell viability of pAb cell viability = 97.3% (SD = 8.45%, p-value = 0.025) and the anti-STEAP2 pADC treated PC3 cells with a cell viability of 93.85% (SD = 8.94%, p-value = 0.008). This highlighted the potency of the highly cytotoxic agent MMAE.

At a dose of 0.1  $\mu\text{g}/\text{ml}$  of drug treatment, only the MMAE treated PC3 cells demonstrated a significant reduction in cell viability of 26.9% (SD = 12.96%) opposed to the untreated control with a cell viability of 117.62%, SD = 12.49%, p-value = 0.003), the anti-IgG Ab treated PC3 cells with a cell viability of 99.35% (SD = 1.8%, p-value = 0.009), the anti-STEAP2 pAb treated PC3 cells with a cell viability of 99.21% (SD = 1.78% , p-value = 0.025) and the anti-STEAP2 pADC treated PC3 cells with a cell viability of 99.21 (SD = 1,79%, p-value = 0.009) (**Figure 5.4**). This result again indicated, that only the MMAE treatment had an impact on reducing the cell viability of the PC3 cells at a dose of 0.1  $\mu\text{g}/\text{ml}$ .

At a dose of 1.0  $\mu\text{g}/\text{ml}$  of drug treatment, a similar decrease in cell viability was exhibited for only the MMAE treated cells (**Figure 5.4**). In detail, the MMAE exposed PC3 cells showed a significant reduction in cell viability of 40.55% (SD = 9.06%) opposed to the untreated control with a cell viability of 99.38% (SD = 13.8%, p-value = 0.01) (**Figure 5.4**). This result indicates, that only the MMAE treatment

had an effect on reducing the cell viability of the PC3 cells. Moreover, the result suggests, that exposure of the PC3 cells to the anti-STEAP2 pAb or anti-STEAP2 pADC did not result in any changes in cell viability.

At a dose of 10.0  $\mu\text{g}/\text{ml}$  of drug treatment, the first substantial decrease in the cell viability of 56.73% (SD = 19.37%, p-value = 0.506) of the PC3 cells after anti-STEAP2 pADC drug exposure was observed compared to the untreated PC3 cells, although not significant (**Figure 5.4**). In addition, PC3 cells treated with anti-STEAP2 pAb exhibited a reduced cell viability of 79.38% (SD = 3.24%, p-value = 0.339) compared to untreated PC3 cells, albeit not significant. MMAE treated PC3 cells exhibited the lowest cell viability of 31.62%, SD = 5.97%, which was significantly lower than the cell viability of PC3 cells treated with either anti-STEAP2 pADC (p-value = 0.009) and anti-STEAP2 pAb (p-value = 0.004) (**Figure 5.4**). This result suggests the anti-STEAP2 pADC may be of poor quality. The data also may imply the anti-STEAP2 pADC could be subjected to an incomplete lysosomal degradation but not the cell free MMAE at a 10.0  $\mu\text{g}/\text{ml}$  dose given its potent cell killing efficiency.

At 100  $\mu\text{g}/\text{ml}$  of drug treatment, a significantly reduced cell viability was observed for anti-STEAP2 pADC treated PC3 cells with cell viability of 11.29% (SD = 2.79%, p-value < 0.001) compared to untreated PC3 cells (**Figure 5.4**). It is important to mention, that based on an initial dose optimisation, the maximum dose of anti-STEAP2 ADC treatment was 100  $\mu\text{g}/\text{ml}$ , thus no further dose increase was conducted (see **Section 5.2.5**). Further, the cell viability was significantly decreased to 38.66% (SD = 6.39%, p-value < 0.001) in PC3 cells exposed to 100  $\mu\text{g}/\text{ml}$  of anti-STEAP2 pAb compared to the untreated PC3 cells (**Figure 5.4**). Interestingly, the anti-STEAP2 pADC treated PC3 cells demonstrated a significantly lower cell viability than the PC3 cells exposed to the unconjugated anti-STEAP2 pAb (p-value = 0.022) at a dose of 100  $\mu\text{g}/\text{ml}$  (**Figure 5.4**). This implies, that the anti-STEAP2 ADC had a stronger effect on reducing the cell viability in PC3 cells when compared to the unconjugated anti-STEAP2 pAb, however at extremely high doses (100  $\mu\text{g}/\text{ml}$ ).

Interestingly, 100  $\mu\text{g}/\text{ml}$  of anti-STEAP2 pADC was more efficient in reducing the cell viability to 11.29% (SD = 2.79%) than its equivalent doses of MMAE treatment with a cell viability of 21.65% (SD = 11.99%), albeit not significant (p-value = 0.393) (**Figure 5.4**). This may be due to the larger error bars of the MMAE treatment at the equivalent dose of 100  $\mu\text{g}/\text{ml}$ . Importantly, this data highlights, that the anti-STEAP2 pADC may have delivered the cytotoxin MMAE more specifically to STEAP2 overexpressed PC3 cells compared to the pure MMAE alone at 100  $\mu\text{g}/\text{ml}$ . In addition, PC3 cells exposed to 100  $\mu\text{g}/\text{ml}$  of anti-IgG Ab isotype control treated cells showed a decreased cell viability of 83.49%, however, not significant (SD = 3.58%, p-value = 0.086) suggesting the cell viability was specifically reduced due to both anti-STEAP2 pAb and anti-STEAP2 pADC.

At a dose of 200  $\mu\text{g}/\text{ml}$  of drug treatment, a significant reduction in cell viability to 21.47% (SD = 3.14%, p-value < 0.0001) was observed after anti-STEAP2 pAb treatment in the PC3 cells opposed to the untreated PC3 cells with a cell viability of 114.52% (SD = 13.62%) (**Figure 5.4**). PC3 cells exposed to 200  $\mu\text{g}/\text{ml}$  of MMAE treatment demonstrated a similar substantial decrease in cell viability to 24.35% (SD = 7.53%, p-value = 0.0008). Interestingly, PC3 cells exposed to 200  $\mu\text{g}/\text{ml}$  of anti-IgG pAb led to a significant reduction in cell viability of 69.21% (SD = 1.35%, p-value = 0.009) in comparison to untreated PC3 cells (**Figure 5.4**). This suggests, that the reduction in cell viability of the PC3 cells was also caused by high doses of the STEAP2 unspecific anti-IgG pAb, regardless of the STEAP2 specificity when using an extremely high dose.

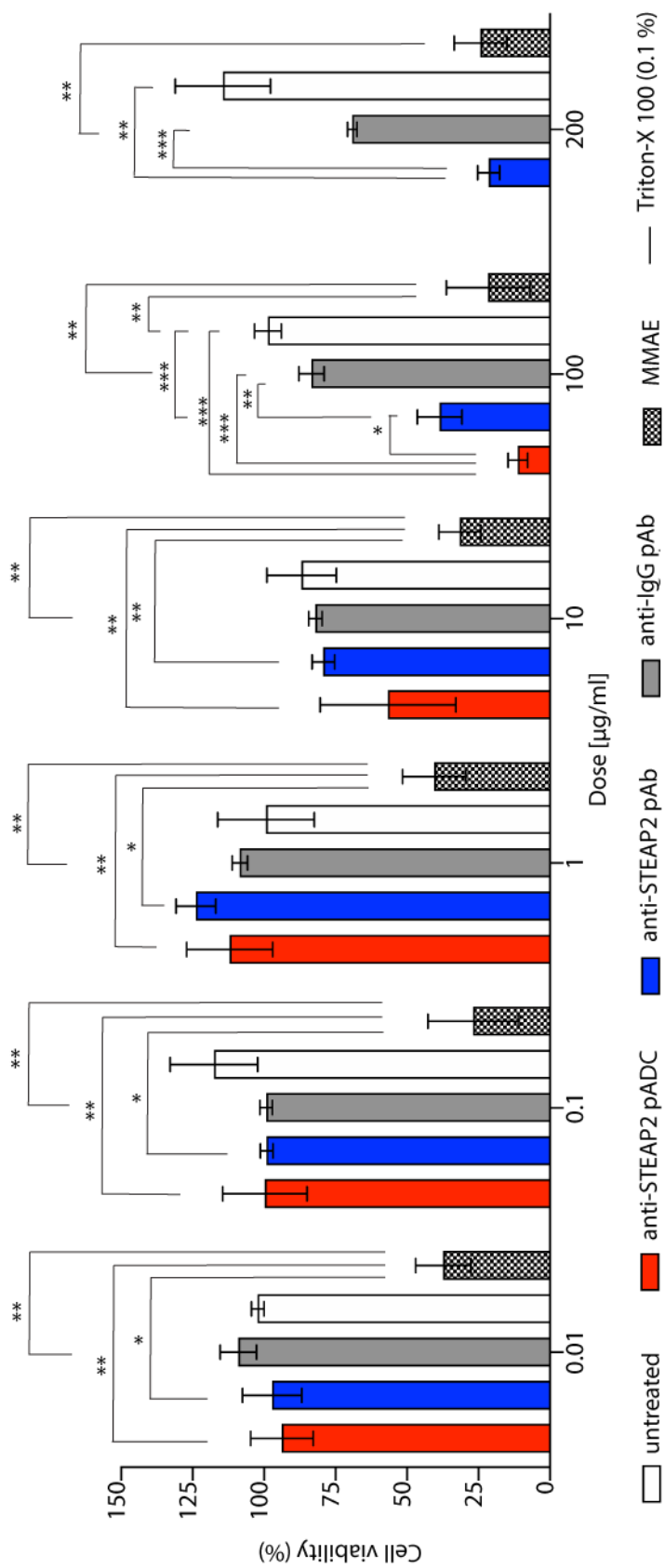


**Figure 5.4 Effect of anti-STEAP2 pADC and pAb on cell viability (PC3 cells)**  
 . The data indicates potential MMAE-ADC catabolite resistance of the PC3 cells. 0.1% Triton X 100: positive control for reduction in cell viability illustrated as horizontal line at 0 % throughout the graph. Statistical analysis was performed using an ANOVA *post-hoc* Dunnett test. p-value of  $\leq 0.05$  (\*), p-value  $\leq 0.01$  (\*\*), p-value of  $\leq 0.001$  (\*\*\*)(N = 3).

### 5.3.3 IC<sub>50</sub> of anti-STEAP2 pADC indicates poor quality

A dose-response curve was generated to compare the ability of the polyclonal anti-STEAP2-MMAE ADC (anti-STEAP2 pADC) and the commercial, unconjugated polyclonal anti-STEAP2 Ab (anti-STEAP2 pAb) on reducing the cell viability of the PC3 cells. No significant differences in cell viability between the anti-STEAP2 pADC and anti-STEAP2 pAb treatments were observed for the doses at 0.01 µg/ml, 0.1 µg/ml, 1.0 µg/ml and 10.0 µg/ml (**Figure 5.5**). However, the data highlights that a dose of 100 µg/ml of anti-STEAP2 pADC significantly reduced the cell viability to 11.2% (SD 2.79%), whilst PC3 cells exposed to the unconjugated anti-STEAP2 pAb exhibited a reduced cell viability of 38.66% (SD = 6.39%, p-value 0.022) (**Figure 5.5**).

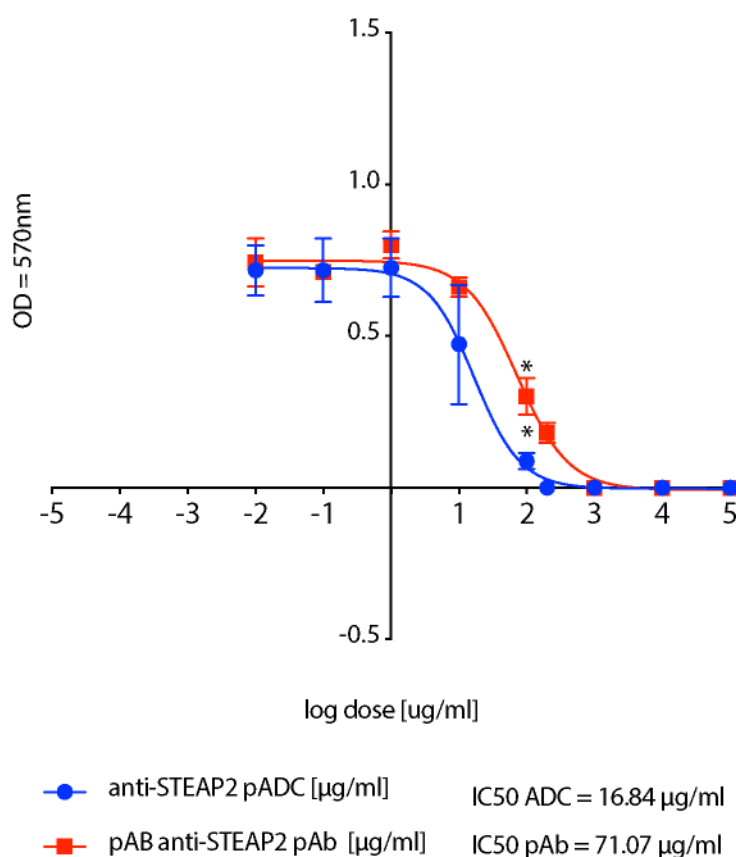


**Figure 5.5** IC<sub>50</sub> values of the anti-STEAP2 pADC and pAb. IC<sub>50</sub> values were estimated by a dose-response-inhibition four-parameter variable slope analysis based on the cell viability data (see Figure 5.4). The data indicates potential MMAE-ADC catabolite resistance of the PC3 cells or a poor ADC quality (N = 3).

Moreover, the anti-STEAP2 pADC exhibited an  $IC_{50}$  of approximately 16.84  $\mu\text{g}/\text{ml}$  and the  $IC_{50}$  value of anti-STEAP pAb was approximately 71.07  $\mu\text{g}/\text{ml}$  (**Figure 5.5**). This suggested, that the anti-STEAP2 pADC was 4.3-fold more efficient than the unconjugated anti-STEAP2 pAb alone, however, only specifically at a dose of 100  $\mu\text{g}/\text{ml}$ . As the most prominent difference in effect between the anti-STEAP2 pADC and the anti-STEAP2 pAb was only observed at approximately 100  $\mu\text{g}/\text{ml}$ , this data indicated potential drug resistance of the PC3 cells against MMAE-catabolites originating from the ADC. The ADC drug could also have been impaired due to an inefficient ADC degradation into its free MMAE drug form in the lysosomes or due to potential ADC instability (and loss of MMAE) *in-vitro* prior to the treatment.

#### **5.3.4 Test sera1 (linear) contain Abs specific to linear STEAP2 antigen**

During Phase I, indirect ELISAs were conducted at Ab Production Services to validate the specificity of the Test sera1 and Test sera2 supernatant containing antibodies to STEAP2. The Test sera1 of Mouse1 - 4 (linear) received an immunisation with the linear STEAP2 antigen and were assayed against linear STEAP2 antigen. The Test sera1 - Mouse1 - 4 (cyclic) was assayed accordingly with cyclic STEAP2 antigen. The Test sera1 - Mouse1 - 4 (linear) were ranked from the highest to the lowest based on their affinity to detect linear STEAP2 antigen based on their absorbance values (OD) starting from the serial dilution of 1:100 - 1:204,800 as follows: Test serum1 - Mouse2 (linear) > Test serum1 - Mouse1 (linear) > Test serum1 - Mouse3 (linear) > Test Serum1 - Mouse4 (linear) (**Figure 5.6**). Amongst the Test sera1 - Mouse1 - 4 (linear) the maximum absorbance was exhibited by the Test serum1 - Mouse2 (linear) which has reached an OD = 0.732 (cut-off = 14.19) at 1:12,800 dilution (**Figure 5.6**).

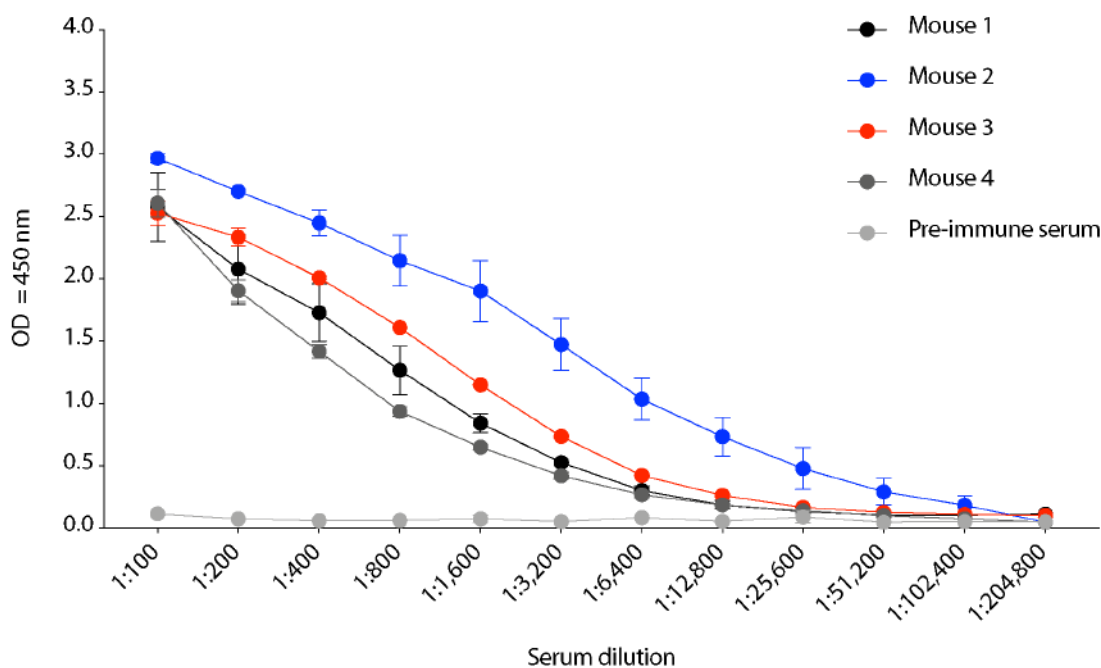


**Figure 5.6** Test sera1 – Mouse1 – 4 (linear) assayed against linear STEAP2 antigen. Provided by APS (N = 1).

Test serum1 - Mouse3 (linear) exhibited the second highest absorbance, yet the absorbance was substantially lower compared to Test serum1 - Mouse2 (linear) with an OD = 0.263 (cut-off = 4.73) suggesting the test serum contained less anti-STEAP2 antibodies than the Test serum1 - Mouse1 (linear) or the antibodies exhibited a low affinity to the antigen (**Figure 5.6**). Lower absorbances were further observed for Test serum1 - Mouse1 (linear) with an OD = 0.186 (cut-off = 3.34) and Test serum1 - Mouse4 (linear) with an OD = 0.184 (cut-off = 3.32), respectively (**Figure 5.6**). This implied, that the immunisation successfully elicited an immune response of the mice against the linear STEAP2 antigen by the production of anti-STEAP2 antibodies. Importantly, the absorbance values of Test sera1 - Mouse1 - 4 (linear) did not reach the ideal absorbance ( $OD \geq 1.0\text{mg/ml}$  at approximately 1:12,800) suggesting additional immunisations may be beneficial to increase their Ab titre prior the hybridoma development (Phase II) (**Figure 5.6**).

### 5.3.5 Test sera1 (cyclic) contain Abs specific to cyclic STEAP2 antigen

The next step in the process involved evaluation of the Test sera1 - Mouse1 - 4 (cyclic) during Phase I, which were ranked from the highest to the lowest based on their affinity to detect cyclic STEAP2 antigen. This was based on their absorbance values (OD) starting from the serial dilution of 1:100 - 1:204,800 as follows: Test serum1 - Mouse4 (cyclic) > Test serum1 - Mouse3 (cyclic) > Test serum1- Mouse2 (cyclic) > Test Serum - Mouse1 (cyclic) (**Figure 5.7**). The highest absorbance was exhibited by Test serum1 - Mouse4 (cyclic) with an OD = 0.585 (cut-off = 10.55). The second strongest absorbance was detected for Test serum1 - Mouse3 (cyclic) with an OD = 0.175 (cut-off = 3.16). Lower absorbances were detected by Test serum1 - Mouse1 (cyclic) (OD = 0.165, cut off = 3.14) and Test serum1 - Mouse2 (OD = 0.225, cut off = 2.96), suggesting their test sera may contain lower Ab titres against STEAP2 than the Test serum1 - Mouse1 (cyclic) and Test serum1 - Mouse4 (cyclic) (**Figure 5.7**).

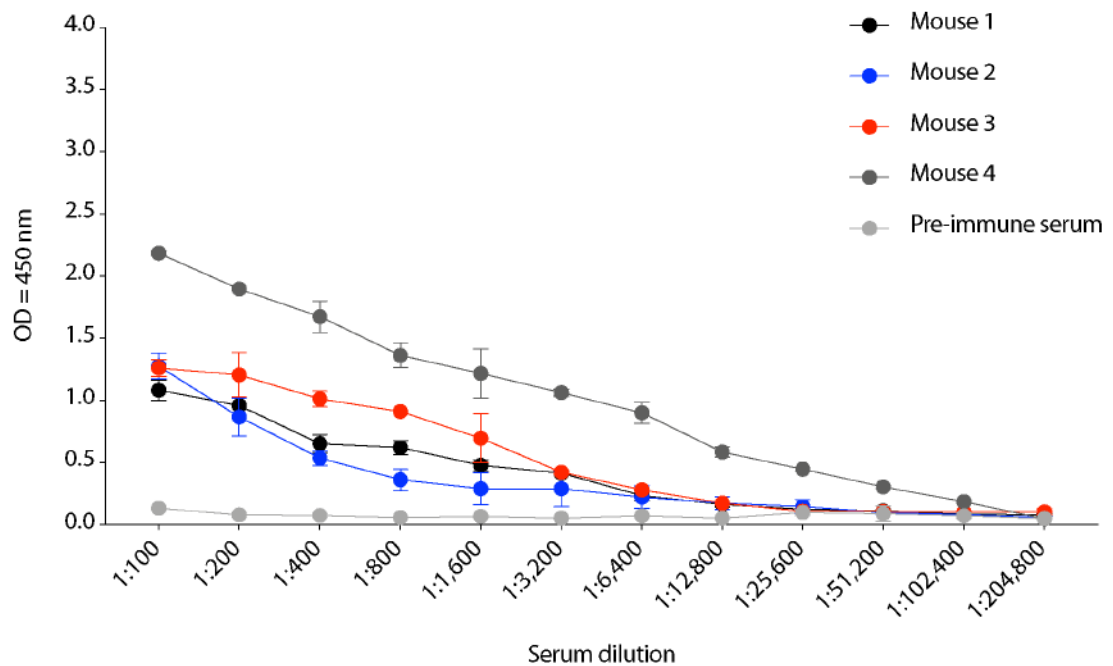


**Figure 5.7** Test sera1 (cyclic) assayed against the cyclic STEAP2 antigen. Provided by APS (N = 1).

Whilst the absorbances of Test sera1 - Mouse1 - 4 (cyclic) did not reach the ideal absorbance ( $OD \geq 1.0\text{mg/ml}$  at approximately 1:12,800), this data suggested the cyclic STEAP2 antigen has successfully triggered the Ab production *in-vivo*. The data also implied additional immunisation should be administered to increase the Ab titres of the mice before the hybridoma development stage (Phase II).

### 5.3.6 Test sera2 (linear) contain Abs specific to linear STEAP2 antigen

During Phase I, the Test sera2 - Mouse1 - 4 (linear) were evaluated after a total of five immunisations of either cyclic or linear STEAP2 peptide. The Test sera2 - Mouse1 - 4 (linear) were ranked from the highest to the lowest based on their affinity to detect linear STEAP2 antigen based on their absorbance values (OD) starting from the serial dilution of 1:100 - 1:204,800 as follows: Test Serum2 - Mouse2 (linear) > Test Serum2 - Mouse1 (linear) > Test Serum2 - Mouse3 (linear) > Test Serum2 - Mouse4 (linear) (**Figure 5.8**). This data indicated, that the Test Serum2 - Mouse2 (linear) contained the highest anti-STEAP2 Ab titre ( $OD = 0.369$ , cut-off = 6.65), followed by Test Serum2 - Mouse1 (linear) ( $OD = 0.248$ , cut-off = 4.45). In addition, Test Serum2 - Mouse3 (linear) exhibited an  $OD = 0.208$  (cut-off = 3.74), while the lowest absorbance was observed for Test Serum2 - Mouse4 (linear) ( $OD = 0.198$ , cut-off = 3.56) (**Figure 5.8**). Further, neither of the absorbance values of the Test sera2 - Mouse1 - 4 (linear) did exhibit the desired  $OD \geq 1.0\text{mg/ml}$  at approximately 1:12,800 as a reference for a strong Ab titre (**Figure 5.8**). Nonetheless, the minimum cut-off value (cut-off = 2) was met by all the Test sera2 - Mouse1 - 4 (linear) compared to the negative control pre-immunisation serum with no substantial absorbance values (**Figure 5.8**). Thus, the data implied the Test sera2 - Mouse1 - 4 (linear) contained anti-STEAP2 antibodies specific to linear STEAP2 antigen.

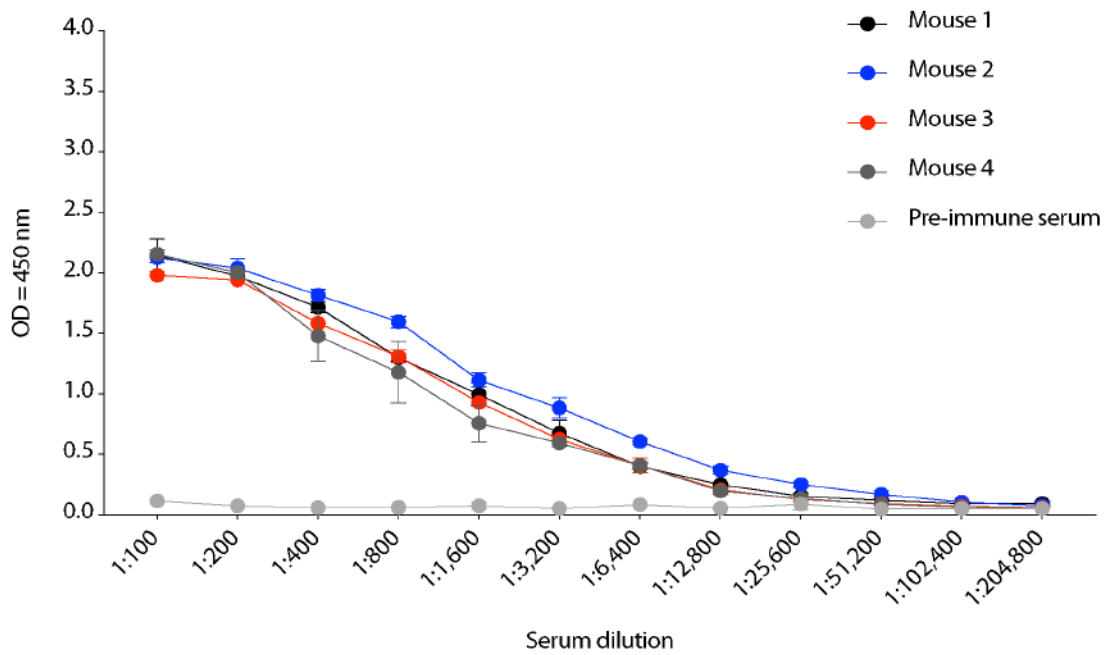


**Figure 5.8** Test sera2 (linear) recognise the linear STEAP2 antigen. Provided by APS (N = 1).

### 5.3.7 Test sera2 (linear) do not recognise cyclic STEAP2 antigen

Test sera2 - Mouse1 - 4 (linear) containing anti-STEAP2 antibodies from species immunised with linear STEAP2 antigen were assayed against cyclic STEAP2 peptide. This test was conducted to determine, if the anti-STEAP2 Ab containing Test-Sera 2 - Mouse1 - 4 (linear) were capable of detecting cyclic STEAP2 antigen without the mice having had experienced any antigen exposure with cyclic peptide. As displayed in **Figure 5.9**, the data showed very low absorbance values for all Test sera2 - Mouse1 - 4 (linear) which were ranked from the highest to the lowest as follows, respectively: OD = 0.065 (cut-off = 1.17) , OD = 0.0625 (cut-off = 1.13) , OD = 0.0625 (cut-off = 0.0525) and OD = 0.035 (cut-off = 0.64). Thus, the Test sera1 - Mouse1 - 4 (linear) were substantially below the desired absorbance and cut-off values (**Figure 5.9**). This suggested the anti-STEAP2 antibodies from Balb/C mice immunised with linear STEAP2 antigen did not possess any sufficient specificity to recognise cyclic the STEAP2 antigen.

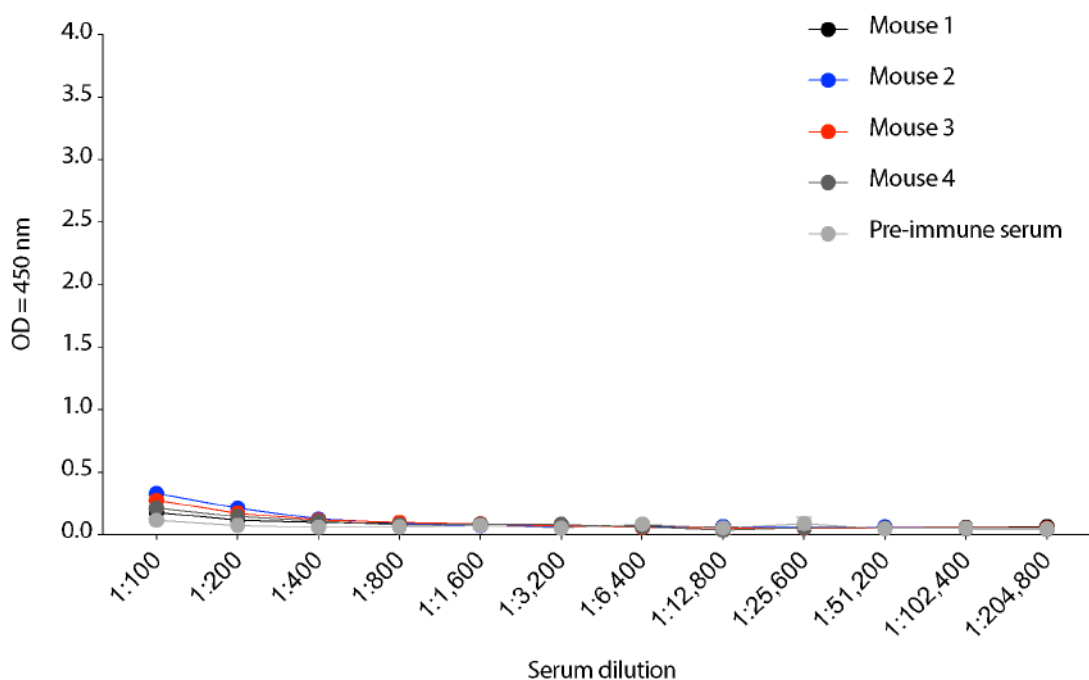


**Figure 5.9** Test sera2 (linear) do not detect the cyclic STEAP2 antigen. Provided by APS (N = 1).

### 5.3.8 Test sera2 (cyclic) contain Abs specific to cyclic STEAP2

The Test sera2 - Mouse1 - 4 (cyclic) were evaluated after a total of five immunisations of either cyclic or linear STEAP2 peptide. The Test sera2 - Mouse1 - 4 (cyclic) demonstrated serum dilution-dependent responses in absorbance values from 1:100 - 1:208,000 (**Figure 5.10**). The higher the serum dilutions, the higher the measured OD. The ability of the Test sera2 - Mouse1 - 4 (cyclic) containing anti-STEAP2 antibodies to bind to cyclic STEAP2 antigen was ranked from the highest to the lowest based on their absorbance value at all given serum dilutions as follows: Test Serum2 - Mouse4 (cyclic) > Test Serum2 - Mouse3 (cyclic) > Test Serum2 - Mouse2 (cyclic) > Test Serum2 - Mouse1 (cyclic) (**Figure 5.10**). Further, Test Serum2 - Mouse4 (cyclic) exhibited the highest OD = 0.357 with a strong cut-off = 11.78 indicating a sufficient high Ab titre. Test Serum2 - Mouse3 (cyclic) and Test Serum2 - Mouse2 (cyclic), absorbance values of OD = 0.160 (cut-off = 5.26) and OD = 0.090 (cut-off = 2.98) were observed, respectively (**Figure 5.10**). Further, both absorbance and cut-off values (OD = 0.057, cut-off = 1.88) reported for Test Serum2 - Mouse1 (cyclic) indicated an insufficient Ab titre during Phase I (**Figure 5.10**). No

substantial absorbance was reported for the pre-immune test serum confirming the absence of specific anti-STEAP2 antibodies. Further, the absorbance values of Test sera2 - Mouse1 - 4 (cyclic) did not meet the reference absorbance value ( $OD \geq 1.0$ mg/ml at approximately 1:12,800) suggesting moderate, but not strong Ab titres (**Figure 5.10**). However, the desired cut-off value was met (cut-off  $\geq 2$ ) by the Test sera2 - Mouse2 - 4 (cyclic) (**Figure 5.10**).

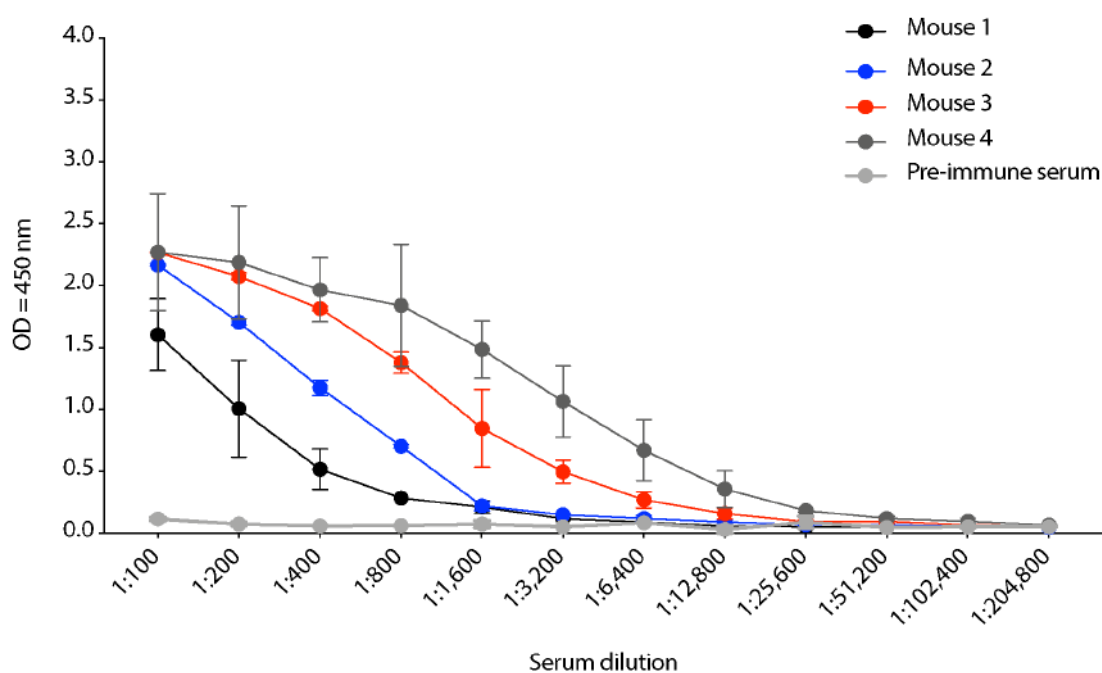


**Figure 5.10** Test sera2 (cyclic) recognise the cyclic STEAP2 antigen. Provided by APS (N = 1).

### 5.3.9 Test sera2 (cyclic) do not recognise linear STEAP2 antigen

Next, it was interesting to evaluate, whether the Test Serum2 - Mouse1 - 4 (cyclic) containing anti-STEAP2 antibodies were able to detect the linear STEAP2 peptide, apart from the cyclic peptide. Therefore, an ELISA was assayed against the linear STEAP2 peptide using the Test sera2 from the cyclic peptide immunisation. The data showed the OD values were very low as stated by their absorbance values at a serum dilution of 1:12,800 for Mouse1 (cyclic), Mouse2 (cyclic), Mouse3 (cyclic) and Mouse4 (cyclic) as follows: OD = 0.0745, OD = 0.105, OD = 0.101 and OD = 0.19, respectively (**Figure 5.11**). All cut-off values for the Test sera2 - Mouse1 - 4

(cyclic) were substantially below  $< 2$  for the Test sera2 - Mouse1 - 3 (cyclic) (cut-off = 1.34, cut-off = 1.88 and cut-off = 1.82) with an exception for Test sera2 - Mouse4 (cut off = 3.42) (**Figure 5.11**). This indicated the Test sera2- Mouse1 - 3 (cyclic) were not capable of recognising linear STEAP2 antigen, while Test Serum2 - Mouse4 (cyclic) may contain some antibodies, which could recognise linear STEAP2 antigen.

Based on the best performance (highest absorbances) of the Test sera2, Mouse1 and 2 (linear) and Mouse3 and 4 (cyclic) for the next Phase II.

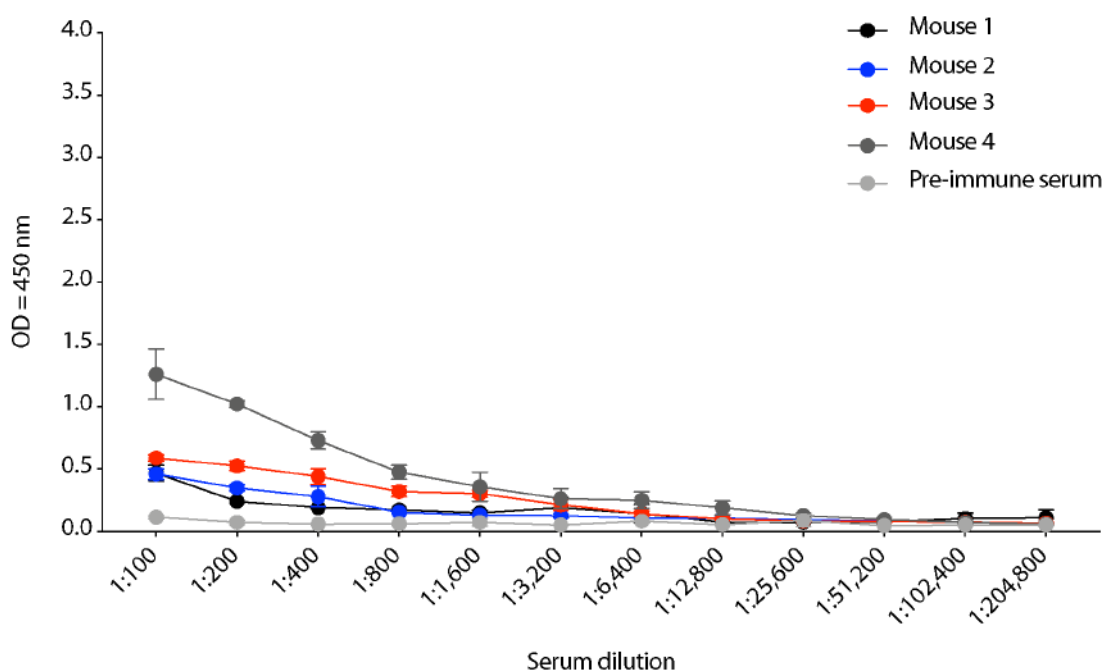


**Figure 5.11** Test sera2 (cyclic) do not detect the linear STEAP2 antigen. Provided by APS (N = 1).

### 5.3.10 Test sera2 (linear/cyclic) detect native STEAP2 in PC3 cells

After the species received a total of 5 rounds of immunisation with either the cyclic or linear STEAP2 peptide, the Test sera2 were examined for the presence of anti-STEAP2 antibodies using confocal microscopy as qualitative analysis. The PC3 cells overexpressing STEAP2 were used as a positive control using the commercial anti-STEAP2 pAb (ECL3), whilst the normal PNT2 cells with low STEAP2 expression were utilised as a negative control. The PC3 cells stained with the anti-

STEAP2 pAb (ECL3) exhibited a green fluorescent signal at the cell periphery suggesting cell surface specific localisation of STEAP2 (**Figure 5.12**). In contrast, the PNT2 cells demonstrated a low fluorescent signal in form of punctuates without cell periphery staining (**Figure 5.12**). This represented the lower STEAP2 expression in healthy PNT2 cells with intracellular localisation in regions such as the Golgi apparatus.

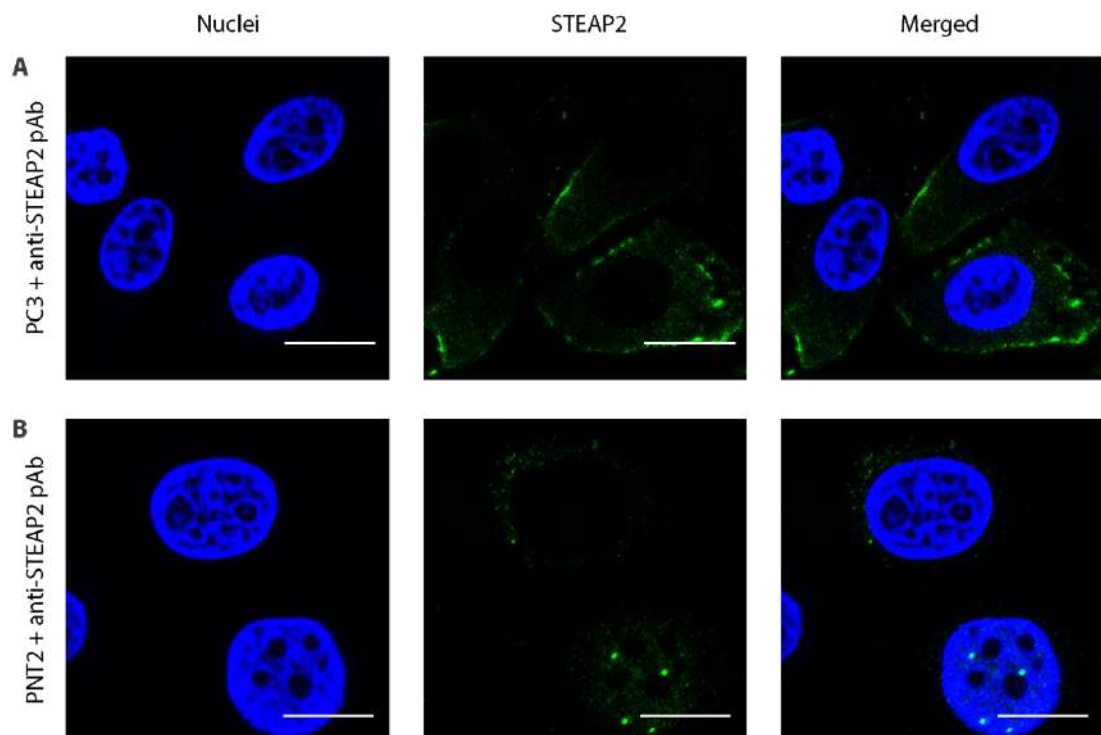


**Figure 5.12 STEAP2 fluorescent staining by the anti-STEAP2 pAb (AB4/ECL3).** PC3 cells: high STEAP expression; PNT2 cells: low STEAP2 expression. Blue: nuclei; green: STEAP2. Images were taken at a 100x objective using the LSM 710 microscope (ZEISS, Germany). Scale bar = 20  $\mu\text{m}$  (N = 3).

Using the Test sera2 - Mouse1 - 4 (linear), the PC3 cells showed a low fluorescent signal in the form of green punctuates distributed throughout the cell with no cell surface specific localisation for STEAP2 (**Figure 5.13**). The fluorescence was ranked from the highest to the lowest in the PC3 cells as follows: Test Serum2 - Mouse1 (linear) > Test Serum2 - Mouse2 (linear) > Test Serum2 - Mouse3 (linear) > Test Serum2 - Mouse4 (linear) (**Figure 5.13**). This result indicated, that the linear STEAP2 peptide had successfully triggered an immune response in the Balb/C mice to produce anti-STEAP2 antibodies.

Further, negligibly low fluorescent signals were exhibited in the normal PNT2 cells using the Test sera2 - Mouse1 - 4 (linear) (**Figure 5.14**). The Test sera2 - Mouse1 - 4 (cyclic) were applied to the PC3 cells, where a substantially stronger fluorescence was detected for STEAP2 using the Test sera2 - Mouse1 - 4 (linear) (**Figure 5.15**). However, the strongest fluorescent signals for STEAP2 appeared as green punctuates becoming more dominant at the cell periphery for Test sera2 - Mouse2 - 3 (cyclic) in PC3 cells (**Figure 5.15**). In contrast, green fluorescent punctuates were observed for the Test serum1 - Mouse1 (cyclic), while the poorest fluorescent signal was exhibited by the Test Serum2 - Mouse4 (cyclic) in PC3 cells (**Figure 5.15**). Further, minimal fluorescent signals, in the form of green punctuates, were observed in the lower STEAP2 expressing normal PNT2 cell line using the Test sera2 - Mouse1 - 4 (cyclic) (

**Figure 5.16**). This data implied, that the cyclic STEAP2 peptide had successfully elicited an immune response in the species to produce anti-STEAP2 antibodies. However, the Test sera2 - Mouse1 - 3 (cyclic) may contain more STEAP2-specific antibodies than the Test Serum2 - Mouse4 (cyclic) (

**Figure 5.16**).

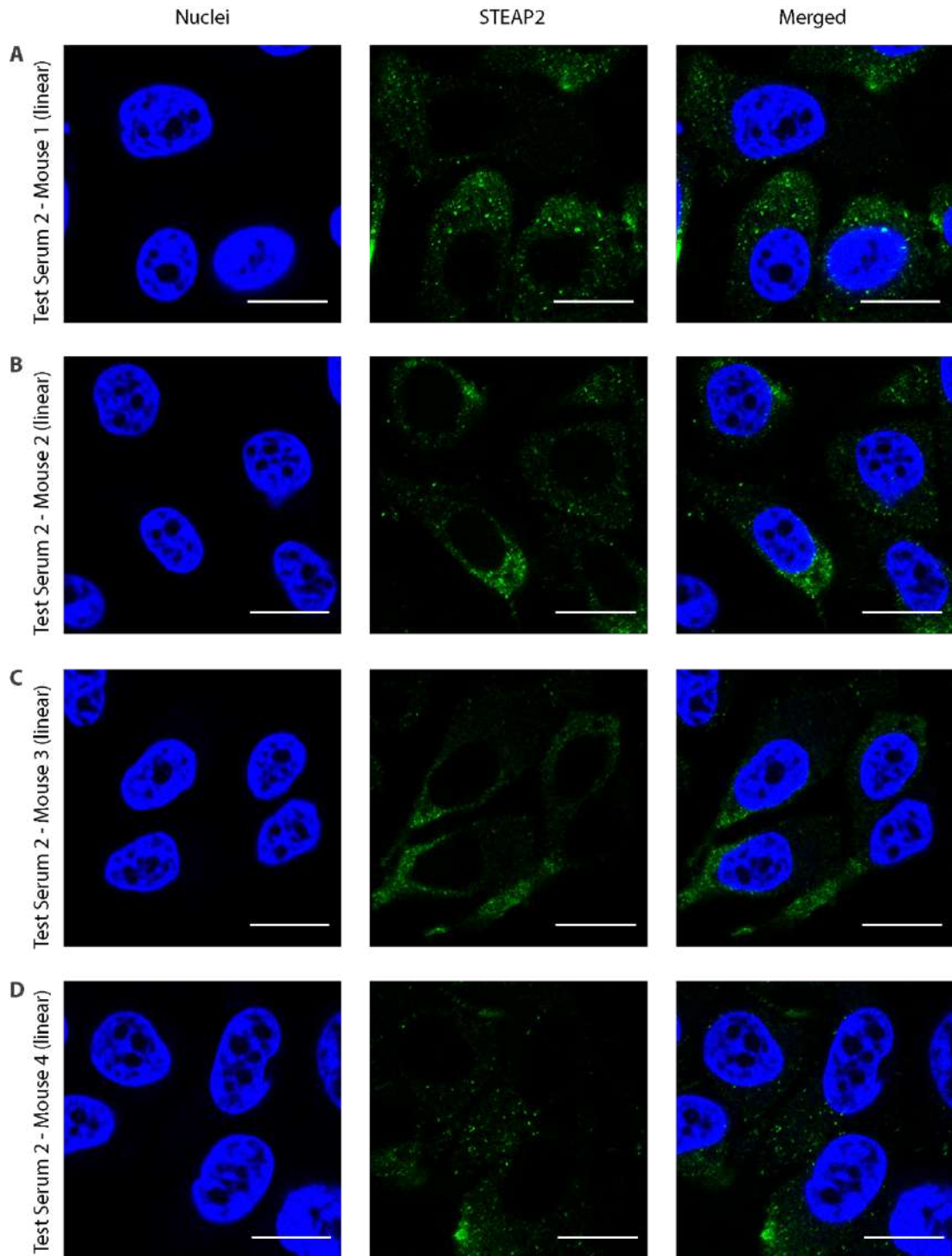


**Figure 5.13 Test sera2 (linear) detect native STEAP2 in PC3 cells.** Blue: nuclei; green: STEAP2. Images were taken at a 100x objective using the LSM 710 microscope (ZEISS, Germany). Scale bar = 20  $\mu$ m. Images were taken at a 100x objective using the LSM 710 microscope (ZEISS, Germany). Scale bar = 20  $\mu$ m (N = 3).

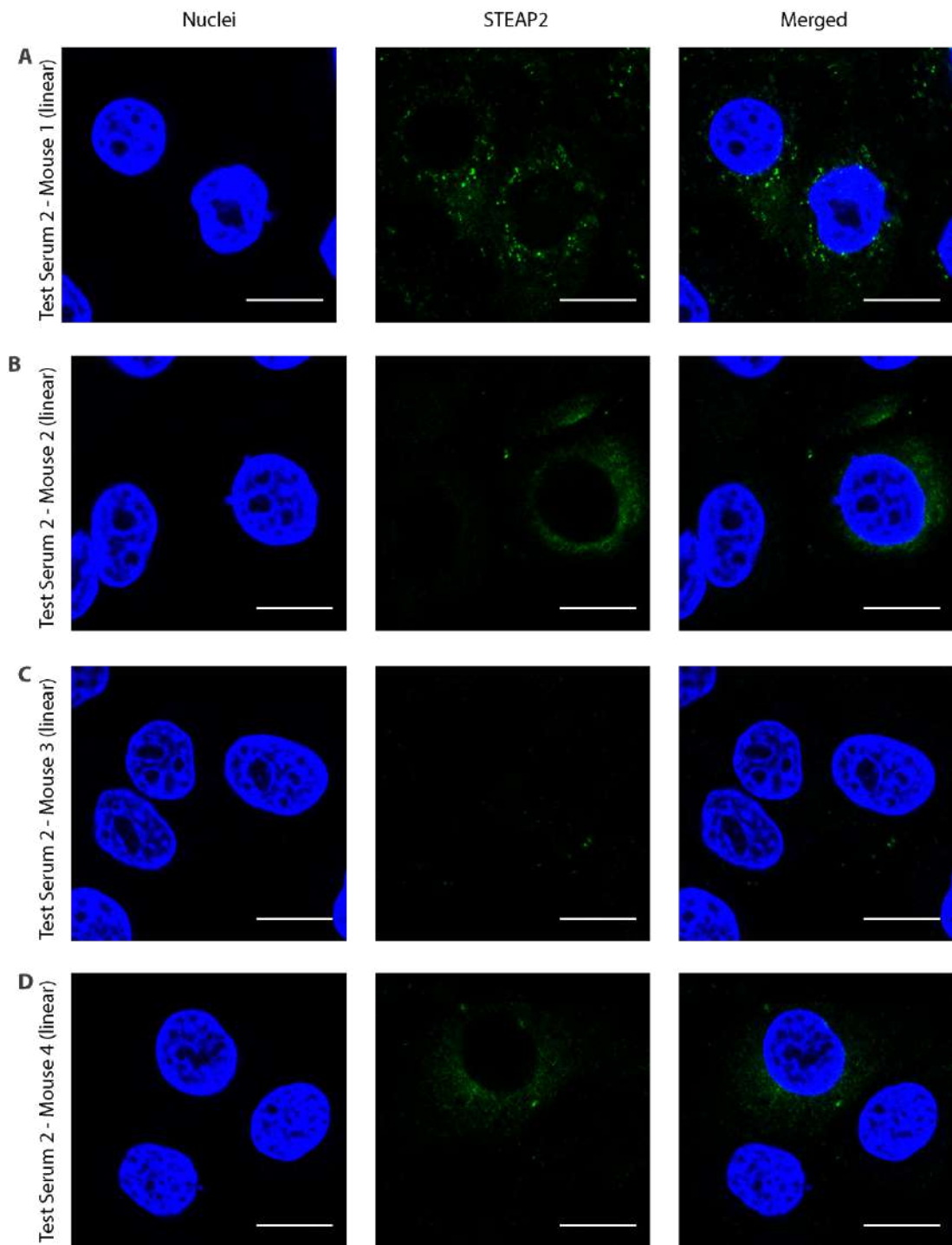


**Figure 5.14 Test sera2 (linear) detect lower STEAP2 levels in PNT2 cells.** Blue: nuclei; green: STEAP2. Images were taken at a 100x objective using the LSM 710 microscope (ZEISS, Germany). Scale bar = 20  $\mu$ m (N = 3).

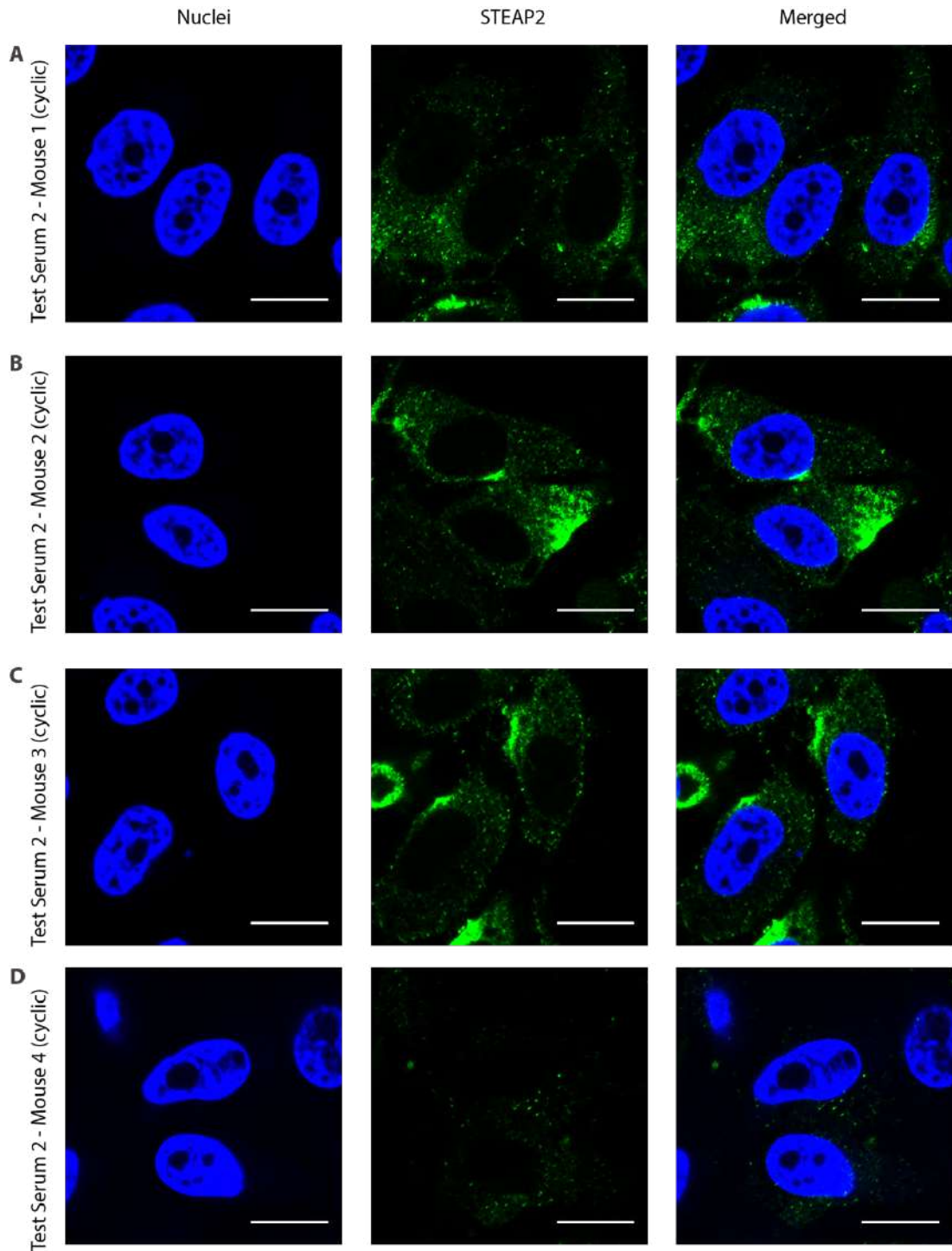


**Figure 5.15 Test sera2 (cyclic) detect native STEAP2 in PC3 cells.** Blue: nuclei; green: STEAP2. Images were taken at a 100x objective using the LSM 710 microscope (ZEISS, Germany). Scale bar = 20  $\mu$ m (N = 3).

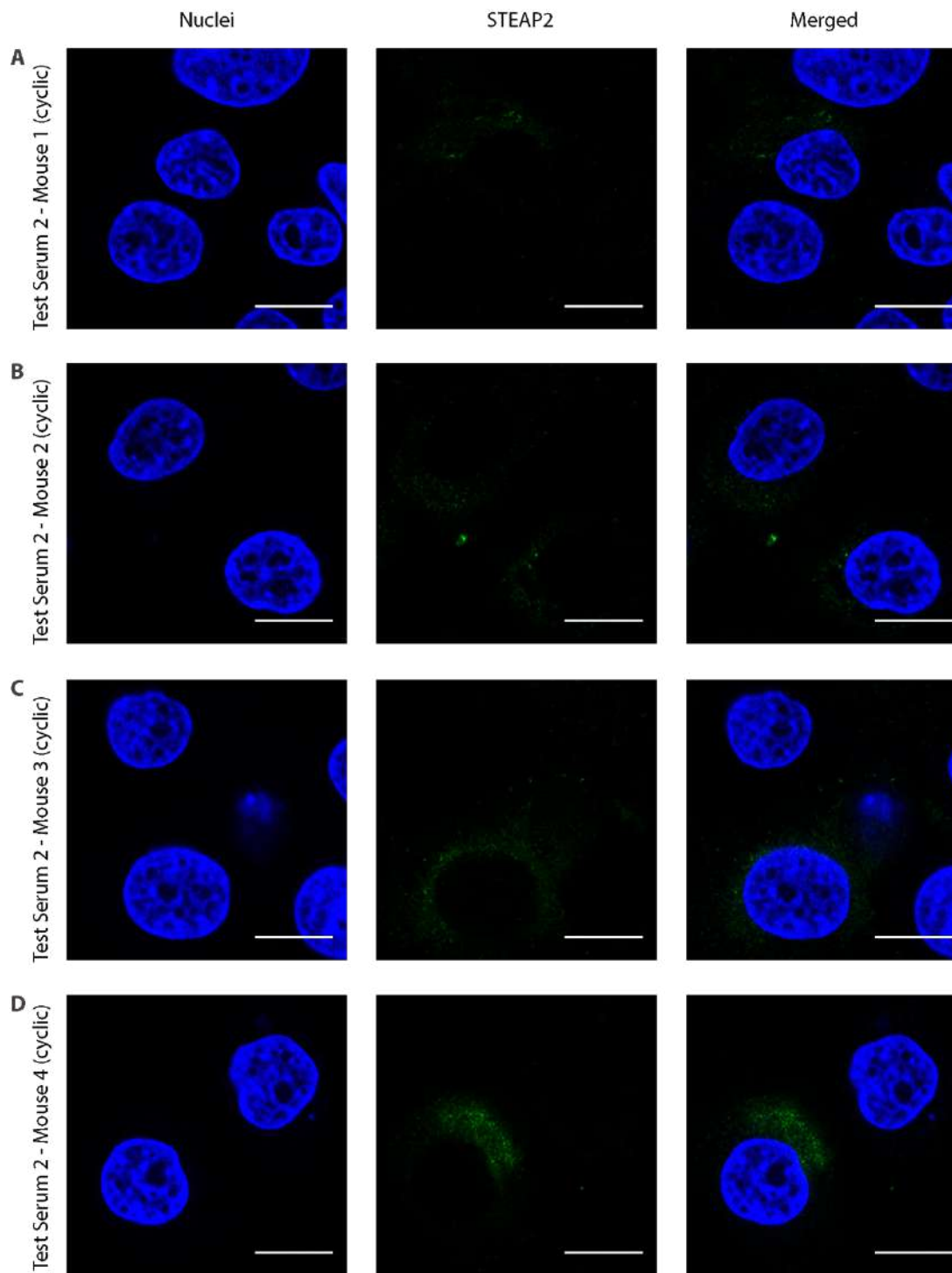


**Figure 5.16 Test sera2 (cyclic) detect minimal STEAP2 levels in PNT2 cells.** Blue: nuclei; green: STEAP2. Images were taken at a 100x objective using the LSM 710 microscope (ZEISS, Germany). Scale bar = 20  $\mu$ m (N = 3).

### **5.3.11 Test sera2 (linear and cyclic) contain a heterogenous pool of anti-STEAP2 pAbs by western blotting**

To complement the screenings process of the Test sera2 – Mouse1 – 4 (linear and cyclic), Western blotting was carried out. It is important to note, that the samples were of limited volume (20 µl), thus one replicate (N = 1) was performed showing high background with no distinct signal for STEAP2 using the Test sera2 (linear and cyclic) (Appendix 3, **Figure A3. 4** and **Figure A3. 5**).

### **5.3.12 Anti-STEAP2 mAbs recognise linear STEAP2 antigen by ELISA**

During Phase II, the mouse myeloma cells were fused with the spleen cells of Mouse1 and 2 (linear) and Mouse3 and 4 (cyclic) to generate the hybridoma cells, which resulted in four colonies of hybridoma cells. The anti-STEAP2 antibodies from the hybridoma cell colonies detected a protein, which was of similar size like STEAP2 by Western blotting in both PNT2 and PC3 cells (Appendix 3, **Figure A3. 6**). The cell culture supernatant of these hybridoma colonies, containing the anti-STEAP2 antibodies, was applied undiluted, in order to increase the Ab concentration for fluorescence microscopy, which demonstrated the anti-STEAP2 antibodies were not capable to detect naïve cell-surface STEAP2 compared to the anti-STEAP2 pAb (ECL3) control in PC3 and PNT2 cells (Appendix 3, **Figure A3. 7**, **Figure A3. 8** and **Figure A3. 9**). During Phase III (Limiting Dilution), the cell number of the four hybridoma cell colonies per well was decreased by a serial dilution step. Limiting dilution yielded four single cell hybridoma clones.

During Phase IV, these four single cell hybridoma clones, which all uniquely produced anti-STEAP2 mAbs, were expanded in cell culture and scaled up to increase the Ab yield uniquely. The anti-STEAP2 mAbs 1 – 3 originated from one mouse species (Mouse1 – linear), which had been exposed to the linear STEAP2 peptide and were therefore given the names: anti-STEAP2 – mAb1 (linear), anti-STEAP2 – mAb2 (linear), anti-STEAP2 – mAb3 (linear). They were further assayed in a serial dilution

(1:100 – 1:12,800) against the linear STEAP2 peptide (**Figure 5.17**). The fourth anti-STEAP2 mAb was obtained from one host species (Mouse4 - cyclic), which was immunised with cyclic STEAP2 peptide and was named anti-STEAP2 mAb4 (cyclic), accordingly. A serial dilution (1:100 – 1:12,800) of the anti-STEAP2 mAb4 was performed to evaluate its ability to detect the linear STEAP2 peptide using ELISA (**Figure 5.17**). The negative control included was the secondary anti-mouse anti-IgG Ab without any primary Ab. As a reference, an optimal absorbance value (OD value) was considered when  $OD > 1$  at a serum dilution of 1:12,800. As a second reference, a cut-off point  $> 2$  was based on the ratio of the OD of the mAbs specific against STEAP2 compared to the negative control. Based on the ELISA data, the anti-STEAP2 mAbs 1 – 4 were ranked from the highest to the lowest absorbance value (OD) at a serum dilution of 1:12,800 as follows: anti-STEAP2 mAb2 (linear)  $>$  anti-STEAP2 mAb4 (cyclic)  $>$  anti-STEAP2 mAb1 (linear)  $>$  anti-STEAP2 mAb3 (linear) (**Figure 5.17**). The anti-STEAP2 mAb2 exhibited the strongest  $OD = 1.29$  ( $SD = 0.087$ ) with a high cut-off value = 12.12, suggesting it specifically detected linear STEAP2 peptide. Further, the second highest absorbance value was observed for the anti-STEAP2 mAb4 (cyclic), although it has been raised against the cyclic STEAP2 antigen. The OD of the anti-STEAP2 mAb4 (cyclic) was  $OD = 0.87$  ( $SD = 0.033$ ) and did not exceed the optimal reference point of  $OD > 1$  at 1:12,800 (**Figure 5.17**). Yet, the cut-off value = 11.59 for the anti-STEAP2 mAb4 (cyclic) was substantially higher than the reference cut-off-value indicating the antibodies were specific against the linear STEAP2 peptide, as opposed to the negative control. In addition, a lower absorbance value was detected using the anti-STEAP2 mAb1 (linear) with an  $OD = 0.5$  ( $SD = 0.02$ ) and a cut-off = 5.5, indicating the samples contained mAbs specific against a linear STEAP2 peptide when compared to the negative control (**Figure 5.17**). The anti-STEAP2 mAb3 (linear) exhibited the lowest absorbance value ( $OD = 0.172$ ,  $SD = 0.012$ ) with a cut-off value = 2.02 (**Figure 5.17**). This result implied the sample contained specific mAbs against the linear STEAP2 peptide compared to the negative control.

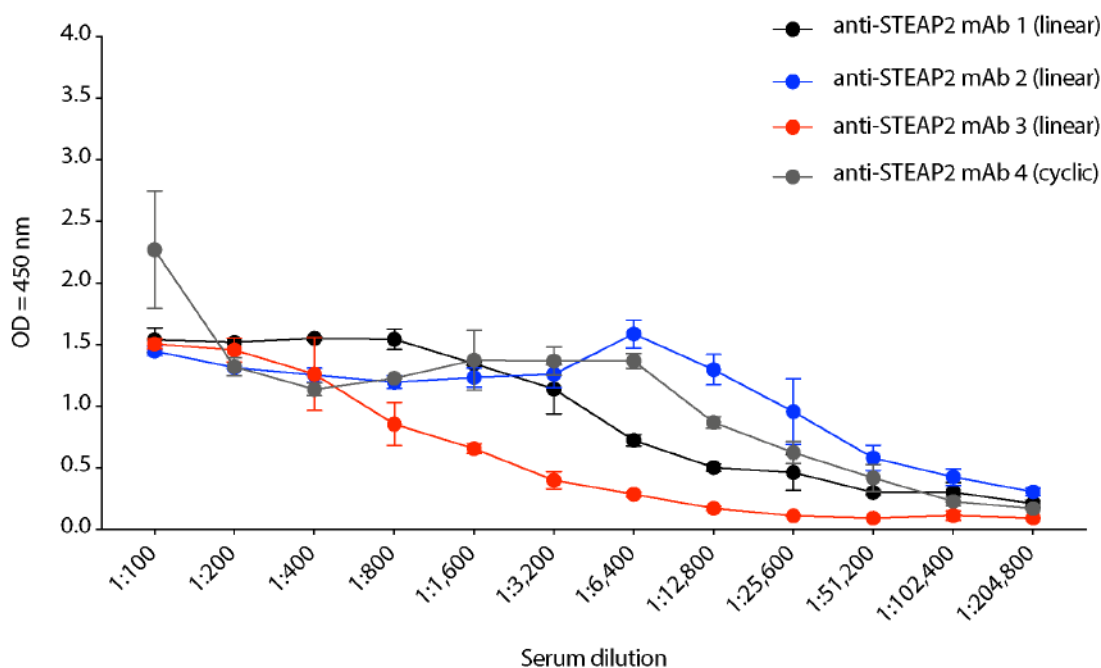


**Figure 5.17** Anti-STEAP2 mAbs recognise the linear STEAP2 antigen. The ELISA was provided by APS (N = 1).

### 5.3.13 Anti-STEAP2 mAbs show distinct IgG heavy and light chains by Nu-PAGE analysis

Nu-PAGE analysis was conducted using the four Protein-G column affinity-purified anti-STEAP2 mAbs1 - 4 to confirm the physicochemical characteristics specific for Immunoglobulin (IgG) molecules. The Ab samples were run alongside a visible marker for the identification of the molecular weight of the detected bands, while PBS served as a negative control. Nu-PAGE analysis of the anti-STEAP2 mAb1 - 3 (linear) and anti-STEAP2 mAb4 (cyclic) clearly showed two major protein fragments (**Figure 5.18 A - D**). The larger fragment was detected above a molecular weight size of 51 kDa suggesting the presence of the IgG heavy chains (HC) fragments (approx. 55 kDa). The second and smaller fragment appeared below the 28 kDa molecular weight size indicating the presence of the light chain (LC) fragments (approx. 25 kDa) of the anti-STEAP2 mAb1 - 4 (**Figure 5.18 A - D**). This data showed, that the anti-STEAP2 mAbs1 - 4 possessed protein fragments which were characteristic for an IgG Ab.

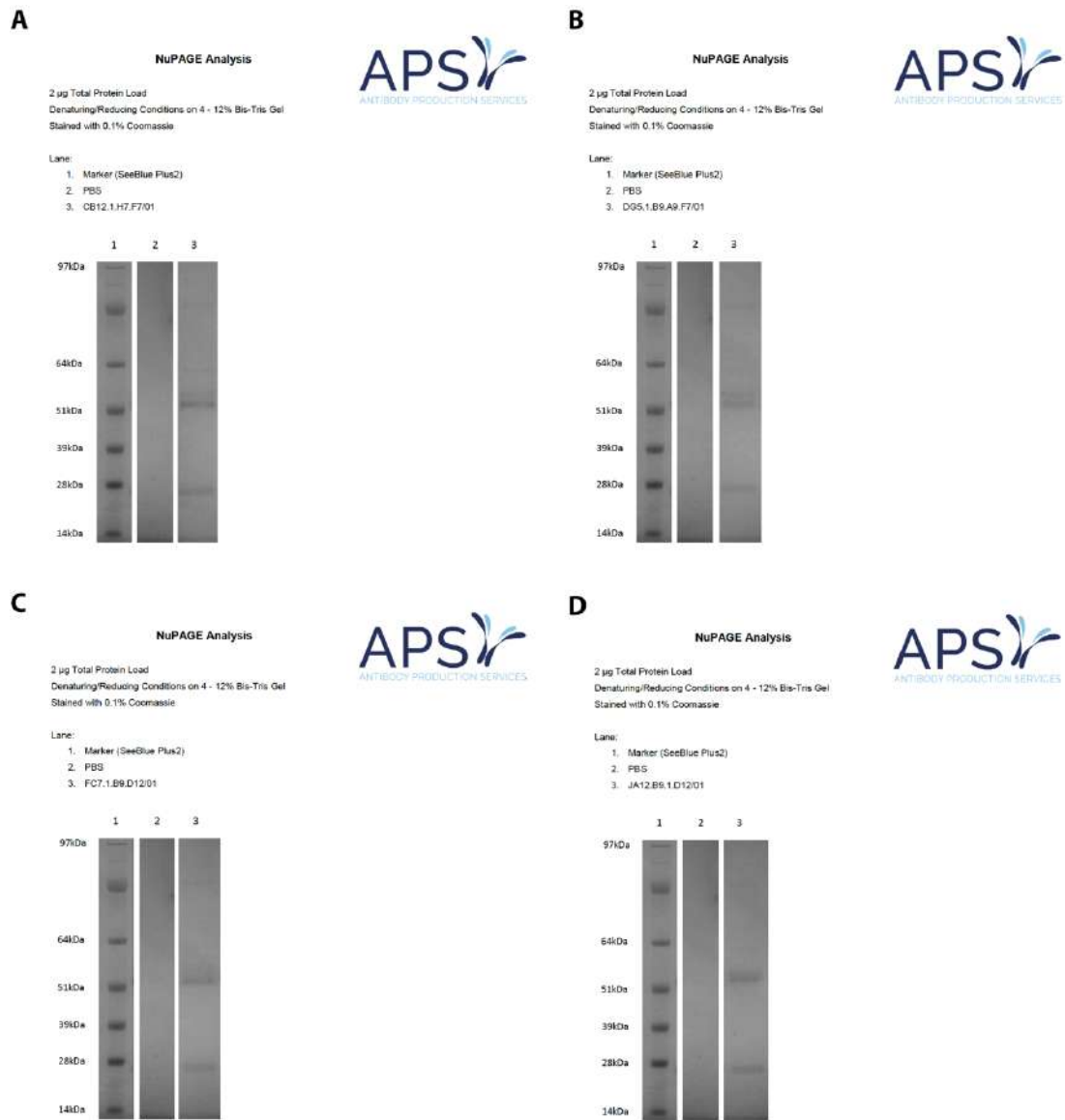


**Figure 5.18 Anti-STEAP2 mAbs contain HC/ LC IgG fragments by Nu-PAGE.** A) Anti-STEAP2 mAb1 (linear). B) Anti-STEAP2 mAb2 (linear). C) Anti-STEAP2 mAb3 (linear). D) Anti-STEAP2 mAb4 (cyclic). 1: Pre-stained molecular weight ladder; 2: PBS (negative control); 3: anti-STEAP2 mAb; HC: IgG heavy chain (approximately 55 kDa); LC: IgG light chain (approximately 25 kDa). Nu-PAGE analysis was conducted by APS (N = 1).

#### 5.3.14 Anti-STEAP2 mAbs do not detect native STEAP2

The monoclonal anti-STEAP2 antibodies (anti-STEAP2 - mAb1 - 4) were further evaluated in PC3 cells for their ability to detect naive STEAP2 protein by confocal microscopy. Due to the different origin of the Balb/C mice between the commercial anti-STEAP2 pAb (ECL3) (rabbit) and the anti-STEAP2 mAb1 - 4 (mouse), the anti-STEAP2 mAb1 - 4 were detected with a different secondary Ab species (**Section 5.2.7.3**). Therefore, the primary mouse anti-golgin97 mAb specific to the Golgi apparatus was utilised to ensure the secondary goat anti-mouse anti-IgG-AlexaFluor-488 Ab was working appropriately. A strong fluorescent signal was observed with predominant localisation to the cell periphery using the commercial anti-STEAP2 pAb (ECL3) suggesting cell surface localisation of STEAP2 (**Figure 5.19A**). In addition, multiple fluorescent punctuates within the cell but not at the cell periphery were detected by the anti-golgin 97 mAb used as an Ab host species control for the respective detecting secondary goat anti-mouse anti-IgG AlexaFluor-488 Ab (**Figure 5.19 B**). The result confirmed the intracellular localisation of the Golgi apparatus and the suitability of the secondary goat anti-mouse anti-IgG-AlexaFluor-488 Ab for evaluation of the anti-STEAP2 mAb1- 4.

Poor fluorescent signals were observed for the PC3 cells using the anti-STEAP2 mAb1 - 4 compared to the strong fluorescence predominantly located at the cell surface using the commercial anti-STEAP2 pAb (ECL3) control (**Figure 5.20 A – D**). The data implies, that the anti-STEAP2 mAb1 - 4 are likely to be unsuitable for fluorescence microscopy.

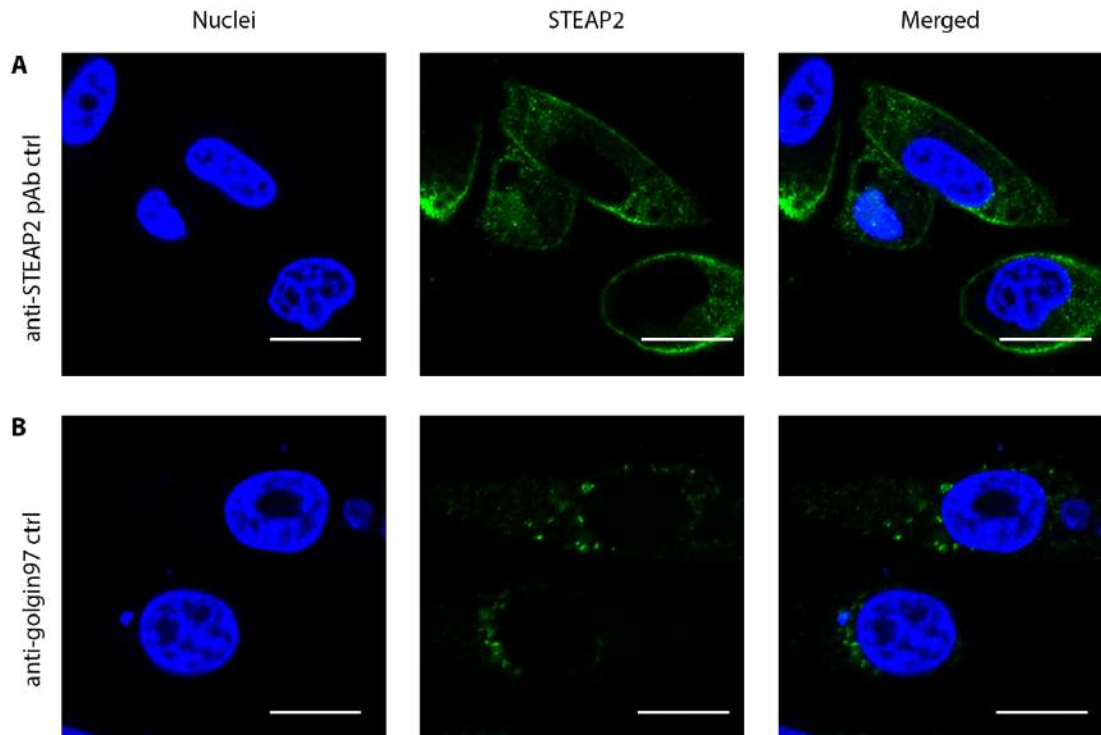


**Figure 5.19 Positive controls used for the anti-STEAP2 mAb evaluation.** A) PC3 cells + commercial anti-STEAP2 pAb (ECL3) showing high levels of cell surface STEAP2 used as a positive control for the matching secondary detection Ab. B) PC3 cells + anti-golgin97 mAb showing the Golgi apparatus used as a positive control for the matching secondary detection Ab. Blue: nuclei; green: STEAP2. Images were taken at a 63x zoom objective using the LSM 710 microscope (ZEISS, Germany). Scale bar = 20  $\mu\text{m}$  (N = 3).

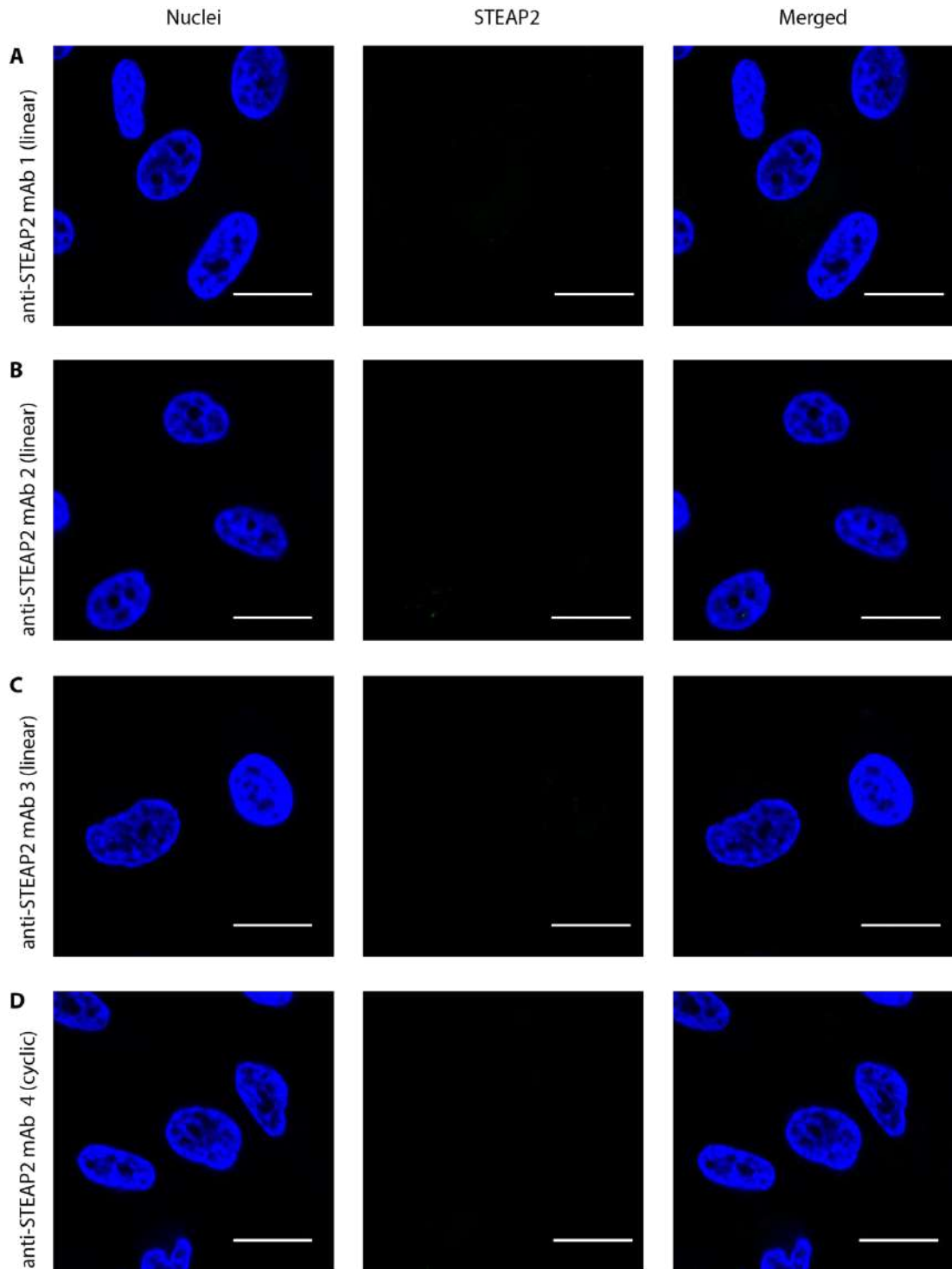


**Figure 5.20** Anti-STEAP2 mAbs do not recognise native STEAP2 in PC3 cells by confocal microscopy. Blue: nuclei; green: STEAP2. Images were taken at a 63x zoom objective using the LSM 710 microscope (ZEISS, Germany). Scale bar = 20  $\mu$ m (N = 3).

### 5.3.15 Anti-STEAP2 mAbs poorly detect linear STEAP2

In order to examine, whether the anti-STEAP mAb1 – 4 were capable of recognising linear STEAP2 protein, western blotting was performed. The

commercial anti-STEAP2 pAb (ECL3) was included as a positive control. Linear regression analysis following densitometry assessment determined the molecular weight of the detected protein specifically at 54.1 kDa with a minor 1.84-fold increase (SD = 0.13-fold) in protein expression in the PC3 cells compared to the PNT2 cells by the anti-STEAP2 mAb1 (linear) (**Figure 5.21 A**). Further, a 1.43-fold increase in protein expression in PC3 cells was detected by the anti-STEAP2 mAb2 (linear) (SD = 1.36-fold) at 46.9 kDa (**Figure 5.21 A**). In comparison, the commercial anti-STEAP2 pAb (ECL3) demonstrated a 2.41-fold (SD = 0.69-fold) higher STEAP2 protein expression level at 52.2. kDa in PC3 cells versus the normal PNT2 cells (**Figure 5.21 A**). Moreover, the anti-STEAP2 mAb3 (linear) detected a protein at 58.4 kDa by a 1.79-fold increase (SD = 0.94-fold) in PC3 cells opposed to the PNT2 cells (**Figure 5.21 B**). In addition, the anti-STEAP2 mAb4 (cyclic) demonstrated a 1.76-fold increase (SD = 1.48-fold) at approximately 60 kDa in PC3 cells as compared to the PNT2 cells (**Figure 5.21 B**). In contrast, the commercial anti-STEAP2 pAb control demonstrated a 15.56-fold increase (SD = 17.23-fold) in STEAP2 expression in the PC3 cells as compared to the normal PNT2 cells at the molecular weight of 58.4 kDa (**Figure 5.21 B**). The data suggested, that ability of the anti-STEAP2 mAb1 – 2 to detect STEAP2 protein by western blotting are inferior to the commercial anti-STEAP2 pAb (ECL3). Moreover, the results imply that extensive optimisation is required in the future to obtain an optimal signal for protein analysis by the anti-STEAP2 mAb1 – 4 (**Figure 5.21 A** compared to **Figure 5.21 B**).

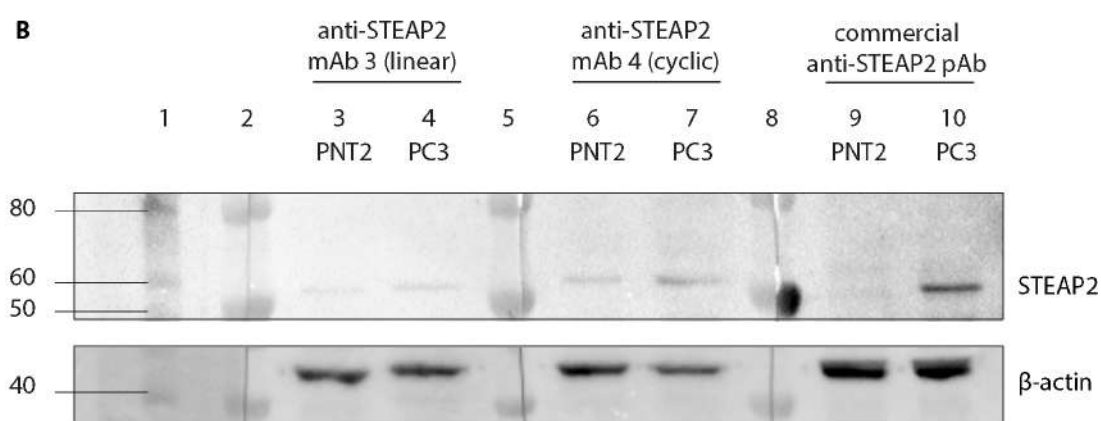
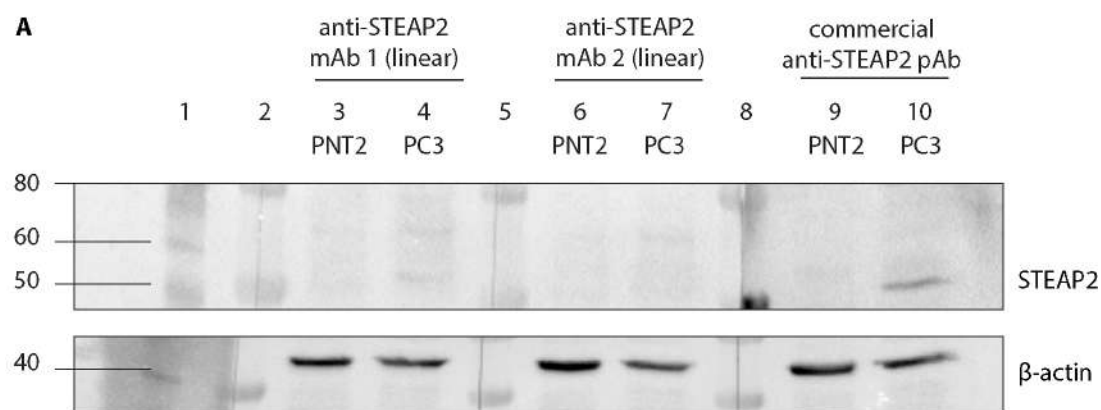


**Figure 5.21 STEAP2 protein analysis using the anti-STEAP2 mAbs.** A) Anti-STEAP2 mAb1 (linear), 2 (linear) and the commercial anti-STEAP2 pAb control. B) Anti-STEAP2 mAb3 (linear), 4 (cyclic) and the commercial anti-STEAP2 pAb (ECL3) control. 1: Unstained molecular weight ladder; 2: pre-stained dual colour molecular weight marker; 3, 6, 9: technical triplicate of PNT2 cell lysate; 4, 7, 10: technical triplicate of PC3 cell lysate (N = 3).

## 5.4 Discussion

---

### 5.4.1 PC3 cell viability following anti-STEAP2 pADC and anti-STEAP2 pAb drug exposure

It was of interest to evaluate, if an anti-STEAP2 monomethyl-auristatin E ADC is more efficient than the unconjugated anti-STEAP2 pAb (ECL3) in reducing the cell viability in PC3 cells. Thus, a polyclonal anti-STEAP2 MMAE ADC (anti-STEAP2 pADC) was commissioned from CellMosaic utilising the commercially available anti-STEAP2 pAb (ECL3). The effects of both the unconjugated anti-STEAP2 pAb (ECL3) and the anti-STEAP2 pADC on the cell viability in the PC3 cell line were then assessed using the MTT assay.

Since the cytotoxins the ADCs carry are substantially more potent than traditional chemotherapeutics, ADCs can be administered in low doses, while ensuring their efficiency in cell killing (Ducry & Stump, 2010). Multiple research findings have achieved significant cell killing effects using various cancer cell lines starting from as little as the pg/ml to ng/ml range for both the ADC and free toxin (Chari *et al.*, 2014; Drachman & Senter, 2013; Nasiri *et al.*, 2018). However, both MTT and IC<sub>50</sub> value data implied, that the use of the anti-STEAP2 pADC only had a significant benefit in reducing the cell viability at extremely high doses (100 µg/ml) opposed to the unconjugated anti-STEAP2 pAb (ECL3). Therefore, this chapter's data is in contrast with the typical (substantially lower) dose range of ADCs *in-vitro*. This key observation raised the question which the underlying cause was for the inefficiency of the anti-STEAP2 pADC in reducing the cell viability in PC3 cells.

The Drug-to-Antibody ratio (DAR) describes the number of payload molecules per antibody and plays a huge role on the therapeutic activity of ADCs *in-vitro* and *in-vivo* (Hamblett *et al.*, 2004). ADCs with higher DARs cause increased cytotoxicity *in-vitro*, whilst ADCs with lower DARs are less cytotoxic (Hamblett *et al.*, 2004). *In-*

*in vivo*, however, ADCs with lower DARs demonstrated better therapeutic activity which was attributed to a slower plasma clearance of the drug (Hamblett *et al.*, 2004). Based on the study's insights, a DAR of 2 - 4 is considered optimal to enhance the ADC efficacy (Hamblett *et al.*, 2004). The SEC analysis conducted as quality control by CellMosaic suggested an average DAR of 3:1 of the anti-STEAP2 pADC meaning approximately three molecules of MMAE were attached per one molecule of pAb and was therefore within the suggested DAR range. Further, the DAR of the pADC of this thesis was similar compared to the one of Brentuximab Vedotin with 4:1 (Schneider, 2017). There are two plausible explanations for the reduced cell killing efficacy of the pADC. Loss of conjugated MMAE payloads of the pADC may have resulted in a lower DAR causing less pronounced *in-vitro* cytotoxicity based on data from Hamblett *et al.*, 2004. Another explanation for the reduced potency of the pADC may have been due to the aggregation of the hydrophobic MMAE payload. Aggregation of the MMAE payload could have masked the antigen-fragment binding domains of the antibody to the epitope of STEAP2 thereby reducing the cell killing efficacy of the pADC (Olivier Jr. & Hurvitz, 2016). The aggregation of hydrophobic MMAE is a common problem within the ADC technology and has been encountered with the design of more hydrophilic ADCs by *e.g.* using PEG4Mal linkers or PEG-spacers to increase the solubility while minimising ADC aggregation (Kovtun *et al.*, 2010; Lyon *et al.*, 2015).

A potential explanation may also be, that the PC3 cell line may be unresponsive to the microtubule inhibitor, MMAE, used in this study. However, equivalent doses in the ng/ml range of the free MMAE were included as a positive control, where it significantly decreased PC3 cell viability. Therefore, this finding demonstrated, that the PC3 cells are sensitive to the free MMAE but not to the anti-STEAP2 pADC. This is in alignment with many studies, which confirmed that using ng/ml doses of MMAE result in substantial cell toxicity in various cancer cell lines (Chari *et al.*, 2014; Chen *et al.*, 2017; Garnock-Jones, 2013; Kratschmer & Levy, 2018; Staudacher & Brown, 2017).

MMAE is one of the most well-studied cytotoxins used for ADC technology and inhibits the microtubule depolymerisation, which ultimately blocks cell growth. MMAE is highly hydrophobic and thus capable of passing the (plasma) membranes (Chalouni & Doll, 2018). To generate the anti-STEAP pADC, the MMAE was attached to the unconjugated anti-STEAP2 pAb (ECL3) via a chemical, cleavable Valine-Citrulline (VC) linker. VC is sensitive to the proteolysis of the lysosomal enzyme, Cathepsin-B (Chalouni & Doll, 2018). Based on the degradation of the ADC in the lysosome organelle, it is anticipated that free MMAE molecules should be able to permeate the lysosomal membrane, entering the cytosol. Further, MMAE inhibit the microtubule polymerisation once they reached the cytosol and exert their cytotoxic effect (Chalouni & Doll, 2018). Given the capability of free MMAE to permeate the lysosomal membrane, it raises the question, if the PC3 cells exhibit drug resistance to retain free MMAE originating from the anti-STEAP2 pADC. Drug resistance to MMAE may be one explanation why high anti-STEAP2 pADC doses were required to reduce the cell viability in PC3 cells. Resistance to ADCs, containing MMAE, have been reported for the commercially available Brentuximab-Vedotin (BV, Adcetris®) (Chen *et al.*, 2016). It is an anti-CD30 VC-PABC-MMAE ADC, used to treat relapsed or refractory Hodgkin lymphoma (HL) and anaplastic large cell lymphoma (ALCL) (Bradley *et al.*, 2013; Garnock-Jones, 2013; Gravanis *et al.*, 2016; Han *et al.*, 2014; Senter & Sievers, 2012). One study has developed an ALCL BV resistant cell line, called KARPAS 299R, by previous constant or pulsatile drug treatment (Chen *et al.*, 2016). A BV resistance was confirmed by the drug exposure to BV and MTS cell viability analysis. It was reported, that the downregulation of CD30 in KARPAS 299R cells but not in KARPAS 299 cells was responsible for the resistance to BV using gene and protein expression profiling by flow cytometry, qRT-PCR and western blotting (Chen *et al.*, 2016). However, a subpopulation of CD30 overexpressing Hodgkin's lymphoma cell line (HL cell line L428R) still exhibited BV-resistance after drug exposure using the MTS assay (Chen *et al.*, 2016). Additional qRT-PCR analysis of the BV-exposed L428R cell line showed the increased gene

expression of the p-glycoprotein *Multi-Drug Resistance Protein1* (*P-gp MDR1*) (Chen *et al.*, 2016). MDR1 is a member of the ATP-binding cassette transporters (ABC transporters), which was accounted for the efflux of MMAE, thereby causing the BV resistance observed in L428R cells (Chen *et al.*, 2016).

Another study reported the liver hepatocellular cell lines HepG2, Hep3B2, the lung squamous cell line NCL-H226 and Hodgkin lymphoma cell line KM-H2 were less sensitive to free MMAE exposure (72 h) than the ovarian cancer cells OVAR3 and the human gastric epithelial cell line NCI-N87 by using the XTT assay (Liu-Kreyche *et al.*, 2019). An approximate cell survival of 20% was observed in the KM-H2 cells treated with high doses of MMAE nearly the 100 µg/ml (Liu-Kreyche *et al.*, 2019). Additional LC-MS analysis of the lysosomal fractions of the cell lines HepG2, Hep3B2, NCL-H22, confirmed the increased presence of MDR proteins. These were namely the Multidrug Resistance-Associated Protein2, 3 and 4 (MRP2, 3 and 4), which are family members of the ABC transporters (Kruh *et al.*, 2007; Liu-Kreyche *et al.*, 2019). To confirm this result, the HepG2, Hep3B2 and NCI-H226 cells were exposed to MMAE or a combination of MMAE and Elacridar, an inhibitor of P-gp MDR-1 and the Breast Cancer Resistance Protein (BCRP) (Hendriks *et al.*, 2014; Liu-Kreyche *et al.*, 2019; Sane *et al.*, 2012). The data showed, that the HepG2, Hep3B2, NCL-H22 cells were more susceptible to the combined treatment. Thus, they concluded the MMAE resistance was due to the expression of the MRP2, MRP3 and MRP4 (Liu-Kreyche *et al.*, 2019). Currently, there is no data available on whether or not MRPs are expressed in the PC3 cells. One limitation of this study is that Elacridar is also a potent blocker of the BCRP, however its expression was not investigated and thus it remains uncertain, if an increased BCRP expression may contribute MMAE resistance (Liu-Kreyche *et al.*, 2019). BCRP overexpression is known for the Non-Small Cell Lung Cell Hodgkin Lymphoma (NSCLC) and triple negative basal-like (TNBL) breast cancer, for instance (Dufour *et al.*, 2015; Galetti *et al.*, 2015). The upregulation of BCRP has been shown to confer MDR and chemotherapeutics like tyrosine-kinase inhibitors, DNA intercalators and nucleoside analogues) are proven substrates of

BCRP (Doyle & Ross, 2003; Westover & Li, 2015). In addition, one study has shown that BCRP is present in the metastatic prostate cancer line LNCaP, which causes resistance to the chemotherapeutic Docetaxel, a BCRP substrate (Xie *et al.*, 2008). Based on these insights, further investigations are required to identify, if a potential MMAE resistance is present in PC3 cells and could be ascribed to the upregulation of both the MRP and BCRP proteins by PCR or Western blotting.

Unlike the cleavable linkers, non-cleavable linkers, the thio-ether conjugation chemistry, attach maytansinoides payloads such as Emtansine (DM1) present in Trastuzumab-DM1 (Kadcyla®) (Jain *et al.*, 2015). Non-cleavable linkers require the catabolic degradation in the lysosomes, in order to release the DM1 toxin (Loganzo *et al.*, 2016). Unlike MMAE, these DM1 catabolites are not capable of translocating across the lysosomal membrane but researchers have suggested there may be a specific transport mechanism in the lysosomes involved (Bissa *et al.*, 2016; Hamblett *et al.*, 2015). Recently, one research group revealed, that maytansinoides, including DM1, are substrates of a unique lysosomal membrane protein (SLC), called SLC46A3 (Hamblett *et al.*, 2015). Researchers have exposed CD70+ cancerous, renal epithelial 786-O cells to an anti-CD70-MCC-DM1 ADC, and then developed shRNA-based libraries. These shRNA-based libraries included both lysosomal and transporter genes, as well as (cell surface) membrane proteins following a phenotypic screening. Besides CD70, the SLC46A3 was identified as the second most common protein. Therefore, *SLC46A3* was knocked down in the 786-O cell line and the cells were further exposed to either anti-CD70-MMAE/F ADC or an anti-CD70-DM1 ADC. The cell viability after drug exposure of the anti-CD70-DM1 ADC was significantly reduced in wild-type 786-O cells using the CelltiterGlo. However, after *SLC46A3* gene knock-down in 786-O cells, no significant reduction in the cell viability was observed suggesting SLC46A3 was required for the transport of catabolic DM1 to unfold its cytotoxic effect. Interestingly, the cell viability of anti-CD70-MMAF ADC exposed 786-O cells remained unaffected indicating MMAF was not likely to be a substrate for SLC46A3 (Hamblett *et al.*, 2015).

Another explanation for the poor efficiency of anti-STEAP2 pADC in reducing the cell viability of PC3 cells could be ascribed to the linker-drug instability of the ADC. It is possible, that the MMAE molecules may have been detached from the linker between the time of shipping from CellMosaic (USA) to Swansea University. However, the anti-STEAP2 pADC was generated using the cleavable VC linker, which should be sensitive to Cathepsin-B, a lysosomal protease. Therefore, the anti-STEAP2 pADC should not have been likely for degradation when not located to the lysosomes. One study has tested the stability of an anti-CD30-MMAE ADC *ex-vivo*, using the same VC linker chemistry as in the present Chapter 5. They exposed the anti-CD30-MMAE ADC to the human blood plasma *in-vitro* at 37°C (Francisco *et al.*, 2003). After 10 days, aliquots of the anti-CD30-MMAE ADC -blood plasma mixture were analysed by LC-MS for the free MMAE drug. It was demonstrated that only 2% of free MMAE was detected by LC-MS highlighting VC as a highly chemically stable linker *ex-vivo* (Francisco *et al.*, 2003). The HIC analysis (CellMosaic) used in the current study showed the absence of protein aggregates after the anti-STEAP2 pADC development, which ruled-out potential instability issues of the ADC at this given time point. Therefore, the HIC analysis was in accordance with the appropriateness of the VC linker and its stability for use in anti-STEAP2 pADC construction. In order to clarify, if the low efficiency of the anti-STEAP2 pADC was due to the instability of the VC linker, HIC analyses should be performed on-site at Swansea University before the treatment in the future.

Taken together, there is evidence, that some cytotoxins used in the ADC technology (e.g. maytansinoides) demand a specific lysosomal transporter to unfold their cytotoxic effect. Other studies report drug resistance of certain cell lines to MMAE or DM1 due to the upregulation of certain MDR proteins, which regulate the efflux of the cytotoxins from the lysosome to the cytosol. It would be exciting to explore the presence of these lysosomal membrane proteins in the PC3 cells. Based on these insights, it is hypothesised, that these (yet unknown) lysosomal transporters

could have been responsible for the efflux of any free, cytosolic MMAE indicated by the low efficiency of the anti-STEAP2 pADC at doses below 100 µg/ml in PC3 cells. Moreover, it is hypothesised that the maximal uptake capacity of this transporter could have been saturated at doses near the 100 µg/ml ADC dose in PC3 cells. If the lysosomal, efflux transporter was no longer capable to retain the free MMAE molecules (originating from the ADC) due to a complete occupation of MMAE ligand binding sites (saturation) at 100 µg/ml, the remaining, free MMAE molecules could have easily passed the lysosomal membrane to the cytosol unfolding their cytotoxic effect. Future work could utilise a validated anti-STEAP2 mAb for the fabrication of a more powerful monoclonal anti-STEAP2-MMAE ADC. This would enable more precise targeting of one specific epitope on the ECL3 of STEAP2 in comparison of multiple epitopes within the ECL3 domain when used by the commercial anti-STEAP2 pAb (Ascoli, 2018; Holzlöhner & Hanack, 2017; Leenaars & Hendriksen, 2005). It would be exciting to construct and compare the efficiency of additional anti-STEAP2 ADCs. These ADCs could be generated by using different linker-payloads such as hydrazone-Ozogamycin (present in Adcetris®) or SMCC-DM1 (included in Trastuzumab-DM1 (Kadcyla®) (Jen *et al.*, 2018; Verma *et al.*, 2012).

#### **5.4.2 Anti-STEAP2 mAb development (Phase I)**

During the Phase I (Immunisation) of the anti-STEAP2 mAb development, the Test sera1 and 2 were obtained from the Balb/C mice, which were exposed to either the linear or cyclic STEAP2 peptide. The Test sera2 (cyclic and linear) were further evaluated to confirm the presence of anti-STEAP2 antibodies using ELISA, Western blot and fluorescence microscopy. The ELISA data suggested the Balb/C mice produced low – moderate but not a high Ab titres. The synthesis of both linear and cyclic STEAP2 antigens was based on the identification of the aa sequence of the immunogen (Peptide 5) on STEAP2 (Chapter3, **Section 3.3.4, Figure 3.13**). According to the AbDesigner tool, Peptide 5 was considered as the most immunogenic peptide region amongst other peptides, albeit a moderate immunogenicity was

ascribed to it (Chapter3, **Section 3.3.4**). Thus, it was not unsurprising, that low - moderate immune response to both linear and cyclic STEAP2 peptides were elicited by the Balb/C mice. Higher immunogenicity does not ultimately guarantee the success of Ab generation (Pisitkun *et al.*, 2014).

The ELISA data further implied, that Abs obtained from the Test sera2 (linear or cyclic) may be less likely to recognise the STEAP2 antigen of which the Balb/C mice have not been exposed to given the low absorbance values. The data implied, that the Test sera2 (linear) contained Abs specifically bind to linear but not to cyclic STEAP2 antigen and vice-versa. This finding is not unsurprising as the Ab production by the plasma B-cells is usually only stimulated once the APCs activate the T- and B-cell dependent humoral immune response (Di Pasquale *et al.*, 2015). However, additional fluorescence microscopy results have additionally proven, that the Test sera2 (linear) obtained from the Balb/C mice, which were exposed to the linear STEAP2 peptide, were indeed capable of recognising native STEAP2 protein. This finding demonstrates, that native STEAP2 may better resemble the linear STEAP2 antigen in a more sterically accessible way for the Test sera2 (linear) containing antibodies than the cyclic STEAP2 antigen (**Figure 5.22 A, B and C**). Cyclic antigens contain several molecules of either different (heterotropic) or the identical, linear antigens (homotropic) conjugated to each other by their lysine residues (Ganeshrao & Vikas, 2013). This gives cyclic antigens a more dendrimer, tree-like antigen structure (Ganeshrao & Vikas, 2013) (**Figure 5.22 B**). Researchers have employed this form to increase the immunogenicity of antigens for the design of vaccines (Ganeshrao & Vikas, 2013).

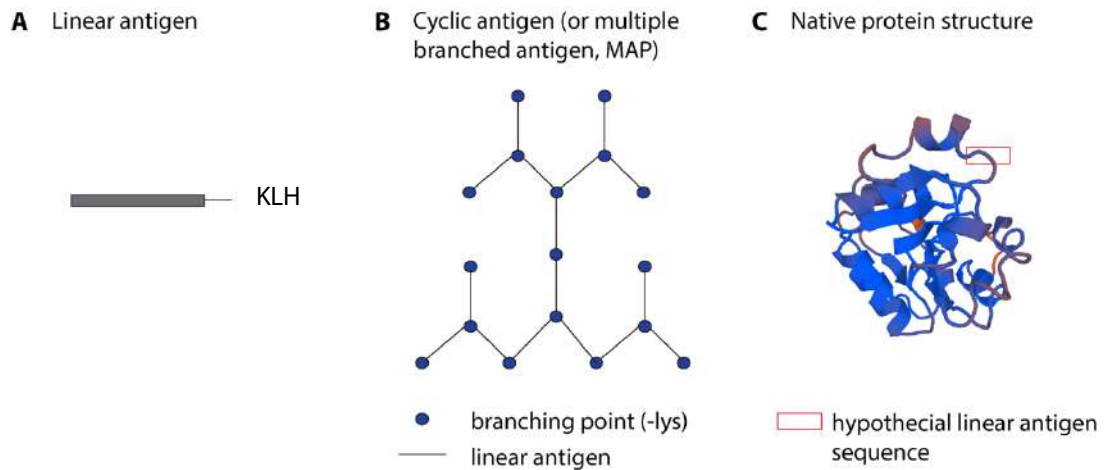


**Figure 5.22 Potential antigen structures for the *in-vivo* immunisation.** A) linear antigen conjugated to KLH. B) Cyclic antigen with lysine branching points. C) Native full-length recombinant protein structure. 3D STEAP2 image was modelled by SWISSPROT (date of retrieval: March 2016).

One study has used a cyclic antigen, which contains the capsid proteins (*i.e.* VP1 and VP3) of the Hepatitis A Virus to develop a vaccine against Hepatitis A (Haro & Pe, 2003). With regards to this current study, the 14 amino acid long, linear STEAP2 antigen („GWKRAFEEYYRFY “) contains one lysine residue (see Chapter3, **Section 3.3.4, Table 3.4**). Since the lysine residue is located within the linear STEAP2 antigen (*i.e.* aa position 3), the linear STEAP2 antigen is divided into two parts, in order to conjugate two additional antigens. Thereby, the utilised lysine conjugation chemistry could have led to a loss of the original configuration of consecutive amino acids within the linear STEAP2 antigen. Therefore, the different arrangement of linear STEAP2 antigen in the cyclic STEAP2 antigen may affect the paratope of the antibodies which is mirrored by the ELISA data (Test sera2 linear against cyclic STEAP2 antigen). In contrast, the confocal data suggests, that the native STEAP2 protein is more likely to fully resemble the linear STEAP2 peptide on the cell surface of the PC3 cells without any steric compromise antigen (**Figure 5.22 C**).

Further, western blot analysis was undertaken, in order to evaluate the Abs obtained from the Test sera2 (linear and cyclic). It was very difficult to draw any

preliminary conclusions based on this data, as the detection of STEAP2 was not distinctive enough when using the Test sera2 (linear and cyclic). At this Phase I stage of the mAb development, it is known, that any Abs produced by the plasma B-cells of the Balb/C mice are of polyclonal origin (Greenfield, 2012). It is known, that the serum of mammals contains a variety of serum proteins such as albumins, which carry other non-soluble proteins or immunoglobulins as part of their humoral immune response and fibrinogens to regulate blood clotting (Hayashi *et al.*, 2011; Sun *et al.*, 2018). It is important to note, that the Test sera2 (linear and cyclic) have not been affinity purified to obtain the Abs. Therefore, it is likely that the Test sera2 (linear and cyclic) contained other serum proteins apart from the primary mouse anti-STEAP2 pAbs. This heterogenous mixture of Abs and other serum proteins may have impeded the Ab binding to STEAP2 during the Western blot analysis resulting in poor signals. Based on this data, it is generally recommended to affinity purify the testing samples at all stages during the mAb development, if possible.

There are several possible reasons for a lower or moderate immune response during Phase I. The main factors considered to affect the host species' immune response are the health condition of the rodents, the time between the Phase I and Phase II and the use of adjuvants during immunisation. Low immune responses can be prevented by maintaining the Balb/C mice in good health condition by providing nutrition on a frequent basis and ensuring the living conditions are appropriate. In addition, the time between administering the final boost and before hybridoma fusion (Phase II) is considered to play a crucial role. Typically, the immune response of the Balb/C mice reaches its maximum 3 - 5 days after the final boost. It is critical to operate within this time frame, whilst exceeding the recommended time may result in a reduced immune response as well as less Ab producing plasma B-cells (Abdollahpour-alitappeh *et al.*, 2017; Greenfield, 2012; Holzlöhner & Hanack, 2017; Page & Thorpe, 2009; Pandey, 2010; Tomita & Tsumoto, 2011).

A variety of different adjuvants are also available for the vaccination (containing the antigen for immunisation). The function of the adjuvants shifted from the original stabilisation of the antigen to its role to increase the immunogenicity of the antigen and therefore the immune response of the host species. Adjuvants promote the recognition of the antigen by Antigen Presenting Cells (APC), which are required activate the humoral immune response. The APCs display the antigen to the T-cells. A specific subtype of the T-cells (*i.e.* CD4+ T-helper cells) release cytokines to recruit B-cells, which then mature to the Ab producing plasma B-cells against the exposed antigen (Apostólico *et al.*, 2016; Bonam *et al.*, 2017; Di Pasquale *et al.*, 2015; Gregorio *et al.*, 2013). The naturally occurring metalloprotein, called the Keyhole-Limpet Hemocyanin (KLH), originates from *Megathura crenulata*. KLH is a large, immunogenic protein, which why it is widely employed as a carrier protein for short antigens for the *in-vivo* production of mAbs (Swaminathan *et al.*, 2014) (**Table 5.3**). Therefore, this thesis has employed KLH to generate the linear STEAP2 antigen-KLH. There is little experience in the use of in-human approved adjuvants for the immunisation of laboratory animals (Apostólico *et al.*, 2016). Besides the use of KLH, the vaccination of animals has been limited to the use of the Freund's (Complete) Adjuvant (FCA) given its proven efficiency which was therefore used in the present study. The FCA belongs to the oil-in-water (O/W) adjuvants. It is formulated on the basis of a mineral oil (paraffin), heat-inactivated, non-pathogenic Mycobacterium and an emulsifier (Arlacel A) to better mix the O/W emulsion (Apostólico *et al.*, 2016; Bonam *et al.*, 2017; Pohanka *et al.*, 2016) (**Table 5.3**). Besides O/W emulsion-based adjuvants, the most common adjuvants are nowadays based on the use of mineral salts (*e.g.* aluminium-salts) or non-pathogenic virosomes. These can be found in FDA approved vaccines (in-human use only) (Di Pasquale *et al.*, 2015; Gregorio *et al.*, 2013).

**Table 5.3 Overview of common vaccine adjuvants.**

Adjuvant	Vaccine	Indication
Mineral salts		
Aluminium hydroxide	Fenderix®	Hepatitis B
Oil/ Water Emulsions		
AS03	Pandemrix®	Swine flu
AS04	Cervarix®	HPV 16/-18
Freunds Comp. Adjuvant*		Laboratory animal use
Virosome		
Phospholipid layer	HAVpur®	Hepatitis A
Other		
Keyhole-Limpet Hemocyanin	-	Carrier-protein

Aluminium hydroxide can be found in the Hepatitis B (Fenderix®) or Diphtheria, Typhus and Pertussis combined vaccination (Di Pasquale *et al.*, 2015; Gregorio *et al.*, 2013) (Table 5.3). In addition, AS03 is an O/W adjuvant, which the swine flu vaccine contains. AS03 combines the naturally occurring squalene with tocopherol and the surfactant polysorbate (Di Pasquale *et al.*, 2015; Gregorio *et al.*, 2013) (Table 5.3). Further, AS04 is an O/W emulsion made up of monophosphorylate lipids obtained from the lipopolysaccharide (LPS) cell wall derivate of *Salmonella minnesota*. AS04 has been efficiently used in Cervarix®, a vaccine used to prevent two common types of the Human Papilloma Virus (HPV-16/-18) causing cervical cancer (Table 5.3). Moreover, the Hepatitis A vaccine (HAVpur®) contains a phospholipid layer virosome, which presents the Hepatitis A specific antigens neuraminidase and haemagglutinin on the virosome surface (Di Pasquale *et al.*, 2015; Gregorio *et al.*, 2013) (Table 5.3).

#### **5.4.3 Anti-STEAP2 mAb development (Phase II)**

After four suitable Balb/C mice were identified to move forward to Phase II, the spleens of the host species (containing the plasma B-cells which produce anti-STEAP2 antibodies) were harvested and fused with mouse myeloma cells. Screening of the initial hybridoma cell colonies was performed by ELISA, which determined four viable hybridoma cell colonies. Yet, the number of viable hybridoma cell colonies was very low. The generation of antibodies using the hybridoma technology may yield from as little as approximately 5 - 25 viable hybridoma colonies. Thus, the poor

hybridoma cell colony yield in this thesis was not surprising (Greenfield, 2012). Potential reasons for a poor yield of hybridoma cells may be a result of chromosomal instability (CIS), the number of B-cells available for cell fusion or the utilised fusion method (Storchova, 2018; Storchova & Kuffer, 2008; Westerwoudt, 1987).

Mammalian cells are diploid but it has been reported, that the hybridoma development results in the generation aneuploid karyotypes by DNA and RNA content analysis using flow cytometry, with evidence of tetraploid (4n), pentaploid (5n) or hexaploid (6n) sets of chromosomes (Andreef *et al.*, 1985). Several checkpoints tightly control the cell division, including the Cyclin-Dependent Kinase CDK-4/6 complex, which detects DNA damage during G1-Phase of the cell cycle. Kinetochores, centromere and spindle-assembly checkpoints ensure the correct segregation of the chromosomes for mitosis (Delespaul *et al.*, 2019; Potapova *et al.*, 2013; Storchova, 2018; Storchova & Kuffer, 2008; Wenzel & Singh, 2018). Positively selected hybridoma cells must not only obtain the parental chromosomes but successfully undergo mitosis, despite their chromosome abnormality (Westerwoudt, 1987). It is anticipated, that many hybridoma cells quickly undergo cell death after the cell fusion given their aneuploidy status, which can result in a poor yield of hybridoma cells. Yet, it poses the question how the remaining hybridoma cell lines actually manage to stabilise their genome despite their aneuploidy. One research group provided insight on how cancer cells adapt and overcome aneuploidy and chromosome instability using *S. Cerevisiae* (Ravichandran *et al.*, 2018). They concluded, that the gain of the chromosome II substantially impacted the gene expression of *SLI15*, an inner centromere-related protein required for appropriate segregation of chromosomes during mitosis (UniProtKB: P38283, SLI15-YEAST) (Ravichandran *et al.*, 2018). They showed, that a specific pattern (subset) of aneuploid chromosome interactions, named the chromosome copy number interaction (CCNI), are either advantageous or disadvantageous for the survival of an optimal karyotype using Next-Generation Sequencing (NGS) (Ravichandran *et al.*, 2018).

There is evidence that the number and ratio of spleen cells fused with myeloma cells affects the number of viable hybridoma cells. The most optimal ratio for intraspecies cell fusion was 5:2 highlighting a substantially higher number of spleen cells than myeloma cells is required (Westerwoudt, 1987). This study has implied, that a synchronous cell cycle of both spleen cells and myeloma cells contributes to a higher number of hybridoma cells obtained after the cell fusion (Westerwoudt, 1987). This study hypothesised, that non-synchronous cell cycles lead to a delay in cell division and therefore impairs the further cell growth (Westerwoudt, 1987). Nowadays the cell cycle phase can be easily determined by analysis of the DNA content (using nuclei stains like PI or DAPI) by flow cytometry (Pozarowski & Darzynkiewicz, 2001). Cell cycle synchronization can be enforced *in-vitro* by transient serum starvation, which can be confirmed by a cell cycle arrest in G0/G1 phase by flow cytometry and fluorescence microscopy (Chen *et al.*, 2007). The use of microtubule inhibitors (*e.g.* Nocodazole, is thought to block the cell cycle in the G2/M phase by inhibiting microtubule polymerisation (Blajeski *et al.*, 2002; Choi *et al.*, 2011; Yiangou *et al.*, 2019). Yet, both options are not feasible because the hybridoma development is limited to absolute sterile working conditions (Greenfield, 2012; Holzlöhner & Hanack, 2017; Tomita & Tsumoto, 2011)

Another option to enhance the success of the hybridoma cell development is the use of a different cell fusion method. The most common technique, which is employed for cell fusion is currently based on the use of polyethylenglycol (PEG), a surfactant (also used in this study) (Greenfield, 2012; Knop *et al.*, 2010). Based on its physicochemical properties, the membranes of single cells are brought in the vicinity of each other by dehydration forcing them to fuse together. Thereby, one mutual cell membrane evolves and results in the generation of the hybridoma cell (Greenfield, 2012; Knop *et al.*, 2010). The downsides of this agent is it, that the dehydration can also lead to the agglomeration of the cells resulting in the generation of unfavoured polykaronts (Pedrazzoli *et al.*, 2011). The use of nano-electropulses has been reported to be more efficient as they led to a higher number of hybridoma cells

(Napotnik & Miklav, 2018; Rems *et al.*, 2013; Yu *et al.*, 2008). The alignment and fusion of the cells can be induced by the use of electric pulses causing a dipole within the cell, which forces the fusion of the cell membranes and leads to the hybridoma cell development (Qian *et al.*, 2014). Besides the higher success rate, this method is also considered to be more reproducible, while allowing real-time monitoring of the cell fusion compared to PEG-based cell fusions (Trontelj *et al.*, 2010).

#### **5.4.4 Anti-STEAP2 mAb development (Phase IV)**

After the Phase III (Limiting Dilution), four viable single cell hybridoma clones were identified and evaluated for their ability to bind linear and cyclic STEAP2 antigen by ELISA, Western blotting and confocal microscopy. Western blotting analysis showed three of four anti-STEAP2 mAbs (anti-STEAP2 mAb1, anti-STEAP2 mAb3 and anti-STEAP2 mAb4) were capable of detecting a protein with a similar molecular weight like STEAP2. Yet, the specificity of these anti-STEAP2 mAbs may be inferior to the commercial anti-STEAP2 pAb (ECL3) control at this stage. The anti-STEAP2 mAbs detected the protein not only in the higher STEAP2 expressing PC3 cells, but also in the normal low STEAP2 expressing PNT2 cells, which is does not align with the commercial anti-STEAP2 pAb (ECL3).

One hypothesis for an inferior specificity of the anti-STEAP2 mAb1 - 4 to STEAP2 opposed to the commercial anti-STEAP2 pAb (ECL3) could be due to the Ab clonality. The commercial anti-STEAP2 pAb (ECL3) is of polyclonal origin and was raised against an immunogen sequence on the ECL3 of STEAP2 between the aa positions 400 - 490 (exact immunogen sequence is not specified by the supplier). This commercial anti-STEAP2 pAb (ECL3) has been generated during Phase I, after the immunisation with the antigen without moving on to Phase II. Given its polyclonal nature, the commercial anti-STEAP2 pAb may bind to multiple epitopes of STEAP2 leading to a greater signal amplification by the secondary anti-IgG-HRP linked conjugate. Unlike the commercial anti-STEAP2 pAb (ECL3), the anti-STEAP2

mAb1 - 4 were all raised against the small 14 aa long Peptide5/ECL3 of STEAP2 and originate from single cell hybridoma clones. Therefore, each of the anti-STEAP2 mAbs recognises one unique epitope region on STEAP2, which may result in a lower signal amplifications.

The anti-STEAP2 mAb1- 4 have not been fully optimised for their application in Western blot or fluorescence microscopy, yet. Unlike the Western blotting result, the fluorescence microscopy data showed none of the anti-STEAP2 mAb1 - 4 were able to detect native STEAP2, albeit neat Ab concentrations were applied and a host species specific primary Ab was included as control for the secondary anti-IgG AlexaFluor-488 detection Ab. It is a common phenomenon, that not all Ab are suitable for each application, which is in line with this present chapter's findings (Bordeaux *et al.*, 2014; Espina & Liotta, 2012; Weller, 2018). On the one hand, an Ab may be useful in Western blotting, but the same Ab may not also be applicable for fluorescence microscopy. Examples are the commercial anti-STEAP2 pAbs 1 - 3 used in the previous Chapter3, were only recommended by the supplier for Western blotting. Thus, poor signals were detected by fluorescence microscopy, which were improved by optimising (i.e. increasing) the anti-STEAP2 pAbs 1 - 3 concentration.

## 5.5 Conclusion

---

The present Chapter5 has shown, that four monoclonal anti-STEAP2 antibodies 1 - 4 (anti-STEAP2 mAbs 1 - 4) were developed (by Ab Production Services) using the hybridoma technology. The data confirmed, that both the linear and cyclic STEAP2 antigens are suitable for the production of anti-STEAP2 mAbs although having elicited a fairly moderate immune response. Future investigations are necessary to evaluate the specificity of the anti-STEAP2 mAb1 - 4 to STEAP2 and to assess the impact on reducing the cancer invasive properties in prostate cancer cells *in-vitro* compared to the commercial anti-STEAP2 pAb (ECL3). The design of a polyclonal anti-STEAP2-MMAE ADC (anti-STEAP2 pADC) and its subsequent assessment versus its unconjugated, commercial, polyclonal anti-STEAP2 Ab (anti-STEAP2 pAb/ECL3) has highlighted the poor quality of the ADC and also suggest potential *in-vitro* processing issues of the ADC. Future studies may also determine the expression profile of MDR proteins in the PC3 cells, to support an appropriate drug-linker selection, in order to design and investigate a panel of highly potent anti-STEAP2 ADCs. .

## 6 General Discussion

Approximately 10% of prostate cancers progress to advanced or metastatic disease with a poor 5-year survival rate with approximately 30% (Cancer Research UK, 2019; NIH, 2016). The main treatment options for advanced prostate cancer are limited to palliative options, which can be accompanied with harsh side-effects (*e.g.*, erectile dysfunction and hair loss) severely compromising patients' quality of life (Cancer Research UK, 2019). Thus, more efficient, targeted drugs need to be established, in order to improve the clinical management of men suffering advanced prostate cancer. More patient-tailored strategies, including mAbs, were developed for oncology applications during the last two decades, since knowledge in the pharmacogenomics of certain cancers have been gained (Ryman & Meibohm, 2017; Schork, 2015). Due to the high specificity of mAbs, they can be utilised as “Magic Bullet” to detect cancer-associated proteins, in order to cause growth inhibition of cancers cells by modulating downstream signalling pathways (Bosch & Rosich, 2008; Strebhardt & Ullrich, 2008; Valent *et al.*, 2016). Although progress has been made to introduce two immunotherapeutics (*i.e.* Sipuleucel-T and Pembrolizumab) to treat mCRPC, the clinical benefit over the standard ADT, radio- and chemotherapy has been debated or limited to a very narrow subset of patients (Graff & Chamberlain, 2014; Hansen *et al.*, 2018; Kantoff *et al.*, 2010). An appropriate (Ab) therapy for men with high-risk, advanced prostate cancer is missing, to minimise side-effects and potentially prevent cancer progression. The cell surface protein STEAP2 is known to drive prostate cancer progression by modulating cancer invasive traits such as cell migration and invasion *in-vitro*.

The aim of this thesis was to determine, whether STEAP2 is a viable drug target with a focus on the application of therapeutic Abs and Antibody-Drug Conjugates (ADCs) to provide a more efficient therapy option for advanced prostate cancer.

The data of this showed (see **Figure 6.1**)

- (1) A low normal tissue expression profile for STEAP2 across 33 tissue specimen by TMA/IHC analysis (Chapter3);
- (2) Peptide5/ECL3 on STEAP2 is a promising immunogen for the generation of anti-STEAP2 mAbs (Chapter3);
- (3) An anti-STEAP2 pAb/ECL3 reduced cancer invasive traits (*e.g.* cell migration, invasion, viability) in prostate cancer cells *in-vitro* and triggered STEAP2 receptor internalisation (Chapter4);
- (4) The suitability of the ADC technology to target STEAP2 (Chapter5).

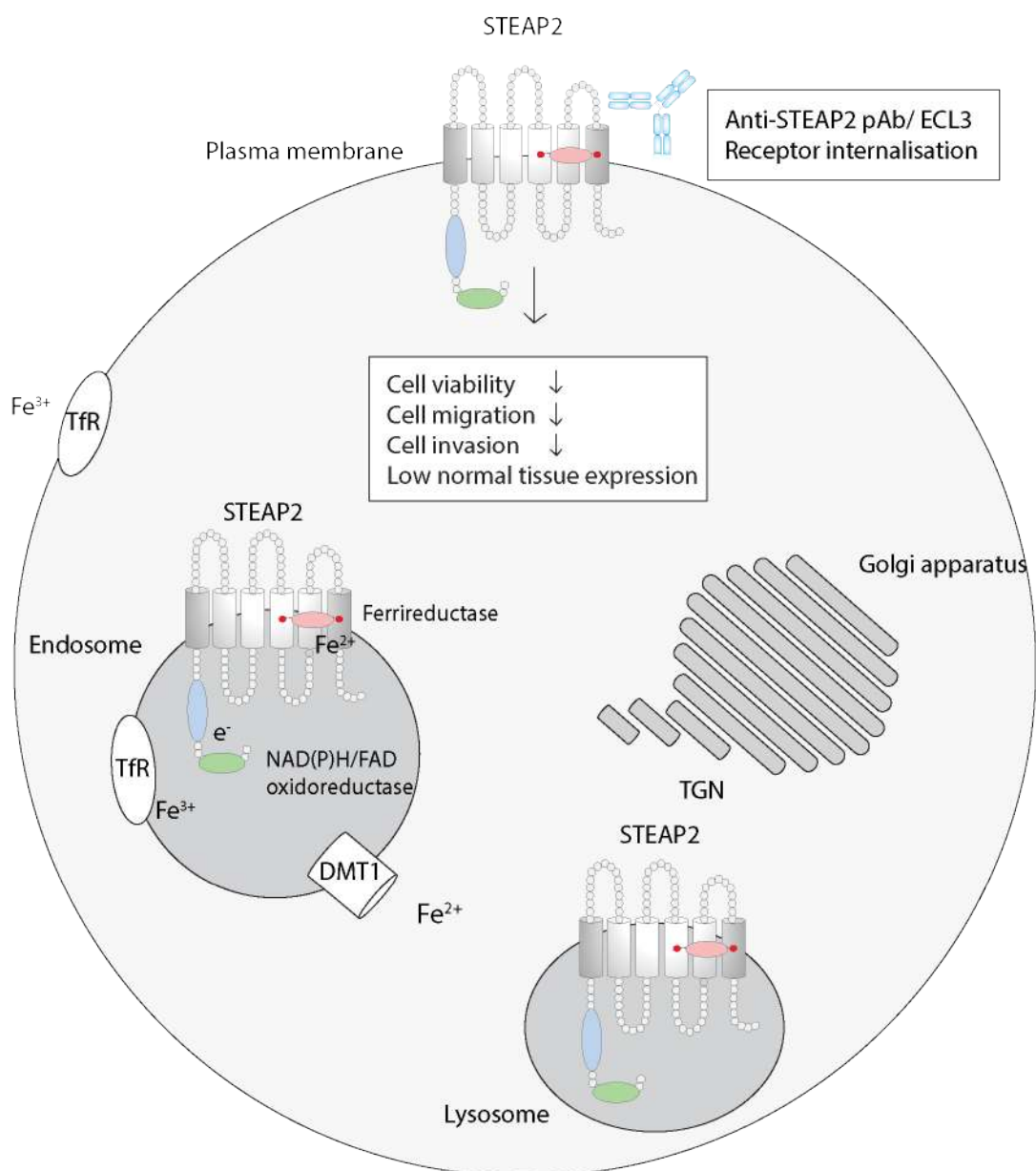


**Figure 6.1 Information gained during this thesis qualifies STEAP2 as a suitable drug target to treat prostate cancer.** Antibody-targeting of STEAP2/ECL3 triggered receptor internalisation of the protein to the endosomes and presumably to the lysosomes and thus makes STEAP2 an attractive drug target for ADC development. Antibody treatment against STEAP2/ECL3 reduces cancer invasive properties of prostate cancer cells PC3 (i.e. cell migration, cell invasion and cell viability). TfR: Transferrin receptor; DMT1: Dimetal-Transporter1; TGN: Trans-Golgi Network; Anti-STEAP2 pAb: Anti-STEAP2 polyclonal antibody; ECL3: Extracellular Loop3 of the STEAP2 protein.

In Chapter3, a low tissue distribution of STEAP2 was observed in 33 healthy tissue specimen by TMA/IHC indicating off-target side-effects are less likely when STEAP2 is used as a drug target for Ab therapeutics. Past results reported STEAP2 is highly expressed in the prostate cancer specimen but not in healthy prostate tissues

and its expression correlates with advanced prostate cancer by an increase in Gleason Score (Burnell *et al.*, 2018; Porkka *et al.*, 2002). The results herein therefore confirm the optimal tissue profile for STEAP2 when used as a drug target for Ab drugs and further imply a potential benefit over standard treatment by causing less side-effects, if these results will translate into *in-vivo*. Hence, future work should address the biodistribution of a validated anti-STEAP2 mAb (ECL3) in prostate cancer xenograft *in-vivo* mouse models. The biodistribution can be investigated by collecting the vital organs (tissues) after Ab treatment following IHC analyses for STEAP2.

During Chapter3, one anti-STEAP2 pAb (ECL3) lead candidate was identified based on the excellent binding ability to detect overexpressed (cell-surface) STEAP2 by confocal microscopy and western blotting. The next step aimed to deliver proof-of-concept *in-vitro* to affirm the suitability for Ab therapies, including when incorporated into ADCs, which might prove the most effective drug in the future treatment of aggressive prostate cancer. Hence, the effects of the selected anti-STEAP2 pAb lead candidate (ECL3) on cancer invasive traits *in-vitro* underlying the metastatic cascade *in-vivo* were investigated (Chapter4). In order to form metastasis, primary cancer cells must gain the capability for an increased movement to disseminate and form secondary tumour sites. The metastatic cascade consists of the following events: (1) Development of the primary tumour, (2) local invasion, (3) intravasation, (4) survival in the blood circulation, (5) extravasation and (6) development of secondary tumour (metastasis) (Lambert *et al.*, 2017). Tumour cells can alter their cell polarity during cytoskeleton remodelling for increased cell movement and migratory capability (Roche, 2018). By upregulating the expression of Matrix-Metalloproteases (MMPs) (*e.g.* MMP2, MMP3, MMP7, MMP9 and MMP11 in prostate cancer), the extracellular matrix (ECM), which confines the primary tumour, can be degraded (Burnell *et al.*, 2018; Escaff *et al.*, 2010; Xie *et al.*, 2016). Consequently, ECM degradation allows the tumour to infiltrate beyond the confined organ. During intravasation, tumour cells enter and survive in the blood circulation (3, 4) (Lambert *et al.*, 2017). By ability to migrate and invade the ECM, tumour cells

reach the distant site during extravasation (5) (Lambert *et al.*, 2017). Further growth and nourishment of the secondary tumour require increased cell proliferation and angiogenesis (6) (Lambert *et al.*, 2017).

Chapter4 showed when targeting the ECL3, the anti-STEAP2 pAb lead candidate was indeed able to completely halt cell migration in PC3 cells (but not in PNT2 cells) in a dose-dependent manner, substantially reduced cancer invasion and led to a reduction in cell viability of PC3 cells. These Chapter4 results were in alignment with past work within the group, which demonstrated STEAP2 plays a significant role in driving cell migration, invasion and proliferation by using an siRNA gene knock-down (and transfection) approach of STEAP2 in PC3 (and PNT2 cells) (Burnell *et al.*, 2018; Whiteland *et al.*, 2014). Since the anti-STEAP2 pAb (ECL3) led to a significant reduction of cancer invasive traits *in-vitro*, it could potentially prevent advanced prostate cancer from cancer metastasis or reduce the spread of metastatic sites *in-vivo*. Indeed, a recent patent application by Regeneron Pharmaceuticals demonstrated the *in-vivo* efficiency of STEAP2-directed mAbs, specific to ECL2, in Severe Compromised Immune-Deficient (SCID) lymph node metastatic prostate cancer (C4-2) xenograft mouse models (Patent Application WO-2018058001-A1, 2018). The anti-STEAP2 mAbs (ECL2) substantially reduced the tumour volume (size) when compared to the untreated control up until 3.5 months after tumour implantation (Patent Application WO-2018058001-A1, 2018). Chapter4 highlighted Ab targeting of either ECL1 or ECL3 was as equally efficient in blocking cancer cell migration completely *in-vitro* (Chapter4). Based on this data (Chapter4) and the findings provided by Regeneron Pharmaceuticals, it is very likely, that anti-STEAP2 mAbs (ECL3) may also be capable of blocking tumour growth *in-vivo* (Patent Application WO-2018058001-A1, 2018). Chapter4 also showed the capability of the selected anti-STEAP2 pAb (ECL3) to trigger receptor internalisation of STEAP2. Indeed, the anti-STEAP2 pAb binding to STEAP2 provoked the uptake of the Ab-STEAP2 complex and suggested the localisation to the endosomes and lysosomes by confocal microscopy (Chapter4). Likewise, Amgen Inc. recently

demonstrated STEAP2 receptor internalisation upon Ab binding to STEAP2 (Hasegawa *et al.*, 2018). They suggested endosomal location of the Ab-STEAP2 complex by confocal microscopy (Hasegawa *et al.*, 2018). However, Hasegawa *et al.* employed an STEAP2-directed mAb, recognising a different domain on the ECL2 of STEAP2, opposed to the ECL3-specific anti-STEAP2 pAb lead candidate used in this thesis (Chapter4). In alignment with Regeneron's patent application and Hasegawa *et al.*, the findings of Chapter4 affirm STEAP2 qualifies as a viable drug target for the application of mAbs and ADCs to treat prostate cancer *in-vitro*. The data set the premises to generate an ADC as a more efficient tumour-cell killing strategy when targeting STEAP2.

The next step was to fabricate and test an ADC for its *in-vitro* cell killing efficiency by using the Ab-STEAP2 pAb lead candidate. The rationale for selecting the VC-PABC linker and the MMAE payload was based on their proven clinical efficacy (*e.g.* Brentuximab-Vedotin, Adcetris®), which is successfully used in the treatment of non-solid tumours (Garnock-Jones, 2013; Gravanis *et al.*, 2016). A polyclonal anti-STEAP2-MMAE ADC (anti-STEAP2 pADC) was produced by CellMosaic (Chapter5). This anti-STEAP2 pADC was 3-fold more efficient in reducing the cell viability of PC3 cells at a dose of 100 µg/ml when compared to its unconjugated version inferring STEAP2 is a viable drug target for ADCs to treat prostate cancer *in-vitro*. However, the free MMAE drug was effective in reducing the cell viability in the ng/ml dose range indicating the anti-STEAP2 pADC quality was poor. The low ADC efficiency could have been due to the polyclonal origin of the anti-STEAP2 pAb lead candidate (ECL3). Polyclonal Abs (pAbs) contain a mixture of antibodies, that recognise multiple epitopes within a specific immunogen region of the antigen (Ascoli, 2018; Leenaars & Hendriksen, 2005; Stills, 2012). Thus, pAbs are considered as a heterogenous pool of antibodies (Abs) (Ascoli, 2018; Leenaars & Hendriksen, 2005; Stills, 2012). Structural analysis of STEAP2 demonstrated Peptide 5/ECL3 as the only accessible binding domain on the ECL3 for the pAbs to STEAP2 given its exposure to the extracellular site (Chapter3). Hence, pAbs, that recognize

immunogen regions on ECL3 other than Peptide 5 cannot bind to the naive STEAP2 protein, which could explain the low ADC efficiency. In contrast to pAbs, mAbs are homogenous Abs as they originate from the identical parent hybridoma cell clone, which recognises one, single epitope (Greenfield, 2012; Stills, 2012). Regeneron Pharmaceuticals recently filed a patent application demonstrating the efficiency of STEAP2-targeted ADCs to substantially reduce the tumour volume in prostate cancer SCID/C4-2 mouse xenograft models up to 30 days after tumour engraftment (Patent Application WO-2018058001-A1, 2018). These STEAP2-directed ADCs were different to the anti-STEAP2 pADC used in this study herein. First, they were of monoclonal origin and second, the ADCs were based on the maytansinoides payload (DM1) compared to the MMAE payload incorporated into the anti-STEAP2 pADC in this thesis (Chapter4) (Patent Application WO-2018058001-A1, 2018). Regeneron Pharmaceuticals' findings, including the Chapter4 data, therefore encourage the hypothesis, that monoclonal anti-STEAP2 ADCs against Peptide5/ECL3, may also be likely to exert an anti-tumour effect *in-vivo*. Future work should use monoclonal anti-STEAP2 mAbs against Peptide5/ECL3 for the fabrication of more efficient ADCs. A panel of different monoclonal anti-STEAP2 ADCs could be designed and screened for the most efficient version *in-vitro* and *in-vivo*. For example, the maytansinoid payload DM1 can be attached via the thio-ether linker to the mAb as exemplified by Regeneron Pharmaceuticals. The DM1/ thio-ether linker payload has also been successfully applied for the treatment of metastatic HER2+ breast cancer by Trastuzumab-Emtansine (Kadcyla®) (Venkatesan, 2016; Verma *et al.*, 2012). Aside from this, the calicheamicin payload Ozogamycin can also be utilised in combination with a hydrazone linker (present in Gemtuzumab Ozogamycin, Mylotarg®) for the treatment of Hodgkin lymphoma (Jen *et al.*, 2018).

The Chapter4 data encouraged the proprietary development of a hybridoma technology-based anti-STEAP2 mAb (ECL3) in collaboration with Ab Production Services (APS, UK) (Chapter5). An identified immunogen region specific to ECL3 of STEAP2 (Peptide5, Chapter3) was utilised as antigen for the mAb production

(Chapter3) and delivered four anti-STEAP2 mAbs (ECL3) (Chapter5). Future work requires the anti-STEAP2 mAbs to be validated for their ability to detect cell-surface STEAP2, to trigger receptor internalisation and their effect on abrogating cancer invasive traits *in-vitro* to identify one anti-STEAP2 mAb (ECL3) lead candidate. Then, the next step is to determine the therapeutic efficiency of validated anti-STEAP2 mAbs (ECL3) *in-vivo* by measuring the reduction in tumour volume (size) over a 3-month period after tumour engraftment. The efficiency of the validated anti-STEAP2 mAbs targeting the ECL3 could be further compared to the ECL2-specific anti-STEAP2 mAb of Regeneron Pharmaceuticals *in-vivo*. The lymph node metastatic (SCID/ C4-2) and bone metastatic prostate cancer xenograft mouse models can be utilised for future *in-vivo* tests.

Within the last 15 years, past research has significantly provided evidence for the immune system to be crucial for both protection and promotion of cancer development (Dunn *et al.*, 2004). Based on these findings, the concept of „cancer immuno-editing“ was been established and described in three phases (Dunn *et al.*, 2004; Mittal *et al.*, 2015). During the first phase, „cancer immunosurveillance“ (1), immune-competent immune cells are able to identify tumour cells, in order to eliminate these before the tumour manifests. However, the „fittest“ tumour cells survive within an immunocompetent tumour environment (2), which leads to tumour progression as the tumour escapes the immune system (3) (Dunn *et al.*, 2004; Schreiber *et al.*, 2011). Tumour cells can escape the immune system by loss of tumour antigenicity, immunogenicity or by exerting an immunosuppressive microenvironment (Beatty & Gladney, 2015). The insights on cancer immuno-editing have introduced „cancer immunotherapy“ as new treatment modality for oncology applications. Cancer immunotherapies are designed to activate the host-immune defence of T-cells against cancer cells to facilitate anti-tumour efficiency. Successful cancer immunotherapy drugs are bispecific antibodies (bsAbs), immune-checkpoint inhibitors (ICIs) and anti-cancer vaccines (Dahlén *et al.*, 2018; Kantoff *et al.*, 2010; Pardoll, 2016; Spiess *et al.*, 2015). In particular, the following proteins have become

attractive drug targets for cancer immunotherapy: Cluster of Differentiation3 (CD3), Programmed-Cell Death Protein1 (PD1), Programmed-Death Ligand1 (PD-L1) and the Cytotoxic T-Lymphocyte-Associated Protein4 (CTLA4) (Hernandez-Hoyos *et al.*, 2016; Ishida *et al.*, 1992; Leach *et al.*, 1996; Pardoll, 2016).

IgG-type mAbs, possess two Fab-binding „arms“, which can be employed for bispecific-targeting of two different epitopes of drug targets to kill tumour cells (Dahlén *et al.*, 2018). Based on this principle, bsAbs have been engineered to recognise a tumour-associated antigen (TAA) with one Fab-region, while the second Fab-domain is used for T-cell activation to elicit anti-tumour response (Dahlén *et al.*, 2018; Spiess *et al.*, 2015; Weidle *et al.*, 2014). CD3 is a co-stimulatory receptor on T-cells, that activates cytotoxic T-cells (CD8+) and T-helper cells (CD4+) for target-cell lysis via a Major-Histocompatibility Complex I or II-dependent manner (Cantrell, 2015; Smith-Garvin *et al.*, 2009). Thereby, bsAbs are capable to redirect T-cells upon binding to CD3 against the TAA for tumour cell elimination (Hernandez-Hoyos *et al.*, 2016; Linke *et al.*, 2010). A recent patent application demonstrated the efficiency of anti-STEAP2xCD3 bsAbs to induce T-cell activation and proliferation *ex-vivo* by using human peripheral blood mononuclear cells (hPBMCs) (Patent Application WO-2018058001-A1, 2018). hPBMC treated with anti-STEAP2xCD3 bsAbs in the presence of prostate cancer lymph node metastatic C4-2 cells resulted in substantial cytotoxicity (Patent Application WO-2018058001-A1, 2018). If bsAbs against the ECL2 of STEAP2xCD3 are capable of inducing a cytotoxic effect in tumour cells, targeting ECL3 of STEAP2xCD3 could elicit a similar cytotoxic effect *ex-vivo*, which remains to be studied in the future. Therefore, there is evidence for STEAP2 to be utilised as a drug target for bsAbs as cancer immunotherapy for advanced prostate cancer.

Activation of T-cells is provoked upon antigen display by the APCs via the Major-Histocompatibility Complex I/II and concurrent binding of the Cluster of Differentiation28 (CD28, T-cell specific) to the B7 receptor on APCs (Buchbinder &

Desai, 2016). This elicits the induction of cytokines (e.g. IL2 and IFN $\gamma$ ) causing T-cell proliferation and immune response (Buchbinder & Desai, 2016). During T-cell activation, the so-called „immune-checkpoints“ serve T-cell suppression to prevent autoimmune reaction, a process called „peripheral tolerance“ (Buchbinder & Desai, 2016; Cantrell, 2015; Smith-Garvin *et al.*, 2009). Anergy of T-cells is achieved by inducing co-inhibitory signalling pathways via the Programmed-Death1 Protein (PD1) and the Cytotoxic T-Lymphocyte Associated Antigen4 (CTLA4) (Buchbinder & Desai, 2016). PD1 is a receptor expressed on T-cells and can be activated by its ligand, Programmed Death-Ligand1(PD-L1) leading to a reduced expression of cytokines to downregulate T-cell activity (Alsaab *et al.*, 2017; Ishida *et al.*, 1992). CTLA4 is a CD28-homologue receptor on T-cells (Kwek *et al.*, 2012; Leach *et al.*, 1996). CTLA4 binding to B7 results in the suppression of T-cell proliferation by reducing INF $\gamma$  expression (Kwek *et al.*, 2012). Cancer cells can upregulate the expression of CTLA4, PD1 or PD-L1 to harness „peripheral tolerance“, in order to escape cancer immunosurveillance (Buchbinder & Desai, 2016). Immune checkpoint-inhibitors (ICIs) bind to CTLA4, PD1 or PD-L1 to suppress co-inhibitory pathways to re-boost T-cell activity for cancer cell elimination (Pardoll, 2016; Schweizer & Drake, 2014). Approved ICIs are Nivolumab and Pembrolizumab specific to PD1 for oncology applications, including prostate cancer, and Ipilimumab (CTLA4) to treat advanced melanoma (Beer *et al.*, 2019; De Bono *et al.*, 2018; Hansen *et al.*, 2018; Johnson *et al.*, 2015; Kwon *et al.*, 2014; MSD, 2019; Slovin *et al.*, 2013). Treatment of ADT, chemo-resistant, mCRPC with positive PD-L1 expression with Pembrolizumab as monotherapy versus placebo showed an improved median progression free survival within 12 months, albeit only effective in a small patient subpopulation (17.4%) (NCT02054806) (Hansen *et al.*, 2018). Follow-on studies reported anti-tumour activity by Pembrolizumab in mCRPC regardless of the PD-L1 status (NCT02787005) (De Bono *et al.*, 2018). Another study indicated the combination of Enzalutamide (ADT) + Pembrolizumab was more beneficial than monotherapy of Pembrolizumab in a subset of mCRPC patients who have been unresponsive to prior Enzalutamide treatment alone (NCT023112557) (Graff *et al.*,

2018). Ipilimumab monotherapy against CTLA4 showed a minimally improved median overall survival of men with mCRPC compared to placebo (11.2 vs. 10 months) (Kwon *et al.*, 2014). In chemo-naive metastatic prostate cancer, progression free survival was increased compared to placebo (5.6 versus 3.8 months) (Beer *et al.*, 2019). A clinical benefit from combination therapy of Ipilimumab + radiotherapy was demonstrated in a subgroup of mCRPC patients of which 50% showed a stable disease leading to ongoing investigations (NCT00232882) (Slovin *et al.*, 2013). These data infer, ICIs monotherapy of prostate cancer are beneficial to a subgroup of prostate cancer patients, while combination therapies of standard treatment (ADT or radiotherapy) appear to be more efficient than ICI therapy alone. A major drawback of ICIs is the lack of predictive biomarkers to risk-stratify these patients to improve the response rate (Spencer *et al.*, 2016). However, the era of ICIs appears to be promising and it would be exciting to assess in the combination of STEAP2-directed mAbs and ICIs future *in-vitro* and *in-vivo*.

Another immune-boosting therapy are anti-cancer vaccines. The only approved agent of this drug class is Sipuleucel-T, an autologous cellular immunotherapy to treat mCRPC, ideally with low disease burden (Kantoff *et al.*, 2010; Sims, 2012). It requires the adoptive cell transfer of patients to collect the hPMBC, including APCs like macrophages and dendritic cells. The dendritic cells are then cultured and exposed to the Prostate Acidic Phosphatase (PAP)xGranulocyte Macrophage-Colony-Stimulating Factor (GM-CSF) recombinant fusion protein *ex-vivo* for activation following reintroduction into the patients' blood circulation (Kantoff *et al.*, 2010; Sims, 2012). Sipuleucel-T significantly improved the median overall survival by 4.1 months versus the placebo control (25.8 vs. 21.7 months) (Kantoff *et al.*, 2010). The major downsides of Sipuleucel-T treatment are the timely organisation and manufacturing of the vaccines, plus predictive biomarkers for treatment response are lacking (Graff & Chamberlain, 2014). To identify the most effective treatment strategy and a suitable patient subgroup, a few combinations of

Sipuleucel-T and sequences with standard therapies have been tested in the past (Antonarakis *et al.*, 2016; Beer *et al.*, 2011).

The research insights about cancer genetics and the role of the immune system in cancer development have set the rationale for the design of novel medicines to boost the immune system to tackle cancer. The major challenge is to define biomarkers to aid the risk stratification of those prostate cancer patients who are most likely to benefit from drug treatments such as ICIs and Sipuleucel-T. Moreover, the evaluation of optimal treatment sequences and the combination of ICIs and Sipuleucel-T with standard therapy is ongoing. Despite these advances, suitable Ab therapies for men with advanced prostate cancer are lacking. The findings of this thesis have provided proof-of-concept for STEAP2 (ECL3) as viable drug target for the application of an anti-STEAP pAb and anti-STEAP2 pADC *in-vitro* to treat aggressive prostate cancer. The data herein suggest STEAP2-targeted Abs represent a valuable therapy option tailored to men with advanced disease to potentially prevent prostate cancer progression, which need to be confirmed by *in-vivo* follow on-studies.

## 6.1 Future Outlook

---

Future studies should focus on the validation of the four delivered anti-STEAP2 mAbs *in-vitro*, in order to identify the most efficient lead candidates for *in-vitro* and *vivo* follow-on studies. Suitable anti-STEAP2 mAb lead candidates provide two possible avenues to take in the future:

- (1) Investigation of the anti-STEAP2 based mAb lead candidates for their therapeutic potential by studying the effect on reducing cancer invasive traits *in-vitro*, their biodistribution and tumour size reduction *in-vivo* (in combination with ICIs);
- (2) Fabrication of more powerful monoclonal anti-STEAP2 ADCs by utilising a panel of different mAbs, linkers and payloads following efficacy assessment (*e.g.* cell killing *in-vitro* and tumour reduction *in-vivo*).

## 6.2 Conclusion

---

The low tissue expression profile of STEAP2 implies few off-target side-effects are likely to occur if STEAP2 is to be utilised as a future drug target. Peptide1 - 5 specific to the ECL1 - 3 of STEAP2 represent potential antigen regions for future mAb development. When ECL3 was evaluated, the anti-STEAP2 pAb lead candidate targeting this region was indeed capable of significantly reducing cancer invasive traits and triggered receptor internalisation in PC3 cells. Assessment of the anti-STEAP2 pADC demonstrated the potential utility of the ADC technology in the future. These findings highlight the therapeutic value of Ab-based strategies against the ECL3 of STEAP2 to block cancer invasive traits underlying cancer metastasis. In summary, the *in-vitro* findings of this thesis provide proof-of-concept, that supports STEAP2 as a viable drug target, with a focus on Abs and ADCs, prior to preclinical *in-vivo* studies to treat men with advanced prostate cancer. The data herein set the rationale for the future development of Ab-based strategies for targeted tumour-cell killing, potentially leading to more powerful medicines tailored to patients with aggressive prostate cancer to improve their clinical management.

## 7 Bibliography

- Abcam. (2019). Tips for designing a good peptide immunogen.
- Abdollahpour-alitappeh, Meghdad, Amanzadeh, Amir, Heidarnejad, Fatemeh, & Habibi-anbouhi, Mahdi. (2017). *Monomethyl Auristatin E*, a Potent Cytotoxic Payload for Development of Antibody-Drug Conjugates against Breast Cancer. *2*, 98–103.
- Abida, W., Armenia, J., Middha, S., Autio, K. A., ... Scher, H. I. (2019). Analysis of the Prevalence of Microsatellite Instability in Prostate Cancer and Response to Immune Checkpoint Blockade. *JAMA Oncology*, *5*(4), 471–478. <https://doi.org/10.1001/jamaoncol.2018.5801>
- Alberts, Bruce. (2015). *Molecular Biology of the Cell* (Sixth).
- Alsaab, H. O., Sau, S., Alzhrani, R., & Tatiparti, K. (2017). PD-1 and PD-L1 Checkpoint Signaling Inhibition for Cancer Immunotherapy: Mechanism, Combinations, and Clinical Outcome. *Frontiers in Pharmacology*, *8*(August), 1–15.
- Amzallag, N., Passer, BJ, Allanic, D., Segura, E., ... Telerman, A. (2004). TSAP6 Facilitates the Secretion of Translationally Controlled Tumor Protein / Histamine-releasing Factor via a Nonclassical Pathway. *The Journal of Biological Chemistry*, *279*(44), 46104–46112. <https://doi.org/10.1074/jbc.M404850200>
- Anderson, Leigh, & Anderson, Norman G. (1977). High resolution two-dimensional electrophoresis of human plasma proteins. *Biochemistry*, *16*(12), 5421–5425.
- Andreef, M., Bartal, A., Feit, C., & Hirshaut, Y. (1985). Clonal stability and heterogeneity of hybridomas: analysis by multiparameter flow cytometry. *Hybridoma*, *4*(3), 277–287.
- Antonarakis, E. S., Kibel, A. S., Yu, E. Y., Karsh, L. I., ... Millard, F. E. (2016). Sequencing of Sipuleucel-T and Androgen Deprivation Therapy in Men with Hormone-Sensitive Biochemically Recurrent Prostate Cancer: A Phase II Randomized Trial. *Clinical Cancer Research*, *23*(10), 1–10.
- Apostólico, Juliana De Souza, Alves, Victória, Lunardelli, Santos, Coirada, Fernanda Caroline, ... Rosa, Daniela Santoro. (2016). Adjuvants: Classification, Modus Operandi, and Licensing. *Journal of Immunology Research*, (April), 1–16. <https://doi.org/10.1155/2016/1459394>
- Arner, P., Stenson, BM, Dungner, El, Na, E., ... Ryden, Mi. (2008). Expression of Six Transmembrane Protein of Prostate 2 in Human Adipose Tissue Associates with Adiposity and Insulin Resistance. *Endocrine Research*, *33*(June), 2249–2254. <https://doi.org/10.1210/jc.2008-0206>
- Ascoli, Carl A. (2018). Overlooked benefits of using polyclonal antibodies. *Biotechniques*, *65*(3), 127–135.
- Bakiu, Erjona, Telhaj, Ervis, Kozma, Elvisa, Ruçi, Ferdinand, & Malkaj, Partizan. (2013). Comparison of 3D CRT and IMRT Treatment Plans. *Acta Inform Med.*,

- 21(July), 211–212. <https://doi.org/10.5455/aim.2013.21.211-212>
- Barupala, D. P., Dzul, S. P., Jo Riggs-Gelasco, P., & Stemmler, T. L. (2017). Synthesis, Delivery and Regulation of Eukaryotic Heme and Fe-S Cluster Cofactors. *Archives of Biochemistry and Biophysics*, 592(313), 60–75. <https://doi.org/10.1016/j.abb.2016.01.010>.Synthesis
- Basak, A., Boudreault, A., Chen, A., Chretien, M., ... Lazure, C. (1995). Application of the multiple antigenic peptides (MAP) strategy to the prpduction of pro-hormone convertase antibodies: synthesis, characterization and use of 8-branched immunogenic peptides. *Journal of Peptide Science*, 1(6), 385–395. <https://doi.org/10.1002/psc.310010606>
- Beatty, Gregory L., & Gladney, Whitney L. (2015). Immune escape mechanisms as a guide for cancer immunotherapy. *Clinical Cancer Research*, 21(4), 687–692. <https://doi.org/10.1158/1078-0432.CCr-14-1860>
- Beer, T. M., Bernstein, G. T., Corman, J. M., Glode, L. M., ... Frohlich, M. W. (2011). Cancer Therapy: Clinical Randomized Trial of Autologous Cellular Immunotherapy with Sipuleucel-T in Androgen-Dependent Prostate Cancer. *Clinical Cancer Research*, 17(13), 4558–4568.
- Beer, T. M., Kwon, E. D., Drake, C. G., Fizazi, K., ... Gerritsen, W. (2019). Randomized, Double-Blind, Phase III Trial of Ipilimumab Versus Placebo in Asymptomatic or Minimally Symptomatic Patients With Metastatic Chemotherapy-Naive Castration-Resistant Prostate Cancer. *Journal of Clinical Oncology*, 35(1), 40–46.
- Bissa, B., Beedle, A. M., & Govindarajan, R. (2016). Lysosomal Solute Carrier Transporters Gain Momentum in Research. *Clinical Pharmacology & Therapeutics*, 100(5), 431–436. <https://doi.org/10.1002/cpt.450>
- Blajeski, April L., Phan, Vy A., Kottke, Timothy J., & Kaufmann, Scott H. (2002). G 1 and G 2 cell-cycle arrest following microtubule depolymerization in human breast cancer cells. *Journal of Clinical Investigation*, 110(1), 91–99. <https://doi.org/10.1172/JCI200213275>.Introduction
- Bogdan, A. R., Miyazawa, M., Hashimoto, K., & Tsuji, Y. (2016). Regulators of Iron Homeostasis : New Players in Metabolism , Cell Death , and Disease. *Trends in Biochemical Sciences*, 41(3), 274–286.
- Bolla, Michel, Tienhoven, Geertjan Van, Warde, Pdraig, Dubois, Jean Bernard, ... Kuten, Abraham. (2010). External irradiation with or without long-term androgen suppression for prostate cancer with high metastatic risk : 10-year results of an EORTC randomised study. *The Lancet Oncology*, 11(November), 1066–1073. [https://doi.org/10.1016/S1470-2045\(10\)70223-0](https://doi.org/10.1016/S1470-2045(10)70223-0)
- Bonam, Srinivasa Reddy, Partidos, Charalambos D., Halmuthur, Sampath Kumar M., Muller, Sylviane, ... Glenney, Alexander T. (2017). An Overview of Novel Adjuvants Designed for Improving Vaccine Ef fi cacy. *Trends in Pharmacological Sciences*, 38(9), 771–793. <https://doi.org/10.1016/j.tips.2017.06.002>
- Boniol, Mathieu, Boyle, Peter, Autier, Philippe, Ruffi, Alain, & Perrin, Paul. (2012). Critical role of prostate biopsy mortality in the number of years of life gained and lost within a prostate cancer screening programme. *British Journal of*

- Urology*, 110, 1648–1652. <https://doi.org/10.1111/j.1464-410X.2012.11513>
- Bordeaux, Jennifer, Welsh, Allison W., Agarwal, Seema, Killiam, Elizabeth, ... Rimm, David L. (2014). Antibody validation. *Biotechniques*, 48(3), 197–209. <https://doi.org/10.2144/000113382.Antibody>
- Bosch, Felix, & Rosich, Laia. (2008). The Contributions of Paul Ehrlich to Pharmacology: A Tribute on the Occasion of the Centenary of His Nobel Prize. *Pharmacology*, 82, 171–179. <https://doi.org/10.1159/000149583>
- Boswell, CA, Mundo, EE, Zhang, C., Bumbaca, D., ... Lin, Kedan. (2011). Impact of Drug Conjugation on Pharmacokinetics and Tissue Distribution of Anti-STEAP1 Antibody À Drug Conjugates in Rats. *Bioconjugate Chemistry*, 22, 1994–2004. <https://doi.org/10.1021/bc200212a>
- Bradbury, Andrew R. M., Trinklein, Nathan D., Thie, Holger, Wilkinson, Ian C., ... Dübel, Stefan. (2018). When monoclonal antibodies are not monospecific: Hybridomas frequently express additional functional variable regions. *MAbs*, 10(4), 539–546. <https://doi.org/10.1080/19420862.2018.1445456>
- Bradley, A. M., Devine, M., & DeRemer, D. (2013). Brentuximab vedotin: An anti-CD30 antibody-drug conjugate. *American Journal of Health-System Pharmacy*, 70(7), 589–597. <https://doi.org/10.2146/ajhp110608>
- Bravo-Cordero, Jose Javier, Magalhaes, Marco A. O., Eddy, Robert J., Hodgson, Louis, & Condeelis, John. (2014). Functions of cofilin in cell locomotion and invasion. *Nature Reviews Molecular Cell Biology*, 14(7), 1–24. <https://doi.org/10.1038/nrm3609.Functions>
- Buchbinder, E. I., & Desai, A. (2016). CTLA-4 and PD-1 Pathways Similarities, Differences, and Implications of Their Inhibition. *American Journal of Clinical Oncology*, 39(1), 98–106.
- Budnik, Justin, Suri, Jaipreet, Bates, James E., Bylund, Kevin C., & Milano, Michael T. (2019). Prognostic Significance of Sites of Visceral Metastatic Disease in Prostate Cancer: A Population-based Study of 12,180 Patients. *Clinical Genitourinary Cancer*, 17(4), 260–267. <https://doi.org/10.1016/j.clgc.2019.03.020>
- Burnell, S., Spencer-Harty, Samantha, Howarth, Suzie, Bodger, Owen, ... Doak, Shareen H. (2019). Utilisation of the STEAP protein family in a diagnostic setting may provide a more comprehensive prognosis of prostate cancer. *PLoS ONE*, 8(August), 1–11. <https://doi.org/10.1371/journal.pone.0220456>
- Burnell, S., Spencer-harty, Samantha, Howarth, Suzie, Owen, B., ... Doak, Shareen H. (2018). STEAP2 Knockdown Reduces the Invasive Potential of Prostate Cancer Cells. *Scientific Reports*, (April), 1–12. <https://doi.org/10.1038/s41598-018-24655-x>
- Cancer Research UK. (2019). Prostate Cancer.
- Cantrell, D. (2015). Signaling in Lymphocyte Activation. *Cold Spring*, 7(a018788), 1–14.
- Carneiro Borra, Ricardo, Andrade Lotufo, Monica, Gagiotti, Sonia Maria, De Mesquita Barros, Fabirna, & Andrade, Priscila Maria. (2009). A simple method to measure cell viability in proliferation and cytotoxicity assays. *Brazilian Oral Research*,

23(3), 255–262.

- Carter, Paul J., & Lazar, Greg A. (2018). Next generation antibody drugs : pursuit of the ‘ high-hanging fruit .’ *Nature Reviews*, 17(March), 197–223. <https://doi.org/10.1038/nrd.2017.227>
- Carter, Paul J., & Senter, Peter D. (2013). Antibody-drug conjugates for cancer therapy. *Cancer Journal (Sudbury, Mass.)*, 14(3), 154–169.
- Challita-Eid, PM, Morrison, K., Etesami, S., & An, Z. (2007). Monoclonal Antibodies to Six-Transmembrane Epithelial Antigen of the Prostate-1 Inhibit Intercellular Communication In vitro and Growth of Human Tumor Xenografts In vivo. *The Journal of Cancer Research*, 67(12), 5798–5805.
- Chalouni, Cécile, & Doll, Sophia. (2018). Fate of Antibody-Drug Conjugates in Cancer Cells. *Journal of Experimental & Clinical Cancer Research*, 37(20), 1–12. <https://doi.org/10.1186/s13046-017-0667-1>
- Channah, E., Tropé, CG, Reich, R., & Davidson, B. (2017). TSAP6 is a novel candidate marker of poor survival in metastatic high-grade serous carcinoma ☆. *Human Pathology*, 60, 180–187. <https://doi.org/10.1016/j.humpath.2016.10.017>
- Chari, Ravi V. J., Miller, Michael L., & Widdison, Wayne C. (2014). Antibody-Drug Conjugates: An Emerging Concept in Cancer Therapy. *Angewandte Chemie International Edition*, 53(15), 3796–3827. <https://doi.org/10.1002/anie.201307628>
- Chen, Elizabeth H., Grote, Eric, & Mohler, William. (2007). Cell – cell fusion. *Federation of European Biochemical Societies Letters*, 581, 2181–2193. <https://doi.org/10.1016/j.febslet.2007.03.033>
- Chen, Hao, Lin, Zongtao, Arnst, Kinsie E., Miller, Duane D., & Li, Wei. (2017). Tubulin Inhibitor-Based Antibody-Drug Conjugates for Cancer Therapy. *Molecules*, 22(1281), 1–28.
- Chen, Ni, & Zhou, Qiao. (2016). The evolving Gleason grading system. *Chinese Journal of Cancer Research*, 28(1), 58–64. <https://doi.org/10.3978/j.issn.1000-9604.2016.02.04>
- Chen, Po Chun, Cheng, Hsu Chen, & Tang, Chih Hsin. (2013). CCN3 promotes prostate cancer bone metastasis by modulating the tumor – bone microenvironment through RANKL-dependent pathway. *Carcinogenesis*, 34(7), 1669–1679. <https://doi.org/10.1093/carcin/bgt103>
- Chen, Robert, Hou, Jessie, Newman, Edward, Kim, Young, ... Kane, Susan E. (2016). CD30 downregulation, MMAE resistance, and MDR1 upregulation are all associated with resistance to brentuximab vedotin. *Molecular Cancer Therapeutics*, 14(6), 1376–1384. <https://doi.org/10.1158/1535-7163.MCT-15-0036>
- Chen, Sonja D., Fava, Joseph L., & Amin, Ali. (2016). Gleason grading challenges in the diagnosis of prostate adenocarcinoma: experience of a single institution. *Vinchrows Archives*, 468, 213–218. <https://doi.org/10.1007/s00428-015-1879-4>
- Chen, Xuan, Wang, Rui, Chen, Anji, Wang, Yongmei, ... Cao, Rongyue. (2019). Inhibition of mouse RM-1 prostate cancer and B16F10 melanoma by the fusion protein of HSP65 & STEAP1. *Biomedicine & Pharmacotherapy*, 111(October

- 2018), 1124–1131. <https://doi.org/10.1016/j.biopha.2019.01.012>
- Cheng, Shi bin, Quinn, Jeffery A., Graeber, Carl T., & Filardo, Edward J. (2011). *GPER downregulation via a TGN-proteasomal pathway* *GPER downregulation via a TGN-proteasomal pathway*. <https://doi.org/10.1074/jbc.M111.224071>
- Choi, Hye Joung, Fukui, Masayuki, & Zhu, Bao Ting. (2011). Role of Cyclin B1 / Cdc2 Up-Regulation in the Development of Mitotic Prometaphase Arrest in Human Breast Cancer Cells Treated with Nocodazole. *PLoS ONE*, *6*(8), 1–13. <https://doi.org/10.1371/journal.pone.0024312>
- Chou, Peter Y., & Fasman, Gerald D. (1974). Conformational Parameters for Amino Acids in Helical, beta-Sheet, and Random Coil Regions Calculated from Proteins. *Biochemistry*, *13*(2), 211–222. <https://doi.org/10.1021/bi00699a001>
- Christian, Ralph, Santos, Delos, Bautista, Stephen, Lucarelli, Stefanie, ... Gruenberg, Jean E. (2014). Selective regulation of clathrin-mediated epidermal growth factor receptor signaling and endocytosis by phospholipase C and calcium. *Molecular Biology of the Cell*, *28*(October), 2802–2818. <https://doi.org/10.1091/mbc.E16-12-0871>
- Clark, Andrew G., & Vignjevic, Danijela Matic. (2015). Modes of cancer cell invasion and the role of the microenvironment. *Current Opinion in Cell Biology*, *36*, 13–22. Retrieved from
- Clementi, Nicola, Mancini, Nicasio, Castelli, Matteo, Clementi, Massimo, & Burioni, Roberto. (2013). Characterization of epitopes recognized by monoclonal antibodies : experimental approaches supported by freely accessible bioinformatic tools. *Drug Discovery Today*, *18*(9–10), 464–471. <https://doi.org/10.1016/j.drudis.2012.11.006>
- Connolly, Erin C., Freimuth, Julia, & Akhurst, Rosemary J. (2012). Complexities of TGF-  $\beta$  Targeted Cancer Therapy. *International Journal of Biological Sciences*, *8*(7), 964–978. <https://doi.org/10.7150/ijbs.4564>
- Corraliza-Gorjon, Isabel, Somovilla-Crespo, Beatriz, Santamaria, Silvia, Garcia-Sanz, Jose A., & Kremer, Leonor. (2017). New Strategies Using Antibody Combinations to increase Cancer Treatment effectiveness. *Frontiers in Immunology*, *8*(December), 1–31. <https://doi.org/10.3389/fimmu.2017.01804>
- Costa, Elisabete C., Moreira, André F., Melo-diogo, Duarte De, Gaspar, Vítor M., ... Correia, Ilídio J. (2016). 3D tumor spheroids: an overview on the tools and techniques used for their analysis. *Biotechnology Advances*, *34*(8), 1427–1441. <https://doi.org/10.1016/j.biotechadv.2016.11.002>
- Coumans, J. V. F., Davey, R. J., & Moens, P. D. J. (2018). Cofilin and profilin : partners in cancer aggressiveness. *Biophysical Reviews*, *10*(5), 1323–1335.
- Crawford, ED, Heidenreich, Axel, Lawrentschuk, Nathan, Tombal, Bertrand, ... Laurence, MJD. (2018). Androgen-targeted therapy in men with prostate cancer : evolving practice and future considerations. *Prostate Cancer and Prostatic Diseases*, 1–15. <https://doi.org/10.1038/s41391-018-0079-0>
- Cytotoxic agents. (n.d.).
- Dahlén, E., Veitonmäki, N., & Norlén, P. (2018). Bispecific antibodies in cancer immunotherapy. *Therapeutic Advances in Vaccines and Immunotherapy*, *6*(1),

3–17.

- Dan, Nirnoy, Setua, Saini, Kashyap, Vivek K., Khan, Sheema, ... Chauhan, Subhash C. (2018). *Antibody-Drug Conjugates for Cancer Therapy: Chemistry to Clinical Implications*. <https://doi.org/10.3390/ph11020032>
- Dason, S., Allard, C., & Shayegan, B. (2012). Androgen deprivation : time to rethink therapy targets. *Urologic Cancer Update*, 11(4), 32–34.
- De Bono, J. S., Goh, J. C. H., Ojamaa, K., Piulats Rodriguez, J. M., ... Antonarakis, E. S. (2018). KEYNOTE\_199: Pembrolizumab (pembro) for docetaxel-refractory metastatic castration-resistant prostate cancer (mCRPC). *Journal of Clinical Oncology*, 36(15).
- Delepaul, Lucile, Merle, Candice, Lesluyes, Tom, Lagarde, Pauline, ... Chibon, Frédéric. (2019). Fusion-mediated chromosomal instability promotes aneuploidy patterns that resemble human tumors. *Oncogene*, 38, 6083–6094. <https://doi.org/10.1038/s41388-019-0859-6>
- Denham, JQ, Steigler, A., Lamb, DS, Joseph, D., ... Este, CD. (2011). Short-term neoadjuvant androgen deprivation and radiotherapy for locally advanced prostate cancer : 10-year data from the TROG 96 . 01 randomised trial. *Lancet Oncology*, 12(5), 451–459. [https://doi.org/10.1016/S1470-2045\(11\)70063-8](https://doi.org/10.1016/S1470-2045(11)70063-8)
- Di Pasquale, A., Preiss, S., Tavares Da Silva, F., Garcon, N., ... Fleming, A. (2015). Vaccine Adjuvants : from 1920 to 2015 and Beyond. *Vaccines*, 3(2), 320–343.
- Diamantis, Nikolaos, & Banerji, Udai. (2016). Antibody-drug conjugates - An emerging class of cancer treatment. *British Journal of Cancer*, 114(4), 362–367. Retrieved from
- Diering, G. H., Numata, M., Putnam, R. W., & State, W. (2014). *Endosomal pH in neuronal signaling and synaptic transmission: role of Na<sup>+</sup>/ H<sup>+</sup> exchanger NHE5*. 4(January), 1–7.
- Donovan, KA, Gonzalez, BB, Nelson, AM, Mayer, N., ... Jacobsen, PB. (2019). Effect of Androgen Deprivation Therapy on Sexual Function and Bother in Men with Prostate Cancer: A Controlled Comparison. *Psychooncology*, 27(1), 316–324. <https://doi.org/10.1002/pon.4463>.Effect
- Dosio, Franco, Brusa, Paola, & Cattell, Luigi. (2011). *The Role of the Linkage between Components*. 848–883. <https://doi.org/10.3390/toxins3070848>
- Doyle, L. Austin, & Ross, Douglas D. (2003). Multidrug resistance mediated by the breast cancer resistance protein BCRP ( ABCG2 ). *Oncogene*, 1(22), 7340–7358. <https://doi.org/10.1038/sj.onc.1206938>
- Drachman, J. G., & Senter, P. D. (2013). Antibody-drug conjugates: the chemistry behind empowering antibodies to fight cancer. *Hematology / the Education Program of the American Society of Hematology. American Society of Hematology. Education Program*, 2013, 306–310.
- Dreyer, AM, Beauchamp, J., Matile, H., & Pluschke, G. (2010). An efficient system to generate monoclonal antibodies against membrane-associated proteins by immunisation with antigen-expressing mammalian cells. *BMC Biotechnology*, 10(87), 1–14.
- Ducry, Laurent, & Stump, Bernhard. (2010). Antibody-drug conjugates: Linking

- cytotoxic payloads to monoclonal antibodies. *Bioconjugate Chemistry*, *21*(1), 5–13.
- Dufour, Robin, Daumar, Pierre, Mounetou, Emmanuelle, Aubel, Corinne, ... Penault-llorca, Frédérique. (2015). BCRP and P-gp relay overexpression in triple negative basal-like breast cancer cell line: a prospective role in resistance to Olaparib. *Scientific Reports*, *5*(22670), 1–9. <https://doi.org/10.1038/srep12670>
- Dunn, G. P., Old, L. J., & Schreiber, R. D. (2004). The Immunobiology of Cancer Immunosurveillance and Immunoediting. *Immunity*, *21*(2), 137–148.
- Dunn, Mary Weinstein, & Kazer, Meredith Wallace. (2011). Prostate cancer overview. *Seminars in Oncology Nursing*, *27*(4), 241–250.
- Ecker, DM, Jones, SD, & Levine, HL. (2015). The therapeutic monoclonal antibody market. *MAbs*, *7*(1), 9–14.
- Edmondson, Rasheena, Broglie, Jessica Jenkins, Adcock, Audrey F., & Yang, Liju. (2014). Three-Dimensional Cell Culture Systems and Their Applications in Drug Discovery and Cell-Based Biosensors. *ASSAY and Drug Development Technologies*, *12*(4), 207–218. Retrieved from
- Epstein, Jonathan I. (2016). New prostate cancer grade group system correlates with prostate cancer death in addition to biochemical recurrence. *British Journal of Cancer*, *114*, 1069–1070. <https://doi.org/10.1038/bjc.2016.102>
- Escaff, S., Fernandez, J. M., Gonzalez, L. O., Suarez, A., ... Vizoso, F. J. (2010). Study of matrix metalloproteinases and their inhibitors in prostate cancer. *British Journal of Cancer*, *102*(5), 922–929.
- Espina, V., & Liotta, L. A. (2012). *Molecular Profiling*.
- Forsström, Björn, Bisławska Axnäs, Barbara, Rockberg, Johan, Danielsson, Hanna, ... Uhlen, Mathias. (2015). Dissecting antibodies with regards to linear and conformational epitopes. *PLoS ONE*, *10*(3), 1–11.
- Francisco, Joseph A., Cervený, Charles G., Meyer, Damon L., Mixan, Bruce J., ... Senter, Peter D. (2003). cAC10-vcMMAE, an anti-CD30-monomethyl auristatin E conjugate with potent and selective antitumor activity. *Blood*, *102*(4), 1458–1465. <https://doi.org/10.1182/blood-2003-01-0039>
- Galetti, Maricla, Petronini, Pier Giorgio, Fumarola, Claudia, Cretella, Daniele, ... Ardizzoni, Andrea. (2015). Effect of ABCG2 / BCRP Expression on Efflux and Uptake of Gefitinib in NSCLC Cell Lines. *PLoS ONE*, (November), 1–18. <https://doi.org/10.1371/journal.pone.0141795>
- Ganeshrao, V., & Vikas, J. (2013). Multiple antigenic peptide (MAP): a synthetic peptide dendrimer for diagnostic , antiviral and vaccine strategies for emerging and re-emerging viral diseases. *Indian Journal of Virology*, *24*(December), 312–320.
- Garnock-Jones, Karly P. (2013). Brentuximab vedotin: A review of its use in patients with hodgkin lymphoma and systemic anaplastic large cell lymphoma following previous treatment failure. *Drugs*, *73*(4), 371–381.
- Gashaw, Isabella, Ellinghaus, Peter, Sommer, Anette, & Asadullah, Khusru. (2012). What makes a good drug target ? §. *Drug Discovery Today*, *17*(February), S24–S30. <https://doi.org/10.1016/j.drudis.2011.12.008>

- Gasparian, Alexander V, Yao, Ya Juan, Kowalczyk, Dariusz, Lyakh, Ludmila A., ... Budunova, Irina V. (2002). The role of IKK in constitutive activation of NF-kappaB transcription factor in prostate carcinoma cells. *Journal of Cell Science*, 115(Pt 1), 141–151. Retrieved from
- Gauss, George H., Kleven, Mark D., Sendamarai, Anoop K., Fleming, Mark D., & Lawrence, C. Martin. (2013). The Crystal Structure of Six-transmembrane Epithelial Antigen of the Prostate 4 ( Steap4 ), a Ferri / Cuprioreductase, Suggests a Novel Interdomain Flavin-binding Site. *The Journal of Biological Chemistry*, 288(28), 20668–20682. <https://doi.org/10.1074/jbc.M113.479154>
- Gioeli, D., Mandell, JW, Petroni, GR, Frierson, HF, & Weber, MJ. (1999). Activation of mitogen-activated protein kinase associated with prostate cancer progression. *Cancer Research*, 59(2), 279–284.
- Goldstein, Neal S., Hewitt, Stephen M., Taylor, Clive R., Yaziji, Hadi, ... Hessling, Jan. (2007). Recommendations for improved standardization of immunohistochemistry. *Applied Immunohistochemistry and Molecular Morphology*, 15(2), 124–133.
- Gomes, I. M., Maia, C. J., & Santos, C. R. (2012). STEAP Proteins: From Structure to Applications in Cancer Therapy. *Molecular Cancer Research*, 10(5), 573–588.
- Gomes, I. M., Sc, M., Arinto, P., Sc, M., ... Ph, D. (2014). STEAP1 is overexpressed in prostate cancer and prostatic intraepithelial neoplasia lesions, and it is positively associated with Gleason score. *Urologic Oncology: Seminars and Original Investigations*, 32(1), e23-29.
- Gomes, Ines M., Maia, Claudio J., & Santos, Cecilia R. (2012). STEAP Proteins : From Structure to Applications in Cancer Therapy. *Molecular Cancer Research*, 1(6), 573–588. <https://doi.org/10.1158/1541-7786.MCR-11-0281>
- Gong, Xue, Lin, Chao, Cheng, Jian, Su, Jiansheng, ... Zhao, Peng. (2015). Generation of multicellular tumor spheroids with microwell-based agarose scaffolds for drug testing. *PLoS ONE*, 10(6), 1–18.
- Gordetsky, Jennifer, & Epstein, Jonathan. (2016). Grading of prostatic adenocarcinoma: current state and prognostic implications. *Diagnostic Pathology*, 11(24), 2–9. <https://doi.org/10.1186/s13000-016-0478-2>
- Gozzelino, R., & Arosio, P. (2016). Iron Homeostasis in Health and Disease. *International Journal of Molecular Sciences*, 17(130), 1–14.
- Grada, Ayman, Otero-vinas, Marta, Prieto-castrillo, Francisco, Obagi, Zaidal, & Falanga, Vincent. (2018). Research Techniques Made Simple: Analysis of Collective Cell Migration Using the Wound Healing Assay. *Journal of Investigative Dermatology*, 137(2), e11–e16. <https://doi.org/10.1016/j.jid.2016.11.020>
- Graff, J. N., ALumkal, J. J., Thompson, R. F., Moran, A., ... Beer, T. M. (2018). Pembrolizumab (Pembro) plus enzalutamide (Enz) in metastatic castration resistant prostate cancer (mCRPC): Extended follow up. *Journal of Clinical Oncology*, 36(15).
- Graff, Julie N., & Chamberlain, Erin D. (2014). Sipuleucel-T in the treatment of prostate cancer: an evidenc-based review of its place in therapy. *Dove Press*

*Journal.*

- Grandchamp, Bernard, Hetet, Gilles, Kannengiesser, Caroline, Oudin, Claire, ... Heimpel, Hermann. (2011). A novel type of congenital hypochromic anemia associated with a nonsense mutation in the STEAP3 / TSAP6 gene. *American Society for Hematology*, 118(25), 6660–6667. <https://doi.org/10.1182/blood-2011-01-329011>.The
- Grant, Gregory A. (2002). *Synthetic Peptides: A User's Guide* (Second Edi; Gregory Grant, Ed.).
- Gravanis, Iordanis, Tzogani, Kyriaki, Van Hennik, Paula, De Graeff, Pieter, ... Pignatti, Francesco. (2016). The European Medicines Agency Review of Brentuximab Vedotin ( Adcetris ) for the Treatment of Adult Patients With Relapsed or Refractory CD30 + Hodgkin Lymphoma or Systemic Anaplastic Large Cell Lymphoma : Summary of the Scientific Assessment of the Commi. *The Oncologist*, 21, 102–109.
- Greenfield, EA. (2012). Generating Monoclonal Antibodies. In Edward A. Greenfield (Ed.), *Antibodies. A Laboratory Manual*. (2nd ed., pp. 201–221).
- Gregorio, Ennio De, Caproni, Elena, & Ulmer, Jeffrey B. (2013). Vaccine adjuvants : mode of action. *Frontiers in Immunology*, 4(July), 1–6. <https://doi.org/10.3389/fimmu.2013.00214>
- Grilo, António L. (2019). The Increasingly Human and Profitable Monoclonal Antibody Market. *Cell Press Reviews.*, 37(1), 9–16.
- Grunewald, TGP, Bach, H., Cossarizza, An, & Matsumoto, I. (2012). The STEAP protein family: Versatile oxidoreductases and targets for cancer immunotherapy with overlapping and distinct cellular functions. *Biology of the Cell*, 104(11), 641–657.
- Grunewald, TGP, Diebold, I., Esposito, I., Plehm, S., ... Burdach, S. (2012). STEAP1 Is Associated with the Invasive and Oxidative Stress Phenotype of Ewing Tumors. *Mol Cancer Res*, 10(1), 52–65.
- Guha, Sonia, & Padh, Harish. (2008). Cathepsins: Fundamental Effectors of Endolysosomal Proteolysis. *Indian Journal of Biochemistry / Biophysics*, 45(April), 75–90.
- Guo, Gang, Xu, Yong, & Zhang, Xu. (2017). TRUS-guided transperineal prostate 12 + X core biopsy with template for the diagnosis of prostate cancer. *Oncology Letters*, 12, 4863–4867. <https://doi.org/10.3892/ol.2017.6051>
- Hamblett, Kevin J., Jacob, Allison P., Gurgel, Jesse L., Tometsko, Mark E., ... Fanslow, William C. (2015). SLC46A3 Is Required to Transport Catabolites of Noncleavable Antibody Maytansine Conjugates from the Lysosome to the Cytoplasm. *Cancer Research*, (December), 5329–5341. <https://doi.org/10.1158/0008-5472.CAN-15-1610>
- Hamblett, KJ, Senter, PD, Chace, DF, Sun, MMC, ... Francisco, JA. (2004). Effects of drug loading on the antitumor activity of a monoclonal antibody drug conjugate. *Clinical Cancer Research*, 10(20), 7063–7070.
- Han, Mingzhi, Xu, Ran, & Wang, Shuai. (2018). Six-Transmembrane Epithelial Antigen of Prostate 3 Predicts Poor Prognosis and Promotes Glioblastoma

- Growth and Invasion. *Neoplasia*, 20(6), 543–554. <https://doi.org/10.1016/j.neo.2018.04.002>
- Han, Tae H., Gopal, Ajay K., Ramchandren, Radhakrishnan, Goy, Andre, ... Connor, Owen A. O. (2014). CYP3A-mediated drug-drug interaction potential and excretion of brentuximab vedotin, and antibody-drug conjugate, in patients in CD30-positive hematologic malignancies. *Journal of Clinical Pharmacology*, 53(8), 866–877. <https://doi.org/10.1002/jcph.116>.CYP3A-mediated
- Hansen, A. R., Massard, C., Ott, P. A., Haas, N. B., ... Keefe, S. M. (2018). Pembrolizumab for advanced prostate adenocarcinoma: findings of the KEYNOTE-028 study. *Annals of Oncology*, 29(July), 1807–1813. <https://doi.org/10.1093/annonc/mdy232>
- Haro, Isabel, & Pe, Silvia. (2003). Liposome entrapment and immunogenic studies of a synthetic lipophilic multiple antigenic peptide bearing VP1 and VP3 domains of the hepatitis A virus: a robust method for vaccine design. *Federation of European Biochemical Societies*, 540, 133.140. [https://doi.org/10.1016/S0014-5793\(03\)00249-7](https://doi.org/10.1016/S0014-5793(03)00249-7)
- Hasegawa, Haruki, Li, Cong, Alba, Benjamin M., Penny, David M., ... Lim, Ai Ching. (2018). Membrane cholesterol modulates STEAP2 conformation during dynamic intracellular trafficking processes leading to broad subcellular distribution. *Experimental Cell Research*, 370(2), 208–226.
- Hatzoglou, Vaios, Patel, GV, Morris, MJ, Curtis, K., ... Holodny, Andrei I. (2016). Brain Metastases from Prostate Cancer: An 11-Year Analysis in the MRI ERA with Emphasis on Imaging Characteristics, Incidence, and Prognosis. *Journal of Neuroimaging*, 24(2), 161–166. <https://doi.org/10.1111/j.1552-6569.2012.00767.x>.Brain
- Heidenreich, Axel, Bastian, PJ, Bellmunt, Joaquim, Bolla, Michel, ... Mottet, Nicolas. (2014). EAU Guidelines on Prostate Cancer. Part II: Treatment of Advanced, Relapsing, and Castration-Resistant Prostate Cancer. *European Urology*, 65(2), 467–479. <https://doi.org/10.1016/j.eururo.2013.11.002>
- Hendriks, J. J. M. A., Lagas, J. S., Wagenaar, E., Rosing, H., ... Schinkel, A. H. (2014). Oral co-administration of elacridar and ritonavir enhances plasma levels of oral paclitaxel and docetaxel without affecting relative brain accumulation. *British Journal of Cancer*, 110(11), 2669–2676. <https://doi.org/10.1038/bjc.2014.222>
- Henry, GH, Malewska, Alicia, Joseph, DB, Hutchinson, RC, ... Reese, JC. (2018). Resource A Cellular Anatomy of the Normal Adult Human Prostate and Prostatic Urethra Resource A Cellular Anatomy of the Normal Adult Human Prostate and Prostatic Urethra. *Cell Reports*, 25(December), 3530–3542. <https://doi.org/10.1016/j.celrep.2018.11.086>
- Hernandez-Hoyos, G., Sewell, T., Bader, R., Bannink, J., ... Blankenship, J. W. (2016). MOR209/ ES414 , a Novel Bispecific Antibody Targeting PSMA for the Treatment of Metastatic Castration-Resistant Prostate Cancer. *Molecular Cancer Therapeutics*, 15(9), 2155–2166.
- Hirschhaeuser, Franziska, Menne, Heike, Dittfeld, Claudia, West, Jonathan, ... Kunz-

- schughart, Leoni A. (2010). *Multicellular tumor spheroids: An underestimated tool is catching up again.* 148, 3–15. <https://doi.org/10.1016/j.jbiotec.2010.01.012>
- Hoarau-Véchet, J., Rafii, A., Touboul, C., Pasquier, J., ... Touboul, C. (2018). Halfway between 2D and animal models: Are 3D cultures the ideal tool to study cancer-microenvironment interactions? *International Journal of Molecular Sciences*, 19(1).
- Hofman, Michael S., Violet, John, Hicks, Rodney J., Ferdinandus, Justin, ... Kong, Grace. (2018). [<sup>177</sup>Lu]-PSMA-617 radionuclide treatment in patients with metastatic castration-resistant prostate cancer (LuPSMA trial): a single-centre, single-arm, phase 2 study. *Lancet Oncology*, 19(6), 825–833. [https://doi.org/10.1016/S1470-2045\(18\)30198-0](https://doi.org/10.1016/S1470-2045(18)30198-0)
- Holzlohner, Pamela, & Hanack, Katja. (2017). Generation of Murine Monoclonal Antibodies by Hybridoma Technology. *Journal of Visualized Experiments*, (119), 1–7. <https://doi.org/10.3791/54832>
- Hopp, T. P., & Woods, K. R. (1981). Prediction of protein antigenic determinants from amino acid sequences. *Proceedings of the National Academy of Sciences of the United States of America*, 78(6), 3824–3828.
- Hricak, H., & Scardino, P. T. (2009). *Prostate cancer*.
- Hu, Yong bo, Dammer, Eric B., Ren, Ru jing, & Wang, Gang. (2015). *The endosomal-lysosomal system: from acidification and cargo sorting to neurodegeneration*. 1–10. <https://doi.org/10.1186/s40035-015-0041-1>
- Huang, Bu wei, & Gao, Jian qing. (2018). Application of 3D cultured multicellular spheroid tumor models in tumor-targeted drug delivery system research. *Journal of Controlled Release*, 270(August 2017), 246–259. <https://doi.org/10.1016/j.jconrel.2017.12.005>
- Hubert, RS, Vivanco, I., Chen, E., Rastegar, S., ... Afar, DE. (1999). STEAP: a prostate-specific cell-surface antigen highly expressed in human prostate tumors. *Proceedings of the National Academy of Sciences of the United States of America*, 96(25), 14523–14528. Retrieved from
- Hudis, Clifford A. (2007). Trastuzumab — Mechanism of Action and Use in Clinical Practice. *New England Journal of Medicine*, 357(1), 39–51. Retrieved from
- Hughes, J. P., Rees, S., Kalindjian, S. B., & Philpott, K. L. (2011). *Principles of early drug*. 1239–1249. <https://doi.org/10.1111/j.1476-5381.2010.01127.x>
- Ishida, Y., Agata, Y., Shibahara, K., & Honjo, T. (1992). Induced expression of PD-1, a novel member of the immunoglobulin gene superfamily, upon programmed cell death. *The EMBO Journal*, 11(11), 3887–3895.
- Ishida, Yoichi, Nayak, Smita, Mindell, Joseph A., & Grabe, Michael. (2013). *A model of lysosomal pH regulation*. 705–720. <https://doi.org/10.1085/jgp.201210930>
- Izumi, Kouji, Ikeda, Hiroko, Maolake, Aerken, Machioka, Kazuaki, ... Namiki, Mikio. (2015). The relationship between prostate-specific antigen and TNM classification or Gleason score in prostate cancer patients with low prostate-specific antigen levels. *The Prostate*, 1042(January), 1034–1042. Retrieved from
- Jain, N., Smith, S. W., Ghone, S., & Tomczuk, B. (2015). Current ADC Linker

- Chemistry. *Pharmaceutical Research*, 32(11), 3526–3540.
- Jen, EY, Ko, CW, Lee, JE, Del Valle, PL, ... Pazdur, R. (2018). FDA Approval: Gemtuzumab Ozogamicin for the Treatment of Adults with Newly Diagnosed CD33-Positive Acute Myeloid Leukemia. *Clinical Cancer Research*, 24(14), 3242–3247. <https://doi.org/10.1158/1078-0432.CCR-17-3179>
- Jin, Renjie, Yi, Yajun, Yull, Fiona E., Blackwell, Timothy S., ... Matusik, Robert J. (2015). NF- $\kappa$ B gene signature predicts prostate cancer progression. *Cancer Research*, 74(10), 2763–2772. <https://doi.org/10.1158/0008-5472.CAN-13-2543.NF->
- Jin, Y., Wang, L., Qu, S., Sheng, X., ... Waehre, H. (2015). STAMP 2 increases oxidative stress and is critical for prostate cancer. *EMBO Molecular Medicine*, 7(3), 315–331.
- Johansson, Mikael P., Maaheimo, Hannu, & Ekholm, Filip S. (2017). New insight on the structural features of the cytotoxic auristatins MMAE and MMAF revealed by combined NMR spectroscopy and quantum chemical modelling. *Scientific Reports*, 7(15920), 1–10. <https://doi.org/10.1038/s41598-017-15674-1>
- John, Rudge, Delfino, Frank, Haber, Lauric, Smith, Eric, ... Nittoli, Thomas. (2018). *Anti-STEAP2 Antibodies, Antibody-Drug Conjugates, and Bispecific Antigen-Binding Molecules That Bind STEAP2 and CD3, And Uses Thereof*.
- Johnson, Douglas B., Peng, Chengwei, & Sosman, Jeffrey A. (2015). *Nivolumab in melanoma: latest evidence and clinical potential*. 97–106. <https://doi.org/10.1177/1758834014567469>
- Jonkman, James E. N., Cathcart, Judith A., Xu, Feng, Bartolini, Miria E., ... Colarusso, Pina. (2014). *An introduction to the wound healing assay using live-cell microscopy*. 8(5), 440–451.
- Junutula, Jagath R., Raab, Helga, Clark, Suzanna, Bhakta, Sunil, ... Mallet, William. (2008). Site-specific conjugation of a cytotoxic drug to an antibody improves the therapeutic index. *Nature Biotechnology*, 26(8), 925–932. <https://doi.org/10.1038/nbt.1480>
- Kaksonen, Marko, & Roux, Aurélien. (2018). Mechanisms of clathrin-mediated endocytosis. *Nature Reviews*, 19(5), 313–326. <https://doi.org/10.1038/nrm.2017.132>
- Kantoff, PW, Higano, CS, Shore, ND, Berger, ER, ... Schellhammer, PF. (2010). Sipuleucel-T Immunotherapy for Castration-Resistant Prostate Cancer. *New England Journal of Medicine*, 363(5), 411–422.
- Kaplon, H., & Reichert, JM. (2018). Antibodies to watch in 2018. *MAbs*, 10(2), 183–203. <https://doi.org/10.1080/19420862.2018.1415671>
- Keating, Gillian M. (2014). *Bevacizumab: A Review of Its Use in Advanced Cancer*. 1891–1925. <https://doi.org/10.1007/s40265-014-0302-9>
- Kim, HY, Park, SY, Lee, MH, Rho, JH, ... Yoo, Young H. (2015). Hepatic STAMP2 alleviates high fat diet-induced hepatic steatosis and insulin resistance. *Journal of Hepatology*, 63(2), 477–485. <https://doi.org/10.1016/j.jhep.2015.01.025>
- Kim, So Woon, Roh, Jin, & Park, Chan Sik. (2016). Immunohistochemistry for Pathologists: Protocols, Pitfalls, and Tips. *Journal of Pathology and*

- Translational Medicine*, 50(6), 411–418.
- Klotz, Laurence, Breau, RH, Collins, LL, Gleave, ME, ... Saad, Fred. (2017). Maximal testosterone suppression in the management of recurrent and metastatic prostate cancer. *CUAJ*, 11(February), 16–23.
- Knop, Katrin, Hoogenboom, Richard, Fischer, Dagmar, & Schubert, Ulrich S. (2010). Drug Delivery Poly ( ethylene glycol ) in Drug Delivery : Pros and Cons as Well as Potential Alternatives Angewandte. *Drug Delivery*, 49, 6288–6308. <https://doi.org/10.1002/anie.200902672>
- Köhler, G., & Milstein, C. (1975). Continuous cultures of fused cells secreting antibody of predefined. *Journal of Immunology*, 256(5517).
- Köhler, G., & Milstein, C. (2019). Continuous cultures of fused cells secreting antibody of predefined specificity. *Nature Immunology*, 256(5517), 495–497.
- Korkmaz, Korkmaz, K., Kurys, Piotr, Elbi, Cem, ... Saatcioglu, Fahri. (2005). Molecular cloning and characterization of STAMP2, an androgen-regulated six transmembrane protein that is overexpressed in prostate cancer. *Oncogene*, 24(31), 4934–4945.
- Korkmaz, KS, Elbi, Cem, Korkmaz, CG, Loda, Massimo, ... Saatcioglu, Fahri. (2002). Molecular Cloning and Characterization of STAMP1, a Highly Prostate-specific Six Transmembrane Protein that Is Overexpressed in Prostate Cancer. *The Journal of Biological Chemistry*, 277(39), 36689–36696. <https://doi.org/10.1074/jbc.M202414200>
- Kovtun, Yelena V., Audette, Charlene A., Mayo, Michele F., Jones, Gregory E., ... Chari, Ravi V. J. (2010). Antibody-maytansinoid conjugates designed to bypass multidrug resistance. *Cancer Research*, 70(6), 2528–2537.
- Krakhmal, N. V., Zavyalova, M. V., Denisov, E. V., Vtorushin, S. V., & Perelmuter, V. M. (2015). Cancer invasion: Patterns and mechanisms. *Acta Naturae*, 7(2), 17–28.
- Kratschmer, Christina, & Levy, Matthew. (2018). Targeted Delivery of Auristatin-Modified Toxins to Pancreatic Cancer Using Aptamers. *Molecular Therapy: Nucleic Acid*, 10(March), 227–236. <https://doi.org/10.1016/j.omtn.2017.11.013>
- Kratz, Felix, Senter, Peter, & Steinhagen, Henning. (2011). *Drug Delivery in Oncology: From Basic Research to Cancer Therapy*.
- Kruh, Gary D., Belinsky, Martin G., Gallo, James M., & Lee, Kun. (2007). Physiological and pharmacological functions of Mrp2 , Mrp3 and Mrp4 as determined from recent studies on gene-disrupted mice. *Cancer Metastasis Review*, 26(5), 5–14. <https://doi.org/10.1007/s10555-007-9039-1>
- Kwek, S. S., Cha, E., & Fong, L. (2012). Unmasking the immune recognition of prostate cancer with CTLA4 blockade. *Nature Publishing Group*, 12(4), 289–297.
- Kwon, ED, Drake, CG, Scher, HI, Fizazi, K., ... Roussy, Gustave. (2014). *Ipilimumab versus placebo after radiotherapy in patients with metastatic castration-resistant prostate cancer that had progressed after docetaxel chemotherapy ( CA184-043 ): a multicentre, randomised, double-blind, phase 3 trial*. 15(June). [https://doi.org/10.1016/S1470-2045\(14\)70189-5](https://doi.org/10.1016/S1470-2045(14)70189-5)
- Lambert, A. W., Pattabiraman, D. R., & Weinberg, R. A. (2017). Emerging Biological

- Principles of Metastasis. *Cell*, 168(4), 670–691.
- Lane, DJR, Merlot, AM, Huang, ML, Bae, D., ... Richardson, DR. (2015). Cellular iron uptake, trafficking and metabolism: Key molecules and mechanisms and their roles in disease. *Biochimica et Biophysica Acta*, 1853(February), 1130–1144. <https://doi.org/10.1016/j.bbamcr.2015.01.021>
- Leach, D. R., Krummel, M. F., & Allison, J. P. (1996). Enhancement of antitumor immunity by CTLA-4 blockade. *Science*, 271(5256), 1734–1736.
- Lee, JJ, Thomas, IC, Nolley, R., Ferrari, M., ... Leppert, JT. (2016). Biologic Differences Between Peripheral and Transition Zone Prostate Cancer. *Prostate*, 75(2), 183–190. <https://doi.org/10.1002/pros.22903>.Biologic
- Leenaars, Marlies, & Hendriksen, Coenraad F. M. (2005). Critical Steps in the Production of Polyclonal and Monoclonal Antibodies: Evaluation and Recommendations. *Institute for Laboratory Animal Research (ILAR) Journal*., 46(3), 269–279.
- Leong, Hon S., Robertson, Amy E., Stoletov, Konstantin, Leith, Sean J., ... Lewis, John D. (2014). Invadopodia Are Required for Cancer Cell Extravasation and Are a Therapeutic Target for Metastasis. *CellReports*, 8(5), 1558–1570. <https://doi.org/10.1016/j.celrep.2014.07.050>
- Lespagnol, A., Duflaut, D., Beekman, C., Blanc, L., ... Telerman, A. (2008). Exosome secretion , including the DNA damage-induced p53-dependent secretory pathway , is severely compromised in TSAP6 / Steap3-null mice. *Cell Death and Differentiation*, 15, 1723–1733. <https://doi.org/10.1038/cdd.2008.104>
- Li, Ping, Jiang, Ning, Nagarajan, Shanmugam, Wohlhueter, Robert, ... Zhu, Cheng. (2007). Affinity and Kinetic Analysis of Fc Receptor IIIa ( CD16a ) Binding to IgG Ligands \*. *The Journal of Biological Chemistry*, 282(9), 6210–6221. <https://doi.org/10.1074/jbc.M609064200>
- Li, Tiezheng, Dilillo, David J., Bournazos, Stylianos, Giddens, John P., ... Wang, Lai xi. (2017). Modulating IgG effector function by Fc glycan engineering. *Proceedings of the National Academy of Sciences of the United States of America*, 114(13), 3485–3490. <https://doi.org/10.1073/pnas.1702173114>
- Liao-chan, Sindy, Daine-matsuoka, Barbara, Heald, Nathan, Wong, Tiffany, ... Theunissen, Jan willem. (2015). *Quantitative Assessment of Antibody Internalization with Novel Monoclonal Antibodies against Alexa Fluorophores*. 1–15. <https://doi.org/10.1371/journal.pone.0124708>
- Lin, Fan, & Chen, Zongming. (2014). Standardization of diagnostic immunohistochemistry: Literature review and Geisinger experience. *Archives of Pathology and Laboratory Medicine*, 138(12), 1564–1577.
- Linke, Martin, Herzog, Volker, & Brix, Klaudia. (2002). Trafficking of lysosomal cathepsin B – green fluorescent protein to the surface of thyroid epithelial cells involves the endosomal / lysosomal compartment. *Journal of Cell Science*, 115, 4877–4889. <https://doi.org/10.1242/jcs.00184>
- Linke, R., Klein, A., & Seimetz, D. (2010). Clinical development and future directions Catumaxomab. *MAbs*, 2(2), 129–136.
- Liu-Kreyche, Peggy, Shen, Hong, Marino, Anthony M., Iyer, Ramaswamy A., ... Lai,

- Y. (2019). Lysosomal P-gp-MDR1 Confers Drug Resistance of Brentuximab Vedotin and Its Cytotoxic Payload Monomethyl Auristatin E in Tumor Cells. *Frontiers in Pharmacology*, 10(July), 1–9. <https://doi.org/10.3389/fphar.2019.00749>
- Loeb, S., Bjurlin, M., Nicholson, J., Tammela, TL, ... Etzioni, R. (2015). Overdiagnosis and Overtreatment of Prostate Cancer. *European Journal for Urology*, 65(6), 1046–1055. <https://doi.org/10.1016/j.eururo.2013.12.062>. Overdiagnosis
- Loganzo, Frank, Sung, Matthew, & Gerber, Hans peter. (2016). Mechanisms of Resistance to Antibody – Drug Conjugates. *Molecular Cancer Therapeutics*, 15(12), 2825–2835. <https://doi.org/10.1158/1535-7163.MCT-16-0408>
- Lohmer, Lauren L., Kelley, Laura C., Hagedorn, Elliott J., & Sherwood, David R. (2014). Invadopodia and basement membrane invasion in vivo. *Cell Adhesion & Migration*, 8(3), 246–255.
- Lopes dos Santos, M., Quintilio, W., Manieri, TM, Tsuruta, LR, & Moro, AM. (2018). Advances and challenges in therapeutic monoclonal antibody drug development. *Brazilian Journal of Pharmaceutical Sciences*, 54.
- Lyon, RP, Bovee, TD, Doronina, SO, Burke, PJ, ... Senter, PD. (2015). Reducing hydrophobicity of homogeneous antibody-drug conjugates improves pharmacokinetics and therapeutic index. *Nature Biotechnology*, 33(7), 733–735.
- Maimaiti, Yusufu, Tan, J., Liu, Zeming, Guo, Yawen, ... Huang, T. (2017). Overexpression of cofilin correlates with poor survival in breast cancer : A tissue microarray analysis. *Oncology Letters*, 14, 2288–2294. <https://doi.org/10.3892/ol.2017.6413>
- Malandrino, Andrea, Kamm, Roger D., & Moeendarbary, Emad. (2018). In Vitro Modeling of Mechanics in Cancer Metastasis. *ACS Biomaterials Science and Engineering*, 4(2), 294–301.
- Mason, M., & Moffat, L. (2010). *Prostate Cancer - The Facts* (Second Edi).
- Mazzola, CR, & Mulhall, JP. (2012). Impact of androgen deprivation therapy on sexual function. *Asian Journal of Andrology*, 14(2), 198–203. <https://doi.org/10.1038/aja.2011.106>
- Miller, M. A. (2014). *When Tissue Antigens and Antibodies Get along : Revisiting the Technical Aspects of Immunohistochemistry — The Red , Brown , and Blue Technique*. 51(1), 42–87. <https://doi.org/10.1177/0300985813505879>
- Mittal, D., Gubin, M. M., Schreiber, R. D., & Smyth, M. J. (2015). New insights into cancer immunoediting and its three component phases - elimination, equilibrium and escape. *Current Opinion in Immunology*, 27(April), 16–25.
- Moreaux, Jerome, Kassambara, Alboukadel, Hose, Dirk, & Klein, Bernard. (2012). STEAP1 is overexpressed in cancers: A promising therapeutic target. *Biochemical and Biophysical Research Communications*, 429, 148–155. <https://doi.org/10.1016/j.bbrc.2012.10.123>
- Mottet, N., Van Den Bergh, RCN, Cornford, P., De Santis, M., ... Willemse, PM. (2018). *EAU - ESTRO - ESUR - SIOG Guidelines on Prostate Cancer*.
- MSD. (2019). *Keytruda (Pembrolizumab) for Injection, for Intravenous Use*.
- Murphy, Danielle A., & Courtneidge, Sara A. (2012). *The “ins” and “outs” of*

- podosomes and invadopodia: characteristics, formation and function*. *12*(7), 413–426. <https://doi.org/10.1038/nrm3141>.The
- Mutschler, E., Geissler, G., Kroemer, HK, Menzel, S., & Ruth, P. (2012). *Arzneimittelwirkungen* (10th ed.).
- Napotnik, Tina Batista, & Miklav, Damijan. (2018). Bioelectrochemistry In vitro electroporation detection methods – An overview. *Bioelectrochemistry*, *120*(August), 166–182. <https://doi.org/10.1016/j.bioelechem.2017.12.005>
- Nasiri, Hadi, Valedkarimi, Zahra, Aghebati-Maleki, Leili, & Majidi, Jafar. (2018). Antibody-drug conjugates: Promising and efficient tools for targeted cancer therapy. *Journal of Cellular Physiology*, *233*(9), 6441–6457.
- Nath, Nidhi, Godat, Becky, Zimprich, Chad, Dwight, Stephen J., ... Urh, Marjeta. (2016). Homogeneous plate based antibody internalization assay using pH sensor fluorescent dye. *431*, 11–21. <https://doi.org/10.1016/j.jim.2016.02.001>
- Naveed, Muhammad, Tehreem, Sana, Mubeen, Shamsa, Nadeem, Fareeha, & Zafar, Fatima. (2016). In-silico analysis of non-synonymous-SNPs of STEAP2: To provoke the progression of prostate cancer. *Open Life Science*, *11*, 402–416. <https://doi.org/10.1515/biol-2016-0054>
- NCCN. (2018). *Prostate Cancer*.
- Nejadmoghaddam, MR, Minai-Tehrani, A., & Ghahremanzadeh, R. (2019). Antibody-Drug Conjugates: Possibilities and Challenges. *Avicenna Journal of Medical Biotechnology*, *11*(1).
- Nelson, A. L. (2010). Antibody fragments. *MAb*, *1*(February), 77–83.
- Neuzillet, Cindy, Tijeras-raballand, Annemiläi, Cohen, Romain, Cros, Jérôme, ... Gramont, Armand De. (2015). Targeting the TGF $\beta$  pathway for cancer therapy. *Pharmacology & Therapeutics*, *147*, 22–31. <https://doi.org/10.1016/j.pharmthera.2014.11.001>
- Nguyen, Daniel P., Li, Jinyi, Yadav, Shalini S., & Tewari, Ashutosh K. (2014). Recent insights into NF- $\kappa$ B signalling pathways and the link between inflammation and prostate cancer. *BJU International*, *114*(2), 168–176.
- NICE. (2019). *Prostate cancer: diagnosis and management*.
- Nicholson, KM, Bibby, MC, & Phillips, RM. (1997). Influence of drug exposure parameters on the activity of paclitaxel in multicellular spheroids. *European Journal of Cancer Part A*, *33*(8), 1291–1298.
- NIH, National Cancer Institute. (2016). SEER Prostate Cancer Statistics 2016.
- Nunes, Ana S., Correia, Ilídio J., & Costa, Elisabete C. (2019). 3D tumor spheroids as in vitro models to mimic in vivo human solid tumors resistance to therapeutic drugs. (May 2018), 206–226. <https://doi.org/10.1002/bit.26845>
- Ohashi, Kazumasa. (2015). Roles of cofilin in development and its mechanisms of regulation. *Development, Growth and Differentiation*., *57*, 275–290. <https://doi.org/10.1111/dgd.12213>
- Ohgami, R., Campagna, De, Greer, E., Antiochos, B., ... Fleming, M. (2005). Identification of a ferrireductase required for efficient transferrin-dependent iron uptake in erythroid cells. *Nature Genetics*, *37*(11), 1264–1269.
- Ohgami, Robert S., Campagna, Dean R., McDonald, Alice, & Fleming, Mark D.

- (2006). The Steap proteins are metalloredoxases. *Blood*, *108*(4), 1388–1394.
- Olivier Jr., KJ, & Hurvitz, SA. (2016). *Antibody-Drug Conjugates: Fundamentals, Drug Development, and Clinical Outcomes to Target Cancer* (1st Editio; KJ Olivier Jr. & SA Hurvitz, Eds.). <https://doi.org/10.1002/9781119060727>
- PacificImmunology. (2019). Selecting a Peptide Sequence.
- Page, Mark, & Thorpe, Robin. (2009). *Screening Hybridoma Culture Supernatants Using ELISA*. 1947–1948.
- Palmer, Trenis D., Ashby, William J., Lewis, John D., & Zijlstra, Andries. (2011). Targeting tumor cell motility to prevent metastasis ☆. *Advanced Drug Delivery Reviews*, *63*(8), 568–581. <https://doi.org/10.1016/j.addr.2011.04.008>
- Pandey, Shivanand. (2010). Hybridoma technology for production of monoclonal antibodies. *International Journal of Pharmaceutical Sciences Review and Research*, *1*(2), 88–94.
- Panowski, Siler, Bhakta, Sunil, Raab, Helga, Polakis, Paul, & Junutula, Jagath R. (2014). *Site-specific antibody drug conjugates for cancer therapy*. *6*(1), 34–45.
- Pardoll, D. M. (2016). The blockade of immune checkpoints in cancer immunotherapy. *Nature Review Cancer*, *12*(4), 252–264.
- Parren, Paul W. H. I., Carter, Paul J., & Plückthun, Andreas. (2017). Changes to International Nonproprietary Names for antibody therapeutics 2017 and beyond : of mice , men and more. *MABs*, *9*(6), 898–906.
- Passer, BJ, Nancy-Portebois, Vanessa, Amzallag, Nathalie, Prieur, Sylvie, ... Telerman, Adam. (2003). The p53-inducible TSAP6 gene product regulates apoptosis and the cell cycle and interacts with Nix and the Myt1 kinase. *PNAS*, *100*(5), 1–6.
- Pedrazzoli, Filippo, Chrysantzas, Iraklis, Dezzani, Luca, Rosti, Vittorio, ... Sitar, Giammaria. (2011). Cell fusion in tumor progression : the isolation of cell fusion products by physical methods. *Cancer Cell International*, *11*(1), 32. <https://doi.org/10.1186/1475-2867-11-32>
- Penson, DF, Redfern, CH, Ferrari, AC, Dreicer, Robert, ... Schellhammer, Paul F. (2012). Sipuleucel-T Immunotherapy for Castration-Resistant Prostate Cancer. *New England Journal of Medicine*, *363*(5), 411–422.
- Peters, Christina, & Brown, Stuart. (2015). Antibody – drug conjugates as novel anti-cancer chemotherapeutics. *Bioscience Reports*, *35*, 1–20. <https://doi.org/10.1042/BSR20150089>
- Petrylak, Daniel P., Kantoff, Philip, Vogelzang, Nicholas J., Mega, Anthony, ... Agarwal, Manish. (2019). Phase 1 study of PSMA ADC , an antibody-drug conjugate targeting prostate-specific membrane antigen , in chemotherapy-refractory prostate cancer. *The Prostate*, *79*(November 2018), 604–613. <https://doi.org/10.1002/pros.23765>
- Phung, Yen T., Barbone, Dario, Broaddus, V. Courtney, & Ho, Mitchell. (2011). *Rapid Generation of In Vitro Multicellular Spheroids for the Study of Monoclonal Antibody Therapy*.
- Pisitkun, Trairak, Dummer, Patrick, Services, Human, Somparn, Poorichaya, & Hirankarn, Nattiya. (2014). Integrated Design of Antibodies for Systems Biology

- Using AbDesigner. *Journal of Proteomics & Bioinformatics*, 7(4), 88–94. <https://doi.org/10.4172/jpb.1000307>
- Poget, Sebastien, Wang, Da Neng, Tsai, Ah ILm, & Zhou, Ming. (2016). Six-Transmembrane Epithelial Antigen of Prostate 1 (STEAP1) Has a Single b Heme and Is Capable of Reducing Metal Ion Complexes and Oxygen. *Biochemis*, 55, 6673–6684. <https://doi.org/10.1021/acs.biochem.6b00610>
- Pohanka, M., Vobornikova, I., & Fusek, J. (2016). Freund ´ s complete adjuvant effect on BALB / c mice: an insight into in fl ammation and oxidative stress after immunity challenge. *Experimental Study*, 117(1), 268–271. <https://doi.org/10.4149/BLL>
- Popova, NV, Deyev, IE, & Petrenko, AG. (2013). Clathrin-Mediated Endocytosis and Adaptor Proteins. *Acta Naturae*, 5(18), 62–73.
- Porkka, KP, Helenius, MA, & Visakorpi, T. (2002). Cloning and Characterization of a Novel Six-Transmembrane Protein STEAP2 , Expressed in Normal and Malignant Prostate. *Laboratory Investigation*, 82(11), 1573–1582. <https://doi.org/10.1097/01.LAB.0000038554.26102.C6>
- Potapova, T., Zhu, J., & Li, R. (2013). Aneuploidy and chromosomal instability: a vicious cycle driving cellular evolution and cancer genome chaos. *Cancer Metastasis Review*, 32(0), 1–20. <https://doi.org/10.1007/s10555-013-9436-6>.Aneuploidy
- Pozarowski, Piotr, & Darzynkiewicz, Zbigniew. (2001). Analysis of Cell Cycle by Flow Cytometry. In *Methods in Molecular Biology* (Vol. 281, pp. 301–311).
- Pritchard, Catrin A., Hayes, Louise, Wojnowski, Leszek, Zimmer, Andreas, ... Norman, Jim C. (2004). B-Raf Acts via the ROCKII / LIMK / Cofilin Pathway To Maintain Actin Stress Fibers in Fibroblasts. *Molecular and Cellular Biology*, 24(13), 5937–5952. <https://doi.org/10.1128/MCB.24.13.5937>
- Qian, Cheng, Huang, Haibo, Chen, Ligu, Li, Xiangpeng, ... Chen, Tao. (2014). Dielectrophoresis for Bioparticle Manipulation. *International Journal of Molecular Sciences*, 15(October), 18281–18309. <https://doi.org/10.3390/ijms151018281>
- Qin, DN, Kou, CZ, Ni, YH, Zhang, CM, ... Zhu, C. (2010). Monoclonal antibody to the six-transmembrane epithelial antigen of prostate 4 promotes apoptosis and inhibits proliferation and glucose uptake in human adipocytes. *International Journal of Molecular Medicine*, 26, 803–811. <https://doi.org/10.3892/ijmm>
- Ravichandran, Madhwesh C., Fink, Sarah, Clarke, Matthew N., Hofer, Franziska Christina, & Campbell, Christopher S. (2018). Genetic interactions between specific chromosome copy number alterations dictate complex aneuploidy patterns. *Genes & Development*, 32, 1–14. <https://doi.org/10.1101/gad.319400.118>.
- Rems, Lea, Usaj, Marko, Kanduser, Masa, Rebersek, Matej, ... Pucihar, Gorazd. (2013). Cell electrofusion using nanosecond electric pulses. *Scientific Reports*, 3(3382), 1–10. <https://doi.org/10.1038/srep03382>
- Rigo, Antonella, & Vinante, Fabrizio. (2017). *Flow Cytometry Analysis of Receptor Internalization / Shedding*. 298(June 2016), 291–298.

<https://doi.org/10.1002/cyto.b.21392>

- Riss, Terry L., Moravec, Richard A., Niles, Andrew L., Benink, Hélène A., & Worzella, Tracy J. (2016). Cell Viability Assays. *Assay Guidance Manual*, 1–31.
- Ritchie, Michael, Tchistiakova, Lioudmila, & Scott, Nathan. (2013). *Implications of receptor-mediated endocytosis and intracellular trafficking dynamics in the development of antibody drug conjugates*. (February), 13–21.
- Roche, Joëlle. (2018). The Epithelial-to-Mesenchymal Transition in Cancer. *Cancers*, 10(52), 10–13. <https://doi.org/10.3390/cancers10020052>
- Roskoski Jr., Robert. (2015). Src protein-tyrosine kinase structure, mechanism, and small molecule inhibitors. *Pharmacological Research*, 94, 9–25. <https://doi.org/10.1016/j.phrs.2015.01.003>
- Ryman, J. T., & Meibohm, B. (2017). Pharmacokinetics of Monoclonal Antibodies. *CPT Pharmacometrics Syst. Pharmacol.*, 6(9), 576–588.
- Sanchez-Pulido, Luis, Rojas, AM, Valencia, Alfonso, Martinez-a, Carlos, & Andrade, MA. (2004). ACRATA: a novel electron transfer domain associated to apoptosis and cancer. *BMC Bioinformatics*, 4(98), 1–6. <https://doi.org/10.1186/1471-2407-4-98>
- Sane, Ramola, Agarwal, Sagar, & Elmquist, William F. (2012). Brain Distribution and Bioavailability of Elacridar after Different Routes of Administration in the Mouse ABSTRACT: *American Society for Pharmacology and Experimental Therapeutics*, 40(8), 1612–1619.
- Sant, Shilpa, & Johnston, Paul A. (2017). The production of 3D tumor spheroids for cancer drug discovery. *Drug Discovery Today: Technologies*, 23, 27–36. <https://doi.org/10.1016/j.ddtec.2017.03.002>
- Sauter, Guido, Simon, Ronald, Hillan, Kenneth, & Francisco, South San. (2003). *TISSUE MICROARRAYS IN DRUG DISCOVERY*. 2(December), 962–973. <https://doi.org/10.1038/nrd1254>
- Scarl, RT, Lawrence, CM, Gordon, HM, & Nunemaker, CS. (2018). STEAP4: its emerging role in metabolism and homeostasis of cellular iron and copper. *Journal of Endocrinology*, 234(3), 1–21. <https://doi.org/10.1530/JOE-16-0594>.STEAP4
- Schellhammer, PPF, Chodak, G., Whitmore, JB, Sims, Robert, ... Kantoff, PW. (2013). Lower Baseline Prostate-specific Antigen Is Associated With a Greater Overall Survival Benefit From Sipuleucel-T in the Immunotherapy for Prostate Adenocarcinoma Treatment (IMPACT) Trial. *Urology*, 81(6), 1297–1302. <https://doi.org/10.1016/j.urology.2013.01.061>
- Schneider, Sonja. (2017). *Analysis of Cysteine-Linked Antibody Drug Conjugates Using Hydrophobic Interaction Chromatography on the*.
- Schork, N. J. (2015). Time for one-person trials. *Nature*, 52(7549), 609–611.
- Schreiber, RD, Old, LJ, & Smyth, MJ. (2011). Cancer immunoediting: integrating immunity's roles in cancer suppression and promotion. *Science*, 331(6024), 1565–1570.
- Schröder, Fritz H., Hugosson, Jonas, Roobol, Monique J., Tammela, Teuvo L. J., ... Auvinen, Anssi. (2009). Screening and Prostate-Cancer Mortality in a

- Randomized European Study — NEJM. *New England Journal of Medicine*, 360(13), 1320–1328.
- Schroeder, Harry W. Jr., & Cavacini, Lisa. (2010). Structure and Function of Immunoglobulins. *Allergy Clinical Immunology*, 125(202), 41–52. <https://doi.org/10.1016/j.jaci.2009.09.046>.Structure
- Schulman, CC, Irani, Jacques, Morote, Juan, Schalken, JA, ... Heidenreich, Axel. (2010). Testosterone Measurement in Patients with Prostate Cancer. *European Urology*, 58(1), 65–74. <https://doi.org/10.1016/j.eururo.2010.04.001>
- Schweizer, Michael T., & Drake, Charles G. (2014). *Immunotherapy for prostate cancer: recent developments and future challenges*. 641–655. <https://doi.org/10.1007/s10555-013-9479-8>
- Senter, Peter D., & Sievers, Eric L. (2012). The discovery and development of brentuximab vedotin for use in relapsed Hodgkin lymphoma and systemic anaplastic large cell lymphoma. *Nature Biotechnology*, 30(7), 631–637. <https://doi.org/10.1038/nbt.2289>
- Sewell, F., Chapman, K., Couch, J., Dempster, M., ... Van der Laan, W. (2017). Challenges and opportunities for the future of monoclonal antibody development : Improving safety assessment and reducing animal use. *MAbs*, 9(5), 742–755.
- Shaikhibrahim, Zaki, Lindstrot, Andreas, Ellinger, Jörg, Rogenhofer, Sebastian, ... Wernert, Nicolas. (2012). The peripheral zone of the prostate is more prone to tumor development than the transitional zone: Is the ETS family the key? *Molecular Medicine Reports*, 5(15), 313–316. <https://doi.org/10.3892/mmr.2011.647>
- Shih, Heather H. (2012). Discovery Process for Antibody-Based Therapeutics Translational Considerations. In Mohammed A. Tabrizi, Gadi G. Bornstein, & Scott L. Klakamp (Eds.), *Development of Antibody-Based Therapeutics Translational Considerations*. (pp. 9–32). <https://doi.org/10.1007/978-1-4419-5955-3>
- Shishkin, Sergey, Eremina, Lidia, Pashintseva, Natalya, Kovalev, Leonid, & Kovaleva, Marina. (2016). Cofilin-1 and Other ADF / Cofilin Superfamily Members in Human Malignant Cells. *International Journal of Molecular Sciences*, 18(10), 1–27.
- Siew, Adeline, & Garofalo, Albert. (2015). *Building Safe and Effective Antibody-Drug Conjugates*.
- Sikkeland, J., Sheng, X., Jin, Y., & Saatcioglu, F. (2016). Molecular and Cellular Endocrinology STAMPing at the crossroads of normal physiology and disease states. *Molecular and Cellular Endocrinology*, 425, 26–36.
- Sikkeland, Jørgen, Sheng, Xia, Jin, Yang, & Saatcioglu, Fahri. (2016). STAMPing at the crossroads of normal physiology and disease states. *Molecular and Cellular Endocrinology*, 425, 26–36.
- Sims, Robert B. (2012). Development of sipuleucel-T: Autologous cellular immunotherapy for the treatment of metastatic castrate resistant prostate cancer. *Vaccine*, 30(29), 4394–4397. Retrieved from

- Sipos, Eva, Dobos, Nikoletta, Rozsa, David, Fodor, Klara, ... Halmos, Gabor. (2018). Characterization of luteinizing hormone-releasing hormone receptor type I ( LH-RH-I ) as a potential molecular target in OCM-1 and OCM-3 human uveal melanoma cell lines. *OncoTargets and Therapy*, 11, 933–941.
- Slovin, S. F., Higano, C., Hamid, O., Tejwani, S., ... Beer, T. M. (2013). Ipilimumab alone or in combination with radiotherapy in metastatic castration-resistant prostate cancer: results from an open-label, multicenter phase I / II study. *Annals of Medicine and Surgery*, 24(7), 1813–1821. <https://doi.org/10.1093/annonc/mdt107>
- Smith-Garvin, J. E., Koretzky, G. A., & Jordan, M. S. (2009). T-Cell Activation. *Annual Review Immunology*, 27, 591–619.
- Sobin, Leslie, Gospodarowicz, Mary, & Wittekind, Christian. (2009). *TNM Classification of Malignant Tumours* (Seventh Ed).
- Soto-Herederó, Gonzalo, Baixauli, Francesc, & Mittelbrunn, María. (2017). Interorganelle Communication between Mitochondria and the Endolysosomal System. *Frontiers in Cell and Developmental Biology*, 5(November), 1–8. <https://doi.org/10.3389/fcell.2017.00095>
- Spencer, K. R., Wang, J., Silk, A. W., Ganesan, S., ... Mehnert, J. M. (2016). Biomarkers for Immunotherapy: Current Developments and Challenges. *American Society of Clinical Oncology*, 35, e493-503.
- Spiess, Christoph, Zhai, Qianting, & Carter, Paul J. (2015). Alternative molecular formats and therapeutic applications for bispecific antibodies &. *Molecular Immunology*, 67, 95–106.
- Staudacher, Alexander H., & Brown, Michael P. (2017). Antibody drug conjugates and bystander killing: is antigen-dependent internalisation required? *British Journal of Cancer*, 117(12), 1736–1742. <https://doi.org/10.1038/bjc.2017.367>
- Stehling, O., & Lill, R. (2013). The Role of Mitochondria in Cellular Iron–Sulfur Protein Biogenesis: Mechanisms, Connected Processes, and Diseases. *Cold Spring Harbor Perspectives Biology*, 5, 1–17.
- Steinhilber, D., Schubert-Zsilavec, M., & Roth, HJ. (2012). *Medizinische Chemie* (2th ed.).
- Stills, Harold F. (2012). Polyclonal Antibody Production. *The Laboratory Rabbit, Guinea Pig, Hamster, and Other Rodents*, 259–274. Retrieved from
- Stoddart, Martin J. (2011). *Mammalian Cell Viability* (Martin Stoddart, Ed.).
- Stoletov, K., Kato, H., Zardoujian, E., Kelber, J., ... Klemke, R. (2010). Visualizing extravasation dynamics of metastatic tumor cells. *Journal of Cell Science*, 123(13), 2332–2341. Retrieved from
- Storchova, Zuzana. (2018). Evolution of aneuploidy: overcoming the original CIN. *Genes & Development*, 32, 1459–1460. <https://doi.org/10.1038/nature10795>
- Storchova, Zuzana, & Kuffer, Christian. (2008). The consequences of tetraploidy and aneuploidy. *Journal of Cell Biology*, 121(23), 3859–3866. <https://doi.org/10.1242/jcs.039537>
- Strebhardt, Klaus, & Ullrich, Axel. (2008). *Paul Ehrlich 's magic bullet concept: 100 years of progress*. 8(june).

- Sun, B. B., Maranville, J. C., Peters, J. E., Stacey, D., ... Butterworth, A. S. (2018). Genomic atlas of the human plasma proteome. *Nature*, *558*(73), 1–24. <https://doi.org/10.1038/s41586-018-0175-2>
- Swaminathan, Ashwin, Lucas, Robyn M., Dear, Keith, & McMichael, Anthony J. (2014). Keyhole limpet haemocyanin – a model antigen for human immunotoxicological studies. *British Journal of Clinical Pharmacology*, *78*(5), 1135–1142. <https://doi.org/10.1111/bcp.12422>
- Tanaka, Yoko, Matsumoto, Isao, Iwanami, Keiichi, Inoue, Asuka, ... Umeda, Naoto. (2012). Six-transmembrane epithelial antigen of prostate4 (STEAP4) is a tumor necrosis factor alpha-induced protein that regulates IL-6, IL-8, and cell proliferation in synovium from patients with rheumatoid arthritis. *Modern Rheumatology*, *22*, 128–136. <https://doi.org/10.1007/s10165-011-0475-y>
- Taylor, Sean C., Berkelman, Thomas, Yadav, Geetha, & Hammond, Matt. (2013). A defined methodology for reliable quantification of western blot data. *Molecular Biotechnology*, *55*(3), 217–226.
- Teixeira Leite, TE, Fernandes da Silva, JL, Capelletti, E., Kalil Haddad, CM, & Nader Marta, G. (2019). Prostate brachytherapy with iodine-125 seeds: analysis of a single institutional cohort. *International Brazilian Journal for Urology*, *45*(2), 288–298. <https://doi.org/10.1590/S1677-5538.IBJU.2018.0142>
- Tewari, A. K., Whelan, P., & Graham, J. (2014). *Prostate Cancer Diagnosis and Clinical Management* (First edit).
- Tolkach, Yuri, Joniau, Steven, & Van Poppel, Hendrik. (2013). Luteinizing hormone-releasing hormone (LHRH) receptor agonists vs antagonists: a matter of the receptors? *British Journal of Urology*, *111*, 1021–1030. <https://doi.org/10.1111/j.1464-410X.2013.11796.x>
- Tomita, M., & Tsumoto, K. (2011). Hybridoma technologies for antibody production Review. *Future Medicine*, *3*(3), 371–380.
- Tomita, Masahiro, & Tsumoto, Kanta. (2011). *Hybridoma technologies for antibody production Review*. *3*, 371–380.
- Tonegawa, S., Steinberg, C., & Bernardin, A. (1974). *Evidence for Somatic Generation of Antibody Diversity*. *71*(10), 4027–4031.
- Trindade, BM, Passos, T., & De Campos, R. (2012). Comparative dosimetry of prostate brachytherapy with I-125 and Pd-103 seeds via SISCODES / MCNP \*. *Radiology Brasil*, *45*(3), 267–272.
- Troiana, Nancy W., Ciovacco, Wendy A., & Kacena, Melissa A. (2010). The Effects of Fixation and Dehydration on the Histological Quality of Undecalcified Murine Bone Specimens Embedded in Methymethacrylate. *Journal of Histotechnology*, *32*(1), 27–31.
- Trontelj, Katja, Ušaj, Marko, & Miklavčič, Damijan. (2010). Cell Electrofusion Visualized with Fluorescence Microscopy. *Journal of Vi*, (41), 1–3. <https://doi.org/10.3791/1991>
- Vainshtein, I., Roskos, L. K., Cheng, J., Sleeman, M. A., ... Liang, M. (2015). Quantitative Measurement of the Target-Mediated Internalization Kinetics of Biopharmaceuticals. *Pharmaceutical Research*, *32*(1), 286–299.

- Valent, P., Groner, B., Schumacher, U., Superti-Furgo, G., ... Sörgel, F. (2016). Paul Ehrlich ( 1854 – 1915 ) and His Contributions to the Foundation and Birth of Translational Medicine. *Journal of Innate Immunity*, 8(February), 111–120. <https://doi.org/10.1159/000443526>
- Van der Poel, Cees E., Spaapen, Robbert M., Van de Winkel, Jan G. J., & Leusen, Jeanette H. W. (2011). Functional Characteristics of the High Affinity IgG Receptor, FcγRI. *The Journal of Immunology*, 186(June), 2699–2704. <https://doi.org/10.4049/jimmunol.1003526>
- Van Eyk, Jennifer E., & Stastna, Miroslava. (2012). Analysis of protein isoforms: can we do it better? *Proteomics*, 12(0), 2937–2948. <https://doi.org/10.1002/pmic.201200161>.Analysis
- Vela, Driton. (2018). Iron Metabolism in Prostate Cancer ; From Basic Science to New Therapeutic Strategies. *Frontiers in Oncology*, 8(November), 1–11. <https://doi.org/10.3389/fonc.2018.00547>
- Velonas, V. M., Woo, H. H., Remedios, C. G., & Assinder, S. J. (2013). Current Status of Biomarkers for Prostate Cancer. *International Journal of Molecular Sciences*, 14(6), 11034–11060.
- Venkatesan, Priya. (2016). Trastuzumab emtansine for HER2-positive breast cancer. *The Lancet. Oncology*, 17(12), e528.
- Verma, Sunil, Miles, David, Gianni, Luca, Krop, Ian E., ... Blackwell, Kim. (2012). Trastuzumab emtansine for HER2-positive advanced breast cancer. *The New England Journal of Medicine*, 367(19), 1783–1791.
- Von Rozycki, T., Yen, MR, Lende, EE, & Milton, HS. (2004). The YedZ Family: Possible Heme Binding Proteins That Can Be Fused to Transporters and Electron Carriers. *Journal of Molecular Microbiology*, 0116(8), 129–140. <https://doi.org/10.1159/000085786>
- Wang, Ling, Jin, Yang, Arnoldussen, Yke Jildouw, Jonson, Ida, ... Mælandsmo, Gunhild M. (2010). STAMP1 Is Both a Proliferative and an Antiapoptotic Factor in Prostate Cancer. *Cancer Research*, 70(14), 5818–5829. <https://doi.org/10.1158/0008-5472.CAN-09-4697>
- Wang, Xinning, Ma, Dangshe, Olson, William C., & Heston, Warren D. W. (2011). In Vitro and In Vivo Responses of Advanced Prostate Tumors to PSMA ADC , an Auristatin-Conjugated Antibody to Prostate-Specific Membrane Antigen. *Molecular Cancer Therapeutics*, 10(September), 13–15. <https://doi.org/10.1158/1535-7163.MCT-11-0191>
- Wang, Y., Yu, L., Ding, J., & Chen, Y. (2019). Iron Metabolism in Cancer. *International Journal of Molecular Sciences*, 20(95), 1–22.
- Webert, Holger, Freibert, Sven andreas, Gallo, Angelo, Heidenreich, Torsten, ... Mu, Ulrich. (2014). Functional reconstitution of mitochondrial Fe/S cluster synthesis on Isu1 reveals the involvement of ferredoxin. *Nature Communications*, 5(May), 1–12. <https://doi.org/10.1038/ncomms6013>
- Weidle, Ulrich H., Kontermann, Roland E., & Brinkmann, Ulrich. (2014). Tumor-Antigen-Binding Bispecific Antibodies for Cancer Treatment. *Seminars in Oncology*, 41(5), 653–660. <https://doi.org/10.1053/j.seminoncol.2014.08.004>

- Weiner, George J. (2015). Building better monoclonal antibody-based therapeutics. *Nature Publishing Group*, 15(6), 361–370. <https://doi.org/10.1038/nrc3930>
- Weiswald, Louis Bastien, Guinebretière, Jean Marc, Richon, Sophie, Bellet, Dominique, ... Dangles-Marie, Virginie. (2010). In situ protein expression in tumour spheres: Development of an immunostaining protocol for confocal microscopy. *BMC Cancer*, 10, 1–11.
- Wellen, KE, Fucho, R., Gregor, MF, Furuhashi, M., ... Hotamisligil, GS. (2008). Coordinated Regulation of Nutrient and Inflammatory Responses by STAMP2 is Essential for Metabolic Homeostasis. *Cell*, 129(3), 537–548.
- Weller, Michael G. (2018). Ten Basic Rules of Antibody Validation. *Analytical Chemistry Insights*, 13, 1–5. <https://doi.org/10.1177/1177390118757462>
- Wenzel, Elizabeth S., & Singh, Amareshwar T. K. (2018). Cell-cycle Checkpoints and Aneuploidy on the Path to Cancer. *In Vivo*, 32, 1–5. <https://doi.org/10.21873/invivo.11197>
- Westerwoudt, Regine. (1987). *Technical aspects of the production and growth of hybridomas*.
- Westover, David, & Li, Fengzhi. (2015). New trends for overcoming ABCG2 / BCRP-mediated resistance to cancer therapies. *Journal of Experimental & Clinical Cancer Research*, 34(159), 1–9. <https://doi.org/10.1186/s13046-015-0275-x>
- Whiteland, Helen, Claire, M., Spencer-Harty, S., Kynaston, H., ... Doak, S. H. (2014). A role for STEAP2 in prostate cancer progression. *Clinical & Experimental Metastasis*, 31, 909–920. <https://doi.org/10.1007/s10585-014-9679-9>
- WHO. (2019). Prostate cancer.
- Wimmers, Florian, Haas, Nienke De, Scholzen, Anja, Schreibelt, Gerty, & Simonetti, Elles. (2017). Monitoring of dynamic changes in Keyhole Limpet Hemocyanin (KLH) -specific B cells in KLH- vaccinated cancer patients. *Scientific Reports*, 7(March), 1–9. <https://doi.org/10.1038/srep43486>
- Wu, Anna M., & Senter, Peter D. (2005). Arming antibodies: prospects and challenges for immunoconjugates. *Nature Biotechnology*, 23(9), 1137–1146. Retrieved from
- Xie, T., Dong, B., Yan, Y., Hu, G., & Xu, Y. (2016). Association between MMP-2 expression and prostate cancer : A meta-analysis. *Biomedical Reports*, 4(2), 241–245.
- Xie, Yingqiu, Xu, Kexin, Linn, Douglas E., Yang, Xi, ... Qiu, Yun. (2008). The 44-kDa Pim-1 Kinase Phosphorylates BCRP / ABCG2 and Thereby Promotes Its Multimerization and Drug-resistant Activity in Human Prostate Cancer Cells \*. *Journal of Biological Chemistry*, 283(6), 3349–3356. <https://doi.org/10.1074/jbc.M707773200>
- Xu, H., & Ren, D. (2015). Lysosomal Physiology. *Annual Review Physiology*, 77(3), 57–80. <https://doi.org/10.1146/annurev-physiol-021014-071649>. Lysosomal
- Xu, Y., Chen, B., Zheng, S., Wen, Y., ... Liu, C. (2016). IgG silencing induces apoptosis and suppresses proliferation, migration and invasion in LNCaP prostate cancer cells. *Cellular & Molecular Biology Letters*, 21(27), 1–10.
- Xue, Xiangt, Bredell, BX, Anderson, ER, Martin, Angelical, ... Nagao-Kitamoto, Hiroko. (2017). Quantitative proteomics identifies STEAP4 as a critical regulator

- of mitochondrial dysfunction linking inflammation and colon cancer. *PNAS*, 9608–9617. <https://doi.org/10.1073/pnas.1712946114>
- Yamamoto, Takashi, Tamura, Yasuaki, & Kobayashi, Jun ichi. (2013). Six-transmembrane epithelial antigen of the prostate-1 plays a role for in vivo tumor growth via intercellular communication. *ScienceDirect*, 319, 2617–2626. <https://doi.org/10.1016/j.yexcr.2013.07.025>
- Yamashita, Makiko, Kitano, Shigehisa, Aikawa, Hiroaki, & Kuchiba, Aya. (2016). A novel method for evaluating antibody-dependent cell-mediated cytotoxicity by flowcytometry using cryopreserved human peripheral blood mononuclear cells. *Nature Publishing Group*, 6(January), 1–10. <https://doi.org/10.1038/srep19772>
- Yang, H., & Kim, D. S. (2015). Peptide Immunotherapy in Vaccine Development : From Epitope to Adjuvant. In *Advances in Protein Chemistry and Structural Biology* (Vol. 99, pp. 1–14).
- Yao, Chengcai, Jiang, Jie, Tu, Yuanrong, Ye, Shefang, ... Zhang, Yi. (2014).  $\beta$  - elemene reverses the drug resistance of A549 / DDP lung cancer cells by activating intracellular redox system , decreasing mitochondrial membrane potential and P-glycoprotein expression , and inducing apoptosis. 5, 304–312. <https://doi.org/10.1111/1759-7714.12093>
- Yao, Ming hua, Zou, Li ling, Wu, Rong, Guo, Le hang, ... Wang, Shuai. (2014). Transperineal Ultrasound-Guided 12-Core Prostate Biopsy : An Extended Approach to Diagnose Transition Zone Prostate Tumors. *PLoS ONE*, 9(2), 1–5. <https://doi.org/10.1371/journal.pone.0089171>
- Yi, Renliang, Chen, Baoxin, Duan, Peng, Zheng, Chanjiao, ... Zhou, Zhiheng. (2016). Sipuleucel-T and Androgen Receptor-Directed Therapy for Castration-Resistant Prostate Cancer: A Meta-Analysis. *Journal of Immunology Research*, 1–10. <https://doi.org/10.1155/2016/4543861>
- Yiangou, Loukia, Grandy, Rodrigo A., Morell, Carola M., Tomaz, Rute A., ... Vallier, Ludovic. (2019). Stem Cell Reports. *Stem Cell Reports*, 12(January), 165–179. <https://doi.org/10.1016/j.stemcr.2018.11.020>
- Yoo, S., Cheong, J., & Kim, H. (2014). STAMPing into Mitochondria. *International Journal of Biological Sciences*, 10(2), 321–326. <https://doi.org/10.7150/ijbs.8456>
- Yu, Xiacong, Mcgraw, Patricia A., House, Frances S., & Jr, James E. Crowe. (2008). An optimized electrofusion-based protocol for generating virus-specific human monoclonal antibodies. *Journal of Immunological Methods*, 336, 142–151. <https://doi.org/10.1016/j.jim.2008.04.008>
- Zanoni, M., Piccinini, F., Arienti, C., Zamagni, A., ... Tessei, A. (2016). 3D tumor spheroid models for in vitro therapeutic screening: A systematic approach to enhance the biological relevance of data obtained. *Scientific Reports*, 6(January), 1–11.
- Zeiler, Marlis, Straube, Werner L., Lundberg, Emma, Uhlen, Mathias, & Mann, Matthias. (2012). A Protein Epitope Signature Tag (PrEST) Library Allows SILAC-based Absolute Quantification and Multiplexed Determination of Protein Copy Numbers in Cell Lines. *Molecular & Cellular Proteomics*, 11(3), O111.009613.

- Zhang, F., Tao, Y., Zhang, Z., Guo, X., ... Wang, F. (2012). Metalloreductase Steap3 coordinates the regulation of iron homeostasis and inflammatory responses. *Iron Metabolism & Its Disorders*, 97(12), 1836–1835.
- Zivny, J., Elson, C. O., Mestecky, J., & Kantele, J. M. (2011). Humoral Immune Response to Keyhole Limpet Haemocyanin , the Protein Carrier in Cancer Vaccines. *Clinical and Developmental Immunology*, 2011, 1–6. <https://doi.org/10.1155/2011/614383>
- Zuber, Simon, Weiß, Susan, Baaske, Dieter, Schöpe, Michael, ... Zwahlen, DR. (2015). Iodine-125 seed brachytherapy for early stage prostate cancer : a single-institution review. *Radiation Oncology*, 10(49), 1–10. <https://doi.org/10.1186/s13014-015-0349-0>

## 8 Appendices

### Appendix 1

NW Score	Identities	Positives	Gaps
490	163/490(33%)	234/490(47%)	151/490(30%)
Query 1	MES-----RK-----		5
Sbjct 1	MES MESISMMSGPKSLSETFLPNGINGIKDARKVTVGVI GSGDFAKSLTIRLIRCGYHVVIGS	RK RK	60
Query 6	-----DITNQEE-----LWKMK-----		17
Sbjct 61	-----D+T+ E+-----LW ++		120
Query 18	-----PRRNLEEDYLHKDT-----GETSMLKRPVLLHLHQTAAHAEFDCPSELQHTQE-----		66
Sbjct 121	-----P N E L D+ + + L + A + C + + Q Q+-----		180
Query 67	-----LFPQWHLPIKIAAIIASLTFLYTLREVIHPLA		99
Sbjct 181	-----LF W P+ +A +A+ FLY+ +R+VIHP A		240
Query 100	TSHQQYFYKIPILVINKVLPVMSITLLALVYLPGVIAAIVQLHNGTKYKFFPHWLDKMWL		159
Sbjct 241	+ Q FYKIPI ++NK LP+V+ITLL+LVYL G++AA QL+ GTKY++FP WL+ W+ RNQSDYFYKIPIEIVNKTLPVAVITLLSLVYLAGLLAAAYQLYYGTYRRFPWLETWLQ		300
Query 160	TRKQFGLLSFFFVAVLHAIYSLSYPMRRSRYRKLNNWAYQQVQNKEDAWIEHDVWRMEIY		219
Sbjct 301	RKQ GLLSFFFA++H YSL PMRRS RY LN AYQQV N E++W E +VWR+E+Y CRKQLGLLSFFFAMVHVAYS LCLPMRRSERYLFLNMAYQQVHANIENSWNEEEVWRIEMY		360
Query 220	VSLGIVGLAILALLAVTSIPSVSDSLTWREFHYIQSKLGI VSLLLGTIHALIFAWNKWID		279
Sbjct 361	+S GI+ L +L+LLAVTSIPSVS++L WREF +IQS LG V+LL+ T H LI+ W + + ISFGIMSLGLLSLLAVTSIPSVSNALNWREFSFIQSTLGYVALLISTFHVLIYGWKRAFE		420
Query 280	IKQFVWYTPPTFMIAVFLPIVVLIFKSI LFLPCLRKKILKIRHWEDVTKINK-----		332
Sbjct 421	+ + +YTPP F++A+ LP +V++ K ILFLPC+ +K+ +I+ GWE + + EEYRFYTPPNFVLALVLP SIVILGKIILFLPCISRKLKRIKKGWEKSQFLEEGMGGTIP		480
Query 333	---TEICSP--- E + Screenshot		
Sbjct 481	HVSPERVTVM 450		

**Figure A.1 1 Protein sequence alignment by BLASTp of STEAP1 and STEAP2.** Protein sequences Q9UHE8 (STEAP1\_Human: STEAP1) and Q8NFT2 (STEAP2\_Human: STEAP2) were retrieved in FASTA format and utilised for BLASTp analysis (date accessed: 11.03.2020; source: <https://blast.ncbi.nlm.nih.gov/Blast>). Sequence identity (“identities”): number of identical amino acids between the query STEAP1 and the subject sequence of STEAP2) was 43%; „+”: amino acids that are different between the query and subject sequences but the two residues have similar chemical properties were 63% between STEAP1 and STEAP2. Explanations for the denotations were retrieved from [https://community.gep.wustl.edu/wiki/images/2/28/2011\\_8b\\_BLASTrv7\\_rev.pdf](https://community.gep.wustl.edu/wiki/images/2/28/2011_8b_BLASTrv7_rev.pdf) (date accessed: 30.03.2020).

NW Score	Identities	Positives	Gaps
1309	255/492(52%)	343/492(69%)	6/492(1%)
Query 1	MPE-EMDKPLISLHLVSDSSLAKVPDEAP-KVGILGSGDFARSLATRLVSGSGFKVVVGS		58
Sbjct 1	M M SL + + + D VG++GSGDFA+SL RL+ G+ VV+GS		60
Query 59	RNPKRTARLFPSAAQVTFQEEAVSSPEVIFVAVFREHYSSLCSLSDQLAGKILVDVSNPT		118
Sbjct 61	RNPK + FP VT E+A++ +IFVA+ REHY+SL L L GKIL+DVSN		120
Query 119	EQEHQLHRESNAEYLASLFPCTCTVVKAFNVISAWTLQAGPRDGNRQVPCGDQPEAKRAV		178
Sbjct 121	Q+ ESNAEYLASLFP +VK FNV+SAW LQ GP+D +RQV IC + +A++ V		178
Query 179	SEMALAMGFMPVDMGSLASAWVEAMPLRLLPAWKVPTLLALGLFVCFYAYNFVRDVLQP		238
Sbjct 179	E+A + F+P+D+GSL+SA E+E +PLRL W+ P ++A+ L F+ Y+FVRDV+ P		238
Query 239	YVQESQNKFFKLPVSVVNTLLPCVAVYLLSLVYLPGLVLAALQLRRGTYQRFDPDWLHW		298
Sbjct 239	Y + Q+ F+K+P+ +VN TLP VA LLSLVYL G+LAAA QL GTKY+RFP WL+ W		298
Query 299	LQHRKQIGLLSFFCAALHALYSFCLPLRRAHRYDLVNLAVKQVLANKSHLWVEEVRME		358
Sbjct 299	LQ RKQ+GLLSFF A +H YS CLP+RR+ RY +N+A +QV AN + W EEEVWR+E		358
Query 359	IYLSLGLVALGTLSELLAVTSLPSIANSLNWREFSFVQSSLGVALVLTSLHTLYGWTRA		418
Sbjct 359	+Y+S G+++LG LSELLAVTS+PS++N+LNWREFSF+QS+LG+VAL++ST H L YGW RA		418
Query 419	FEESRYKFYLPPTFTLTLVPCVVILAKALFLLPCISRRLARIRRGWERESTIKFTL--P		476
Sbjct 419	FEE Y+FY PP F L L++P +VIL K + LPCISR+L RI++GWE+ ++ +		478
Query 477	TDHALAEKTSHV 488		
Sbjct 479	H E+ + + IPHVSPERTVM 490		

**Figure A.1 2 Protein sequence alignment by BLASTp of STEAP3 and STEAP2.** Protein sequences Q658P3 (STEAP3\_Human: STEAP3) and Q8NFT2 (STEAP2\_Human: STEAP2) were retrieved in FASTA format and utilised for BLASTp analysis (date accessed: 11.03.2020; source: <https://blast.ncbi.nlm.nih.gov/Blast>). Sequence identity (“identities”): number of identical amino acids between the query STEAP3 and the subject sequence of STEAP2) was 52%; „+”: amino acids that are different between the query and subject sequences but the two residues have similar chemical properties were 69% between STEAP3 and STEAP2. Explanations for the denotations were retrieved from [https://community.gep.wustl.edu/wiki/images/2/28/2011\\_8b\\_BLASTrv7\\_rev.pdf](https://community.gep.wustl.edu/wiki/images/2/28/2011_8b_BLASTrv7_rev.pdf) (date accessed: 30.03.2020).

NW Score	Identities	Positives	Gaps
1105	212/490(43%)	310/490(63%)	31/490(6%)
Query 1	MEKTCIDALPLTMNSS-----EKQETVCIFGTGDFGRSLGLKMLQCGYSVVF		49
Sbjct 1	ME + P +++ + ++ TV + G+GDF +SL +++++CGY VV GS		60
Query 50	RNPQ-KTLLPSGAEVLSEAAKKSIIIHREHYDFLTELTEVLNGKILVDISNNL		108
Sbjct 61	RNP+ + P +V + +A K+ II +AIHREHY L +L +L GKIL+D+SNN+		120
Query 109	KINQYVESNAEYLAHLVPGAHVVKAFNTISAWALQSGALDASRQVFCVGNDSKAKQVMD		168
Sbjct 121	+INQYVESNAEYLA L P + +VK FN +SAWALQ G DASRQV++C N+ +A+Q+V++		180
Query 169	IVRNLGLTPMDQGSMAAKEIEKYPLQFPMWRFPFYL SAVLCVFLFFYCVIRDVIYPYV		228
Sbjct 181	+ R L P+D GSL +A+EIE PL+LF +WR P ++ L F F Y +RDVI+PY		240
Query 229	YEKDNTRFMAISIPNRFIPITALTLALVYLPGVIAAILQLYRGTKYRRFPDWDHWM		288
Sbjct 241	++ + +++ I I N+ PI A+TLL+LVYL G++AA QLY GTKYRRFP WL+ W+		300
Query 289	CRKQLGLVALGFALHVLVYTLVPIRYYVRWRLGNLTVTQAILKKNPFSTSSAWLSDSY		348
Sbjct 301	CRKQLGL++ FA +HV Y+L +P+R R+ N+ Q EN ++ W + Y		360
Query 349	VALGILGFFLVLLGITSLSVSNVWREFRFVQSKLGYLTLILCTAHTLVYGGKRFLS		408
Sbjct 361	++ GI+ L LL +TS+PSVSNVWREF F+QS LGY+ L++ T H L+YG KR		420
Query 409	PSNLRWYLPAAVYVGLIIPCTVLVIKFLVIMPCVDNTLRIRQGWERN-----		456
Sbjct 421	R+Y P +VL L++P V++ K +L +PC+ L RI++GWE++		480
Query 457	-----SKH 459		
Sbjct 481	+ HVSPERVTVM 490		

**Figure A.1 3 Protein sequence alignment by BLASTp of STEAP4 and STEAP2.** Protein sequences Q687X5 (STEAP4\_Human: STEAP4) and Q8NFT2 (STEAP2\_Human: STEAP2) were retrieved in FASTA format and utilised for BLASTp analysis (date accessed: 11.03.2020; source: <https://blast.ncbi.nlm.nih.gov/Blast>). Sequence identity (“identities”): number of identical amino acids between the query STEAP4 and the subject sequence of STEAP2) was 43%; „+”: amino acids that are different between the query and subject sequences but the two residues have similar chemical properties were 63% between STEAP4 and STEAP2. Explanations for the denotations were retrieved from [https://community.gep.wustl.edu/wiki/images/2/28/2011\\_8b\\_BLASTrv7\\_rev.pdf](https://community.gep.wustl.edu/wiki/images/2/28/2011_8b_BLASTrv7_rev.pdf) (date accessed: 30.03.2020).

**Table A1. 1 Overview of the statistical analysis of the 33 analysed normal, healthy human tissues across the human body compared to the high-grade prostate cancer tissue specimen used as a positive control for high STEAP2 expression.** +ctrl (PCa): high-grade prostate cancer tissue specimen used as positive control with high STEAP2 expression. Data was analysed by a non-parametric one-way ANOVA post-hoc Kruskis-Wallis test for statistical significance.

Comparison of tissues	Significant?	Summary	Adjusted p-value	Tissue
+ control (PCa) vs. Adrenal gland	No	ns	0.2432	Adrenal gland
+ control (PCa) vs. Bladder	Yes	**	0.0056	Bladder
+ control (PCa) vs. Bone marrow*	No	ns	>0.9999	Bone marrow*
+ control (PCa) vs. Eye*	No	ns	0.1049	Eye*
+ control (PCa) vs. Breast	No	ns	0.3332	Breast
+ control (PCa) vs. Cerebellum*	No	ns	0.4129	Cerebellum*
+ control (PCa) vs. Cerebral cortex*	Yes	*	0.0107	Cerebral cortex*
+ control (PCa) vs. Fallopian tube	No	ns	0.3475	Fallopian tube
+ control (PCa) vs. GI-esophagus	Yes	*	0.0208	GI-esophagus
+ control (PCa) vs. GI-stomach	No	ns	0.1534	GI-stomach
+ control (PCa) vs. GI-small intestine	No	ns	0.2829	GI-small intestine
+ control (PCa) vs. GI-colon	No	ns	0.1534	GI-colon
+ control (PCa) vs. GI-rectum	No	ns	>0.9999	GI-rectum
+ control (PCa) vs. Heart*	No	ns	>0.9999	Heart*
+ control (PCa) vs. Kidney	No	ns	0.1448	Kidney
+ control (PCa) vs. Liver	No	ns	0.8240	Liver
+ control (PCa) vs. Lung	No	ns	0.1036	Lung
+ control (PCa) vs. Ovary	Yes	*	0.0379	Ovary
+ control (PCa) vs. Pancreas*	Yes	**	0.0034	Pancreas*
+ control (PCa) vs. Pituitary gland*	No	ns	0.7006	Pituitary gland*
+ control (PCa) vs. Placenta	No	ns	>0.9999	Placenta
+ control (PCa) vs. Prostate	Yes	*	0.0107	Prostate
+ control (PCa) vs. Skin	Yes	*	0.0107	Skin
+ control (PCa) vs. Spinal cord*	Yes	*	0.0107	Spinal cord*
+ control (PCa) vs. Spleen	No	ns	>0.9999	Spleen
+ control (PCa) vs. Striated muscle*	No	ns	0.1955	Striated muscle*
+ control (PCa) vs. Testis	Yes	**	0.0034	Testis
+ control (PCa) vs. Thymus*	Yes	**	0.0056	Thymus*
+ control (PCa) vs. Thyroid	Yes	*	0.0254	Thyroid
+ control (PCa) vs. Tonsil	Yes	**	0.0034	Tonsil
+ control (PCa) vs. Ureter	Yes	*	0.0208	Ureter
+ control (PCa) vs. Uterus-cervix	Yes	*	0.0208	Uterus-cervix
+ control (PCa) vs. Uterus-endometrium	Yes	**	0.0034	Uterus-endometrium

**Table A1. 2 Commercial anti-STEAP2 Ab list for Ab-ECL mapping.** Anti-STEAP2 antibodies were evaluated and listed for their clonality, host species origin and recommended applications, immunogen regions the Ab has been raised against (if available) and supplier with catalogue number. Poly: polyclonal, rb: rabbit, ELISA: Enzyme-Linked Immunosorbent Assay; IHC: Immunohistochemistry; ICC: Immunocytochemistry; FC: Flow cytometry; WB: Western blotting; aa: amino acid number of immunogen; N/A: not available. Date accessed: 03/2016.

Clonality	Host	Application	Immunogen (aa)	Supplier, cat. #
Poly	Rb	ELISA, IF, IHC, WB	N/A	Abbiotec, # 253762
Poly	Rb	FC, IHC, WB	233 – 262	Abcam, # ab174978
Poly	Rb	ICC/IF, IHC	N/A	Abcam, # ab196661
Poly	Rb	IHC	N/A	Abcam, # ab133392
Poly	Rb	IHC	N/A	Abcam, # ab188809
Poly	Rb	ELISA	455 – 467	Abnova Corpor., # PAB1062
Poly	Rb	IHC, WB	N/A	Abnova Corpor., # PAB13007
Poly	Rb	ELISA, ICC/IF, WB	N/A	Acris antibodies, # AP30834PU-N
Poly	Rb	IHC, WB	N/A	Acris antibodies, # AP-07354PU-N
Poly	Rb	ELISA, IHC, WB	N/A	Antibodies online, # ABIN500821
Poly	Rb	ELISA, IHC, WB	N/A	Antibodies online, # ABIN1003201
Poly	Rb	IHC	131-201	Atlas Antibodies, # HPA029115
Poly	Rb	WB, IHC, ELISA	226 – 253	Avivasystems. # OAA02995
Poly	Rb	ELISA, IF, IHC	431-480	Avivasystems, # OAAF02556
Poly	Rb	IHC	N/A	Avivasystems, # OALA01481
Poly	Rb	IHC, WB	N/A	Avivasystems, # OALA01897
Poly	Rb	ELISA, IHC, WB	N/A	Avivasystems. # OAPB00563
Poly	Rb	IF, IHC, ELISA	400 – 480	Avivasystems, # OASG06901
Poly	Rb	IHC	N/A	Biorbyt, # orb96663
Poly	Rb	IHC	N/A	Biorbyt, # orb96740
Poly	Rb	FC, IHC, WB	233 – 262	Creative Diagn., # DPABH-11394
Poly	Rb	IHC	N/A	Creative Diagn., # DPABH-25313
Poly	Rb	IF, IHC, WB	N/A	EMD Millipore, # ABC341
Poly	Rb	ELISA, IHC, WB	N/A	Fitzgerald Ind., # 70R-21712
Poly	Rb	IHC, WB	N/A	GeneTex, # GTX85648
Poly	Rb	IHC	N/A	Invitrogen, # PA5-33060
Poly	Rb	FC, IHC, WB	226 – 253	LifeSpan Bio,

				# LS-C161555
Poly	Rb	IHC	N/A	LifeSpan Bio, # LS-A9239
Poly	Rb	ELISA, IF, IHC	431 – 480	LifeSpan Bio, # LS-C119155
Poly	Rb	IHC, WB	N/A	MyBioSource, # MBS241319
Poly	Rb	IF, IHC, WB	N/A	OriGene Tech, # TA306464
Poly	Rb	IHC	N/A	OriGene Tech, # TA341329
Poly	Rb	ELISA, IF, IHC, WB	N/A	ProSci, # 4307
Poly	Rb	ELISA, IHC, WB	68 – 88	Proteintech, # 20201-1-AP
Poly	Rb	IHC, WB	N/A	RayBiotech, # 119-12134
Poly	Rb	IHC	N/A	RayBiotech, # 119-17551
Poly	Rb	ELISA, IF, IHC, WB	N/A	Santa Cruz, # sc-368248
Poly	Rb	ELISA, IF, WB	N/A	Santa Cruz, # sc-82365
Poly	Rb	ELISA, IF, WB	N/A	Santa Cruz, # sc-82367
Poly	Rb	IHC	131 – 201	Sigmaaldrich, # HPA029115
Poly	Rb	IHC, WB	N/A	Sigmaaldrich, # PRS4307
Poly	Rb	IF, WB	6 - 127	Sigmaaldrich, # HPA055603
Poly	Rb	IHC	N/A	Source Bio, # SBS401504
Poly	Rb	IHC	N/A	Source Bio, # SBS401506

## Appendix 2

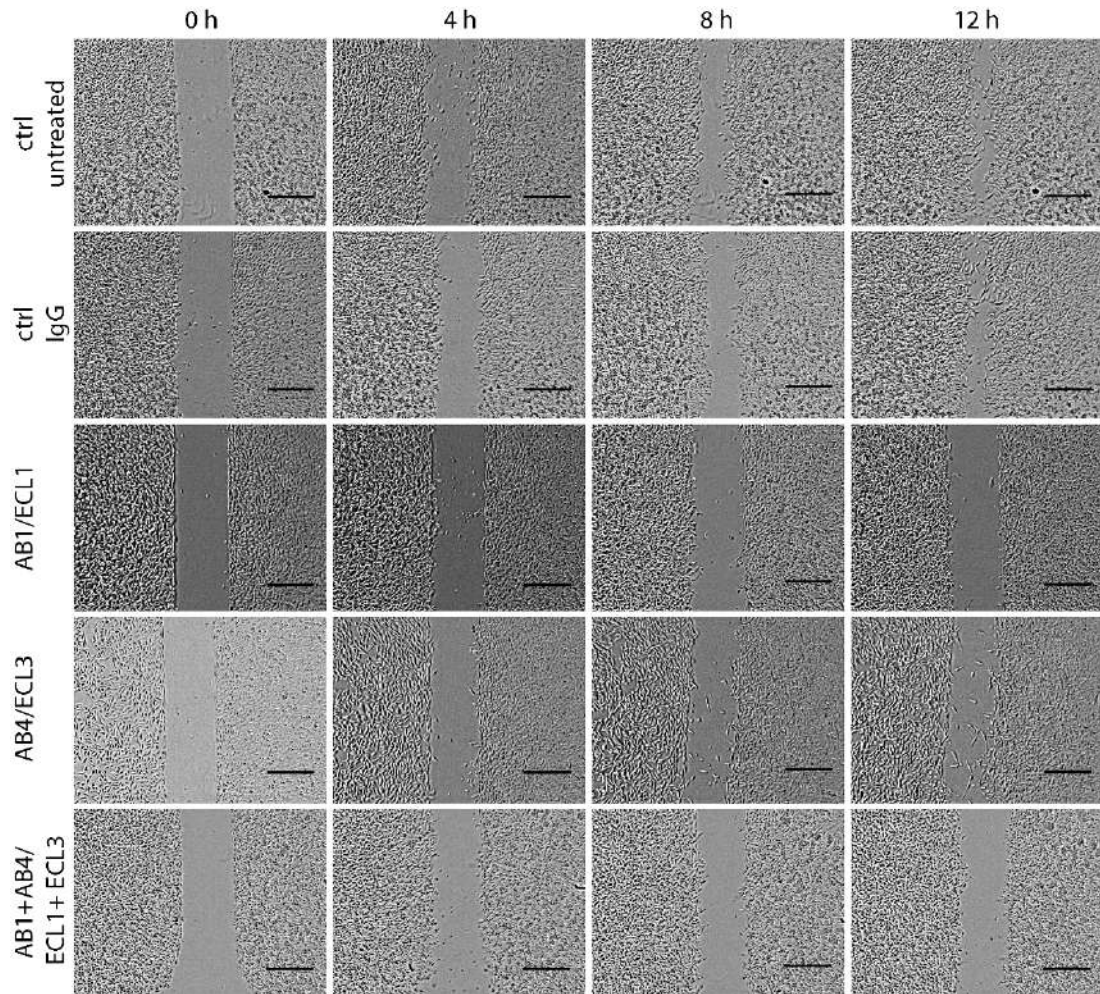


**Figure A2. 1 Similar inhibition of cell migration in PC3 cells is observed by either single or dual Ab STEAP2 targeting.** Time points at which the images were taken: 0h, 4h, 8h and 12h; +ctrl, untreated PC3 cells, + ctrl IgG: PC3 cells treated with anti-IgG isotype Ab (20  $\mu\text{g}/\text{ml}$ ); AB1/ECL1: single anti-STEAP2 Ab targeting an epitope of the ECL1 (20  $\mu\text{g}/\text{ml}$ ); AB4/ECL3: single anti-STEAP2 Ab targeting an epitope of the ECL3 (20  $\mu\text{g}/\text{ml}$ ); AB1+AB4/ECL1+ECL3: dual anti-STEAP2 Ab targeting of two unique epitopes on ECL1 and ECL3. Images were acquired using an inverted light microscope with a 5x objective (AxioCam ERC5s, ZEISS, Germany). Scale bar = 500  $\mu\text{m}$  (N = 2).

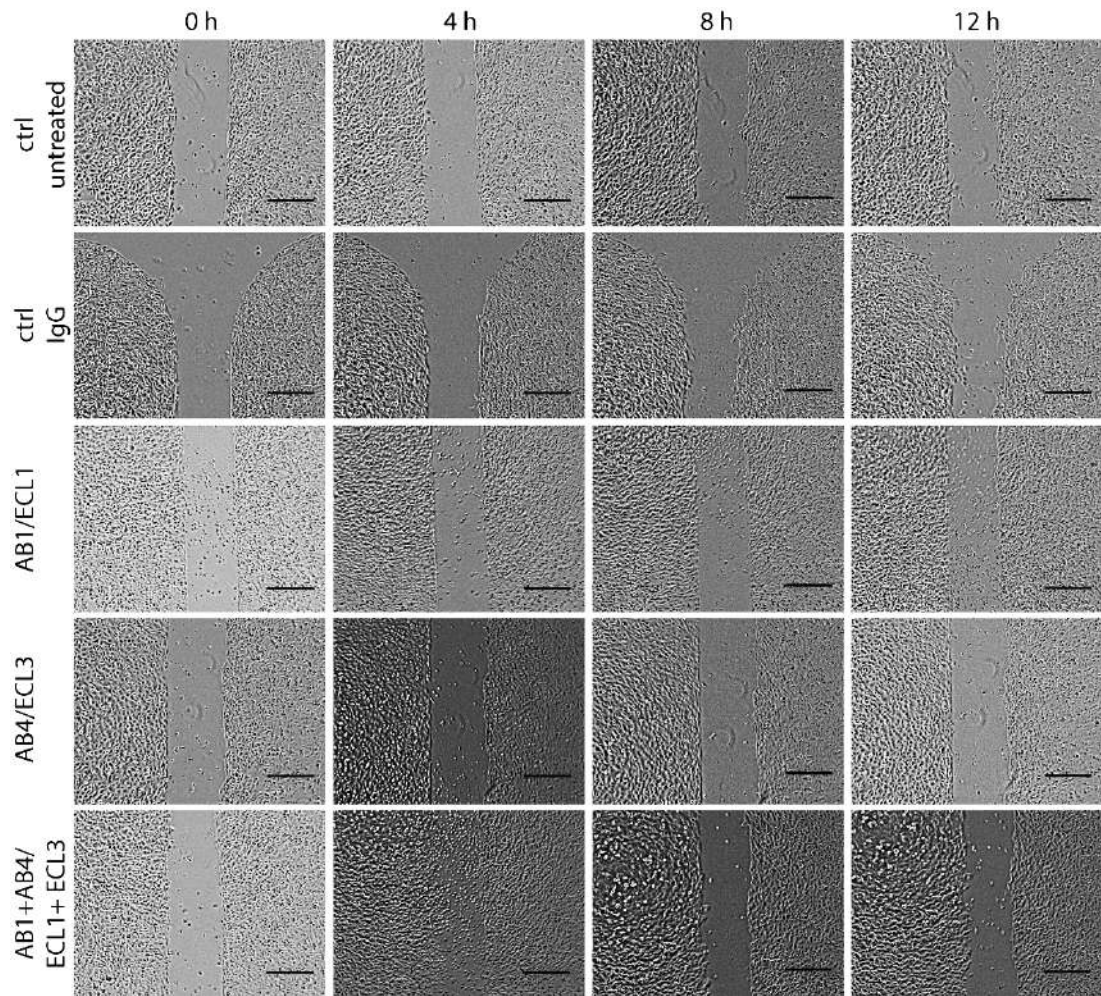


**Figure A2.2 Cell migration of PNT2 cells remains unaffected after anti-STEAP2 Ab (ECL3) exposure.** Time points at which the images were taken: 0h, 4h, 8h and 12h; +ctrl, untreated PC3 cells, + ctrl IgG: PC3 cells treated with anti-IgG isotype Ab (20  $\mu\text{g}/\text{ml}$ ); AB1/ECL1: single anti-STEAP2 Ab targeting an epitope of the ECL1 (20  $\mu\text{g}/\text{ml}$ ); AB4/ECL3: single anti-STEAP2 Ab targeting an epitope of the ECL3 (20  $\mu\text{g}/\text{ml}$ ); AB1+AB4/ ECL1+ECL3: dual anti-STEAP2 Ab targeting of two unique epitopes on ECL1 and ECL3. Images were acquired using an inverted light microscope with a 5x objective (AxioCam ERC5s, ZEISS, Germany). Scale bar = 500  $\mu\text{m}$  (N = 2).

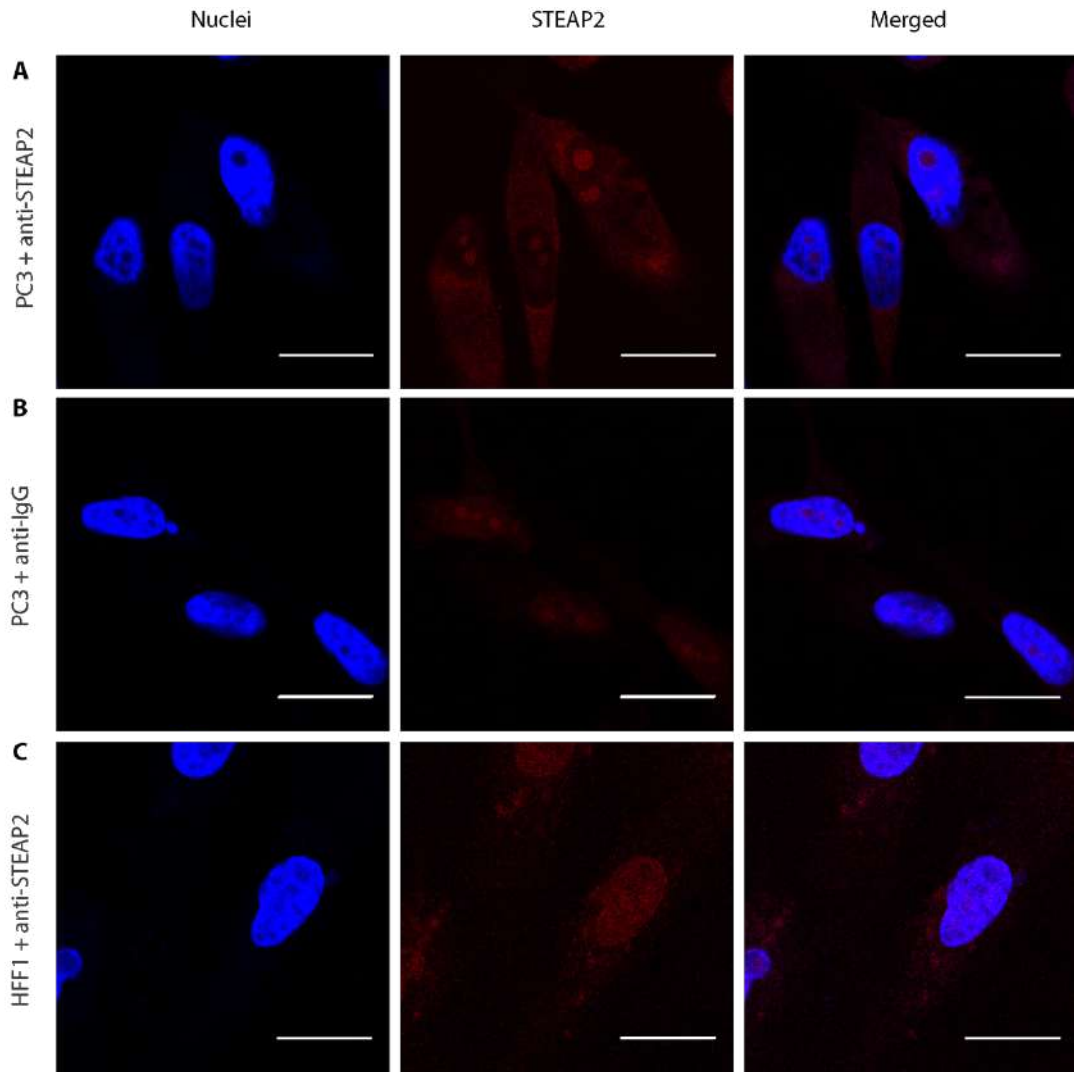


**Figure A2. 3 Cellular localisation of STEAP2 is located to the cell membrane at the 0 min time point during receptor internalisation studies in cancerous PC3 cells but not in normal HFF1 cells (after fluorescence activation).** Cell surface STEAP2 was visualised by the addition of acid (pH 5.0) before receptor internalisation. A) PC3 + anti-STEAP2 pHAb Amine Reactive Dye Conjugate showing cell surface STEAP2. B) PC3 + anti-IgG pHAb Amine Reactive Dye Conjugate: Ab isotype control unspecific to STEAP2 with no cell-surface fluorescence observed. C) HFF1 + anti-STEAP2 pHAb Amine Reactive Dye Conjugate, a STEAP2 low expressing used as negative control cell line showing low fluorescence without cell-surface staining. Blue: nuclei, red: STEAP2. Images were acquired with the Confocal LSM 710 (ZEISS, Germany) at a 63x zoom objective. Scale bar = 20  $\mu\text{m}$  (N = 2).

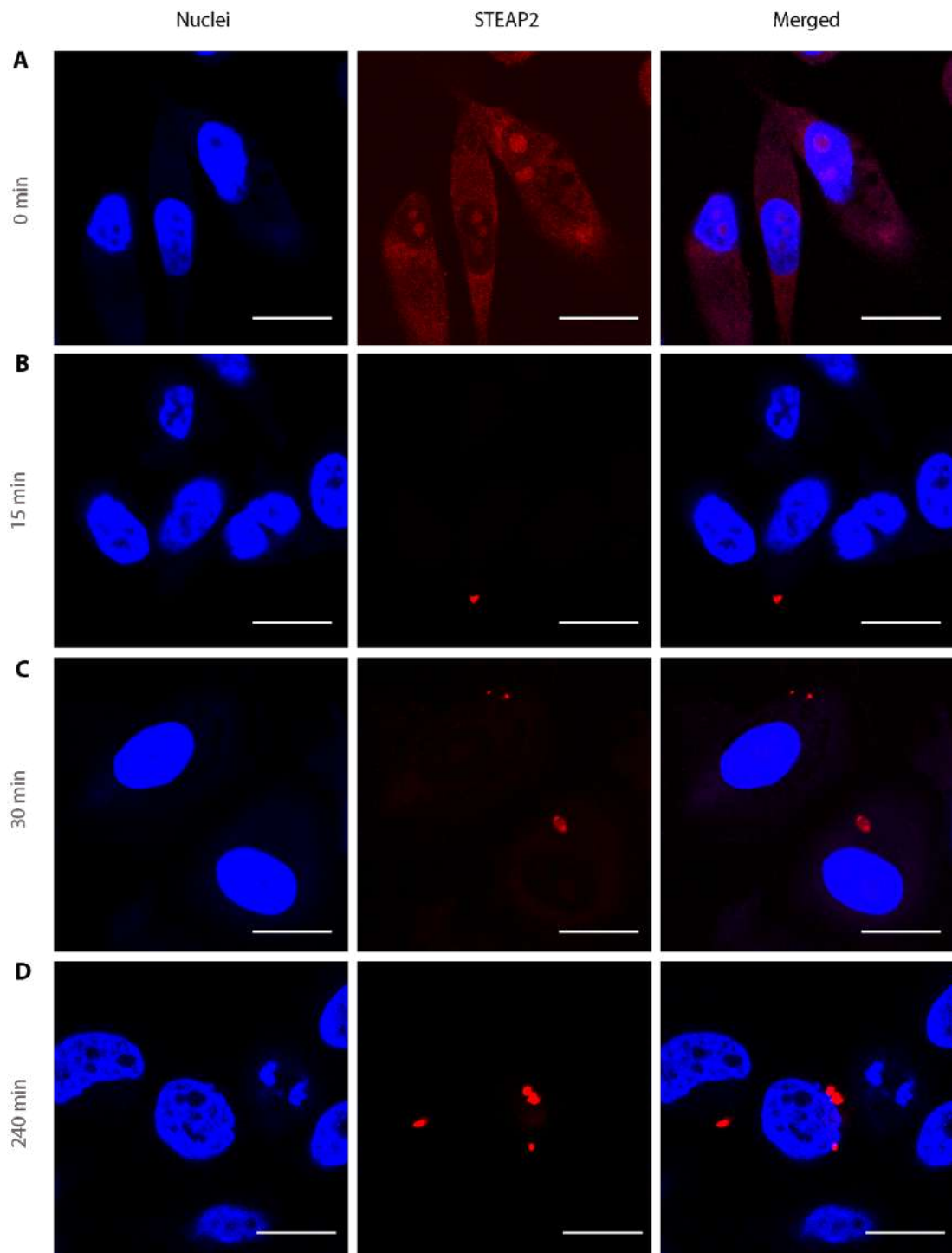


**Figure A2. 4 STEAP2 receptor internalisation was triggered after Ab binding and accumulated accumulation in the endosomal/ lysosomal organelles.** A) 0 min: cell surface STEAP2 was visualised by the addition of acid (pH 5.0) before receptor internalisation. B) 15 min: receptor internalisation was initiated. C) 30 min: first internalised cell surface STEAP2. (D) 240 min: fully internalised STEAP2 shown as red puncta. Blue: nuclei, red: internalised STEAP2 (endosomes/ lysosomal location). Images were acquired with a Confocal LSM 710 with a 63x zoom objective (ZEISS, Germany). Scale bar = 20  $\mu$ m (N = 2).

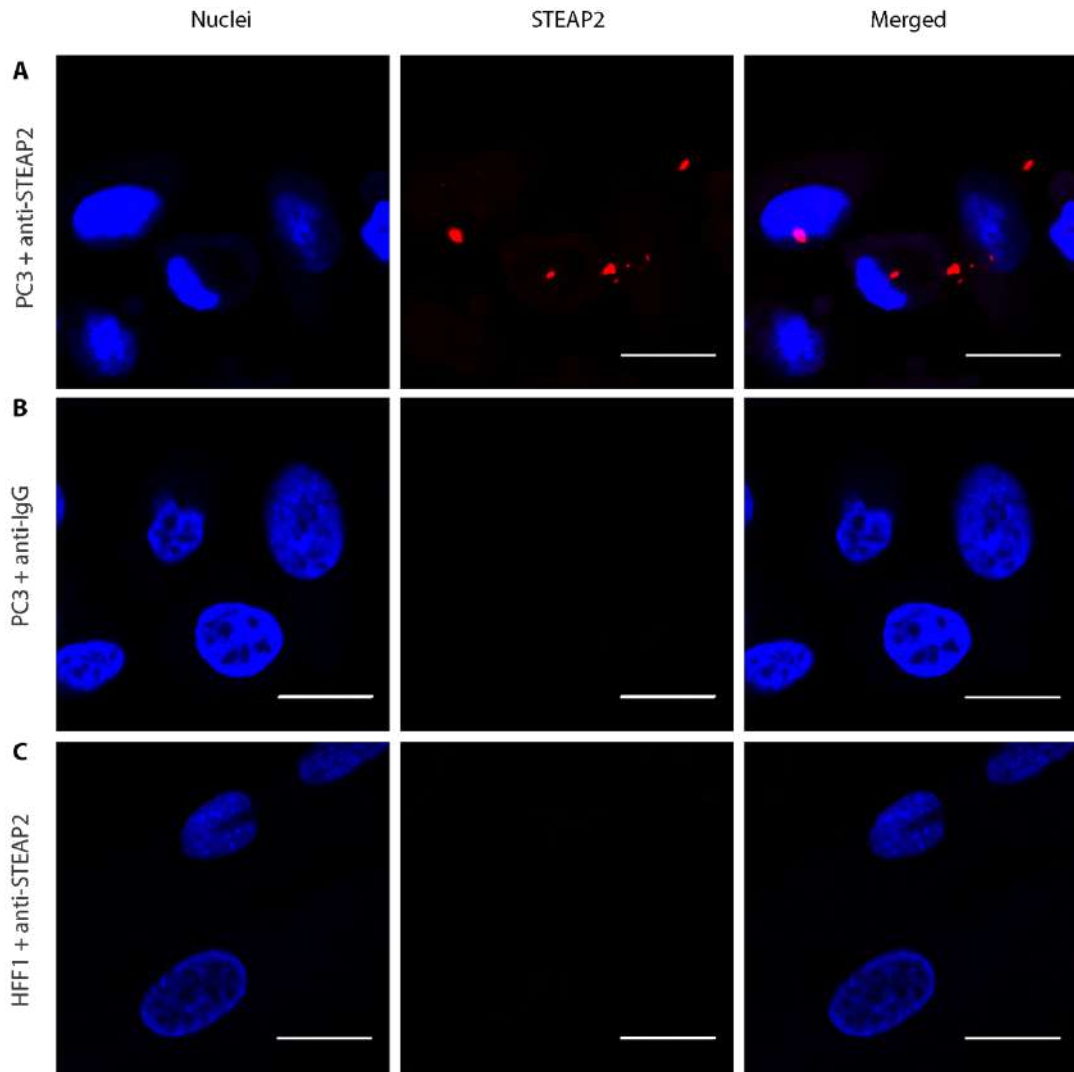


**Figure A2. 5 STEAP2's is localised in the endosomal and lysosomal organelles after 240 min of receptor internalisation in cancerous PC3 cells but is not present in normal HFF1 cells.** A) PC3 + anti-STEAP2 pHAb Amine Reactive Dye Conjugate Ab. B) PC3 + anti-IgG pHAb Amine Reactive Dye Conjugate Ab isotype control. C) STEAP2 low expressing negative control cell line HFF1 + anti-STEAP2 pHAb Amine Reactive Dye Conjugate. Blue: nuclei, red: internalised STEAP2. Images were acquired with the Confocal LSM 710 with a 63x zoom objective (ZEISS, Germany). Scale bar = 20  $\mu\text{m}$  (N = 2).

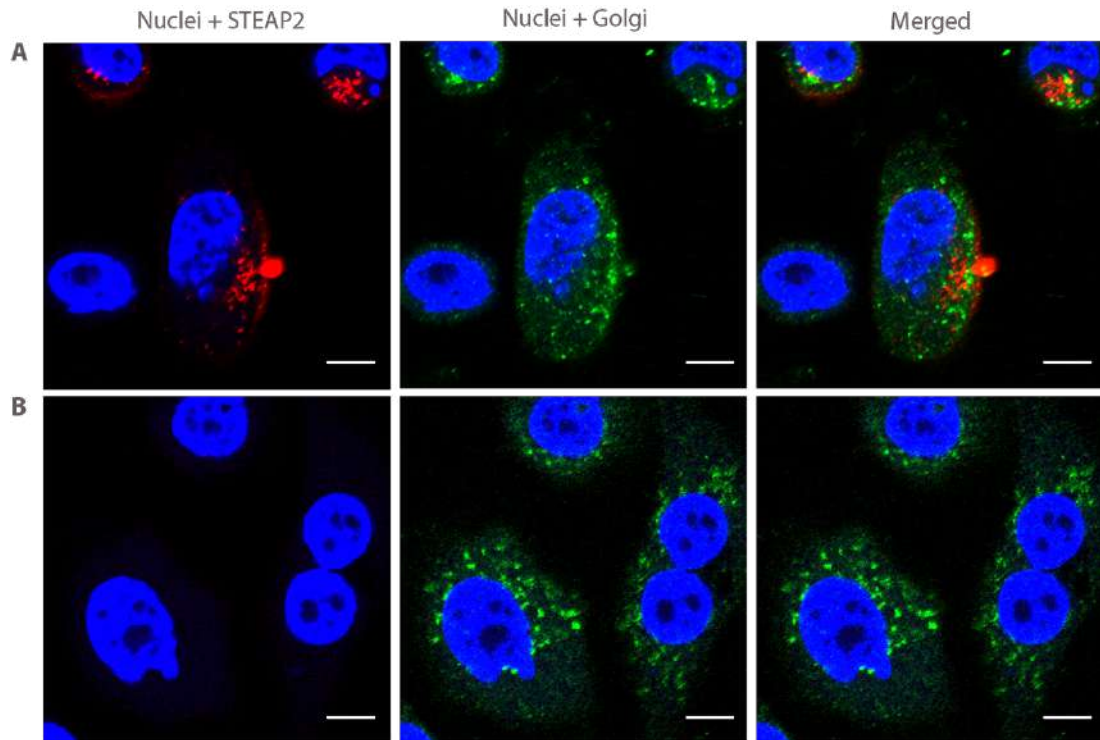


**Figure A2. 6 Internalised cell surface STEAP2 protein did not co-localise with the Golgi apparatus indicating it accumulated in the endosomal/ lysosomal organelles after 240min of receptor internalisation in cancerous PC3.** A) PC3 cells + anti-STEAP2 pHAb Amine Reactive Dye Conjugate Ab. B) PC3 cells + anti-IgG pHAb Amine Reactive Dye Conjugate isotype control Ab. Blue: nuclei, red: internalised STEAP2, green: Golgi. Images were acquired with the Confocal LSM 710 with a 63x zoom objective (ZEISS, Germany). Scale bar = 10  $\mu$ m (N = 2).

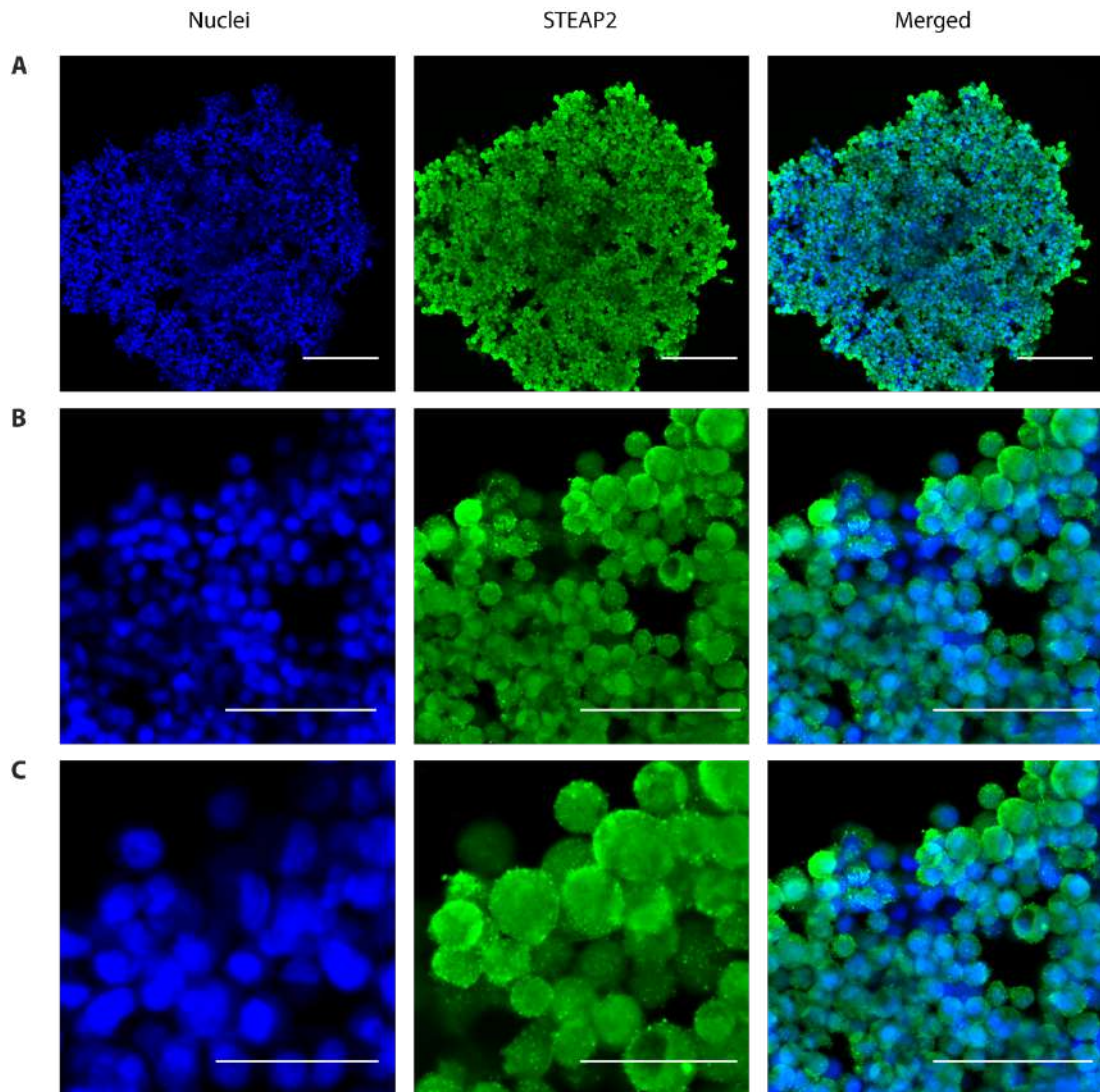


**Figure A2. 7 STEAP2 protein expression and localisation in 3D PC3 cell spheroids using fluorescence microscopy analysis demonstrated it is evenly distributed throughout the spheroid and overexpressed in the PC3 cells. A)** Protein expression of STEAP2 in 3D PC3 spheroid cells at 10x magnification showing the full spheroid. Scale bar = 200  $\mu\text{m}$ . **B)** Protein expression of STEAP2 in 3D PC3 spheroid cells at 10x magnification with 1x standard zoom application showing a strong, evenly distributed protein expression evident both intracellular as well as at the cell membrane. Scale bar = 100  $\mu\text{m}$ . **C)** STEAP2's protein expression in 3D PC3 cell spheroids at 10x magnification showing the full spheroid with 2x standard zoom application. Scale bar = 50  $\mu\text{m}$ . Blue: nuclei, green: STEAP2 protein expression. Images were acquired with the Confocal LSM 710 (ZEISS, Germany) (N = 2).

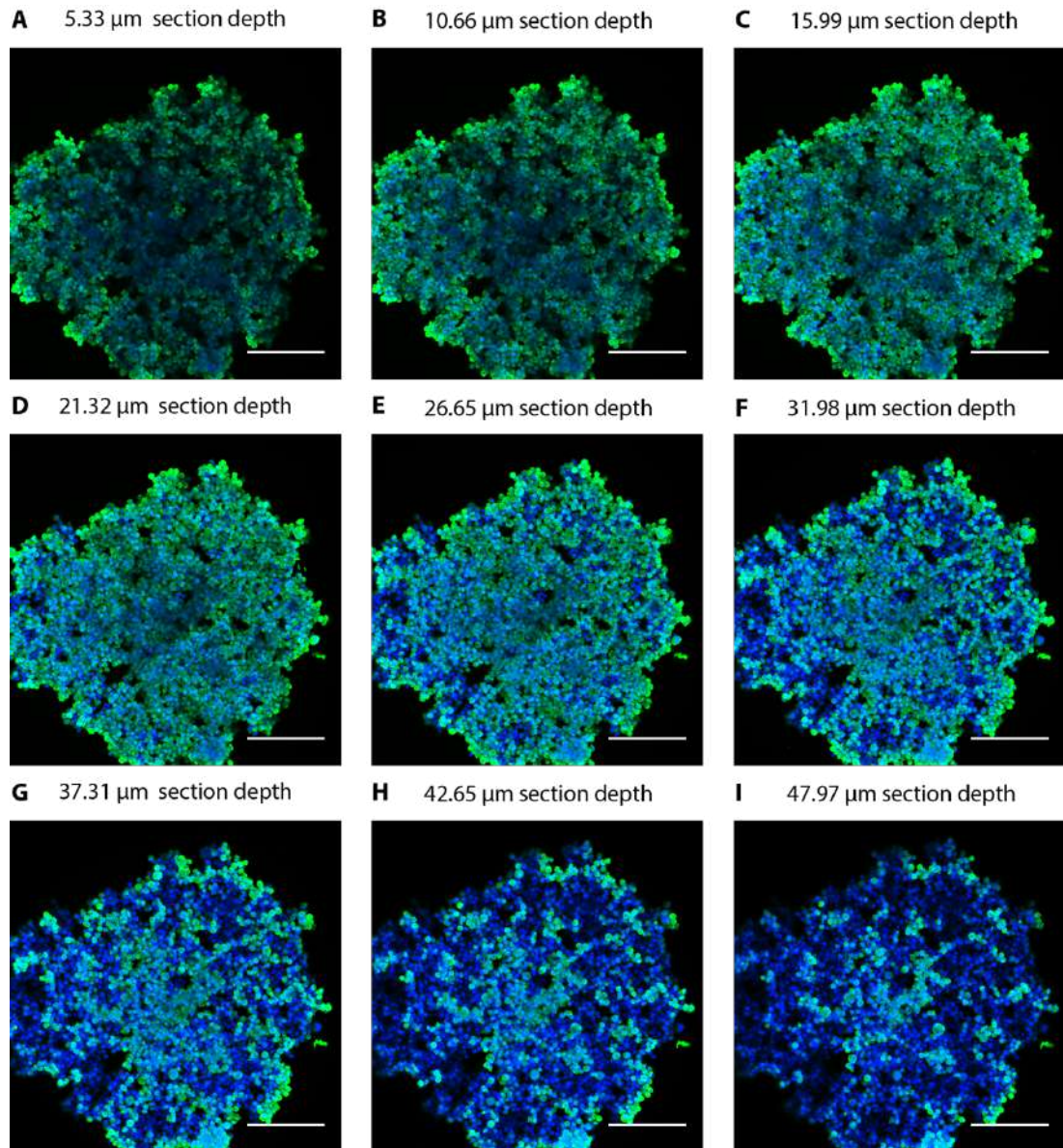


**Figure A2. 8 A z-stack of 3D PC3 cell spheroids over 50  $\mu\text{m}$  depth using fluorescence microscopy analysis demonstrated strong STEAP2 expression throughout the spheroid and good Ab penetration which decreased towards the deeper the sections. A) 5.33  $\mu\text{m}$  section depth, starting point of the z-stack. B) 10.66  $\mu\text{m}$  section depth. C) 15.99  $\mu\text{m}$  section depth. D) 21.32  $\mu\text{m}$  section depth. E) 26.65  $\mu\text{m}$  section depth. F) 31.98  $\mu\text{m}$  section depth. G) 37.31  $\mu\text{m}$  section depth. H) 42.647  $\mu\text{m}$  section depth. I) 47.97  $\mu\text{m}$  section depth, final z-stack. Blue: nuclei, green: STEAP2 protein expression. Images were acquired with the Confocal LSM 710 with a 10x objective (ZEISS, Germany). The z-stack was taken over a 50  $\mu\text{m}$  depth with 5  $\mu\text{m}$  interval slices. Scale bar = 200  $\mu\text{m}$  (N = 2).**

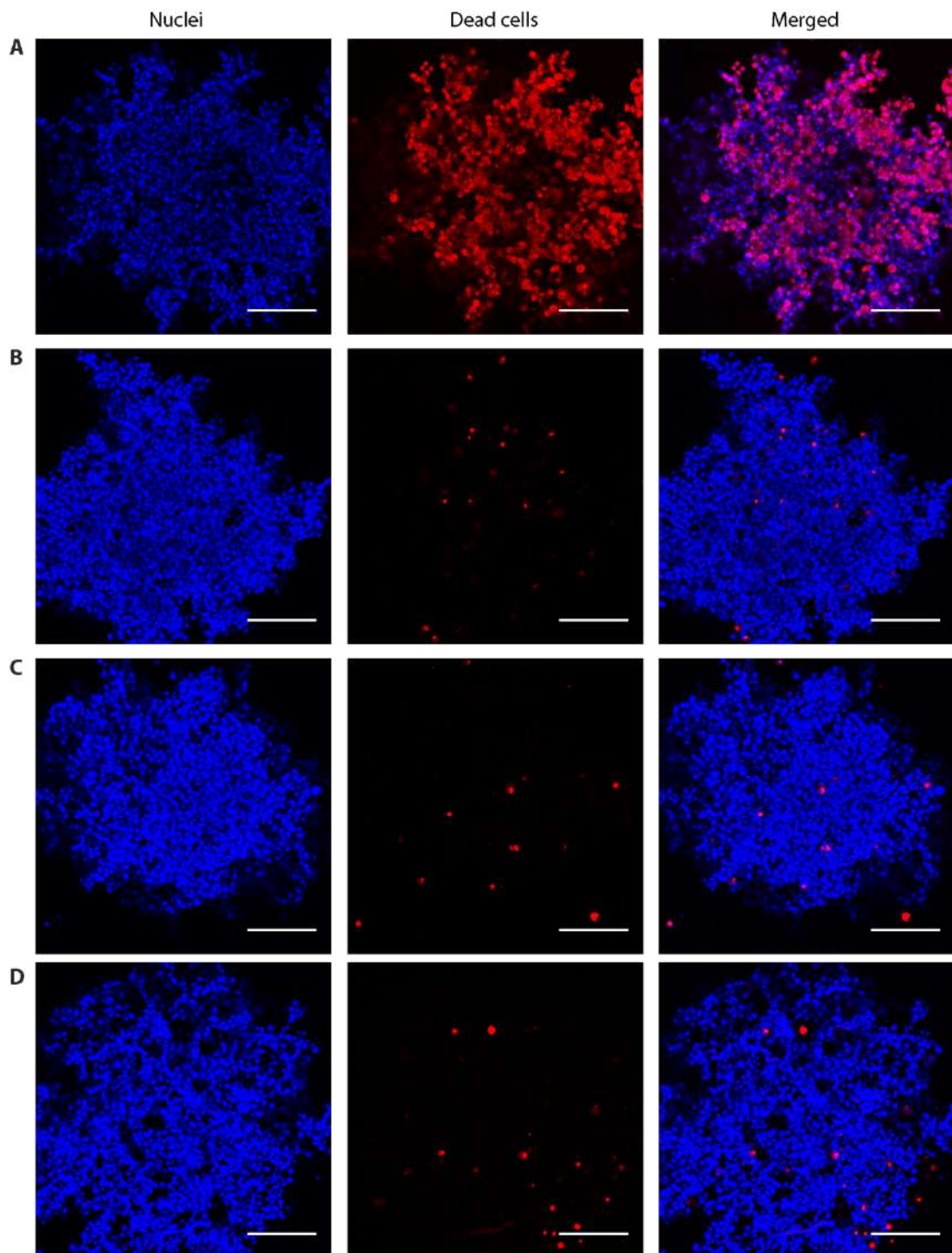


**Figure A2. 9** No difference in cell viability was observed after anti-STEAP2 Ab treatment in 3D PC3 spheroid cells over 24 h using the PI staining and fluorescence microscopy analysis. A) Fixed 3D PC3 spheroid cells to demonstrate dead cells stained with PI. B) Untreated 3D PC3 spheroid cells, negative control. C) 3D PC3 spheroid cells treated with anti-IgG isotype control Ab. D) 3D PC3 spheroid cells treated with 75 µg/ml of anti-STEAP2 Ab (Ab4/ ECL3 specific). Blue: nuclei, red: PI, dead cells. Images were acquired with the Confocal LSM 710 with a 10x objective (ZEISS, Germany). Scale bar = 200 µm (N = 2).

## Appendix 3

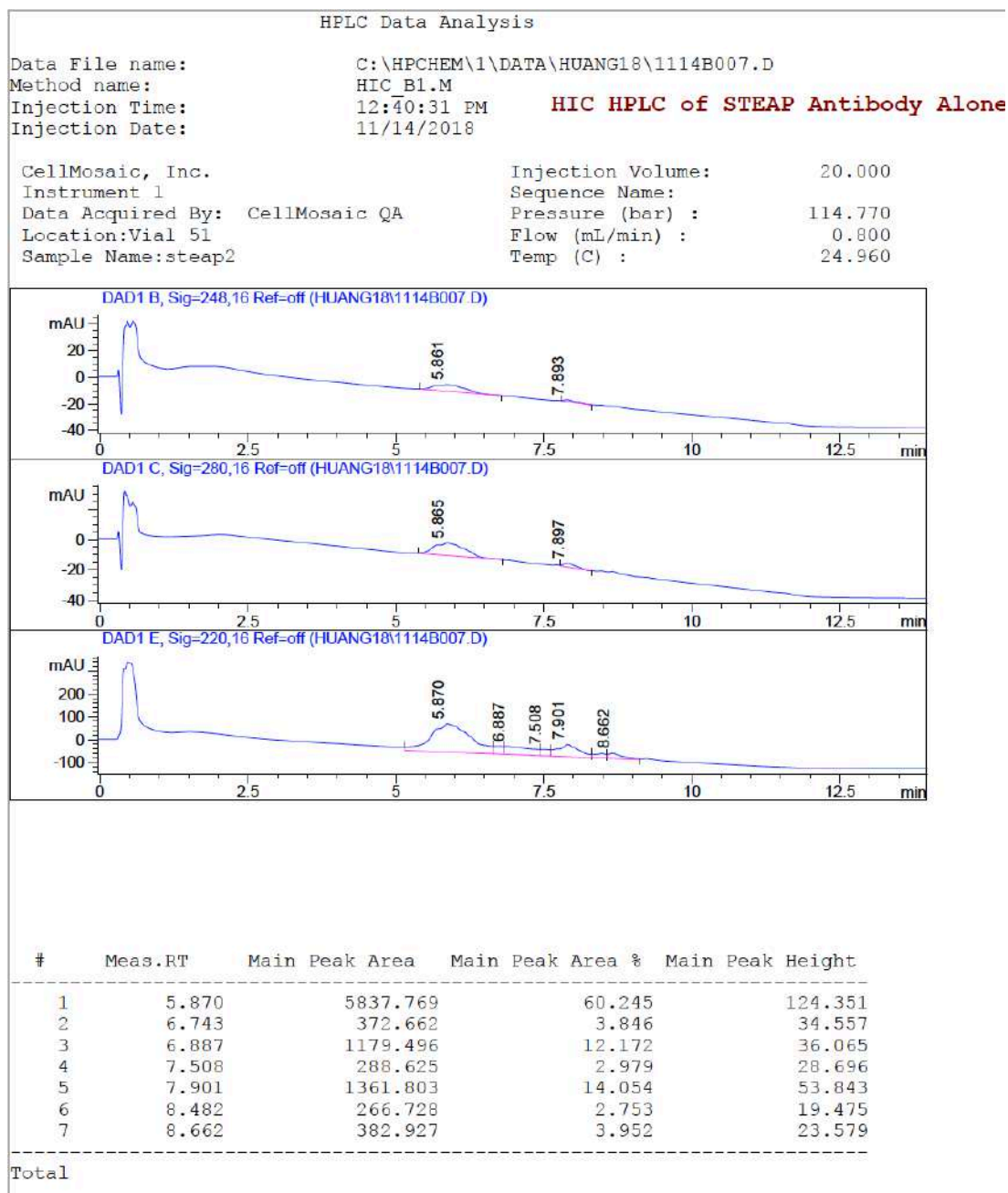


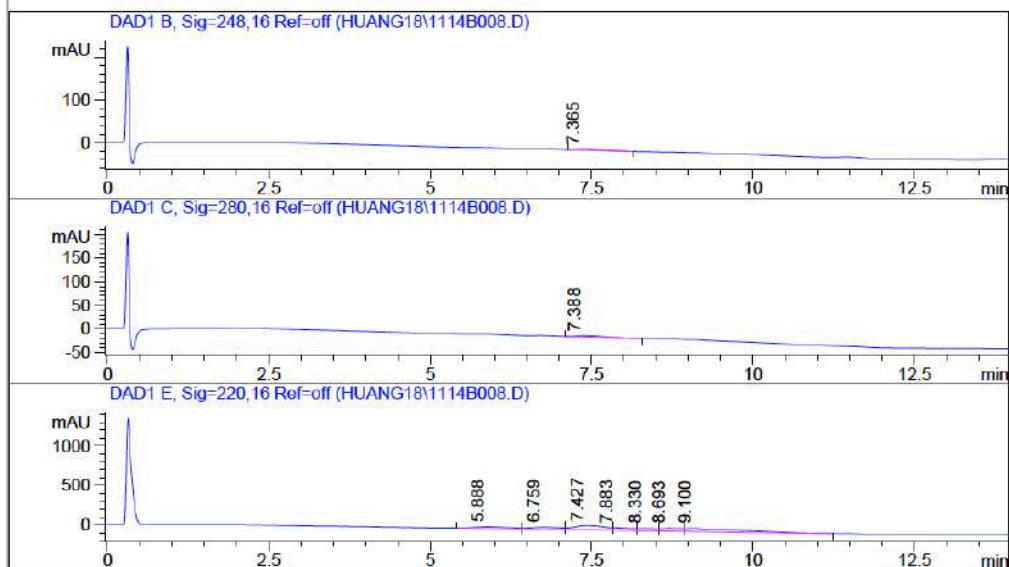
**Figure A3. 1 HIC of the anti-STEAP2 pADC (CellMosaic).** The three graphs represent the absorbances measured at  $\lambda = 280$  nm: protein (IgG) (top);  $\lambda = 248$  nm: MMAE (middle);  $\lambda = 220$  nm: amide bonds of proteins or peptides (bottom) (N =1).

HPLC Data Analysis

Data File name: C:\HPCHEM\1\DATA\HUANG18\1114B008.D  
 Method name: HIC\_B1.M  
 Injection Time: 1:00:04 PM  
 Injection Date: 11/14/2018

HIC HPLC of Product

CellMosaic, Inc. Injection Volume: 20.000  
 Instrument 1 Sequence Name:  
 Data Acquired By: CellMosaic QA Pressure (bar) : 113.640  
 Location:Vial 52 Flow (mL/min) : 0.800  
 Sample Name:7E7.111318 Temp (C) : 24.950



#	Meas.RT	Main Peak Area	Main Peak Area %	Main Peak Height
1	5.888	866.908	10.522	21.526
2	6.759	897.319	10.891	28.066
3	7.388	70.464	100.000	2.557
4	7.427	1923.917	23.351	55.908
5	7.883	668.085	8.109	34.185
6	8.330	630.289	7.650	31.018
7	8.693	833.082	10.112	36.972
8	9.100	2419.359	29.365	40.285

Total

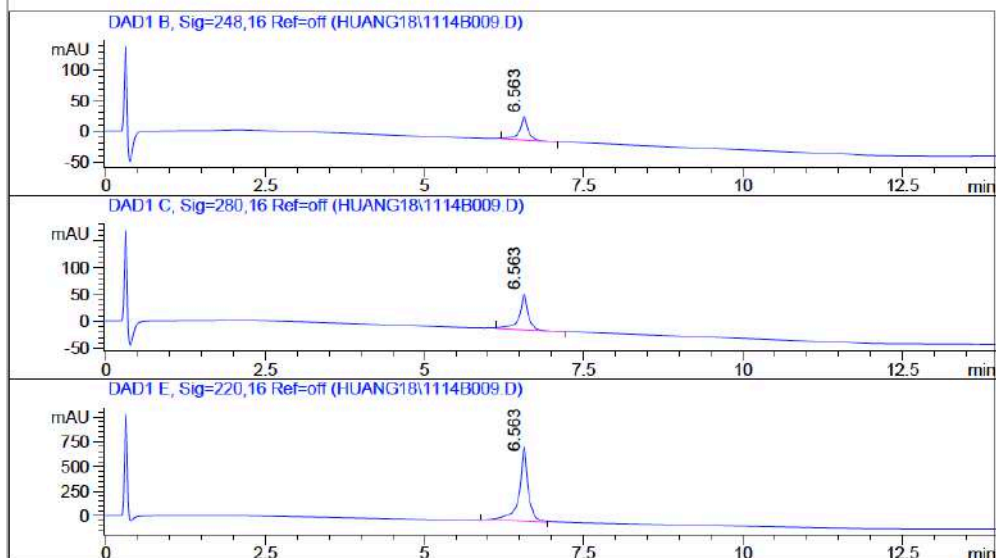
Figure A3. 2 HIC of the unconjugated anti-STEAP2 pAb showing no evident protein aggregation (CellMosaic). The three graphs represent the absorbances measured at A 280 nm: protein (IgG) (top); A 248 nm: MMAE (middle); A 220 nm: amide bonds of proteins or peptides (bottom) (N =1).

HPLC Data Analysis

Data File name: C:\HPCHEM\1\DATA\HUANG18\1114B009.D  
 Method name: HIC\_B1.M  
 Injection Time: 1:19:32 PM  
 Injection Date: 11/14/2018

HIC HPLC of Monoclonal Human IgG1

CellMosaic, Inc. Injection Volume: 20.000  
 Instrument 1 Sequence Name:  
 Data Acquired By: CellMosaic QA Pressure (bar) : 113.920  
 Location:Vial 53 Flow (mL/min) : 0.800  
 Sample Name:herceptin Temp (C) : 25.050



#	Meas.RT	Main Peak Area	Main Peak Area %	Main Peak Height
1	6.563	7456.452	100.000	750.573
Total				

Figure A3. 3 HIC of the human anti-IgG1 Ab control showing no protein aggregation (CellMosaic). The three graphs represent the absorbances measured at A 280 nm: protein (IgG) (top); A 248 nm: MMAE (middle); A 220 nm: amide bonds of proteins or peptides (bottom) (N =1).

### Calculation of equivalent MMAE doses

A 10 mM (10,000  $\mu$ M) MMAE stock (MedChemExpress, USA) was used to prepare 1 ml of the maximum MMAE dose equivalent to 1,000  $\mu$ g/ml pADC dose as below. The desired MMAE doses, equivalent to the pADC doses with a DAR of 3:1 were calculated based on the result of (3) (**Table A3. 1**).

Where: MW: Molecular weight (Da); MW ADC = MW pAb + MW VC-MMAE;  
pAb: commercial polyclonal anti-STEAP2 Ab (rabbit IgG isotype); pADC: commercial polyclonal anti-STEAP2 ADC (rabbit IgG isotype); VC-MMAE: Valine-Citrulline Monomethylauristatin-E (Linker-Drug). MW VC-MMAE = 717.98 Da; MW pAb (rabbit IgG isotype) = 150,000 Da; MW pADC = 151,316.33 Da; Drug-to-Ab Ratio = 3:1

(1) Ratio (MW ADC to number of MMAE drugs)

= MW ADC : number of MMAE drugs

= MW 1x ADC : MW 3x MMAE molecules

= 151.316,33 Da : 2,153.94 Da

= 70.251.

(2) Amount of MMAE per 1  $\mu$ g/ml of pADC

1  $\mu$ g/ml of pADC contains amount of MMAE [ $\mu$ g/ml]:

= 1  $\mu$ g/ml of pADC (containing 3x MMAE drugs) : Ratio

= 1  $\mu$ g/ml of pADC(containing 3x MMAE drugs) : 70.251

= 0.001423  $\mu$ g/ml of MMAE

= 14,23 ng/ml of MMAE

→ 1  $\mu$ g/ml of pADC contains 14,23 ng/ml of MMAE.

(3) Conversion of ng/ml to nM (MMAE)

14.23 ng/ml of MMAE x 717.98 Da = 10.27 nM of MMAE

→ 1 µg/ml of pADC contains 10.27 nM of MMAE.

→ 1 µg/ml of pADC contains 0.01027 µM of MMAE.

$$C_{\text{final}} \times V_{\text{final}} : C_{\text{initial}}$$

$$= 20.54 \text{ } \mu\text{M (MMAE)} \times 1 \text{ ml} : 10,000 \text{ } \mu\text{M (MMAE stock)}$$

$$= 0.002054 \text{ ml of } 10,000 \text{ } \mu\text{M (MMAE stock)}$$

$$= 2.05 \text{ } \mu\text{l of } 10,000 \text{ } \mu\text{M (MMAE stock)}$$

→ 2.05 µl of 10 mM (MMAE stock) + 997.95 µl (DMEM)

→ 2.05 µl of 10 mM MMAE stock are required to represent an equivalent dose of 1,000 µg/ml of pADC.

Where:  $C_{\text{final}}$ : final concentration;  $V_{\text{final}}$  = final volume;  $C_{\text{initial}}$ : initial concentration; DMEM: cell culture medium.

**Table A3. 1 Calculation of the MMAE doses equivalent to the MMAE molecules per anti-STEAP2 ADC dose (DAR of 3:1).** MMAE<sub>f</sub>: final MMAE dose.

Calculations of the MMAE doses				
pADC [µg/ml]	MMAE [ng/ml]	MMAE [nM]	MMAE[ µM]	MMAE <sub>f</sub> [ µM]
1,000	14,230.0 (X)	10,270.0	10.27	20.54
200	2,846.0	2054.0	2.05	4.11
100	1,423.0	1,027.0	1.03	2.05
10	142.3	102.7	0.11	0.21
1	14.23	10.27	0.01	0.02
0.1	1.423	1.027	0.001	0.002
0.01	0.1423	0.1027	0.0001	0.0001
Preparations of the MMAE doses				
MMAE	Dose [ng/ml]*	Volume [µl]	DMEM [µl]	
A	14,300.0	2.0 of stock	997.9	
B	2,846.0	17.5 of (A)	157.5	
C	1,423.0	17.5 of B	157.5	
D	142.3	17.5 of C	157.5	
E	14.23	17.5 of D	157.5	
F	1.423	17.5 of E	157.5	
G	0.1423	17.5 of F	157.5	

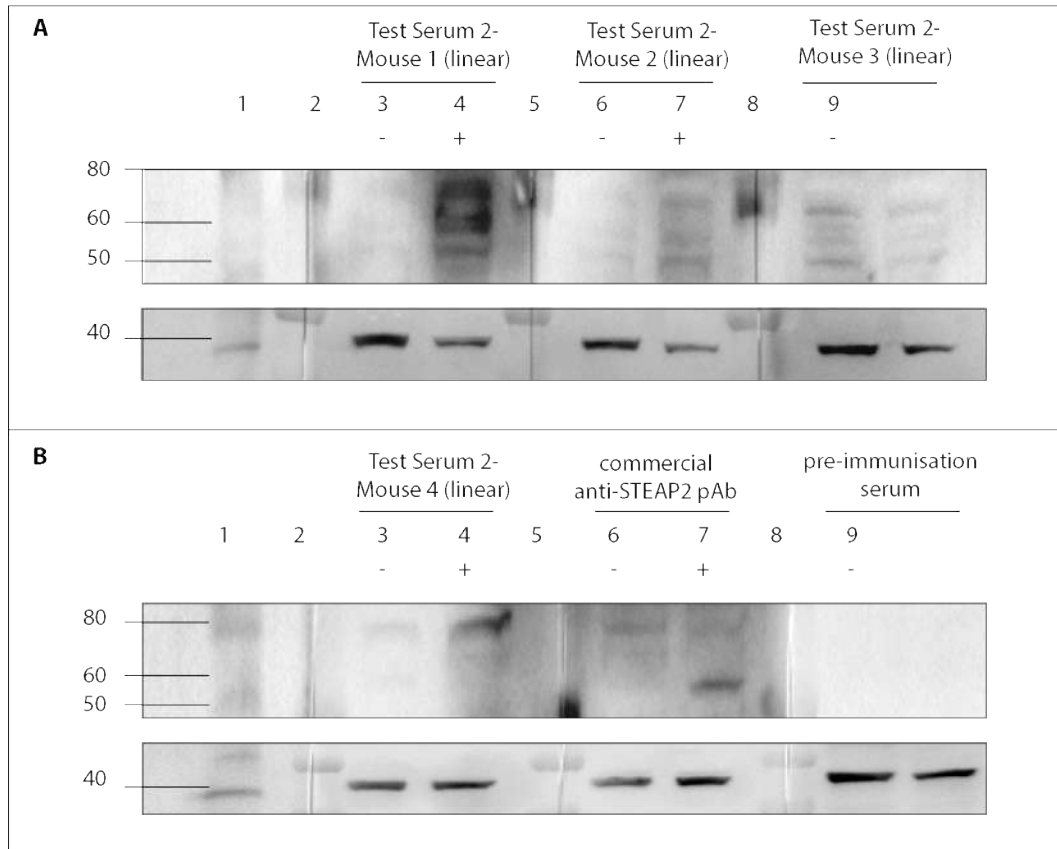


**Figure A3. 4 STEAP2 protein analysis using the Test sera2 (linear).** A) Test Serum2 – Mouse1 (linear), 2 (linear), Mouse3 (linear). B) Test Serum2 – Mouse4 (linear), commercial anti-STEAP2 pAb control and the pre-immunisation serum used as a negative control. 1:Unstained molecular weight ladder; 2: pre-stained dual colour molecular weight marker; 3, 6, 9 (-): technical triplicate of PNT2 cell lysate; 4, 7, 10 (+): technical triplicate of PC3 cell lysate (N = 1).

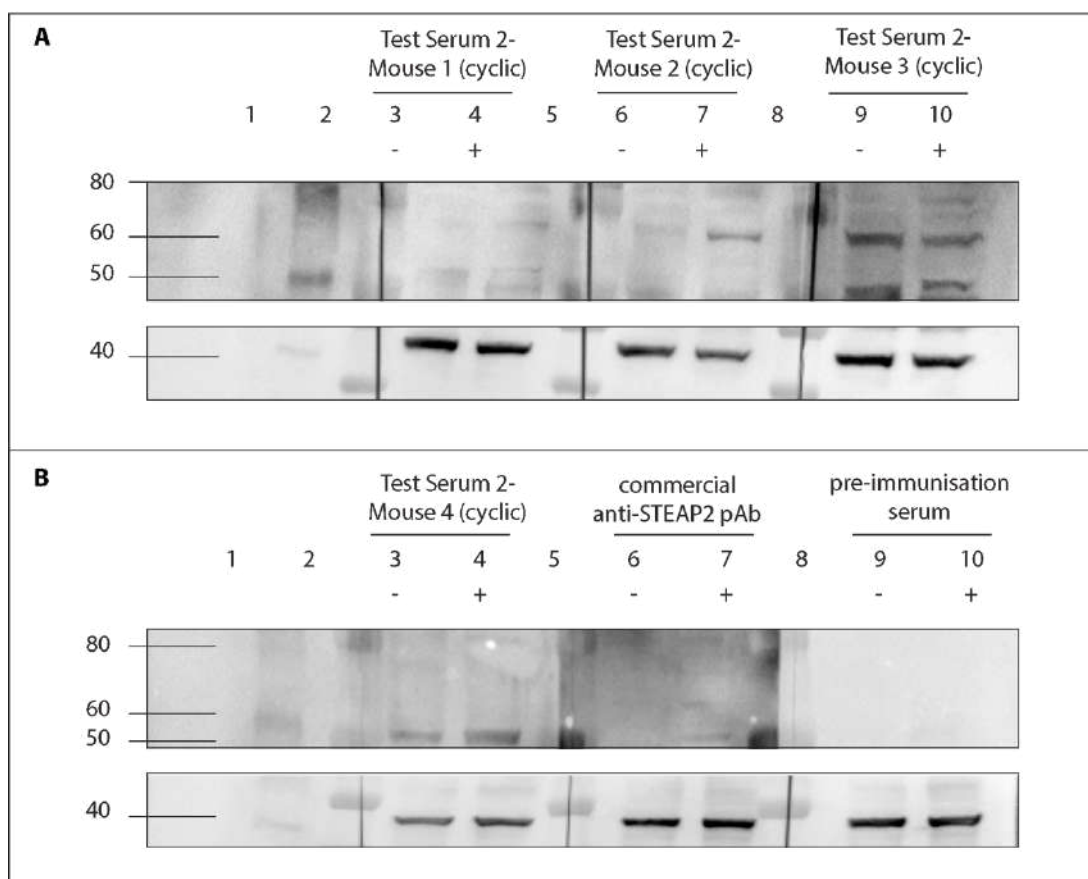


**Figure A3. 5 STEAP2 protein analysis using the Test sera2 (cyclic).** A) Test Serum2 (cyclic)1, 2 and the commercial anti-STEAP2 pAb control. B) Test Serum2 (cyclic) 3, 4 and the commercial anti-STEAP2 pAb control. 1:Unstained molecular weight ladder; 2: pre-stained dual colour molecular weight marker; 3, 6, 9: technical triplicate of PNT2 cell lysate; 4, 7, 10: technical triplicate of PC3 cell lysate (N = 1).

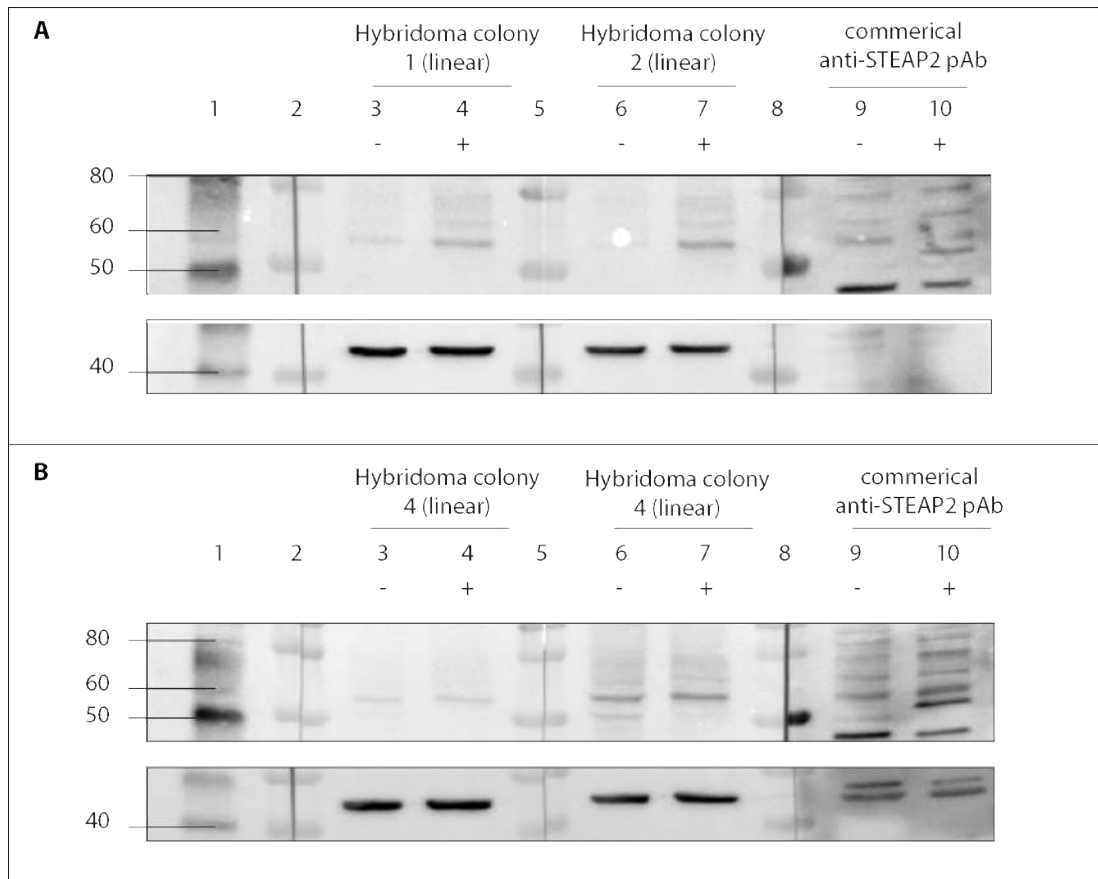


**Figure A3. 6 STEAP2 protein analysis using the supernatant of the hybridoma colonies.** A) Hybridoma colony 1 (linear), 2 (linear) and the commercial anti-STEAP2 pAb control. B) Hybridoma colony 3 (linear), 4 (cyclic) and the commercial anti-STEAP2 pAb control. 1: Unstained molecular weight ladder; 2: pre-stained dual colour molecular weight marker; 3, 6, 9: technical triplicate of PNT2 cell lysate; 4, 7, 10: technical triplicate of PC3 cell lysate (N = 1).

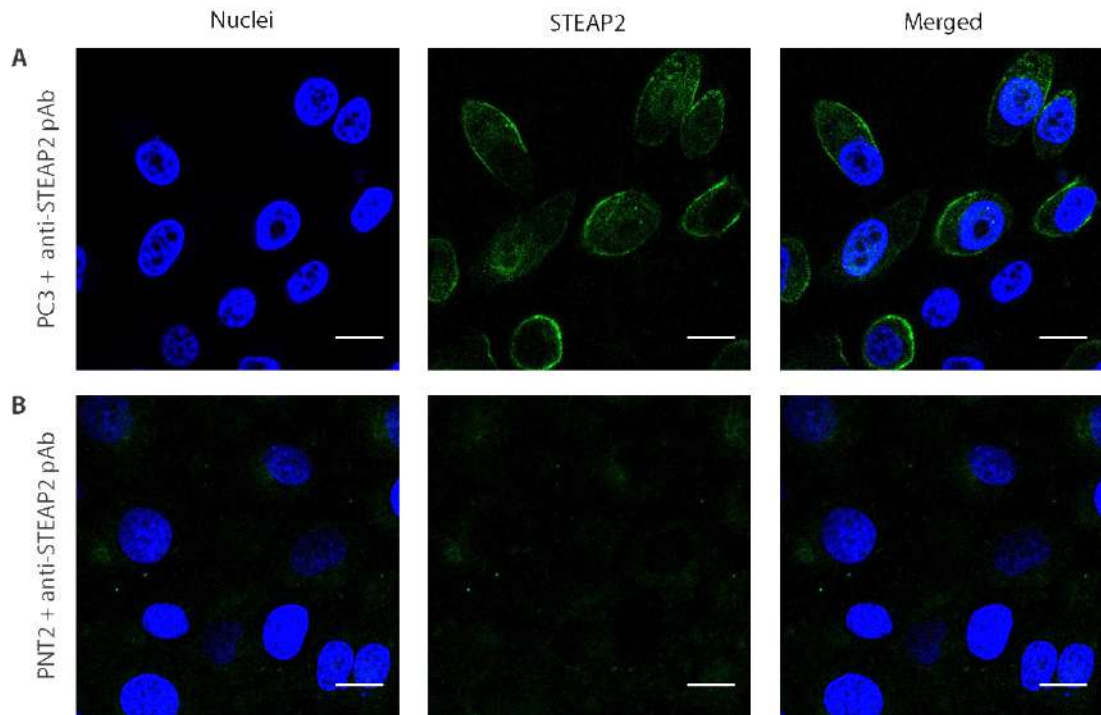


**Figure A3. 7** Fluorescent staining of STEAP2 using the commercial anti-STEAP2 pAb control to evaluate the hybridoma colony supernatants. A) PC3 cells + anti-STEAP2 pAb showing high STEAP2 (cell surface) expression. B) PNT2 cells + anti-STEAP2 pAb showing low STEAP2 expression. Blue: nuclei; green: STEAP2. Images were taken at a 63x objective using the LSM 710 microscope (ZEISS, Germany). Scale bar = 20  $\mu\text{m}$  (N = 1).

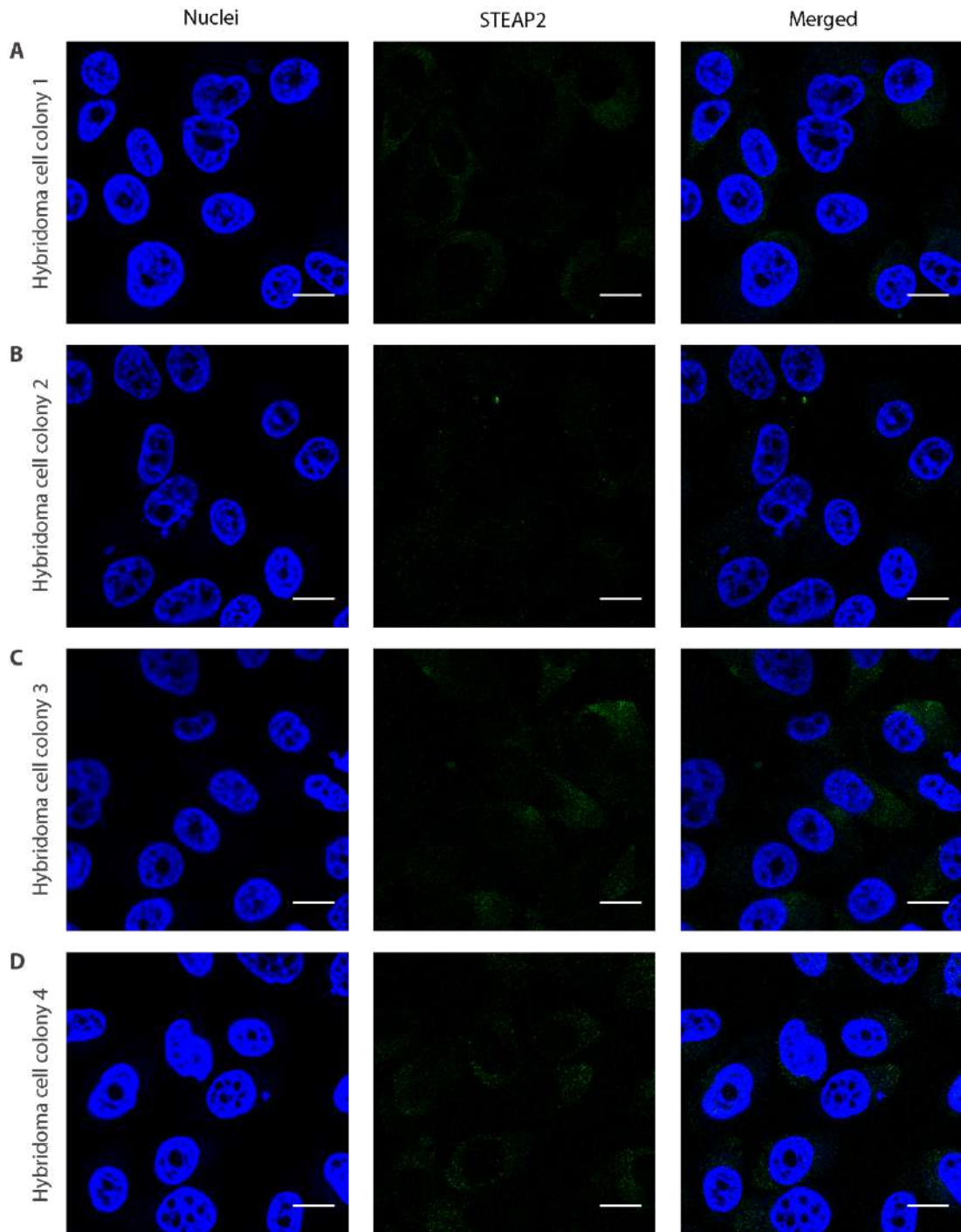


**Figure A3. 8** The supernatants of the hybridoma colonies do not recognise native STEAP2 protein in the PC3 cells. Blue: nuclei; green: STEAP. Images were taken at a 63x objective using the LSM 710 microscope (ZEISS, Germany). Scale bar = 20  $\mu\text{m}$  (N = 1).

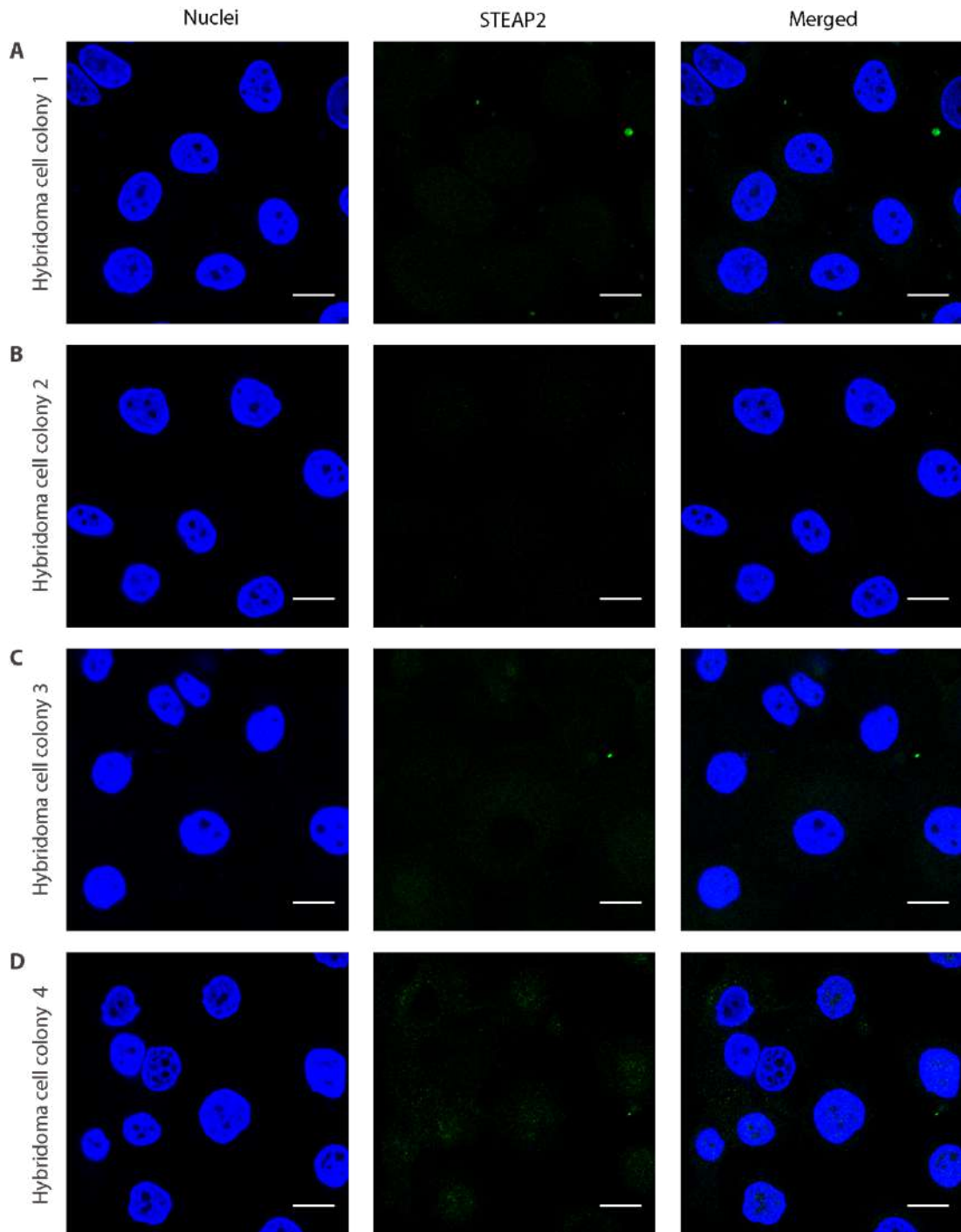


**Figure A3. 9** The supernatants of the hybridoma colonies do not recognise native STEAP2 protein in the PNT2 cells. Blue: nuclei; green: STEAP2. Images were taken at a 63x objective using the LSM 710 microscope (ZEISS, Germany). Scale bar = 20  $\mu\text{m}$  (N = 1).